DEVELOPMENT OF BIOMIMETIC MATERIALS FOR ENHANCED MATURATION OF ENGINEERED CARDIAC TISSUE

by

Alexander Jay Hodge

A dissertation submitted to the Graduate Faculty of
Auburn University
in partial fulfillment of the
requirements for the Degree of
Doctor of Philosophy

Auburn, Alabama
May 8, 2016

Approved by

Elizabeth A. Lipke, Chair, Mary and John H. Sanders Endowed Associate Professor of Chemical Engineering
Mark E. Byrne, Daniel F. & Josephine Breeden Associate Professor of Chemical Engineering
Jin Wang, Walt and Virginia Woltosz Endowed Associate Professor of Chemical Engineering
Rajesh Amin, Assistant Professor of Drug Discovery and Development

Abstract

The creation of cardiac tissue constructs holds potential in the development of clinical and diagnostic platforms, including the creation of novel treatments for patients with heart disease and cost-effective platforms for drug discovery. Many materials and techniques have been investigated for use in creating engineered cardiac tissue; however, formation of engineered myocardium in vitro, particularly when derived from pluripotent cell sources, often results in the creation of cardiac tissue or cardiomyocytes with functional properties that are markedly different from the native adult myocardium. The use of biomimetic materials, those materials that emulate one or more properties of native tissue, may be necessary for obtaining cardiac tissue demonstrating physiologically-relevant electrophysiological properties. In this document, the ability of biomimetic materials to drive pluripotent stem cell derived cardiac tissue maturation has been investigated.

This document first introduces the overall challenges associated with heart disease and drug discovery, which emphasizes the need for biomimetic material-based solutions. A review on current biomaterial-based methods for treating heart disease, as well as background on work utilizing biomimetic materials for cardiac regeneration is presented, as well as current methods for evaluating functional maturity (with an emphasis on quantifying electrophysiology) of cardiomyocytes and cardiac tissue. Next, the design and implementation of an optical mapping platform for assessing calcium wave velocity and calcium transient duration is presented. This combined macroscopic and microscopic

imaging system was capable of capturing optical mapping data from samples ranging 21 to 0.5 mm in size at rates in excess of 500 frames per second. After, a study utilizing biomimetic nitric oxide donor S-nitrosocysteine (CysNO) to direct maturation of stem cell derived cardiomyocytes (SC-CMs) is discussed. Differentiating embryoid bodies treated with CysNO developed greater numbers of faster contracting cardiomyocytes in comparison to controls; dissociated SC-CMs treated with CysNO demonstrated improvement in calcium handling via faster calcium transient velocities and shorter calcium transient durations. Next, a study utilizing the conductive polymer polypyrrole (PPy) is presented which evaluated cardiomyocyte survival and development when grown on the novel material. HL-1 cardiomyocytes cultured on PPy-polycaprolactone (PPy-PCL) films demonstrated greater numbers of connexin-43 positive cells in conjunction with faster calcium transient velocities and shorter calcium transient durations in comparison to cells grown on PCL alone. Finally, the response of SC-CMs differentiated on the surface of the novel PPy-PCL material is reported; PPy-PCL supported the growth and viability of dissociated SC-CMs at a comparable number to PCL alone. Together, these studies provide insight into how novel biomimetic materials can be implemented in the creation of functionally-mature cardiac tissue. Additionally, this work demonstrates how a custom optical mapping apparatus can be adapted to assess cardiac maturation among a gamut of different platforms. The ability to direct and evaluate maturity of differentiating cardiomyocytes contributes to the development of clinical and research platforms for improving treatment of heart disease.

Acknowledgements

Assembly of this document has been a challenging endeavor that reflects my time, skills, and patience while at Auburn University. Although I would like to claim sole responsibility for all work contained within the manuscript, I cannot alone take credit for this effort. In truth, there have been a number of individuals which have assisted me throughout the course of my graduate studies. These individuals include a number of graduate students that personally invested their time and intellect to assist with many facets of my project: Aaron Seeto, Samuel Chang, Petra Kerscher, and Shantanu Pradhan. During my time at Auburn University, I had the opportunity to mentor several undergraduate students that all contributed in part to the completion of my program. I would like to thank: Benjamin Spearman, James Morris, Wesley Grove, John Porter, and Alec Castinado for their hard work and dedication. I must also thank my PI, Dr. Elizabeth Lipke, for her continued dedication and guidance throughout my project, as well as my other committee members and faculty that have devoted time and knowledge to my work.

Furthermore, I could not have completed this document without the support of my friends and family. I would like thank my parents, Pat and Dale Hodge, and my in-laws, Katherine and Jerry Shearin, for all the support they have given me during this process. Lastly, I would like to dedicate this document to my wife Laura for her unyielding support, patience, and motivation for me during this challenging time in my life.

Table of Contents

List of Figures

List of Tables

List of Abbreviations

ATP	adenosine triphosphate
bFGF	basic fibroblast growth factor
BMP-2	bone morphogenic protein 2
CCD	charge coupled device
cGMP	cyclic guanosine monophosphate
CPLA	crystalized polylactic acid
cTnT	cardiac troponin T
Cx43	connexin-43
CysNO	*S*-nitrosocysteine
DAPI	4',6-diamidino-2-phenylindole
DMEM	Dulbecco's Modified Eagle Medium
DMSO	dimethyl sulfoxide
EB	embryoid body
ECM	extracellular matrix
EGTA	ethylene glycol tetraacetic acid
eNOS	endothelial nitric oxide synthase
ESC	embryonic stem cell
FBS	fetal bovine serum
FGF-2	basic fibroblast growth factor
GAG	glycosaminoglycan

GTP	guanosine triphosphate
HBS	HEPES buffered saline
HEPES	4-(2-hydroxyethyl)-1-piperazineethanesulfonic acid
IGF-1	insulin-like growth factor 1
iNOS	inducible nitric oxide synthase
L-NAME	Nω-nitro-L-arginine methyl ester
LIF	leukemia inhibitory factor
MEA	microelectrode array
mEF	mouse embryonic fibroblast
mESC	mouse embryonic stem cell
MHC	myosin heavy chain
MSC	mesenchymal stem cell
Nkx2.5	NK2 homeobox 5
nNOS	neuronal nitric oxide synthase
NO	nitric oxide
NOS	nitric oxide synthase
P4HB	prolyl 4-hydroxylase subunit beta
PBS	phosphate-buffered saline
PCL	polycaprolactone
PCR	polymerase chain reaction
PDMS	polydimethylsiloxane
PEG	polyethylene glycol
PEUU	poly(etherurethane urea)

PGA	polyglycolic acid
PGS	poly(glycerol-sebacate)
PKG	phosphate kinase G
PLA	polylactic acid
PLGA	poly(lactic acid-co-glycolic acid)
PNIPAAm	poly(N-isopropylacrylamide)
poly(HEMA)	poly(hydroxyl)ethyl-methacrylate
SC-CM	stem cell-derived cardiomyocyte
SEM	scanning electron microscopy
SERCA	sarcoendoplasmic reticulum calcium transport ATPase
sGC	soluble guanylyl cyclase
SNAP	*S*-nitroso-N-acetylpenicillamine
SR	sarcoplasmic reticulum
TEM	transmission electron microscopy
TGF-β	transforming growth factor β
VEGF	vascular endothelial growth factor
WCA	water contact angle
XPS	X-ray photoelectron spectroscopy

1. THE NEED FOR ENGINEERED MYOCARDIUM

The heart is an intricate organ with intensive structural and functional demands when compared to other tissues in the body. In a healthy adult, the heart must supply an output of five liters each minute on average to adequately supply oxygen and nutrients to the body; however, sudden increases in physiological demand resulting from hormonal and paracrine signaling pathways may generate cardiac outputs as high as thirty liters per minute. Furthermore, with rates of contraction in the range of 60-70 beats per minute, an average individual may experience in excess of three billion contractions over the course of a lifetime. Taken together, these facts demonstrate the stressful, transient demands which are placed on the heart on a daily basis. Indeed, with the complexity of the cardiac mechanical, electrical, and chemical systems integrated into an organ the size of a fist, these statements constitute an oversimplification of the heart's physiological importance. It should be no surprise that given the complexity of the heart, the propensity for heart disease remains an ongoing risk, resulting in debilitating conditions for patients experiencing such pathologies.

Heart disease constitutes the highest cause of mortality in the developed world (Kirkpatrick, Vannan et al. 2007), translating to over one in four deaths within the United States alone (Fig. 1.1). When combined with all other forms of cardiovascular disease, the mortality rate increases to include over 34% of all American deaths (Lloyd-Jones, Adams et al. 2009). In addition to the widespread cost in lives and lost economic opportunity, the financial burden for heart disease and related treatments has been estimated at hundreds of billions of dollars every year (Lloyd-Jones, Adams et al. 2010). Perhaps even more devastating is the loss in quality of life experienced by a patient with

heart disease, which can place a burden on family members and care providers. Taken together, these problems represent considerable challenges and present opportunities for both saving lives and recuperating cost in the form of more effective cardiac therapies.

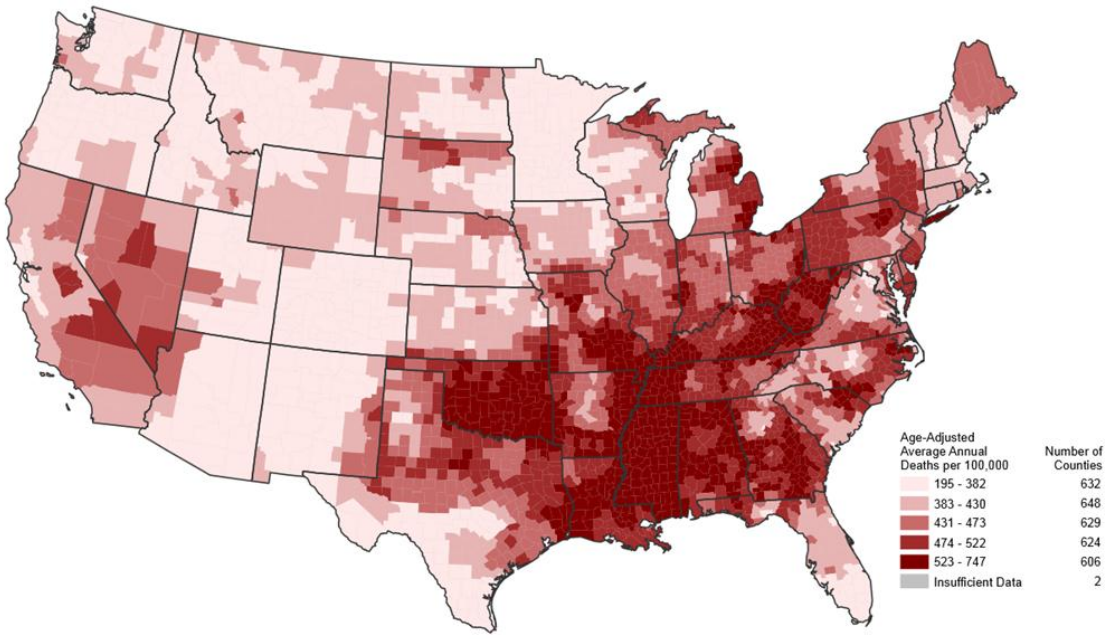

Figure 1.1. Map of the United States listing annual deaths from heart disease by county. (Image from CDC.gov)

1.1. Current methods and challenges in the treatment of heart disease

Heart disease is a blanket statement which may be applied to a number of cardiac pathologies. In general use, this term often refers to ischemic heart disease and cardiomyopathy; however, the term is also extended to include valvular disease and congenital heart defects (Fig. 1.2). Ischemic heart disease often results from an occlusion in a coronary artery, leading to hypoxic conditions in the heart which result in cell necrosis or apoptosis. In the case of reperfusion following ischemia, large numbers of free radicals formed from inflammation in the myocardium cause significant damage to

surrounding tissue, including the heart wall. Cardiomyopathy is a condition in which the performance or function of the heart has diminished, placing an individual at risk for arrhythmias and cardiac arrest. While the principal causes of cardiomyopathy are numerous, dilated cardiomyopathy, a condition in which an enlarged cardiac tissue leads to progressive damage and hypertrophy, is the most commonly diagnosed form. In both cases of ischemic heart disease and cardiomyopathy, the damage left to the underlying tissue is extensive, resulting in poor electrical conduction and a reduction in output.

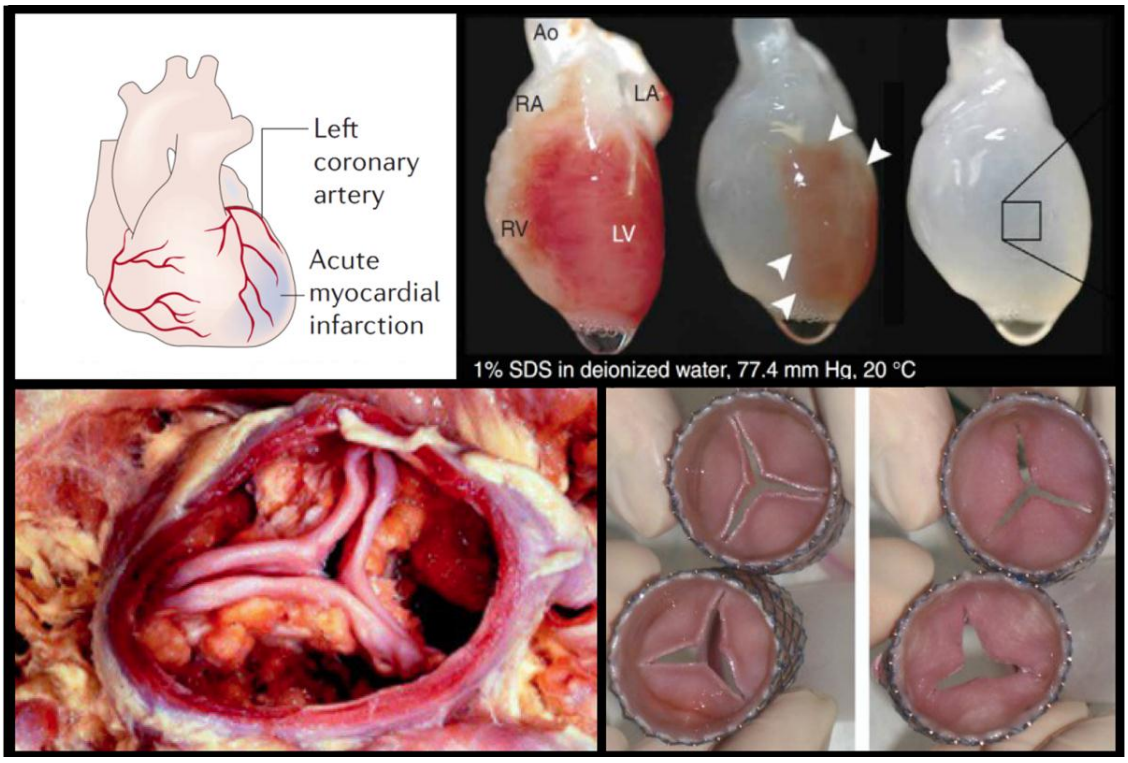

Figure 1.2. Heart function can be negatively impacted by diseases and by the presence of congenital heart defects. These effects can be treated with biomaterial approaches. (Top-Left) Graphic of a myocardial infarction (Top-Right) Creation of a decellularized scaffold. (Bottom-Left) Diseased aortic valve. (Bottom-Right) Tissue engineered valve replacements with cells grown on a synthetic scaffold.

Understanding the extent of disease, as well as the means for treating or reversing disease, requires investigation into the physiology of cardiac tissue. The myocardium is

composed primarily of three cell types: cardiomyocytes, cardiac fibroblasts, and endothelial cells. Cardiomyocytes, the muscle cells responsible for contraction in the heart, constitute approximately 75% of the total volume of heart tissue (Ju and Dixon 1996). Although these contractile cells are regenerated slowly over the lifespan of the individual, disruptions in the heart caused by disease cannot be rapidly repaired by endogenous cardiomyocytes; thus, cardiac fibroblasts are largely responsible for repairing damage left by disease, resulting in the formation of scar tissue (Laflamme and Murry 2011).

In order to restore function to these regions, both the mechanical and electrical properties of the native myocardium must be reinstated, which means replacing the fibrotic tissue with functional cardiomyocytes. The course of treatment for individuals with heart disease varies from patient to patient depending on a number of factors including age, pathology, and overall health of the individual. Virtually all patients with myocardial damage are treated with minimally-invasive therapies, which include the prescribing of pharmaceutical drugs (diuretics, alpha/beta blockers, nitrates, anti-coagulant/platelet, etc.) and through changes in diet and lifestyle. Further care may be provided in the form of surgical intervention, which can vary depending on the pathology as well as the severity of the condition. Catheterization labs are specialized facilities for assessment and treatment of cardiovascular disease; treatments range from diagnostic imaging, such as angiography, to angioplasty procedures to open occluded arteries and even pacemaker implantation. Stents may be employed in patients with coronary artery or ischemic heart disease to enlarge occluded vessels, improving circulation to damaged regions in the myocardium; in more severe cases, diseased vessels may be replaced in a

total cardiac bypass. Congenital heart defects are typically treated surgically, with septal defects currently being repaired using synthetic patches, such as Dacron and Gore-Tex®, or patches derived from decellularized human or bovine pericardium. End stage heart failure patients may have a total heart transplant or receive a ventricular assist device or other artificial heart as bridge to transplant. State-of-the-art adult stem cell therapies have demonstrated some improvement in cardiac output (Taccardi, Lux et al. 1997); this change may be a result of increased nutrient transport through angiogenesis, or from improvements in extracellular matrix regeneration. Therefore, these treatments have not resulted in the generation of new cardiomyocytes to replace fibrotic scar tissue. Although these treatments as a whole may extend the life of the individual, modern medicine cannot erase long-term damage inflicted on the myocardium. In contrast to existing therapies, engineered cardiac tissue grown in a controlled laboratory environment could offer one approach to repair damaged tissue within the heart. Unlike other techniques, engineered tissue would replace diseased, fibrotic myocardium, reducing mortality and increasing quality of life.

1.2. The use of engineered myocardium in diagnostic applications

In addition to the benefits of engineered cardiac tissue in clinical medicine, emphasis has been placed on development of cardiac tissue for drug discovery applications. Many widely prescribed pharmaceuticals, including: antiarrhythmics, antidepressants, antipsychotics, and anesthetics have been shown to contribute to the formation of drug-induced long QT syndrome, torsade de pointes, Brugada syndrome and other conditions with a propensity for forming arrhythmias (Ayad, Assar et al. 2010, Letsas, Kavvouras et al. 2013). Hundreds of millions of dollars may be spent over a

decade or more when moving from drug discovery to market, thus, technology to evaluate drug toxicity in the myocardium would provide an important tool for the pharmaceutical industry to screen new chemical formulations prior to testing on humans (Fig. 1.3). Development of tissue-engineered myocardium for clinical applications could be utilized by the pharmaceutical industry to reduce costs both in money and lives. Similarly, development of cardiac tissue models could assist in areas of basic biology, allowing for research into organismal development and formation of pathologies.

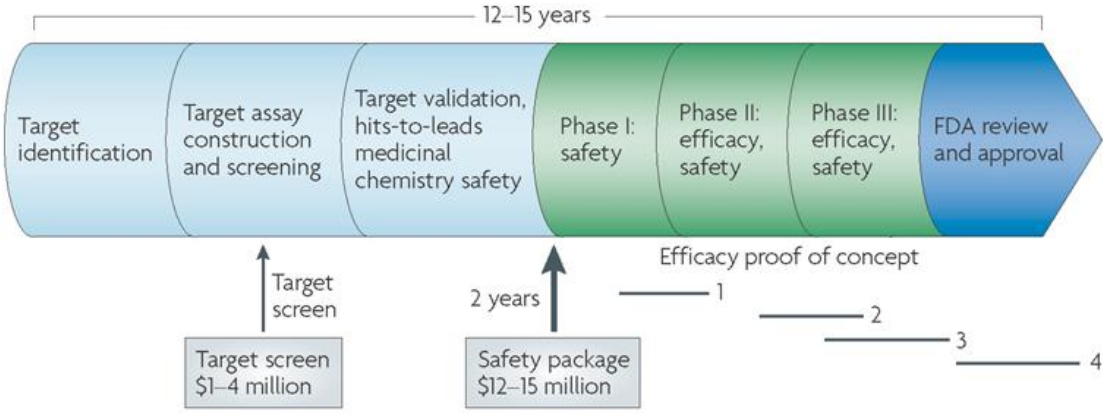

Figure 1.3. Timeline illustrating the individual stages of drug discovery and clinical trials. (Image from Roses, 2008).

Taken together, these clinical and diagnostic applications present a unique challenge to the field of cardiac regeneration. Herein, the goal of the proposed research is to develop a platform for creating engineered myocardium (Fig. 1.4). In the following chapter, a background on current treatments for heart disease will be presented, as well as biomaterials investigated for use in cardiac regeneration and methods for determination of electrophysiological maturation. Next, the motivation for collecting electrophysiological data on cardiomyocytes, as well as work involved in the fabrication

of an optical mapping platform, will be discussed. The experimental effects of a soluble nitric oxide donor on the maturation of stem cell-derived cardiomyocytes will be examined. The application of a conductive polymer as a cardiac scaffold, as well as data demonstrating growth and viability of cardiomyocytes on the material, will be presented in Chapter 5. A subsequent study utilizing stem cell-derived cardiomyocytes on the conductive polymer will also be discussed in Chapter 6. The remaining chapter will summarize the work presented in the document and present overarching conclusions regarding the lessons learned in driving cardiomyocyte maturation.

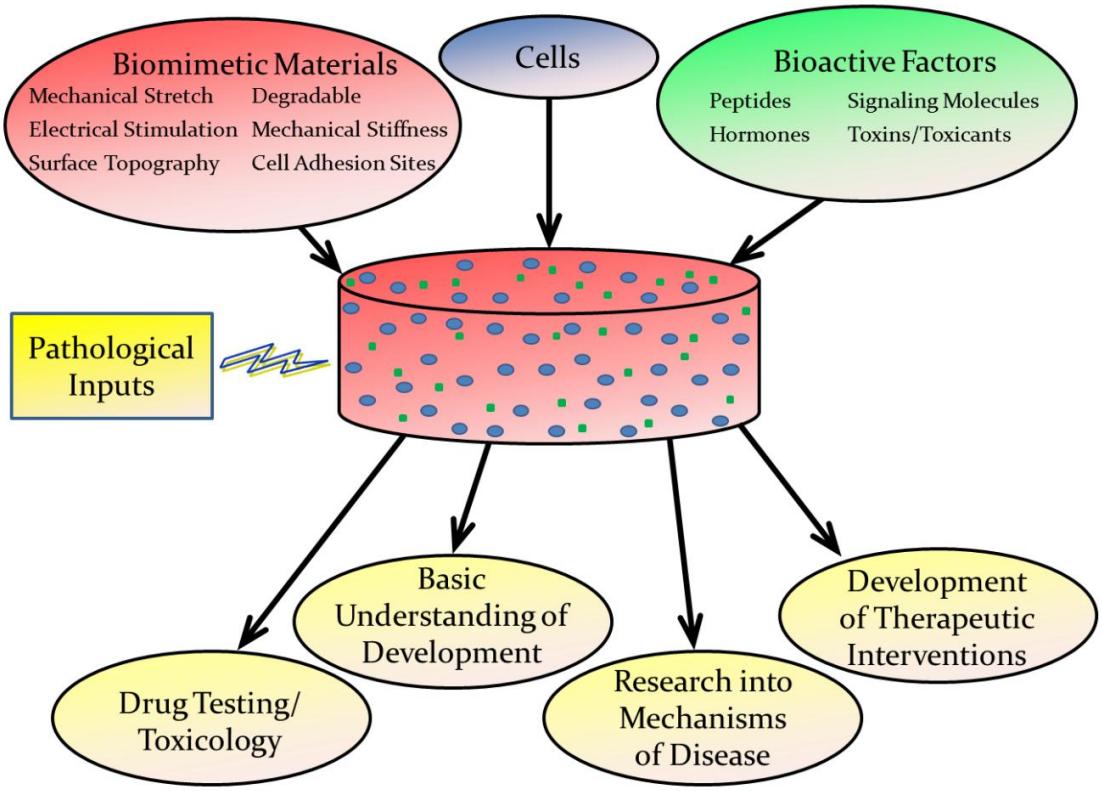

Figure 1.4. Biomaterials seeded with bioactive factors and cultured cells support engineered tissue formation.

References

Ayad, R. F., M. D. Assar, L. Simpson, J. B. Garner and J. M. Schussler (2010). "Causes and management of drug-induced long QT syndrome." Proc (Bayl Univ Med Cent) 23(3): 250-255.

Ju, H. and I. M. Dixon (1996). "Extracellular matrix and cardiovascular diseases." Can J Cardiol 12(12): 1259-1267.

Kirkpatrick, J. N., M. A. Vannan, J. Narula and R. M. Lang (2007). "Echocardiography in heart failure: applications, utility, and new horizons." J Am Coll Cardiol 50(5): 381-396.

Laflamme, M. A. and C. E. Murry (2011). "Heart regeneration." Nature 473(7347): 326-335.

Letsas, K. P., C. Kavvouras, G. Kollias, S. Tsikrikas, P. Korantzopoulos, M. Efremidis and A. Sideris (2013). "Drug-induced brugada syndrome by noncardiac agents." Pacing Clin Electrophysiol 36(12): 1570-1577.

Lloyd-Jones, D., R. Adams, M. Carnethon, G. De Simone, T. B. Ferguson, K. Flegal, E. Ford, K. Furie, A. Go, K. Greenlund, N. Haase, S. Hailpern, M. Ho, V. Howard, B. Kissela, S. Kittner, D. Lackland, L. Lisabeth, A. Marelli, M. McDermott, J. Meigs, D. Mozaffarian, G. Nichol, C. O'Donnell, V. Roger, W. Rosamond, R. Sacco, P. Sorlie, R. Stafford, J. Steinberger, T. Thom, S. Wasserthiel-Smoller, N. Wong, J. Wylie-Rosett, Y. Hong, C. American Heart Association Statistics and S. Stroke Statistics (2009). "Heart disease and stroke statistics--2009 update: a report from the American Heart Association Statistics Committee and Stroke Statistics Subcommittee." Circulation 119(3): 480-486.

Lloyd-Jones, D., R. J. Adams, T. M. Brown, M. Carnethon, S. Dai, G. De Simone, T. B. Ferguson, E. Ford, K. Furie, C. Gillespie, A. Go, K. Greenlund, N. Haase, S. Hailpern, P. M. Ho, V. Howard, B. Kissela, S. Kittner, D. Lackland, L. Lisabeth, A. Marelli, M. M. McDermott, J. Meigs, D. Mozaffarian, M. Mussolino, G. Nichol, V. L. Roger, W. Rosamond, R. Sacco, P. Sorlie, R. Stafford, T. Thom, S. Wasserthiel-Smoller, N. D. Wong, J. Wylie-Rosett, C. American Heart Association Statistics and S. Stroke Statistics (2010). "Executive summary: heart disease and stroke statistics--2010 update: a report from the American Heart Association." Circulation 121(7): 948-954.

Taccardi, B., R. L. Lux, P. R. Ershler, R. MacLeod, T. J. Dustman and N. Ingebrigtsen (1997). "Anatomical architecture and electrical activity of the heart." Acta Cardiol 52(2): 91-105.

2. METHODS FOR REPAIRING CARDIAC FUNCTION

2.1. Biomaterials for myocardium regeneration

Materials play an integral role in the ability to direct cardiac regeneration and cardiomyocyte differentiation. As a unique organ with complex structural and functional properties, the heart requires an environment capable of withstanding the stresses associated with systematic contraction and oxidative (or free radical) degradation while supporting the intimate cell-cell interaction and coupling necessary for wide spread, organized electrical propagation. Scaffolds used in cardiac regeneration should therefore be comprised of biomimetic materials which can replicate the inherent properties of native myocardium on the tissue, cellular, and molecular scales in order to develop physiologically-accurate cardiac tissue (Fig. 2.1). In the context of cell differentiation, this requires engineering a cell niche capable of delivering the complex sequence of biomimetic physical and chemical stimuli necessary to direct early cell lineage towards a cardiomyocyte fate. Design of materials capable of suppressing spontaneous differentiation among pluripotent cell populations is also a crucial step in the creation of billions of cells necessary for cardiac regeneration therapy; differentiated, mature cardiomyocytes rarely divide. Addressing these issues requires fundamental knowledge of the biomaterials which can be modified to accommodate the needs of the developing tissue while also adapting to the complex structure and function of native myocardium.

Biomimetic materials hold promise in addressing the inadequacies of contemporary heart repair techniques. Biomimetic materials are materials which act to emulate properties from a natural biological environment. In the context of cardiac regeneration, this involves creating materials which: maintain the mechanical and

electrical properties of native tissue, direct cell and tissue orientation (Bursac, Loo et al. 2007, Kim, Lipke et al. 2010), deliver cardiac-promoting drugs and growth factors (Hempel, Hintze et al. 2012), and degrade in response to enzymes secreted by cells (Moon, Saik et al. 2010). Furthermore, these materials can be designed to promote cell adhesion (Gandaglia, Huerta-Cantillo et al. 2012), mechanical stretch (Shachar, Benishti et al. 2012) and electrical conduction (Mooney, Mackle et al. 2012). Overall, biomaterials can be engineered to produce functional cardiac tissue with highly controlled, defined properties.

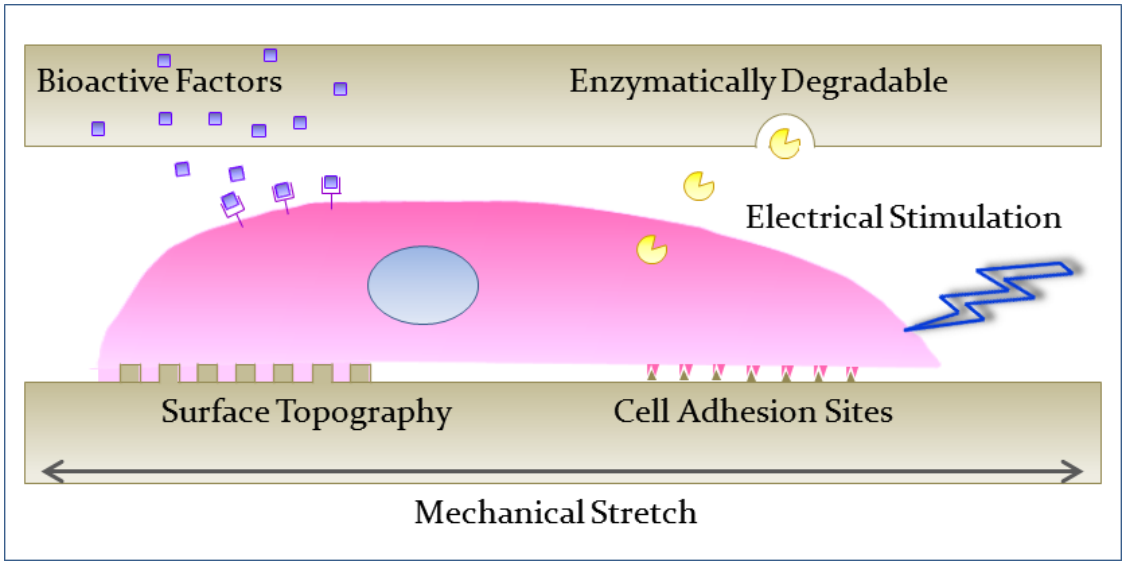

Figure 2.1. Biomimetic materials can be engineered to elicit a number of different chemical, mechanical and electrical stimuli to influence cellular behavior.

The human heart is a complex organ with unique functional and mechanical demands. With approximately 2 to 3 billion contractions over the lifetime of an individual, the myocardium requires significant flexibility and strength to withstand the cyclical, biological responses associated with physical activity and development.

Selecting an optimal material for the design of a myocardial scaffold or cell differentiation platform requires knowledge of how the surface and bulk properties of the material influence cellular behavior and host response. The ability of a substrate to replicate the environment of the native myocardial ECM is an important consideration when choosing a biomaterial for cardiac regeneration. The ECM provides structural support, a pattern for spatial conformation, cellular binding sites and reserves of signaling molecules. The scope of this microenvironmental control includes physiologically-consistent organization and integration of mature cells, as well as the facilitation of differentiation and maturation of precursor cell types.

Bulk properties of a biomaterial contribute significantly to the success of a cardiac implant and must be weighed heavily in the selection process. An engineered scaffold must accurately reflect the native physiological mechanics of the heart, in terms of stiffness and elasticity, in order to integrate correctly with native myocardium. To facilitate electrical propagation across the tissue characteristic of native myocardium, the engineered structure must incorporate conductive materials or enable adequate cell-cell coupling. Additionally, long-term medical consequences of implantable devices must be considered. This may include designing scaffolds with the flexibility for use in developing children and adults, as well as the ability to withstand long-term implantation or degrade systematically into non-toxic byproducts while limiting foreign body immune response, as well as thrombosis. As the tissue grows and develops, vascularization must also be considered to supply the organ with nutrients and oxygen. Taken together, these objectives provide a unique challenge to the engineer when considering biomaterial choice for an effective biomimetic cardiac regeneration platform.

2.2. *Properties of biomimetic materials for cardiac regeneration*

By definition, a biomimetic material is a substrate or support which mimics or emulates some aspect of the native tissue microenvironment. Biomimicry plays a critical role in selecting a material for a particular application; this may include the augmentation of bulk materials, which may not be directly biomimetic in their own right, in order to encourage greater growth, development, and engraftment of cardiac cells and tissues. In general, the materials which closely recapitulate the properties of native tissue: mechanical, electrical, and surface properties, offer greater opportunity in the creation of mature cardiomyocytes or cardiac tissue.

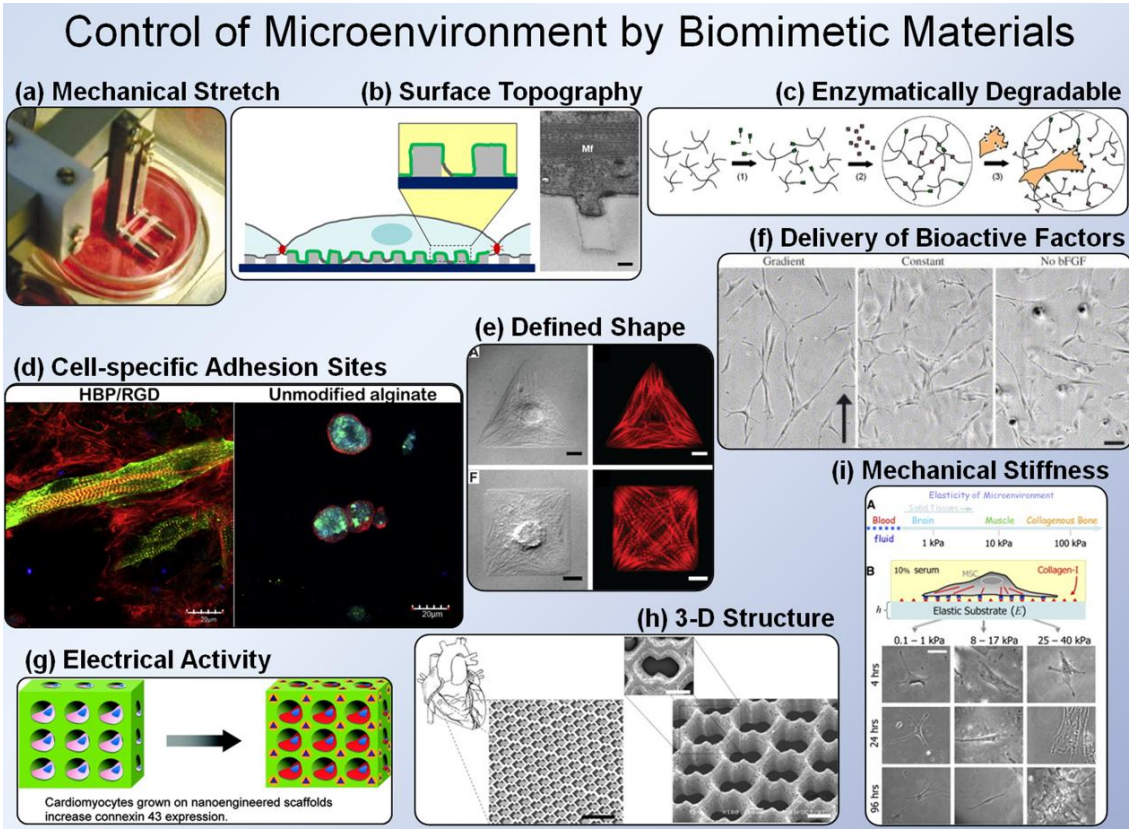

Figure 2.2. An overview of different properties which can be controlled and incorporated into biomimetic materials to direct cardiomyocyte behavior.

In practice, this may include fabrication of materials with well-defined: mechanical or structural properties, capable of enhancing cell alignment via engineered topography (Costa, Lee et al. 2003, Badie, Scull et al. 2012); electrically conducting components, supporting or augmenting the propagation of electrical current through adjacent cardiomyocytes (You, Rafat et al. 2011); bioactive factors, which promote cellular adhesion (Webber, Tongers et al. 2010), deliver signaling molecules and therapeutics (Sapir, Kryukov et al. 2011, Hammers, Sarathy et al. 2012), or capacity for enzymatic degradation (Benton, Fairbanks et al. 2009, Frisman, Seliktar et al. 2011, Leslie-Barbick, Saik et al. 2011) (Fig. 2.2).

Creation of a suitable platform for cardiac regeneration necessitates the replication of mechanical properties of native tissue. On the bulk scale, myocardium demonstrates a Young's Modulus of approximately 0.2-0.5 MPa (Jawad, Ali et al. 2007), which must be replicated in engineered constructs. The mechanical properties of cardiac tissue also impact cellular behavior; ECM stiffness on the cell and molecular scale has been demonstrated to influence gene expression of the surrounding cell types by virtue of mechanical transducer proteins (Engler, Sen et al. 2006). Common methods for directing mechanical properties of engineered constructs include the use of applied mechanical force (Eschenhagen, Didié et al. 2002) as well as the formation of surfaces supplying mechanical resistance (Taylor, Kim et al. 2012) (Fig. 2.3). It has been demonstrated that systematically applied shear stress or strain significantly enhances cardiomyocyte differentiation of mESCs (Gwak, Bhang et al. 2008) and improves stem cell-derived cardiomyocyte α-actinin organization (Shimko and Claycomb 2008).

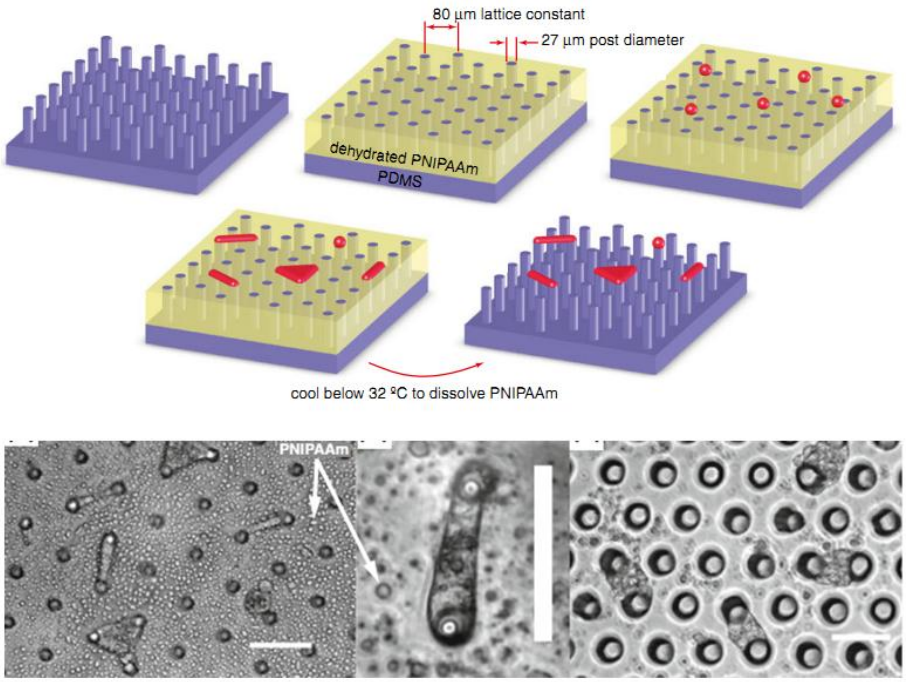

Figure 2.3. Example of a biomimetic material containing engineered micro-posts to supply mechanical resistance to cultured cardiomyocytes.

Like other cells, cardiomyocytes are responsive to material topography by virtue of adhesion molecules on their surface (Segers and Lee 2011). Structural organization on the cellular or molecular scale has been shown to influence a number of cardiomyocyte behaviors, including: protein and gene expression, proliferation, movement, morphology (McNamara, McMurray et al. 2010, McCain and Parker 2011), shape (Parker, Tan et al. 2008), and contractile strength (Feinberg, Alford et al. 2012). In the context of cardiac cell types, surface topography can also significantly impact cell-cell coupling, which influences the electrical conduction characteristics of the underlying tissue (Kim, Lipke et al. 2010). Biomimetic materials have been utilized for the creation of functional cardiac tissue with highly aligned structural components, allowing for synchronous contraction

and anisotropic electrical propagation (Fig. 2.4); success in this area depends on the creation of materials with strictly defined topography, fiber diameter, and molecular conformations (Segers and Lee 2011). Methods for creating cell (micro)-scale topography on materials include: material stamping using bioactive adhesive factors, laser microablation (Engelmayr, Cheng et al. 2008) and photolithography (Kim, Lipke et al. 2010). Structure and function of cardiac tissue on the cellular level can also be directed through the use of scaffold materials containing topographical features on the nano-scale, which reflects the scale of the ECM. Creation of nano-topography has been accomplished using a number of techniques, including sputter coating (Luna, Ciriza et al. 2011), electrospinning (Hosseinkhani, Hosseinkhani et al. 2010), and incorporation of environment-sensing materials (Elloumi-Hannachi, Yamato et al. 2010). Knowledge of cell-substrate interactions has the potential to further the development of biomimetic materials capable of manipulating the complex signaling pathways necessary for control of cellular behavior.

Synchronous contraction, which is facilitated by rhythmic electrical pacing, is a property unique to cardiomyocytes and essential to the function of healthy myocardium. On a cellular level, the speed and direction of electrical signal propagation is influenced by the presence of gap junction proteins, which link the cytosol of adjacent cardiomyocytes, as well as ion channels, which regulate the depolarization and repolarization phases of cardiomyocytes. The proteins which constitute the gap junctions in cardiomyocytes, primarily connexin-43 in ventricular cardiomyocytes and connexin-45 in atrial or nodal cardiomyocytes, are organized along the intercalated discs, which contribute to the anisotropic conduction behavior observed in these cell types.

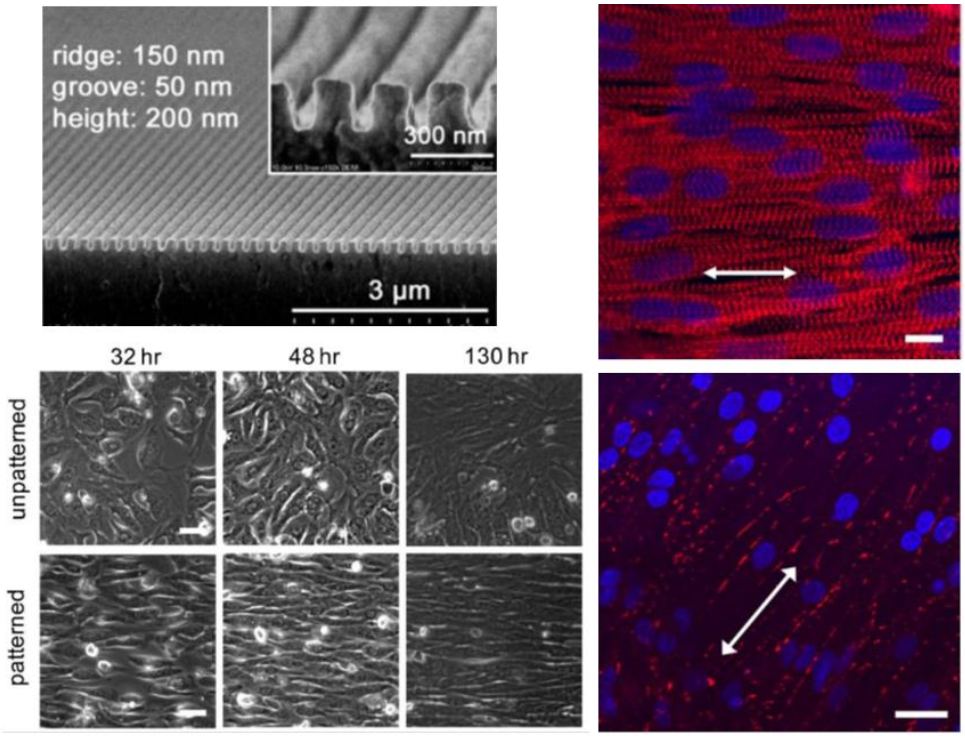

Figure 2.4. PDMS substrate with nanotopography directs alignment of cardiomyocytes.

Enhancement of electrical propagation and action potential duration in engineered heart constructs may be realized by influencing the development of gap junction proteins or ion channels, or by augmenting the cardiac ECM with conductive materials. Application of external electrical fields has been demonstrated to impact alignment and contraction strength by influencing the expression of gap junctions (Maidhof, Tandon et al. 2011). Engineered scaffolds containing conductive materials, either extracellular or transcellular (Dvir, Timko et al. 2011), have also been utilized to augment electrical propagation (Fig. 2.5).

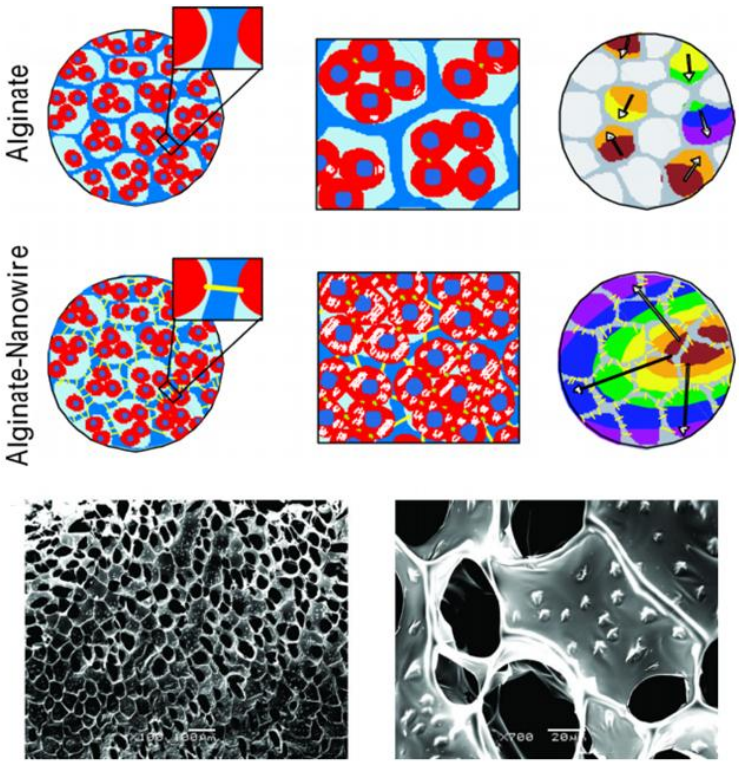

Figure 2.5. Alginate scaffold containing embedded gold nanowires.

A number of signaling molecules are instrumental in the development of native cardiac tissue. Indeed, while delivery of specific molecules remains an important aspect in the context of cardiac tissue development, the concentration or volume of release, as well as the timing of release, constitute equally important considerations. Thus, the ability to deliver drugs or other effector molecules in a controlled manner, as well as respond to degradation enzymes secreted by the developing myocardium, are desirable properties for materials used in cardiac regeneration. Functionalized materials have been designed for release of cardiogenic factors, including TGF-β (Mann, Schmedlen et al. 2001, Hempel, Hintze et al. 2012) and BMP-2 (Henslee, Spicer et al. 2011, Hou, Wang et al. 2012). Other important cardiac-promoting small molecules, such as nitric oxide, have

been successfully delivered from functionalized materials for other tissue engineering applications (Lipke and West 2005, Cabrales, Han et al. 2010). While not cardiogenic in its own right, insulin-like growth factor-1 (IGF-1) has been successfully delivered from degradable PEG-fibrin gels for restoration of skeletal myocyte function after ischemia-reperfusion injury (Hammers, Sarathy et al. 2012). Another approach which utilizes functional surfaces to direct cellular behavior involves use of self-assembling materials, namely peptide amphiphiles, to form hydrogels that can influence cell adhesion and proliferation (Matson, Zha et al. 2011). These materials are currently being investigated for multiple applications, including use in vascular repair (Andukuri, Kushwaha et al. 2011) and cardiac regeneration (Zhang, Greenfield et al. 2010). As we learn which stimuli are important for maturation, additional small molecules, time points for release, and dosages of effectors will become important considerations in cardiac material design (Table 2-1).

Table 2-1. Important biomimetic properties for heart tissue regeneration

Property	Native function	Example Materials
Mechanical Property Modulation	Mechanical properties of myocardium, including stiffness and elasticity, defined by ECM composition	Collagen/Matrigel Gelatin
Directing Cell Alignment/ Anisotropy	Anisotropic alignment of myocardium enables unidirectional electrical propagation and contraction	PEG PDMS/Fibronectin Collagen
Enhancing Electrical Propagation	Myocardium conduction rate: 50 cm/s Establishment of organized gap junction proteins	Gold nanowires Gold nanoparticles Polypyrrole Carbon nanotubes Tin Oxide Electrodes
Bioactive / Functionalized Surface	Cardiomyocyte development is closely regulated by a number of bioactive molecules released by cells in the surrounding niche	RGDS Peptide Amphiphiles PEG-Fibrin HPB/RGDS
Degradable Support	Native tissue relies derives its structural integrity from ECM and supporting cell types Synthetic materials used for cardiac regeneration should be replaceable with ECM over time	PEG-fibrinogen PEG PEGDA

2.3. Classes of Biomaterials

Previous work in creating engineered cardiac tissues has utilized a number of different polymeric materials to augment cardiac regeneration and control cardiomyocyte differentiation. In general, these materials can be categorized as either natural or synthetic in origin; however, combinations of the two classes have been developed to create hybrid materials which express a unique combination of different properties. While the materials covered here represent just a partial list of the materials utilized in scaffold design and niche engineering, each contains unique biomimetic characteristics which contribute to its individual success for different applications. The development of these biomimetic substrates offers novel approaches for addressing the challenges associated with creating functional engineered cardiac tissue. These materials will be discussed in further detail.

Natural Materials

Natural materials constitute the class of materials derived from proteins, polysaccharides, and other derivatives of these substances. The use of substrates derived from naturally occurring materials has been employed in numerous ways to promote cardiac regeneration, taking advantage of the inherent cell signaling aspects of these moieties. In particular, the use of heart structural proteins offers a significant advantage in the improvement of cellular activity by virtue of surface properties which are characteristic of native cardiac tissue. Other natural materials, many of which do not possess the same surface properties of native proteins, may contain unique properties which facilitate their use in the myocardium. Despite their inherent biomimetic nature, natural materials also possess a number of undesirable qualities which can hinder their effectiveness. In particular, the bulk properties of these materials are often considerably

different than the structure of native myocardium, leading to poor engraftment of these materials in native tissue (Pêgo, Siebum et al. 2003). With the exception of decellularized heart ECM, natural materials do not maintain their native organization; many may also lose their mechanical properties with repetitive cycling or degrade further over time. Furthermore, because many natural materials are derived from animal sources, lot to lot variability and the potential for disease transmission and immune complications are drawbacks that require serious consideration. Intense efforts are being made to overcome these disadvantages.

The use of natural materials, particularly those materials which constitute the native extracellular matrix of myocardium, is an attractive option when attempting to replicate the complex microenvironment of the heart. As explained earlier in detail, the extracellular matrix plays an important role in the determining the mechanical properties of the underlying tissue; this role is dictated by composition of the matrix as well as the ability of the material to direct and organize cellular morphology and geometry. The extracellular matrix is comprised of collagen interspersed with elastin, providing the tissue with tensile strength and plasticity; these properties are further defined by the size, shape, and organization of collagen fibers within the tissue space. The use of collagen alone as a substrate for cardiac regeneration has been met with criticism, as the material has poor mechanical properties, limited stability, and chronic batch-to-batch variability in its production (Pêgo, Siebum et al. 2003, Radisic, Deen et al. 2005). Despite these undesirable aspects, collagen (Dai, Hale et al. 2009) and Matrigel (Laflamme, Chen et al. 2007) have been utilized as soluble substrates for direct injection of stem cell-derived cardiomyocytes into native myocardium, facilitating an environment for improving

cellular viability and engraftment. Collagen, as well as gelatin, has also been utilized in concert with other materials in the creation of co-polymer blends which provide a suitable environment for cell expansion, modulating cellular mechanical transduction (Zimmermann, Schneiderbanger et al. 2002, Baraniak, Cooke et al. 2012) while maintaining structural integrity (Kai, Prabhakaran et al. 2011, Liu, Peng et al. 2011).

Other natural materials constituting the extracellular matrix, including fibronectin, laminin, and GAGs, have also been used in cardiac regeneration applications for enhancing the adhesion and proliferation of cells in a scaffold (Heydarkhan-Hagvall, Gluck et al. 2012). Hyaluronic acid, a common GAG, has demonstrated important roles involved in integrin signaling pathways responsible for directing cardiomyocyte fate and behavior (Chopra, Lin et al. 2012); others have used hyaluronic acid scaffolds to directly influence the activity of mesenchymal stem cells and neonatal cardiomyocytes (Fiumana, Pasquinelli et al. 2012, Gallina, Dolgetta et al. 2012). Decellularized cardiac tissue, which retains the native properties of heart extracellular matrix, has also been prepared for use in scaffolds.

A number of other natural materials demonstrate favorable properties for cardiac regeneration therapy. Fibrin has been utilized as a structural material for scaffolds, valuable for its ability to recreate tissue with a biologically-consistent ECM profile (Ross and Tranquillo 2003). Scaffolds containing fibrin have been used to encapsulate neonatal rat ventricular myocytes in a defined three-dimensional environment while promoting viability over a period of 13 days (Yuan Ye, Sullivan et al. 2011). Alginates, although demonstrating poor cell adhesion and proliferative capacity, have been combined with other materials to promote cell viability among encapsulated neonatal rat ventricular

myocytes (Bai, Zheng et al. 2011). Given their innate solubility characteristics, alginates have been employed in other tissue engineering approaches, including cell encapsulation (Bai, Zheng et al. 2011) and cell printing technology (Gaetani, Doevendans et al. 2012).

Synthetic Materials

Synthetic materials constitute a significant portion of the engineered constructs designed for cardiac regeneration therapy. Unlike natural materials, synthetic materials do not suffer from inherently different structural properties compared to native tissue, nor do they introduce xenogenic compounds which can prompt immune response. Synthetic scaffolds may be engineered with tunable properties capable of emulating the structural characteristics of native tissue. Furthermore, these materials may be augmented to interact with cells or respond to changes in the environment, resulting in a shift of physical properties or release of a drug or growth factor. Unlike decellularized tissue or other natural materials, which must be harvested and treated prior to use in cardiac regeneration, synthetic materials can be produced in sufficiently large quantities to handle to increasing demand for these devices. One major consideration when using this class of materials for cardiac regeneration is the creation of toxic or immune-compromising products which can ultimately prevent successful incorporation or repair.

While a number of synthetic materials have been utilized for cardiac therapies, the more promising applications involve the use of materials which emulate native tissue properties or incorporate functional components to mimic biological function. Among these include hydrogels, environmentally-responsive polymers, and conductive materials. Hydrogels are attractive for cardiac regeneration given their inherent mechanical properties similar to that of native tissue (Slaughter, Khurshid et al. 2009). Hydrogels are

strong hydrophiles, capable of supporting nutrient transport and controlled degradation (Cristallini, Gagliardi et al. 2012) to allow for cell proliferation. Moreover, many techniques have been developed to functionalize the polymers with biological cues to tightly regulate the cellular microenvironment (Kraehenbuehl, Zammaretti et al. 2008, Gupta, Walthall et al. 2011).

Temporally-changing or externally-modifiable materials can be engineered to provide biomimetic properties that facilitate cardiac regeneration. Materials that fall into this category are unique in their ability to change structure based on changes in input (temperature, pH, photoactive, mechanical/electrical stress). Poly(N-isopropylacrylamide) (PNIPAAm), a hydrogel known for its reversible phase transition at 32°C, has been utilized for creating individual layers of cardiomyocytes in vitro (Masuda, Shimizu et al. 2008, Haraguchi, Shimizu et al. 2011). Although potentially toxic, PNIPAAm has also been investigated as a medium for controlled drug delivery among implantable devices, which may be utilized in the future for delivery of therapeutics directly into myocardium. Other external modulation has been employed in the controlled manipulation of tunable materials, including the use of photodegradation to allow for manual control of material structural integrity (Fairbanks, Singh et al. 2011).

In addition to emulating the mechanical and cell-signaling behavior necessary for cardiac regeneration or cardiomyocyte maturation, materials have been engineered to promote electrical conduction among cardiac cell types in synthetic tissue. Incorporation of gold nanowires (Dvir, Timko et al. 2011), gold nanoparticles (You, Rafat et al. 2011), or polypyrrole (Kai, Prabhakaran et al. 2011) into conventional polymers has been utilized to improve electrical conduction between adjacent cardiomyocytes. Another

method has involved the incorporation of electrically conducting materials, such as carbon nanotubes (Mooney, Mackle et al. 2012), for external stimulation of cardiac cell types.

2.4. Cell types for cardiac regeneration

Novel cardiac regeneration strategies necessitate the creation of large, readily available cell populations capable of incorporating into the native myocardium. In the past, cardiac regeneration has been limited to total heart replacements from deceased donors; however, this source remains insufficient to match the demand for cardiac regeneration therapies. Since adult cardiomyocytes rarely divide, another cell source is needed. In particular, pluripotent stem cells have the potential to provide the large numbers of cardiomyocytes needed, due to their ability to be expanded in vitro while maintaining the capacity to differentiate into almost every cell type in the body. The use of many types of cells for cardiac differentiation, including embryonic stem cells, induced pluripotent stem cells, and other lines have been reviewed by others (Siepe, Akhyari et al. 2008).

2.5. *Biomimetic materials for expansion and differentiation of cardiac cells*

In the past, biomaterials have been utilized to aid in both stem cell expansion as well as cardiac differentiation. Accomplishing each task requires knowledge of the complex microenvironment which directs (or impedes) progression into the cardiomyocyte lineage.

Biomimetic materials for expansion of stem and cardiac cells

Biomimetic materials will play an important role in the expansion and differentiation of cells for use in cardiac regeneration (Fig. 2.6) (Maidhof, Marsano et al. 2010). For safety reasons, including immunogenicity and transmission of infectious disease, it is desirable to move away from traditional methods of co-culture with non-human cells and undefined, xenogenic cell culture reagents when culturing cells that will be used clinically (Mallon, Park et al. 2006). Biomimetic material design can be used to provide cues to undifferentiated stem cells during expansion, facilitating the creation of feeder-free, xeno-free, chemically-defined culture systems for expansion of pluripotent cells. By investigating integrin expression profiles and integrin-surface interactions of pluripotent stem cells, synthetic peptide-conjugated materials have been developed that engage these same integrin receptors, enabling maintenance of stem cells in their undifferentiated state in the absence of naturally-derived protein coatings (Lee, Yun et al. 2009, Meng, Eshghi et al.). In addition to surface protein display, physical rigidity was shown to play an important role in directing lineage-specific differentiation potentially facilitating the replacement of xenogenic culture reagents (Engler, Sen et al. 2006). A number of synthetic substrates, such as aminopropylmethacrylamide (Irwin, Gupta et al. 2011), peptide-acrylate surfaces (Melkoumian, Weber et al.), poly(methyl vinyl ether-alt-maleic anhydride) (Brafman, Chang et al.), and poly[2-(methacryloyloxy)ethyl dimethyl-(3-sulfopropyl)ammonium hydroxide] (Villa-Diaz, Nandivada et al.), have been used successfully to support human pluripotent stem cell expansion and/or differentiation without the use of murine-derived Matrigel or fibroblast feeder layers (Fig. 2.6) (Melkoumian, Weber et al. 2010, Young and Engler 2011). Combinatorial development

of biomaterials for stem cell expansion has shown that material properties such as wettability, surface topography, surface chemistry and indentation elastic modulus can be optimized for maintenance of pluripotency without feeder layers (Mei, Saha et al.).

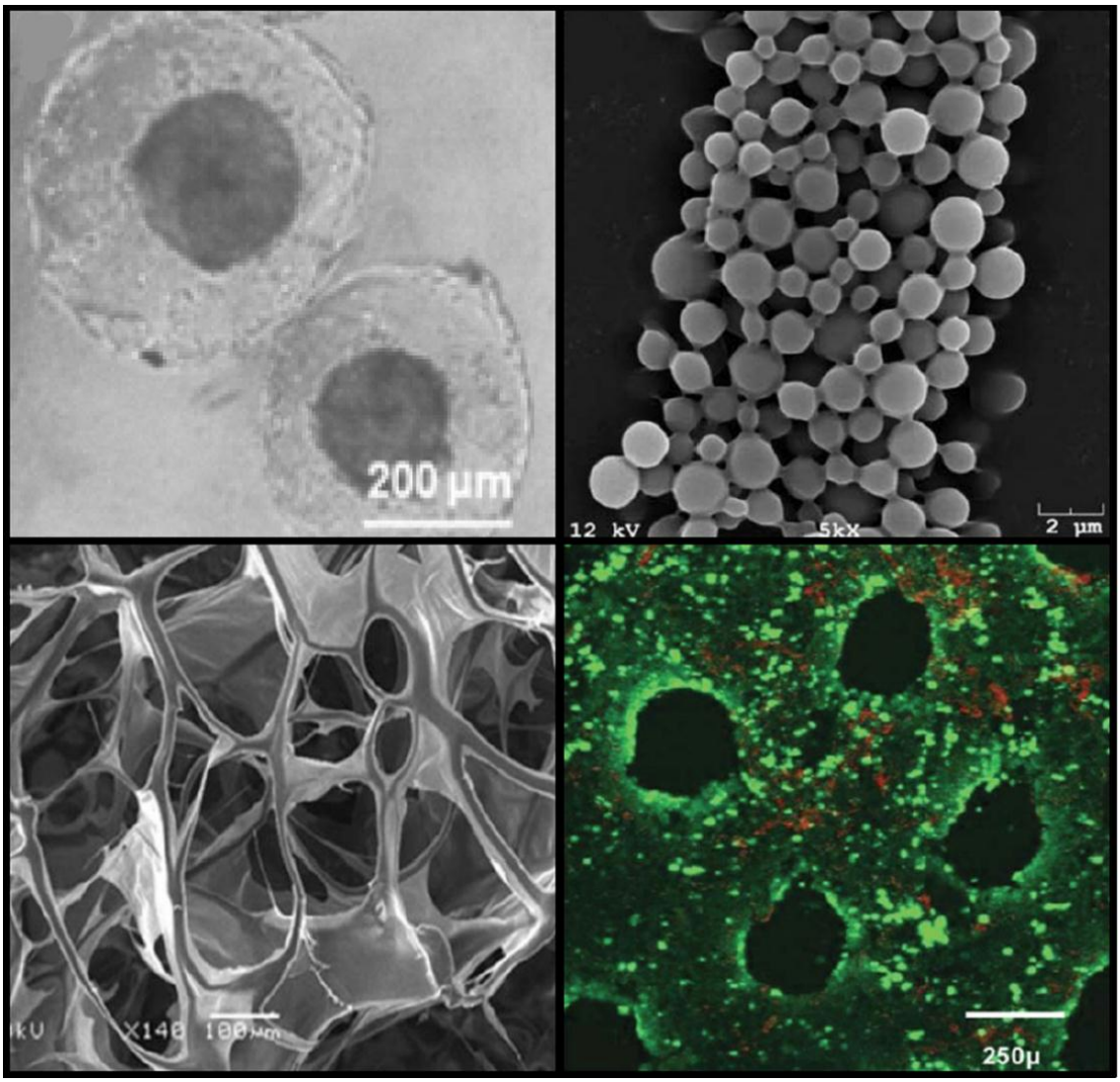

Figure 2.6. Biomimetic materials for the expansion of of stem cells.

Biomimetic materials for cardiac differentiation of stem cells

Biomaterials can also be fabricated to create engineered microenvironments designed to direct stem cell differentiation, including cardiogenesis (Dawson, Mapili et

al. 2008, Burdick and Vunjak-Novakovic 2009, Lutolf, Gilbert et al. 2009, Murtuza, Nichol et al. 2009). An important aspect in cellular differentiation, migration and homing is the ability of cells to remodel, to traverse through, and to take various cues from, engineered scaffolds. To address these issues, biomimetic materials can be designed to be enzymatically degraded (Moon, Saik et al. 2010, Patterson and Hubbell 2010), to provide specific cell-adhesion ligands (Gonzalez, Gobin et al. 2004, DeLong, Gobin et al. 2005, Sapir, Kryukov et al. 2011), and to support localized delivery of growth factors (Gobin and West 2003), therapeutics (Tulis, Bohl Masters et al. 2002), and/or signaling molecules (Lipke and West 2005). For example, the creation of a poly(ethylene glycol) (PEG)-vinylsulfone based hydrogel containing the peptide RGDSP, which emulates the integrin signaling found in early stage cardiogenesis, was shown to increase expression of cardiac markers Nkx2.5 and MHC in embryonic carcinoma cells by 1.5- and 6-fold respectively in comparison to cells cultured in suspension (Kraehenbuehl, Zammaretti et al. 2008). Regulation of spatial presentation of bioactive factors can also direct local cellular response; for example, by covalently immobilizing the growth factor bFGF in a hydrogel scaffold, cells preferentially aligned in the direction of the gradient (DeLong, Moon et al. 2005). Materials that provide localized delivery of factors for retaining stem cell pluripotency or for guiding cardiac differentiation can be used to reduce concentration gradients of these bioactive molecules, improving homogeneity (Bratt-Leal, Carpenedo et al. 2009) and potentially reducing the overall cost. Other work has examined the potential of sustainable release platforms for long-term delivery of drugs and growth factors for promoting expansion or differentiation of stem cells (Sahoo, Ang et al. 2010). Electrical activity has also been shown to play a role in directing stem cell

differentiation (Serena, Figallo et al. 2009, Limpitikul, Christoforou et al. 2010); for example, providing electrical signaling through exogenous pacing has been shown to reduce the heterogeneity of stem cell-derived cardiomyocytes (Limpitikul, Christoforou et al. 2010), which is important prior to the use of these cells for clinical applications. Acquiring the enormous cell numbers required for cardiac regenerative therapy necessitates the creation of novel cellular expansion platforms, capable of promoting proliferation while directing cardiac differentiation and maturation (Fig. 2.7). Whether the goal of the system is maintenance of pluripotency or tightly controlled differentiation into cardiac lineages, definition and fabrication of a cell niche, the microenvironment containing sources of mechanical, electrical and chemical stimuli, is necessary to promote the desired behavior for a given cell type (Bratt-Leal, Carpenedo et al. 2009).

Bioreactor culture of anchorage dependent cells, such as those for cardiac regeneration, typically relies on the cells having a carrier system to provide support and potentially to manipulate cellular microenvironment (Fig. 2.6) (Carpenedo, Bratt-Leal et al. 2010, Jing, Parikh et al. 2010). Stirred-flask bioreactors are the platform most commonly implemented for large scale-cell production. The use of bioreactor platforms for the production of both undifferentiated cells and cardiomyocytes has been well reviewed (Kehoe, Jing et al. 2010). A number of platforms have been developed to direct cardiogenesis within specialized scalable bioreactor culture systems (Kehoe, Jing et al. 2010). Success in directing cardiogenesis within a bioreactor depends greatly on the cell line utilized, the concentration of oxygen in the system, the substrate for expansion (whether or not one exists), and the concentration of nutrients, growth factors, and other

signaling molecules in the environment and timing of all these characteristics (Burridge, Thompson et al. 2011).

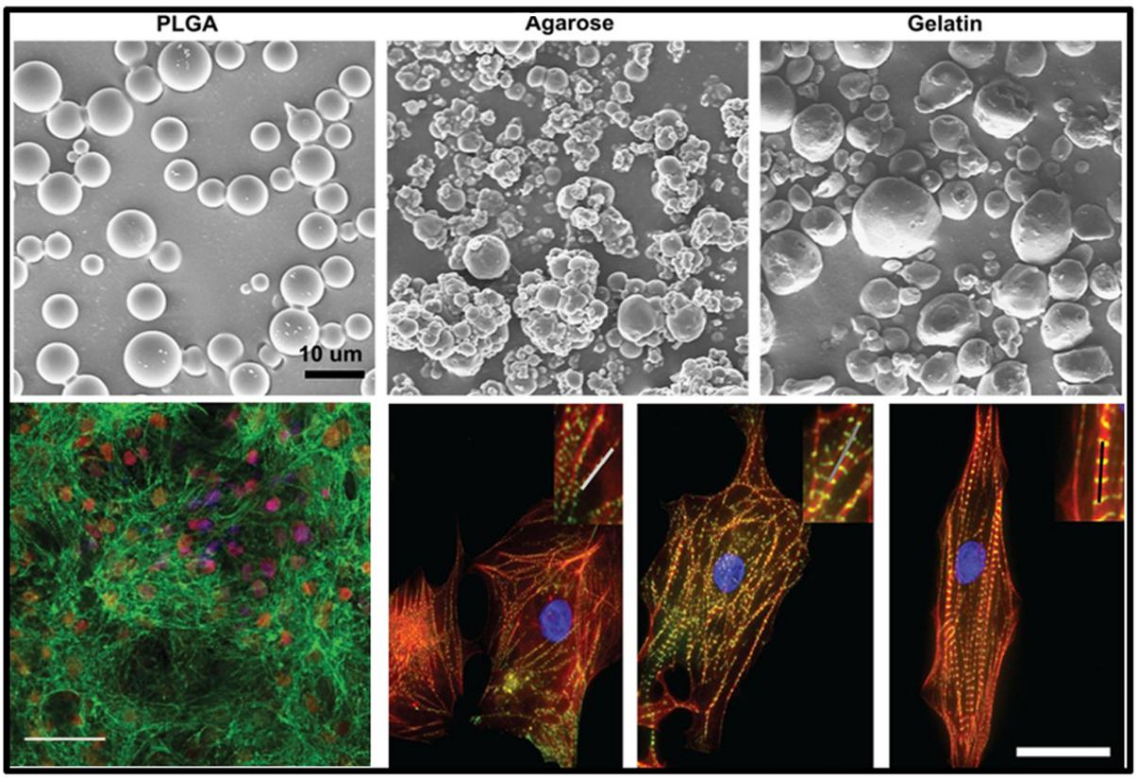

Figure 2.7. Biomimetic materials for the differentiation of cardiomyocytes.

Biomimetic materials have been used to enhance yields of cardiac cells by controlling cell microenvironment during bioreactor culture. For example, embryoid bodies (EBs) created on micropatterned Matrigel surfaces were shown to tightly regulate aggregate size prior to inoculation into bioreactor culture, allowing for up to a 6-fold increase in contraction in EBs compared to static culture (Niebruegge, Bauwens et al. 2009). ESCs aggregated with gelatin and PLGA microparticles (Fig. 2.7) in a rotary orbital culture platform were shown to exhibit greater spatial homogeneity in sarcomeric α-actinin (a marker for cardiac muscle) expression than ES cells aggregated without

incorporating the microparticles (Bratt-Leal, Carpenedo et al. 2011). Stem cell encapsulation in alginate beads has also been used to direct cardiac differentiation in bioreactor cultures, with higher percentages of cells encapsulated in liquid core alginate beads expressing cardiac markers than those encapsulated in solid beads (Lock and Tzanakakis 2009, Kehoe, Jing et al. 2010). A micro-scale bioreactor system containing electrodes on a patterned substrate was shown to increase beating focal areas in EBs by 10% with a two-fold increase the presence of connexin-43 in adipose-derived stem cells (Tandon, Marsano et al. 2010). Development of carrier systems capable of producing the cells needed for cardiac regeneration will be substantially advanced by using the toolbox of approaches available for biomimetic material design.

2.6. *Biomimetic materials for cardiac tissue patches*

Material requirements for cardiac tissue patches

The use of engineered patches for cardiac regeneration requires incorporation of biomimetic facets to direct the creation of physiologically-accurate tissues. A number of considerations must be addressed in the creation of cardiac patches for organ regeneration, including structural integrity, electrical propagation, and flexible integration in native myocardium. Engineered patches should facilitate development of new cardiac tissue which integrates appropriately with native myocardium. In the context of the growing heart, patches used for correcting congenital heart defects must conform to the needs and changes associated with developing cardiac tissue (Mirensky and Breuer 2008, Pok and Jacot 2011). Cardiac patches should include cues for controlling cellular maturation and structural organization, while also supporting vascularization to support

the significant nutrient requirements of cardiac tissue. Nutrient transport can be facilitated by the incorporation of angiogenesis factors (Miyagi, Chiu et al. 2011) and through the development of high-perfusion bioreactors (Koch, Vrij et al. 2010). For long term implants, patch materials should be degradable, producing non-toxic byproducts which do not generate an immune response (Lutolf, Lauer-Fields et al. 2003). Several materials have been identified for use in cardiac patches, including naturally occurring polymers, synthetic polymers, and natural-synthetic hybrid materials (Wang and Guan 2010, Pok and Jacot 2011). One alternative to traditional materials is the use of decellularized heart tissue, which has demonstrated the capacity to transform stem cells into cardiomyocytes (Duan, Liu et al. 2011). A different approach involves layering functional cardiac cell layers, which can be coupled directly to native cell types (Stevens, Kreutziger et al. 2009, Haraguchi, Shimizu et al. 2011).

Biomimetic materials for cardiac tissue patches

Tissue engineered patches for cardiac regeneration employ biomimetic principles in their design to direct the formation of mechanically and electrically functional tissues (Fig. 2.8). Cardiac patches are necessary to address some causes of cardiac dysfunction, including repair of congenital heart defects (Pok and Jacot 2011). However, even the decellularized biological patches currently used as surgical interventions for pediatric congenital heart defects suffer from insufficient capacity to grow with the patient and suboptimal durability (Mirensky and Breuer 2008). Numerous materials have been tested for use in cardiac patches, including naturally occurring polymers such as collagen, collagen-glycosaminoglycan chitosan, fibrin, alginate and gelatin; synthetic polymers such as polycaprolactone (PCL), poly(glycolic acid) (PGA), poly-4-hydroxybutyrate

(P4HB), poly(lactic acid) (PLA) and poly(lactic-co-glycolic acid) (PLGA), poly(glycerol–sebacate) (PGS) (Fig. 2.8), poly(trimethylene carbonate–co-lactide), polyester urethane urea (PEUU) (Fujimoto, Tobita et al. 2012) and polyurethane; and co-polymers of natural and synthetic materials (Martin and Williams 2003, Maidhof, Marsano et al. 2010, Wang and Guan 2010, Pok and Jacot 2011). Recently, tissue-engineered patches have also been employed for cell therapy to overcome limitations of poor cell engraftment and survival using cell injection strategies. In one study, patch material made from PEGylated fibrin gel was used as a delivery vehicle for improving viability of mesenchymal stem cells after delivery to infarcted myocardium (Zhang, Wang et al. 2006). Mechanical support provided by cardiac patches to the heart wall at the site of infarct may also improve cardiac function (Fig. 2.8) (Fujimoto, Tobita et al. 2007).

Biomimetic strategies for improving on the current surgical patches utilize scaffold materials onto which cells are seeded or matrices within which cells can be incorporated. These cardiac patches typically include cues for cellular maturation and structural organization, while also supporting vascularization for ample nutrient transport. Biomimetic cardiac patches, whether natural or synthetic, should be degradable, generating byproducts which do not damage surrounding tissue or elicit a systemic immune response or inflammation (Lutolf, Lauer-Fields et al. 2003). Degradation needs to take place on the same time scale as cells replace the patch material with ECM; biomimetic synthetic materials can achieve this through the incorporation of enzymatically degradable segments in the patch material (Lutolf, Lauer-Fields et al. 2003, Patterson and Hubbell 2010). Nutrient transport in cardiac tissue patches has been

enhanced by culture in perfusion bioreactor systems (Koch, Vrij et al. 2010) or by incorporation of angiogenesis factors to elicit vascularization (Miyagi, Chiu et al. 2011). Mechanical stretch or electrical pacing has been used to guide tissue formation and alignment (Eschenhagen, Didie et al. 2002, Zimmermann, Schneiderbanger et al. 2002) and electrical conduction (Limpitikul, Christoforou et al. 2010). Incorporation of gold nanoparticles (You, Rafat et al. 2011) or gold nanowires (Dvir, Timko et al. 2011) into cell-seeded scaffolds for patch fabrication led to enhanced electrical/conductive properties. Materials with micro- and nanotopography and structure have also been used to direct the alignment of cardiomyocytes within the engineered tissue, such that the organization of these tissues resembles that of native cardiac tissue and that they exhibit similar anisotropic electrical conduction (Bursac, Loo et al. 2007, Kim, Lipke et al. 2010, Liau, Christoforou et al. 2011, Parrag, Zandstra et al. 2012). The use of decellularized cardiac tissue has been examined as an alternative to synthetic polymer scaffolds (Ott, Matthiesen et al. 2008) and has been shown to facilitate differentiation of stem cells into cardiac cell types (Duan, Liu et al. 2011). Cell sheet engineering (Haraguchi, Shimizu et al. 2011), which utilizes electrically and mechanically coupled layers of cells without exogenous scaffold materials, has also been examined as an alternative to scaffold-based tissues (Fig. 2.8) (Stevens, Kreutziger et al. 2009), allowing for engraftment of functional cells without sutures or vascularization (Sekine, Shimizu et al. 2006). A large number of studies have been published investigating discrete aspects of cardiac tissue patch design and function. As future research provides combinatorial blends of these approaches, barriers to the clinical use of cardiac tissue patches will be overcome.

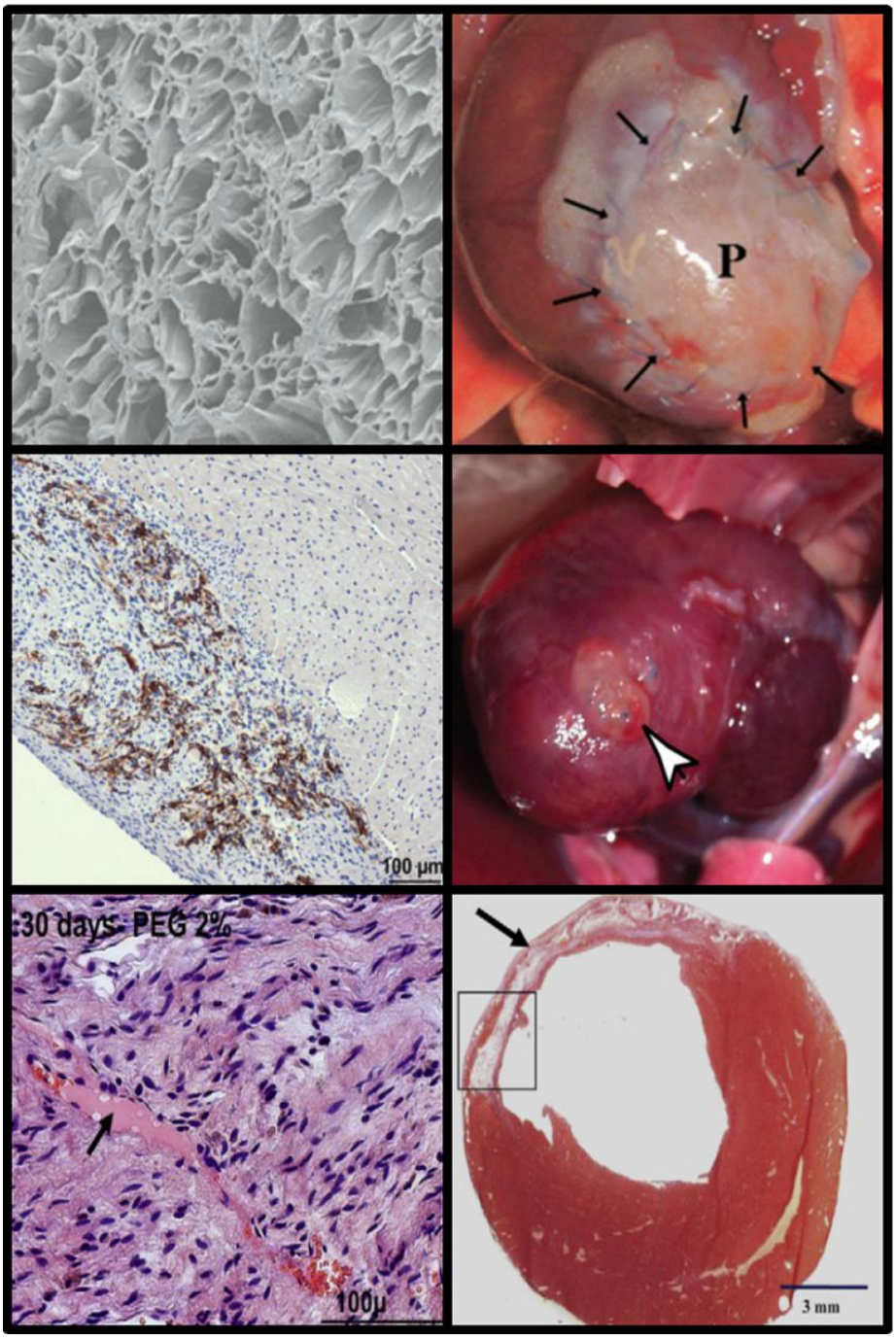

Figure 2.8. Examples of cardiac patches for the restoration of the myocardium.

2.7. Biomimetic materials for injectable cardiac therapies

Material requirements for injectable cardiac therapies

Biomimetic materials are also needed to support cells during and following cell injection procedures. Direct injection of cells into diseased myocardium as a medium for cardiac regeneration is crippled by high incidence of cell mortality (Aguado, Mulyasasmita et al. 2012) coupled with consistently low cell retention (Terrovitis, Lautamäki et al. 2009). Cell injection technology is benefitting from advances in biomimetic materials which are able to provide a carrier system to aid in the delivery of cells and then form a scaffold architecture *in situ*. In the context of injectable cardiac patches, biomimetic materials may be incorporated to improve cellular viability (Zhang, Wang et al. 2006), increase cell retention within native myocardium, and provide a suitable environment for cardiomyocyte integration and development (Singelyn, DeQuach et al. 2009). Materials that have been used to support cells during injection include: fibrin, collagen, alginate and chitosan (Gupta, Walthall et al. 2011).

Biomimetic materials for injectable cardiac therapies

Biomimetic materials have the potential to support cells during injection for cardiac regeneration, aid in the retention of the injected cells at the desired location, and facilitate incorporation of the cells by providing a supportive microenvironment following injection. Materials that have been used to support cells during injection include fibrin, collagen, self-assembling peptides, Matrigel, alginate and chitosan (Gupta, Walthall et al.). Although application of these materials may improve cellular survivability and promote angiogenesis, multiple factors must be addressed in order to

facilitate regeneration of damaged cardiac tissue. In particular, materials used in cell injection must approximate the native physical and chemical environment and be able to deliver or propagate physiological stimuli in order to better direct cell differentiation and engraftment; furthermore, the materials must have slow degradation rates to allow the delivered cells to electrically couple with existing tissue (Wang and Guan 2010).

In order to address problems with *in vivo* cellular injection, a number of techniques have been developed to facilitate cellular viability, differentiation and engraftment by use of biomimetic materials (Bursac 2009, Balasubramanian, Prabhakaran et al. 2011, Prabhakaran, Venugopal et al. 2011). One common method for improving viability involves mixing cells directly with a soluble gel prior to injection. In one study, cardiomyocytes derived from human ESCs were delivered using Matrigel mixed with immunosuppressant drugs and pro-survival growth factors (Laflamme, Chen et al. 2007). Injection of the resulting product was shown to reduce the incidence of apoptosis in injected cells while producing grafts four times larger in infarcted rat hearts than injections of cells with Matrigel alone. Additionally, alginates, which degrade readily in sodium-rich solutions, have been utilized for a number of encapsulation techniques. In one recent report, human umbilical vein endothelial cells that were encapsulated using an alginate solution demonstrated a 20% increase in cell viability after ejection through a syringe needle (Aguado, Mulyasasmita et al. 2012). Likewise, injection of MSCs encapsulated in peptide-modified alginate resulted in 15% smaller infarct sizes compared to PBS injected controls (Yu, Du et al. 2010). Other novel encapsulation materials, including a chitosan-collagen hydrogels containing a conjugated angiopoietin-1 peptide (Reis, Chiu et al. 2012) and degradable PEG-based hydrogels

(Franco, Price et al. 2011, Habib, Shapira-Schweitzer et al. 2011), have been developed and tested as platforms for cellular injection. Cell encapsulation using degradable materials, both natural and synthetic, is a promising technique for providing protection to a number of different cell types during injection.

2.8. Use of Nanotechnology for Cardiac Regeneration

The potential of engineered scaffolds for tissue regeneration has been significantly advanced by nano- and micro-fabrication techniques (Dvir, Timko et al. 2011). Creation of biomimetic materials for use in cardiac tissue engineering has benefitted from advancements in nanotechnology, allowing for manipulation of surfaces to influence behavior of individual cells. Nanoscale cues regulate the structure and function of macroscopic cardiac tissue constructs (Kim, Kim et al. 2006) and the application of micro-patterned surfaces containing functional moieties (Badie, Scull et al. 2012). A recent review on micro- and nano-fabrication approaches in cardiac tissue engineering has identified goals for nanotechnology-mediated functionality, including surface-mediated cell assembly, scaffold engineering, and functional vascularization (Zhang, Xiao et al. 2011).

Advancements in the field of nanotechnology have permitted researchers to manipulate cell behavior and differentiation, for example, by triggering cardiogenic signaling pathways, and also to track the differentiation of non-committed cells into the cardiomyocyte lineage. Superparamagnetic iron oxide nanoparticles have been investigated for tracking cell development (Au, Liao et al. 2009) and migration (Hoshino, Ly et al. 2007) in vivo through magnetic resonance imaging (Cromer Berman, Walczak et al. 2011). Differences in gold nanoparticle uptake within embryoid bodies have been

used to identify individual stages of cardiac differentiation by characterizing unique response signatures through surface-enhanced Raman scattering (Sathuluri, Yoshikawa et al. 2011). Additionally, the use of specialized binding moieties has allowed for detection of stem cells expressing specific cardiac markers; for example, NaYF4 nanocrystals with near-infrared emission spectra were conjugated to primary antibodies, detecting cellular gap junction proteins in vitro (Nagarajan and Zhang 2011).

Knowledge of nanoscale cell-substrate interactions has furthered the development of biomimetic materials capable of manipulating complex signaling pathways necessary for control of cellular behavior. Nanoscale topographical features have been used to direct the structure and function of engineered cardiac tissues on the cellular and tissue levels (Fig. 2.9) (Elloumi-Hannachi, Yamato et al. 2010, Hosseinkhani, Hosseinkhani et al. 2010, Luna, Ciriza et al. 2011). The native ECM matrix is a nanostructured substrate, which is responsible for the direction of cellular function and tissue organization (Kelleher and Vacanti 2010). Mimicking the nanostructure of native cardiac tissue ECM can therefore play an important role in guiding the formation of engineered cardiac tissue. Nanotopography has the ability to direct not only the alignment of cardiomyocytes, but also cytoskeletal organization and the expression of gap junctions (Fig. 2.9) (Kim, Lipke et al. 2010).

Photolithography, electrospinning, and peptide self-assembly are commonly used techniques for generating substrate materials with features on the nano-scale. Polymer supports created from photolithographic molds have been used to enhance alignment of cardiac cell types through the formation of nanotopography (Kim, Lipke et al. 2010). Non-photolithographic approaches have also been utilized for creating molds with nano-

scale features. A soft lithography mold was created by sputter-coating gold-palladium particles on a polystyrene sheet (Luna, Ciriza et al. 2011). PDMS substrates created from the molds were shown to directly influence the orientation of junction proteins connexin-43 and N-cadherin in stem cell-derived cardiomyocytes.

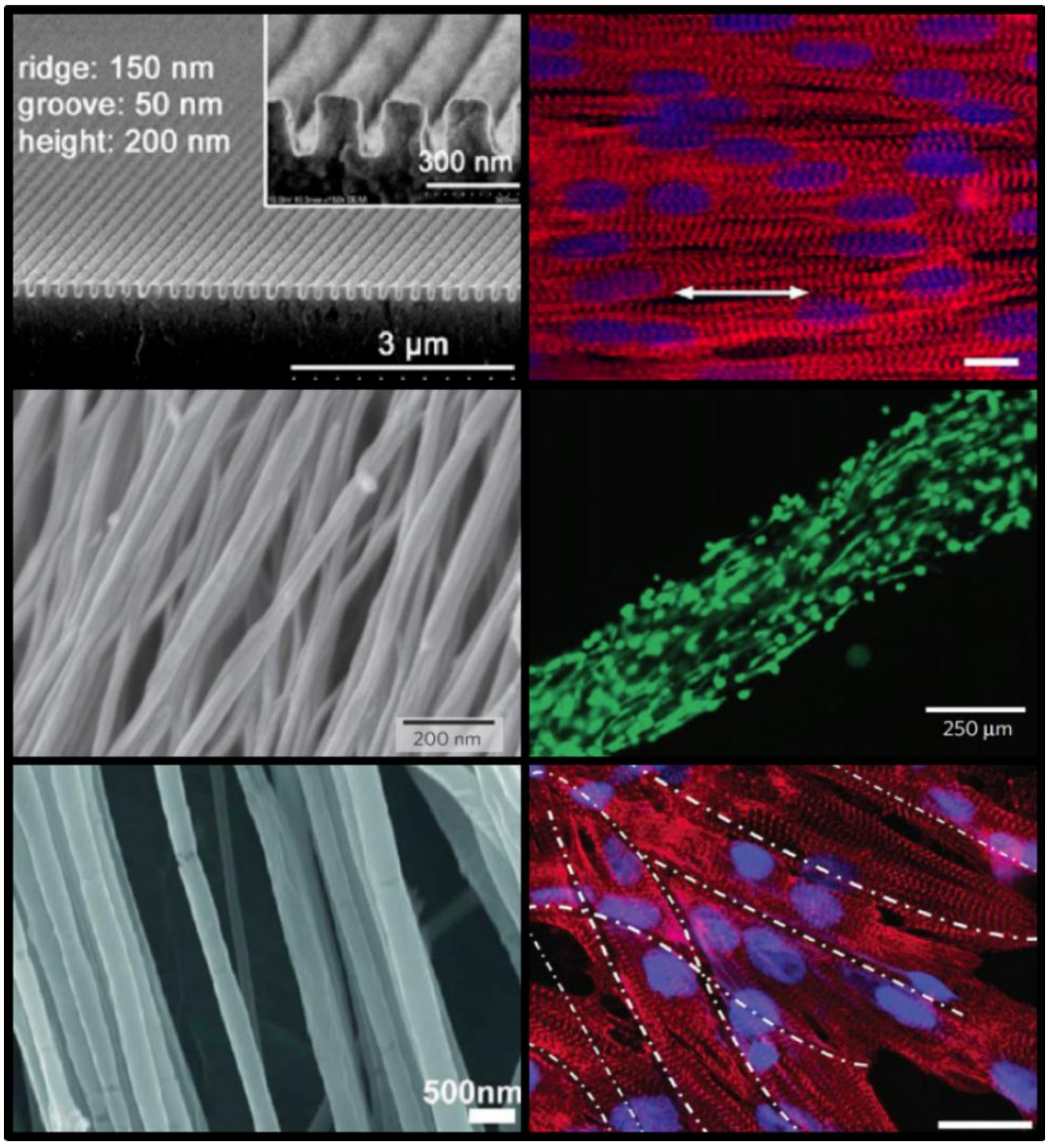

Figure 2.9. Biomimetic materials with features on the nano-scale are capable of directing alignment of cardiomyocytes.

The use of electrospun fibers in the production of bioactive scaffold systems is a topic of active research and has been reviewed extensively (Szentivanyi, Chakradeo et al. 2011). Methods have been developed to augment electrospun nano-structures with drug-eluting materials, functionalized surfaces, and polymer blends with specified mechanical and chemical properties to influence cellular behavior. A specialized scaffold system containing PEG-PLA-CPLA nanofibers demonstrated a two-fold increase in the expression level of the cardiac structural marker α-myosin heavy chain by mouse ES cell-derived cardiomyocytes compared to cells grown without a scaffold (Gupta, Walthall et al. 2011). Nanofibers have also been produced using rotary extrusion, a similar approach to electrospinning. Neonatal rat ventricular myocytes cultured on PLA fibers generated from this system demonstrated strong sarcomeric alignment in the direction of the material nanofibers (Fig. 2.9) (Badrossamay, McIlwee et al. 2010).

Incorporation of bioactive molecules into nanostructured materials can have a marked phenotypic effect. Self-assembling peptides are amphiphilic materials which spontaneously develop into nanofiber niches; these peptides may be modified to elicit bioactive signals capable of directing cellular differentiation and other events. A biotin-streptavidin system was developed which created in vivo nanostructures capable of delivering insulin growth factor-1, a protein shown to promote cardiomyocyte growth and survival (Davis, Hsieh et al. 2006). As a method for promoting angiogenesis in damaged myocardium, materials containing nanoscale filaments of vascular endothelial growth factor (VEGF)-mimicking peptide were injected into mouse models and shown to significantly increase circulation in damaged tissue (Webber, Tongers et al. 2011). Aligned peptide amphiphile nanofibers have been shown to direct cell alignment,

including cardiac cells (Fig. 2.9) (Zhang, Greenfield et al. 2010). Biomimetic material design will continue to exploit advances in nanotechnology to better recreate the cellular microenvironment and advance cardiac regeneration.

While the development of techniques for incorporating nanotopography or influencing molecular arrangement of materials has provided new platforms in the context of cardiac regeneration, the field as a whole remains in its infancy. Common protocols for influencing nanoscale cellular behavior are often limited by the creation of materials with few cell-signaling moieties or structural components, which do not fully replicate the complex environment of the cell niche on the micro- and nano-scale. Furthermore, imaging technologies incorporating nanoscale features may be limited by issues associated with lack of specificity to cardiac tissue types or retention of these components when used *in vivo*. Future progress in this area will require the development of biomimetic materials which can accurately replicate cellular microenvironments to enhance engraftment and accuracy of imaging elements or, in the context of cardiac regeneration, enhance the development of physiologically suitable tissue.

2.9. Ongoing Challenges for Cardiac Tissue Regeneration

Given the degree of complexity associated with heart physiology and heart disease pathology, successful cardiac regeneration strategies require innovation in overcoming challenges associated with the incorporation of new, functioning tissue. Fibrotic scar tissue, which develops post-infarction, may need to be denuded prior to transplantation to allow for efficient engraftment of donor cells. As seen with the various cell delivery platforms, successful delivery and engraftment of cells is often compromised by low cellular viability. Because diseased hearts lose the function of

potentially billions of cardiomyocytes, creating the numbers of cells necessary for therapy through in vitro sources is difficult (Yoshida and Yamanaka 2011). Generating a tissue patch containing multiple cell types that will couple with the electrical, mechanical and vascular networks of the surrounding tissue requires a novel engineering platform. Whereas using cells and materials to improve heart function through changes in heart wall stiffness or formation of new blood vessels has been well-established, it is much more difficult to achieve functional coupling of cells or grafts with the native myocardium such that they actively contribute to mechanical force generation and increasing cardiac output. In the post-myocardial infarction heart, success of implanted materials is dependent on the ability of a these materials to promote cardiomyocyte differentiation, survival and/or functional coupling with surrounding tissue while maintaining structural integrity of the heart. While multiple material properties are important in influencing cardiac function, their comparative value, as well as the importance of interactions between these material properties remain to be fully characterized. In addition, successful incorporation of donor cells often requires an immunosuppressant to prevent rejection. Similarly, tissue prepared using animal-derived products, such as Matrigel, may also elicit a pyrogenic response. Furthermore, depending on the progression of the disease, certain treatments may prove to be insufficient for reversing tissue damage.

2.10. The Need for Electrophysiological Characterization of Cardiac Tissue

The analysis of cardiomyocytes, either derived from pluripotent cell types or isolated from primary tissue sources, in an in vitro culture environment is a complex process which requires expertise in many academic areas and techniques. In the past,

characterization of cardiac differentiation has relied extensively on the use of microscopy techniques; phase contrast, brightfield, fluorescence, confocal, SEM and TEM microscopy have all been utilized in the identification of cardiomyocyte structure. Quantification of cardiomyocyte gene and protein expression has relied heavily on: PCR, Western blot, flow cytometry, and similar techniques. Quantification of cellular metabolism, either through direct mitochondrial analysis or through measurements of oxygen consumption and lactate production, has also been investigated to provide information about extent of cardiomyocyte development and cellular activity (Dedkova and Blatter 2012, Robertson, Tran et al. 2013). While these techniques (and others) provide insight into the composition and organization of cultured cells, knowledge about these properties reveals little about the functionality of cardiomyocytes and cardiac tissue. Techniques that evaluate contractile strength and cardiac electrophysiology offer valuable insight into the potential performance of in vitro cultured cardiomyocytes in clinical or diagnostic applications.

As a biological pump, the main function of the heart is to supply oxygenated blood and nutrients to the body's tissues while returning deoxygenated blood to the lungs. To this end, the heart relies on the myocardium, with cardiomyocytes acting as individual functional units, to engage in precise excitation-contraction coupling in response to external electrical stimulation, a process which requires cardiomyocytes with well-defined mechanical properties. A number of techniques have been developed in order to assess the mechanical strength of cardiomyocytes grown in vitro. One popular method for stress-strain determination involves the implementation of glass pipet or a stainless steel needle attached directly to the cardiomyocyte using vacuum or silicone adhesive (van der

Velden, Klein et al. 1998). This probe acts as a cantilever, relaying the signal to a mechanical transducer, such as a semiconductor strain gauge, as well as a piezoelectric translator, such as a motor (Sugiura, Yasuda et al. 2003, Malkin, Kramer et al. 2005). This technique, often utilized as an endpoint determination of cardiomyocyte strength, has been incorporated into a bioreactor platform to record stress and strain of cultured cardiomyocytes over a period of multiple weeks (Kensah, Gruh et al. 2011). While measurement of contraction strength of individual cardiomyocytes provides unique information into the functionality of these cell types, this analysis fails to capture function of the myocardium as a whole. In the context of cardiac tissue mechanical analysis, incorporation of cantilevers can lead to inaccuracies in force measurement due to pre-loading forces and incomplete fixation within the myocardium (Malkin, Kramer et al. 2005). Furthermore, this form of data collection provides no information on the electrical activity of the underlying cardiomyocyte or myocardial tissue. Improvements on this design have consisted of electromechanical sensors which detect both electrical activity and force generation. Another unique approach for mechanical assessment consists of seeding cardiomyocytes directly onto polymer micro-cantilevers which can be translated and quantified using imaging techniques (Park, Ryu et al. 2005). Similarly, atomic force microscopy has been utilized to directly evaluate elasticity of myocardial tissue (Hiesinger, Brukman et al. 2012). Despite these advancements in monitoring technology, direct acquisition of mechanical force data from cardiomyocytes or cardiac tissue remains an ongoing challenge.

The electrophysiology of the heart, which is correlated with the excitation-contraction coupling process, is perhaps the most important functional property of

cardiomyocytes considered for tissue engineering. In addition to identifying physiologically-healthy cells, electrophysiological analysis can be used to identify certain pathologies, including the formation of deadly arrhythmias. In practice, the electrophysiology of cardiomyocytes can be evaluated using several different techniques, each containing their own benefits and drawbacks; these will be examined in greater detail.

2.11. Techniques for measuring electrophysiology in cardiomyocytes

While many techniques exist for monitoring the electrical activity of cardiomyocytes and cardiac tissue (either in vitro or in vivo), a small number of approaches have emerged as popular methods for evaluating electrophysiology. Herein, a brief overview of some of these techniques will be presented and discussed.

Calcium transient analysis

While not directly measuring electrophysiology in its own right, the evaluation of calcium transients has been utilized by researchers to assess functionality of cardiomyocytes. In healthy myocardium, initiation of muscle contraction begins with a sudden, rapid increase in cytosolic calcium ion concentration. This begins when electrical signaling triggers opening of L-type calcium channel proteins, forming a local elevated concentration of cytosolic calcium (Shacklock, Wier et al. 1995). In turn, this local increase in calcium triggers the opening of ryanodine receptor, releasing large stores of calcium from the sarcoplasmic reticulum (SR). As the cardiomyocyte relaxes, calcium is pumped back into the SR using the SERCA protein complex or outside of the cell using the sarcolemma sodium-calcium exchange (Bers 2000). The magnitude and duration of

this calcium transient must be tightly controlled in order to maintain cardiac output and increase force of contraction when necessary (Eisner, Choi et al. 2000). Issues in this signaling pathway have been implemented in a number of cardiac pathologies.

Because the duration of these calcium transients lasts on the order of tens of milliseconds, a number of unique approaches have been devised in order to detect the rapid changes in intracellular calcium. A number of fluorescent calcium-indicating dyes, such as fura-2, indo-1, and rhod-2, have been proven effective in detecting intracellular calcium within myocytes. The combination of fluorescent indicator with an exogenous electrical signal and a photometric detector, such as a photodiode, photomultiplier, or CCD camera, has been used to acquire data on intracellular calcium concentrations (Vergara, DiFranco et al. 1991). Together, this approach represents a simple, minimally-invasive technique for evaluating the calcium-handling capabilities of cardiomyocytes.

Patch clamping

While calcium transient analysis provides insight into the calcium handling of cardiomyocytes or cardiac tissue, it does not directly provide information about the electrophysiology of the cell. In order to quantify the currents generated from single or multiple ion channels, a technique called patch clamping has been developed and applied to cardiomyocytes (Cerbai, Sartiani et al. 2000). In principle, this technique utilizes a glass microelectrode filled with an electrolyte solution which is connected to a recording device, such as an oscilloscope. A small "patch" of cell membrane is electrically isolated by using suction to attach the microelectrode flush against the membrane surface (Bebarova 2012). Using different combinations of microelectrode positioning and

electrolyte solution presentation, measurements may be recorded on individual ion channels or on net current generation from the entire cell (whole cell patch clamp).

Patch clamp is useful for its specificity in measuring the currents from multiple independent ion channels as well as currents from specific types of ion channels. This technique, however, is limited by its ability to measure currents only from individual cardiomyocytes. Patch clamping is a time-consuming, labor-intensive technique with large technician variability. Furthermore, progressive dialyzation of the cellular cytosol with the electrolyte solution limits the time in which data can be acquired from samples; this can also limit the use of patched samples for other analytical purposes.

Microelectrode Array

Given the invasiveness of patch clamp technique in recording electrophysiological data from cardiomyocytes, additional techniques have been developed to allow for extracellular acquisition of electrical activity. The microelectrode array (MEA) is a variant on the patch design which allows for extracellular acquisition of changes in membrane potential. Electrically-active cells or tissue is placed on top of an MEA containing hundreds of individual electrodes spaced within tens of microns apart. These specially-designed chips can be mounted on microscope stages to visualize cardiomyocytes or neurons during the course of acquisition (Spira and Hai 2013). Additionally, efforts have been made to implement electrodes on MEAs that protrude the cell membranes, allowing for intracellular recordings. MEAs have many inherent advantages compared to patch clamping apparatuses, including the ability to: select and record data from multiple locations simultaneously within a sample, establish a control

electrode in stimulation experiments, and record voltage data over an extended period of time.

MEAs, while providing a unique platform for detecting cardiomyocyte electrophysiology, require careful consideration before implementation. MEAs are often limited by low spatial resolution compared to other techniques. Electrical interference, particularly in cases of exogenous electrical stimulation, can exacerbate the signal-to-noise ratio, increasing the complexity of data analysis (Spira and Hai 2013). Depending on the cell type, maintaining close contact between the cell membrane and the electrodes is potentially problematic. Because the cardiomyocytes must be plated onto the MEA prior to recording, this technique is not suitable for measuring electrical activity of cardiomyocytes in or on novel materials. Additionally, the high cost of implementing MEAs can also be a limiting factor in their use.

Optical mapping

Given the problems associated with electrical artifacts and invasive equipment when implementing microelectrode-based techniques, optical mapping has emerged as a popular technique for characterizing electrophysiology of cardiomyocytes. Unlike other techniques which rely on electrodes to directly record current or voltage, optical mapping utilizes calcium or voltage-sensitive fluorescent dyes which bind to intracellular calcium or membrane-bound proteins. Voltage-sensitive dyes record transmembrane potential; this data can be used to evaluate cellular depolarization, spatial distribution of action potential duration, or repolarization events (Malkin, Kramer et al. 2005). In addition to these analyses, calcium wave propagation can be visualized using photodiodes, photomultiplier tubes, laser scanning systems, and CCD cameras at high spatial temporal

resolution (Herron, Lee et al. 2012). Taken together, optical mapping systems represent a valuable approach for visualizing both conduction velocities and action potential durations of cardiomyocytes.

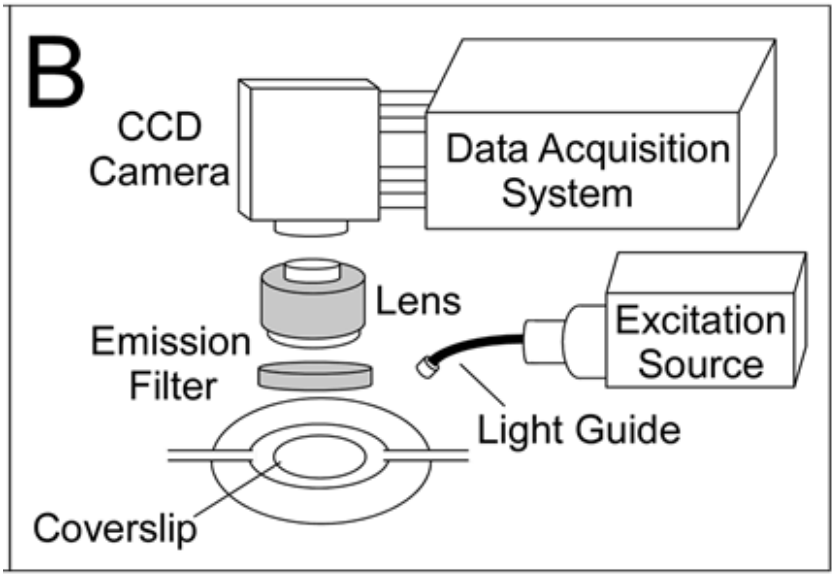

Figure 2.10. An example schematic of an optical mapping setup with all associated equipment (Image from Weinberg, 2010).

One major limitation of the optical mapping approach for electrophysiological characterization is the incompatibility of simultaneous electrical and mechanical mapping. Motion artifacts can arise from the movement of contractile cell types; changes in fluorescence intensity due to re-positioning of tissue can lead to challenges in the analysis of acquired signal (Brandes, Figueredo et al. 1992). Motion artifacts due to contraction can be mitigated in part through the use of pharmaceutical agents (Pertsov, Davidenko et al. 1993); however, ratiometric analysis has also been considered for optical mapping of moving tissues (Grynkiewicz, Poenie et al. 1985). Additionally, imaging of multilayered tissues can lead to photon scattering effects by which multiple

interfering signals are acquired over the thickness of the sample (Baxter, Mironov et al. 2001). Given the potential for issues to arise during the mapping process, many considerations must be addressed in the fabrication of an optical mapping platform; these concepts will be explored in greater detail.

2.12. Considerations for the design of an optical mapping platform

Optical mapping requires a complex set of equipment to support the viability of the cardiac sample while correctly filtering and acquiring the signal from the fluorescent dye. Perhaps the most important pieces of equipment in an optical mapping setup are the photodetector and light source. Because the propagating electrical impulse from cardiac tissue produces a short-lived weak signal via a fluorescent reporter dye, a detector-illuminator combination that can successfully capture transient, low light is required for mapping applications. Selecting a correct filter which can block out background light from the illuminator is important in reducing the signal-to-noise ratio of the acquired data. Selecting a stimulator that can maintain exogenous electrical pacing of the cardiac sample is critical for reducing noise from spontaneous depolarizations. Cost considerations in the acquisition of these components must also be addressed. In successfully maintaining the cardiac sample as to maximize signal acquisition and minimize cell death, many considerations must be made in the design of the pacing chamber and apparatus. These design parameters include maximizing perfusion of Tyrode's solution (without causing motion artifacts from turbulence), maintaining physiological temperature of Tyrode's solution, and minimizing motion artifacts from the surrounding environment. Together, these challenges require thoughtful design and consideration to successfully acquire mapping data.

2.13. Conclusions

Heart disease continues to be the leading cause of death worldwide. This fact underscores the need for new clinical developments to treat a wide range of cardiovascular conditions. Since the majority of current therapies treat the symptoms of heart disease rather than repairing the damaged tissue, the long-term goal of cardiovascular clinicians and researchers is development of novel therapeutic modalities with cardiac regeneration as their hallmark. Thus, there is a great need for future regenerative therapies involving biomimetic materials. In order to reverse the pathologic changes that occur in heart disease, conditions which mimic native healthy tissue must be present, allowing endogenous or exogenous cells to populate the diseased area and form functional tissue. The past decade has led to intense investigation into methods for cardiac regeneration, addressing challenges in replacement cell source and expansion, material design of scaffolds on which to grow these cells, and construct delivery. The selection of cell types for a given therapy, as well as the technique(s) for their expansion, requires the development of platforms capable of producing the billions of cardiomyocytes and other cell types required for myocardial and valvular repair. The choice of materials for scaffold design must provide the mechanical and electrical environment necessary for cardiac function. The method of construct delivery to a diseased tissue site requires a vehicle which aids in maintaining cellular viability and functional engraftment. Additionally, the electrophysiological of the resulting cardiomyocytes or cardiac tissue must be determined before the samples can be employed in clinical or diagnostic research applications.

Various biomimetic materials have demonstrated potential for achieving cardiac regeneration. Biomimetic materials have been designed to direct differentiation and maturation of cardiomyocytes in vitro, providing a basis for large-scale production of clinical-grade cells. Scaffolds have been created imparting functional features incorporating biological (stretch, bioactive peptides, signaling molecules and cell adhesion sites) and physical (surface topography, shape, electrical conductivity, three-dimensional structure and stiffness) properties that are important in directing the formation and alignment of functionalized tissue. Injectable scaffold systems designed for in situ tissue formation have been tailored to enhance cell targeting and viability. Also, design of enzymatically degradable materials has opened the door for scaffolds capable of being completely replaced by the regenerating functional tissue. While these accomplishments have laid the groundwork for many exciting future developments, the field of cardiac tissue engineering remains in its infancy. Although many of the existing materials for cardiac tissue regeneration show promise, they are currently still limited in scope, incorporating few cardiogenic factors and producing tissue with immature properties. Future advancement in this area will require incorporation of multiple stimuli (mechanical, electrical, and biological) into novel substrates to further control the fate of differentiating cells and promote material integration into native tissue. Continuing investigation into the design and implementation of biomimetic materials promise to move us ever closer to the reality of making regenerative medicine therapies available to the multitudes of people suffering from heart disease.

In the following chapters, a novel study will be described which investigates the connection between biomaterials and maturation of cardiomyocytes for use in different

applications. First, the method for constructing and optimizing an optical mapping platform for quantifying the electrophysiological properties of cardiomyocytes will be described. Next, a series of experiments will be described which show how different biomimetic materials can be employed to promote maturation of cardiomyocytes.

References

Aguado, B. A., W. Mulyasasmita, J. Su, K. J. Lampe and S. C. Heilshorn (2012). "Improving viability of stem cells during syringe needle flow through the design of hydrogel cell carriers." Tissue Eng Part A 18(7-8): 806-815.

Andukuri, A., M. Kushwaha, A. Tambralli, J. M. Anderson, D. R. Dean, J. L. Berry, Y. D. Sohn, Y. S. Yoon, B. C. Brott and H. W. Jun (2011). "A hybrid biomimetic nanomatrix composed of electrospun polycaprolactone and bioactive peptide amphiphiles for cardiovascular implants." Acta Biomater 7(1): 225-233.

Au, K. W., S. Y. Liao, Y. K. Lee, W. H. Lai, K. M. Ng, Y. C. Chan, M. C. Yip, C. Y. Ho, E. X. Wu, R. A. Li, C. W. Siu and H. F. Tse (2009). "Effects of iron oxide nanoparticles on cardiac differentiation of embryonic stem cells." Biochem Biophys Res Commun 379(4): 898-903.

Badie, N., J. A. Scull, R. Y. Klinger, A. Krol and N. Bursac (2012). "Conduction block in micropatterned cardiomyocyte cultures replicating the structure of ventricular cross-sections." Cardiovasc Res 93(2): 263-271.

Badrossamay, M. R., H. A. McIlwee, J. A. Goss and K. K. Parker (2010). "Nanofiber assembly by rotary jet-spinning." Nano Lett 10(6): 2257-2261.

Bai, X. P., H. X. Zheng, R. Fang, T. R. Wang, X. L. Hou, Y. Li, X. B. Chen and W. M. Tian (2011). "Fabrication of engineered heart tissue grafts from alginate/collagen barium composite microbeads." Biomed Mater 6(4): 045002.

Balasubramanian, P., M. P. Prabhakaran, A. A. Al Masri and S. Ramakrishna (2011). "Injectable Polymeric Materials and Evaluation of Their In Vivo Functional Assessment in Cardiac Tissue Engineering." Journal of Biomaterials and Tissue Engineering 1(2): 149-165.

Baraniak, P. R., M. T. Cooke, R. Saeed, M. A. Kinney, K. M. Fridley and T. C. McDevitt (2012). "Stiffening of human mesenchymal stem cell spheroid microenvironments induced by incorporation of gelatin microparticles." J Mech Behav Biomed Mater 11: 63-71.

Baxter, W. T., S. F. Mironov, A. V. Zaitsev, J. Jalife and A. M. Pertsov (2001). "Visualizing excitation waves inside cardiac muscle using transillumination." Biophys J 80(1): 516-530.

Bebarova, M. (2012). "Advances in patch clamp technique: towards higher quality and quantity." Gen Physiol Biophys 31(2): 131-140.

Benton, J. A., B. D. Fairbanks and K. S. Anseth (2009). "Characterization of valvular interstitial cell function in three dimensional matrix metalloproteinase degradable PEG hydrogels." Biomaterials 30(34): 6593-6603.

Bers, D. M. (2000). "Calcium fluxes involved in control of cardiac myocyte contraction." Circ Res 87(4): 275-281.

Brafman, D. A., C. W. Chang, A. Fernandez, K. Willert, S. Varghese and S. Chien (2010). "Long-term human pluripotent stem cell self-renewal on synthetic polymer surfaces." Biomaterials 31(34): 9135-9144.

Brandes, R., V. M. Figueredo, S. A. Camacho, B. M. Massie and M. W. Weiner (1992). "Suppression of motion artifacts in fluorescence spectroscopy of perfused hearts." Am J Physiol 263(3 Pt 2): H972-980.

Bratt-Leal, A. M., R. L. Carpenedo and T. C. McDevitt (2009). "Engineering the embryoid body microenvironment to direct embryonic stem cell differentiation." Biotechnol Prog 25(1): 43-51.

Bratt-Leal, A. M., R. L. Carpenedo, M. D. Ungrin, P. W. Zandstra and T. C. McDevitt (2011). "Incorporation of biomaterials in multicellular aggregates modulates pluripotent stem cell differentiation." Biomaterials 32(1): 48-56.

Burdick, J. A. and G. Vunjak-Novakovic (2009). "Engineered microenvironments for controlled stem cell differentiation." Tissue Eng Part A 15(2): 205-219.

Burridge, P. W., S. Thompson, M. A. Millrod, S. Weinberg, X. Yuan, A. Peters, V. Mahairaki, V. E. Koliatsos, L. Tung and E. T. Zambidis (2011). "A universal system for highly efficient cardiac differentiation of human induced pluripotent stem cells that eliminates interline variability." PLoS One 6(4): e18293.

Bursac, N. (2009). "Cardiac tissue engineering using stem cells [Cellular/Tissue Engineering]." Engineering in Medicine and Biology Magazine, IEEE 28(2): 80, 82, 84-86, 88-89.

Bursac, N., Y. Loo, K. Leong and L. Tung (2007). "Novel anisotropic engineered cardiac tissues: studies of electrical propagation." Biochem Biophys Res Commun 361(4): 847-853.

Cabrales, P., G. Han, C. Roche, P. Nacharaju, A. J. Friedman and J. M. Friedman (2010). "Sustained release nitric oxide from long-lived circulating nanoparticles." Free Radic Biol Med 49(4): 530-538.

Carpenedo, R. L., A. M. Bratt-Leal, R. A. Marklein, S. A. Seaman, N. J. Bowen, J. F. McDonald and T. C. McDevitt (2010). "Homogeneous and organized differentiation within embryoid bodies induced by microsphere-mediated delivery of small molecules." Biomaterials 30(13): 2507-2515.

Cerbai, E., L. Sartiani, P. De Paoli and A. Mugelli (2000). "Isolated cardiac cells for electropharmacological studies." Pharmacol Res 42(1): 1-8.

Chopra, A., V. Lin, A. McCollough, S. Atzet, G. D. Prestwich, A. S. Wechsler, M. E. Murray, S. A. Oake, J. Y. Kresh and P. A. Janmey (2012). "Reprogramming cardiomyocyte mechanosensing by crosstalk between integrins and hyaluronic acid receptors." J Biomech 45(5): 824-831.

Costa, K. D., E. J. Lee and J. W. Holmes (2003). "Creating alignment and anisotropy in engineered heart tissue: role of boundary conditions in a model three-dimensional culture system." Tissue Eng 9(4): 567-577.

Cristallini, C., M. Gagliardi, N. Barbani, D. Giannessi and G. D. Guerra (2012). "Novel biodegradable, biomimetic and functionalised polymer scaffolds to prevent expansion of post-infarct left ventricular remodelling." J Mater Sci Mater Med 23(1): 205-216.

Cromer Berman, S. M., P. Walczak and J. W. Bulte (2011). "Tracking stem cells using magnetic nanoparticles." Wiley Interdiscip Rev Nanomed Nanobiotechnol 3(4): 343-355.

Dai, W., S. L. Hale, G. L. Kay, A. J. Jyrala and R. A. Kloner (2009). "Delivering stem cells to the heart in a collagen matrix reduces relocation of cells to other organs as assessed by nanoparticle technology." Regen Med 4(3): 387-395.

Davis, M. E., P. C. Hsieh, T. Takahashi, Q. Song, S. Zhang, R. D. Kamm, A. J. Grodzinsky, P. Anversa and R. T. Lee (2006). "Local myocardial insulin-like growth factor 1 (IGF-1) delivery with biotinylated peptide nanofibers improves cell therapy for myocardial infarction." Proc Natl Acad Sci U S A 103(21): 8155-8160.

Dawson, E., G. Mapili, K. Erickson, S. Taqvi and K. Roy (2008). "Biomaterials for stem cell differentiation." Advanced Drug Delivery Reviews 60(2): 215-228.

Dedkova, E. N. and L. A. Blatter (2012). "Measuring mitochondrial function in intact cardiac myocytes." J Mol Cell Cardiol 52(1): 48-61.

DeLong, S. A., A. S. Gobin and J. L. West (2005). "Covalent immobilization of RGDS on hydrogel surfaces to direct cell alignment and migration." J Control Release 109(1-3): 139-148.

DeLong, S. A., J. J. Moon and J. L. West (2005). "Covalently immobilized gradients of bFGF on hydrogel scaffolds for directed cell migration." Biomaterials 26(16): 3227-3234.

Duan, Y., Z. Liu, J. O'Neill, L. Q. Wan, D. O. Freytes and G. Vunjak-Novakovic (2011). "Hybrid gel composed of native heart matrix and collagen induces cardiac differentiation of human embryonic stem cells without supplemental growth factors." J Cardiovasc Transl Res 4(5): 605-615.

Dvir, T., B. P. Timko, M. D. Brigham, S. R. Naik, S. S. Karajanagi, O. Levy, H. Jin, K. K. Parker, R. Langer and D. S. Kohane (2011). "Nanowired three-dimensional cardiac patches." Nat Nano 6(11): 720-725.

Dvir, T., B. P. Timko, D. S. Kohane and R. Langer (2011). "Nanotechnological strategies for engineering complex tissues." Nat Nano 6(1): 13-22.

Eisner, D. A., H. S. Choi, M. E. Diaz, S. C. O'Neill and A. W. Trafford (2000). "Integrative analysis of calcium cycling in cardiac muscle." Circ Res 87(12): 1087-1094.

Elloumi-Hannachi, I., M. Yamato and T. Okano (2010). "Cell sheet engineering: a unique nanotechnology for scaffold-free tissue reconstruction with clinical applications in regenerative medicine." J Intern Med 267(1): 54-70.

Engelmayr, G. C., Jr., M. Cheng, C. J. Bettinger, J. T. Borenstein, R. Langer and L. E. Freed (2008). "Accordion-like honeycombs for tissue engineering of cardiac anisotropy." Nat Mater 7(12): 1003-1010.

Engler, A. J., S. Sen, H. L. Sweeney and D. E. Discher (2006). "Matrix elasticity directs stem cell lineage specification." Cell 126(4): 677-689.

Eschenhagen, T., M. Didié, J. Heubach, U. Ravens and W. H. Zimmermann (2002). "Cardiac tissue engineering." Transpl Immunol 9(2-4): 315-321.

Fairbanks, B. D., S. P. Singh, C. N. Bowman and K. S. Anseth (2011). "Photodegradable, Photoadaptable Hydrogels via Radical-Mediated Disulfide Fragmentation Reaction." Macromolecules 44(8): 2444-2450.

Feinberg, A. W., P. W. Alford, H. Jin, C. M. Ripplinger, A. A. Werdich, S. P. Sheehy, A. Grosberg and K. K. Parker (2012). "Controlling the contractile strength of engineered cardiac muscle by hierarchal tissue architecture." Biomaterials 33(23): 5732-5741.

Fiumana, E., G. Pasquinelli, L. Foroni, M. Carboni, F. Bonafé, C. Orrico, B. Nardo, M. Tsivian, F. Neri, G. Arpesella, C. Guarnieri, C. M. Caldarera and C. Muscari (2012). "Localization of mesenchymal stem cells grafted with a hyaluronan-based scaffold in the infarcted heart." J Surg Res.

Franco, C. L., J. Price and J. L. West (2011). "Development and optimization of a dual-photoinitiator, emulsion-based technique for rapid generation of cell-laden hydrogel microspheres." Acta Biomater 7(9): 3267-3276.

Frisman, I., D. Seliktar and H. Bianco-Peled (2011). "Nanostructuring PEG-fibrinogen hydrogels to control cellular morphogenesis." Biomaterials 32(31): 7839-7846.

Fujimoto, K. L., K. Tobita, J. Guan, R. Hashizume, K. Takanari, C. M. Alfieri, K. E. Yutzey and W. R. Wagner (2012). "Placement of an elastic biodegradable cardiac patch on a subacute infarcted heart leads to cellularization with early developmental cardiomyocyte characteristics." J Card Fail 18(7): 585-595.

Fujimoto, K. L., K. Tobita, W. D. Merryman, J. Guan, N. Momoi, D. B. Stolz, M. S. Sacks, B. B. Keller and W. R. Wagner (2007). "An Elastic, Biodegradable Cardiac Patch Induces Contractile Smooth Muscle and Improves Cardiac Remodeling and Function in Subacute Myocardial Infarction." Journal of the American College of Cardiology 49(23): 2292-2300.

Gaetani, R., P. A. Doevendans, C. H. Metz, J. Alblas, E. Messina, A. Giacomello and J. P. Sluijter (2012). "Cardiac tissue engineering using tissue printing technology and human cardiac progenitor cells." Biomaterials 33(6): 1782-1790.

Gallina, C., S. Dolgetta, G. Alloatti, R. Levi and M. P. Gallo (2012). "Development of morphology and function of neonatal mouse ventricular myocytes cultured on a hyaluronan-based polymer scaffold." J Cell Biochem 113(3): 800-807.

Gandaglia, A., R. Huerta-Cantillo, M. Comisso, R. Danesin, F. Ghezzo, F. Naso, A. Gastaldello, E. Schittullo, E. Buratto, M. Spina, G. Gerosa and M. Dettin (2012). "Cardiomyocytes in vitro adhesion is actively influenced by biomimetic synthetic peptides for cardiac tissue engineering." Tissue Eng Part A 18(7-8): 725-736.

Gobin, A. S. and J. L. West (2003). "Effects of epidermal growth factor on fibroblast migration through biomimetic hydrogels." Biotechnol Prog 19(6): 1781-1785.

Gonzalez, A. L., A. S. Gobin, J. L. West, L. V. McIntire and C. W. Smith (2004). "Integrin interactions with immobilized peptides in polyethylene glycol diacrylate hydrogels." Tissue Eng 10(11-12): 1775-1786.

Grynkiewicz, G., M. Poenie and R. Y. Tsien (1985). "A new generation of Ca2+ indicators with greatly improved fluorescence properties." J Biol Chem 260(6): 3440-3450.

Gupta, M. K., J. M. Walthall, R. Venkataraman, S. W. Crowder, D. K. Jung, S. S. Yu, T. K. Feaster, X. Wang, T. D. Giorgio, C. C. Hong, F. J. Baudenbacher, A. K. Hatzopoulos and H. J. Sung (2011). "Combinatorial polymer electrospun matrices promote physiologically-relevant cardiomyogenic stem cell differentiation." PLoS One 6(12): e28935.

Gwak, S. J., S. H. Bhang, I. K. Kim, S. S. Kim, S. W. Cho, O. Jeon, K. J. Yoo, A. J. Putnam and B. S. Kim (2008). "The effect of cyclic strain on embryonic stem cell-derived cardiomyocytes." Biomaterials 29(7): 844-856.

Habib, M., K. Shapira-Schweitzer, O. Caspi, A. Gepstein, G. Arbel, D. Aronson, D. Seliktar and L. Gepstein (2011). "A combined cell therapy and in-situ tissue-engineering approach for myocardial repair." Biomaterials 32(30): 7514-7523.

Hammers, D. W., A. Sarathy, C. B. Pham, C. T. Drinnan, R. P. Farrar and L. J. Suggs (2012). "Controlled release of IGF-I from a biodegradable matrix improves functional recovery of skeletal muscle from ischemia/reperfusion." Biotechnol Bioeng 109(4): 1051-1059.

Haraguchi, Y., T. Shimizu, M. Yamato and T. Okano (2011). "Regenerative therapies using cell sheet-based tissue engineering for cardiac disease." Cardiol Res Pract 2011: 845170.

Hempel, U., V. Hintze, S. Möller, M. Schnabelrauch, D. Scharnweber and P. Dieter (2012). "Artificial extracellular matrices composed of collagen I and sulfated hyaluronan with adsorbed transforming growth factor β1 promote collagen synthesis of human mesenchymal stromal cells." Acta Biomater 8(2): 659-666.

Henslee, A. M., P. P. Spicer, D. M. Yoon, M. B. Nair, V. V. Meretoja, K. E. Witherel, J. A. Jansen, A. G. Mikos and F. K. Kasper (2011). "Biodegradable composite scaffolds incorporating an intramedullary rod and delivering bone morphogenetic protein-2 for stabilization and bone regeneration in segmental long bone defects." Acta Biomater 7(10): 3627-3637.

Herron, T. J., P. Lee and J. Jalife (2012). "Optical imaging of voltage and calcium in cardiac cells & tissues." Circ Res 110(4): 609-623.

Heydarkhan-Hagvall, S., J. M. Gluck, C. Delman, M. Jung, N. Ehsani, S. Full and R. J. Shemin (2012). "The effect of vitronectin on the differentiation of embryonic stem cells in a 3D culture system." Biomaterials 33(7): 2032-2040.

Hiesinger, W., M. J. Brukman, R. C. McCormick, J. R. Fitzpatrick, 3rd, J. R. Frederick, E. C. Yang, J. R. Muenzer, N. A. Marotta, M. F. Berry, P. Atluri and Y. J. Woo (2012). "Myocardial tissue elastic properties determined by atomic force microscopy after stromal cell-derived factor 1alpha angiogenic therapy for acute myocardial infarction in a murine model." J Thorac Cardiovasc Surg 143(4): 962-966.

Hoshino, K., H. Q. Ly, J. V. Frangioni and R. J. Hajjar (2007). "In vivo tracking in cardiac stem cell-based therapy." Prog Cardiovasc Dis 49(6): 414-420.

Hosseinkhani, H., M. Hosseinkhani, S. Hattori, R. Matsuoka and N. Kawaguchi (2010). "Micro and nano-scale in vitro 3D culture system for cardiac stem cells." J Biomed Mater Res A 94(1): 1-8.

Hou, J., J. Wang, L. Cao, X. Qian, W. Xing, J. Lu and C. Liu (2012). "Segmental bone regeneration using rhBMP-2-loaded collagen/chitosan microspheres composite scaffold in a rabbit model." Biomed Mater 7(3): 035002.

Irwin, E. F., R. Gupta, D. C. Dashti and K. E. Healy (2011). "Engineered polymer-media interfaces for the long-term self-renewal of human embryonic stem cells." Biomaterials 32(29): 6912-6919.

Jawad, H., N. N. Ali, A. R. Lyon, Q. Z. Chen, S. E. Harding and A. R. Boccaccini (2007). "Myocardial tissue engineering: a review." J Tissue Eng Regen Med 1(5): 327-342.

Jing, D., A. Parikh and E. S. Tzanakakis (2010). "Cardiac cell generation from encapsulated embryonic stem cells in static and scalable culture systems." Cell Transplant 19(11): 1397-1412.

Kai, D., M. P. Prabhakaran, G. Jin and S. Ramakrishna (2011). "Guided orientation of cardiomyocytes on electrospun aligned nanofibers for cardiac tissue engineering." J Biomed Mater Res B Appl Biomater 98B(2): 379-386.

Kai, D., M. P. Prabhakaran, G. Jin and S. Ramakrishna (2011). "Polypyrrole-contained electrospun conductive nanofibrous membranes for cardiac tissue engineering." J Biomed Mater Res A 99(3): 376-385.

Kehoe, D. E., D. Jing, L. T. Lock and E. S. Tzanakakis (2010). "Scalable stirred-suspension bioreactor culture of human pluripotent stem cells." Tissue Eng Part A 16(2): 405-421.

Kelleher, C. M. and J. P. Vacanti (2010). "Engineering extracellular matrix through nanotechnology." Journal of The Royal Society Interface 7(Suppl 6): S717-S729.

Kensah, G., I. Gruh, J. Viering, H. Schumann, J. Dahlmann, H. Meyer, D. Skvorc, A. Bar, P. Akhyari, A. Heisterkamp, A. Haverich and U. Martin (2011). "A novel miniaturized multimodal bioreactor for continuous in situ assessment of bioartificial cardiac tissue during stimulation and maturation." Tissue Eng Part C Methods 17(4): 463-473.

Kim, D. H., P. Kim, I. Song, J. M. Cha, S. H. Lee, B. Kim and K. Y. Suh (2006). "Guided three-dimensional growth of functional cardiomyocytes on polyethylene glycol nanostructures." Langmuir 22(12): 5419-5426.

Kim, D. H., E. A. Lipke, P. Kim, R. Cheong, S. Thompson, M. Delannoy, K. Y. Suh, L. Tung and A. Levchenko (2010). "Nanoscale cues regulate the structure and function of macroscopic cardiac tissue constructs." Proc Natl Acad Sci U S A 107(2): 565-570.

Koch, M. A., E. J. Vrij, E. Engel, J. A. Planell and D. Lacroix (2010). "Perfusion cell seeding on large porous PLA/calcium phosphate composite scaffolds in a perfusion bioreactor system under varying perfusion parameters." J Biomed Mater Res A 95(4): 1011-1018.

Kraehenbuehl, T. P., P. Zammaretti, A. J. Van der Vlies, R. G. Schoenmakers, M. P. Lutolf, M. E. Jaconi and J. A. Hubbell (2008). "Three-dimensional extracellular matrix-directed cardioprogenitor differentiation: systematic modulation of a synthetic cell-responsive PEG-hydrogel." Biomaterials 29(18): 2757-2766.

Laflamme, M. A., K. Y. Chen, A. V. Naumova, V. Muskheli, J. A. Fugate, S. K. Dupras, H. Reinecke, C. Xu, M. Hassanipour, S. Police, C. O'Sullivan, L. Collins, Y. Chen, E. Minami, E. A. Gill, S. Ueno, C. Yuan, J. Gold and C. E. Murry (2007). "Cardiomyocytes derived from human embryonic stem cells in pro-survival factors enhance function of infarcted rat hearts." Nat Biotech 25(9): 1015-1024.

Lee, S. T., J. I. Yun, Y. S. Jo, M. Mochizuki, A. J. van der Vlies, S. Kontos, J. E. Ihm, J. M. Lim and J. A. Hubbell (2009). "Engineering integrin signaling for promoting embryonic stem cell self-renewal in a precisely defined niche." Biomaterials 31(6): 1219-1226.

Leslie-Barbick, J. E., J. E. Saik, D. J. Gould, M. E. Dickinson and J. L. West (2011). "The promotion of microvasculature formation in poly(ethylene glycol) diacrylate hydrogels by an immobilized VEGF-mimetic peptide." Biomaterials 32(25): 5782-5789.

Liau, B., N. Christoforou, K. W. Leong and N. Bursac (2011). "Pluripotent stem cell-derived cardiac tissue patch with advanced structure and function." Biomaterials 32(35): 9180-9187.

Limpitikul, W., N. Christoforou, S. Thompson, J. Gearhart, L. Tung and E. Lipke (2010). "Influence of Electromechanical Activity on Cardiac Differentiation of Mouse Embryonic Stem Cells." Cardiovascular Engineering and Technology 1(3): 179-193.

Lipke, E. A. and J. L. West (2005). "Localized delivery of nitric oxide from hydrogels inhibits neointima formation in a rat carotid balloon injury model." Acta Biomater 1(6): 597-606.

Liu, S. J., K. M. Peng, C. Y. Hsiao, K. S. Liu, H. T. Chung and J. K. Chen (2011). "Novel biodegradable polycaprolactone occlusion device combining nanofibrous PLGA/collagen membrane for closure of atrial septal defect (ASD)." Ann Biomed Eng 39(11): 2759-2766.

Lock, L. T. and E. S. Tzanakakis (2009). "Expansion and differentiation of human embryonic stem cells to endoderm progeny in a microcarrier stirred-suspension culture." Tissue Eng Part A 15(8): 2051-2063.

Luna, J. I., J. Ciriza, M. E. Garcia-Ojeda, M. Kong, A. Herren, D. K. Lieu, R. A. Li, C. C. Fowlkes, M. Khine and K. E. McCloskey (2011). "Multiscale biomimetic topography for the alignment of neonatal and embryonic stem cell-derived heart cells." Tissue Eng Part C Methods 17(5): 579-588.

Lutolf, M. P., P. M. Gilbert and H. M. Blau (2009). "Designing materials to direct stem-cell fate." Nature 462(7272): 433-441.

Lutolf, M. P., J. L. Lauer-Fields, H. G. Schmoekel, A. T. Metters, F. E. Weber, G. B. Fields and J. A. Hubbell (2003). "Synthetic matrix metalloproteinase-sensitive hydrogels for the conduction of tissue regeneration: engineering cell-invasion characteristics." Proc Natl Acad Sci U S A 100(9): 5413-5418.

Maidhof, R., A. Marsano, E. J. Lee and G. Vunjak-Novakovic (2010). "Perfusion seeding of channeled elastomeric scaffolds with myocytes and endothelial cells for cardiac tissue engineering." Biotechnol Prog 26(2): 565-572.

Maidhof, R., N. Tandon, E. J. Lee, J. Luo, Y. Duan, K. Yeager, E. Konofagou and G. Vunjak-Novakovic (2011). "Biomimetic perfusion and electrical stimulation applied in concert improved the assembly of engineered cardiac tissue." J Tissue Eng Regen Med.

Malkin, R. A., N. Kramer, B. Schnitz, M. Gopalakrishnan and A. L. Curry (2005). "Advances in electrical and mechanical cardiac mapping." Physiol Meas 26(1): R1-14.

Mallon, B. S., K.-Y. Park, K. G. Chen, R. S. Hamilton and R. D. G. McKay (2006). "Toward xeno-free culture of human embryonic stem cells." The International Journal of Biochemistry & Cell Biology 38(7): 1063-1075.

Mann, B. K., R. H. Schmedlen and J. L. West (2001). "Tethered-TGF-beta increases extracellular matrix production of vascular smooth muscle cells." Biomaterials 22(5): 439-444.

Martin, D. P. and S. F. Williams (2003). "Medical applications of poly-4-hydroxybutyrate: a strong flexible absorbable biomaterial." Biochemical Engineering Journal 16(2): 97-105.

Masuda, S., T. Shimizu, M. Yamato and T. Okano (2008). "Cell sheet engineering for heart tissue repair." Adv Drug Deliv Rev 60(2): 277-285.

Matson, J. B., R. H. Zha and S. I. Stupp (2011). "Peptide Self-Assembly for Crafting Functional Biological Materials." Curr Opin Solid State Mater Sci 15(6): 225-235.

McCain, M. L. and K. K. Parker (2011). "Mechanotransduction: the role of mechanical stress, myocyte shape, and cytoskeletal architecture on cardiac function." Pflugers Arch 462(1): 89-104.

McNamara, L. E., R. J. McMurray, M. J. Biggs, F. Kantawong, R. O. Oreffo and M. J. Dalby (2010). "Nanotopographical control of stem cell differentiation." J Tissue Eng 2010: 120623.

Mei, Y., K. Saha, S. R. Bogatyrev, J. Yang, A. L. Hook, Z. I. Kalcioglu, S.-W. Cho, M. Mitalipova, N. Pyzocha, F. Rojas, K. J. Van Vliet, M. C. Davies, M. R. Alexander, R. Langer, R. Jaenisch and D. G. Anderson (2010). "Combinatorial development of biomaterials for clonal growth of human pluripotent stem cells." Nat Mater 9(9): 768-778.

Melkoumian, Z., J. L. Weber, D. M. Weber, A. G. Fadeev, Y. Zhou, P. Dolley-Sonneville, J. Yang, L. Qiu, C. A. Priest, C. Shogbon, A. W. Martin, J. Nelson, P. West, J. P. Beltzer, S. Pal and R. Brandenberger (2010). "Synthetic peptide-acrylate surfaces for long-term self-renewal and cardiomyocyte differentiation of human embryonic stem cells." Nat Biotech 28(6): 606-610.

Meng, Y., S. Eshghi, Y. J. Li, R. Schmidt, D. V. Schaffer and K. E. Healy (2010). "Characterization of integrin engagement during defined human embryonic stem cell culture." The FASEB Journal 24(4): 1056-1065.

Mirensky, T. L. and C. K. Breuer (2008). "The development of tissue-engineered grafts for reconstructive cardiothoracic surgical applications." Pediatr Res 63(5): 559-568.

Miyagi, Y., L. L. Chiu, M. Cimini, R. D. Weisel, M. Radisic and R. K. Li (2011). "Biodegradable collagen patch with covalently immobilized VEGF for myocardial repair." Biomaterials 32(5): 1280-1290.

Moon, J. J., J. E. Saik, R. A. Poché, J. E. Leslie-Barbick, S. H. Lee, A. A. Smith, M. E. Dickinson and J. L. West (2010). "Biomimetic hydrogels with pro-angiogenic properties." Biomaterials 31(14): 3840-3847.

Mooney, E., J. N. Mackle, D. J. Blond, E. O'Cearbhaill, G. Shaw, W. J. Blau, F. P. Barry, V. Barron and J. M. Murphy (2012). "The electrical stimulation of carbon nanotubes to provide a cardiomimetic cue to MSCs." Biomaterials 33(26): 6132-6139.

Murtuza, B., J. W. Nichol and A. Khademhosseini (2009). "Micro- and nanoscale control of the cardiac stem cell niche for tissue fabrication." Tissue Eng Part B Rev 15(4): 443-454.

Nagarajan, S. and Y. Zhang (2011). "Upconversion fluorescent nanoparticles as a potential tool for in-depth imaging." Nanotechnology 22(39): 395101.

Niebruegge, S., C. L. Bauwens, R. Peerani, N. Thavandiran, S. Masse, E. Sevaptisidis, K. Nanthakumar, K. Woodhouse, M. Husain, E. Kumacheva and P. W. Zandstra (2009). "Generation of human embryonic stem cell-derived mesoderm and cardiac cells using

size-specified aggregates in an oxygen-controlled bioreactor." Biotechnol Bioeng 102(2): 493-507.

Ott, H. C., T. S. Matthiesen, S.-K. Goh, L. D. Black, S. M. Kren, T. I. Netoff and D. A. Taylor (2008). "Perfusion-decellularized matrix: using nature's platform to engineer a bioartificial heart." Nat Med 14(2): 213-221.

Park, J., J. Ryu, S. K. Choi, E. Seo, J. M. Cha, S. Ryu, J. Kim, B. Kim and S. H. Lee (2005). "Real-time measurement of the contractile forces of self-organized cardiomyocytes on hybrid biopolymer microcantilevers." Anal Chem 77(20): 6571-6580.

Parker, K. K., J. Tan, C. S. Chen and L. Tung (2008). "Myofibrillar architecture in engineered cardiac myocytes." Circ Res 103(4): 340-342.

Parrag, I. C., P. W. Zandstra and K. A. Woodhouse (2012). "Fiber alignment and coculture with fibroblasts improves the differentiated phenotype of murine embryonic stem cell-derived cardiomyocytes for cardiac tissue engineering." Biotechnology and Bioengineering 109(3): 813-822.

Patterson, J. and J. A. Hubbell (2010). "Enhanced proteolytic degradation of molecularly engineered PEG hydrogels in response to MMP-1 and MMP-2." Biomaterials 31(30): 7836-7845.

Pêgo, A. P., B. Siebum, M. J. Van Luyn, X. J. Gallego y Van Seijen, A. A. Poot, D. W. Grijpma and J. Feijen (2003). "Preparation of degradable porous structures based on 1,3-trimethylene carbonate and D,L-lactide (co)polymers for heart tissue engineering." Tissue Eng 9(5): 981-994.

Pertsov, A. M., J. M. Davidenko, R. Salomonsz, W. T. Baxter and J. Jalife (1993). "Spiral waves of excitation underlie reentrant activity in isolated cardiac muscle." Circ Res 72(3): 631-650.

Pok, S. and J. G. Jacot (2011). "Biomaterials advances in patches for congenital heart defect repair." J Cardiovasc Transl Res 4(5): 646-654.

Prabhakaran, M. P., J. Venugopal, D. Kai and S. Ramakrishna (2011). "Biomimetic material strategies for cardiac tissue engineering." Materials Science and Engineering: C 31(3): 503-513.

Radisic, M., W. Deen, R. Langer and G. Vunjak-Novakovic (2005). "Mathematical model of oxygen distribution in engineered cardiac tissue with parallel channel array perfused with culture medium containing oxygen carriers." Am J Physiol Heart Circ Physiol 288(3): H1278-1289.

Reis, L. A., L. L. Y. Chiu, Y. Liang, K. Hyunh, A. Momen and M. Radisic (2012). "A peptide-modified chitosan–collagen hydrogel for cardiac cell culture and delivery." Acta Biomater 8(3): 1022-1036.

Robertson, C., D. D. Tran and S. C. George (2013). "Concise review: maturation phases of human pluripotent stem cell-derived cardiomyocytes." Stem Cells 31(5): 829-837.

Ross, J. J. and R. T. Tranquillo (2003). "ECM gene expression correlates with in vitro tissue growth and development in fibrin gel remodeled by neonatal smooth muscle cells." Matrix Biol 22(6): 477-490.

Sahoo, S., L. T. Ang, J. C.-H. Goh and S.-L. Toh (2010). "Growth factor delivery through electrospun nanofibers in scaffolds for tissue engineering applications." Journal of Biomedical Materials Research Part A 93A(4): 1539-1550.

Sapir, Y., O. Kryukov and S. Cohen (2011). "Integration of multiple cell-matrix interactions into alginate scaffolds for promoting cardiac tissue regeneration." Biomaterials 32(7): 1838-1847.

Sathuluri, R. R., H. Yoshikawa, E. Shimizu, M. Saito and E. Tamiya (2011). "Gold nanoparticle-based surface-enhanced Raman scattering for noninvasive molecular probing of embryonic stem cell differentiation." PLoS One 6(8): e22802.

Segers, V. F. and R. T. Lee (2011). "Biomaterials to enhance stem cell function in the heart." Circ Res 109(8): 910-922.

Sekine, H., T. Shimizu, S. Kosaka, E. Kobayashi and T. Okano (2006). "Cardiomyocyte Bridging Between Hearts and Bioengineered Myocardial Tissues With Mesenchymal Transition of Mesothelial Cells." The Journal of Heart and Lung Transplantation 25(3): 324-332.

Serena, E., E. Figallo, N. Tandon, C. Cannizzaro, S. Gerecht, N. Elvassore and G. Vunjak-Novakovic (2009). "Electrical stimulation of human embryonic stem cells: Cardiac differentiation and the generation of reactive oxygen species." Experimental Cell Research 315(20): 3611-3619.

Shachar, M., N. Benishti and S. Cohen (2012). "Effects of mechanical stimulation induced by compression and medium perfusion on cardiac tissue engineering." Biotechnol Prog.

Shacklock, P. S., W. G. Wier and C. W. Balke (1995). "Local Ca2+ transients (Ca2+ sparks) originate at transverse tubules in rat heart cells." J Physiol 487 (Pt 3): 601-608.

Shimko, V. F. and W. C. Claycomb (2008). "Effect of mechanical loading on three-dimensional cultures of embryonic stem cell-derived cardiomyocytes." Tissue Eng Part A 14(1): 49-58.

Siepe, M., P. Akhyari, A. Lichtenberg, C. Schlensak and F. Beyersdorf (2008). "Stem cells used for cardiovascular tissue engineering." Eur J Cardiothorac Surg 34(2): 242-247.

Singelyn, J. M., J. A. DeQuach, S. B. Seif-Naraghi, R. B. Littlefield, P. J. Schup-Magoffin and K. L. Christman (2009). "Naturally derived myocardial matrix as an injectable scaffold for cardiac tissue engineering." Biomaterials 30(29): 5409-5416.

Slaughter, B. V., S. S. Khurshid, O. Z. Fisher, A. Khademhosseini and N. A. Peppas (2009). "Hydrogels in regenerative medicine." Adv Mater 21(32-33): 3307-3329.

Spira, M. E. and A. Hai (2013). "Multi-electrode array technologies for neuroscience and cardiology." Nat Nanotechnol 8(2): 83-94.

Stevens, K. R., K. L. Kreutziger, S. K. Dupras, F. S. Korte, M. Regnier, V. Muskheli, M. B. Nourse, K. Bendixen, H. Reinecke and C. E. Murry (2009). "Physiological function and transplantation of scaffold-free and vascularized human cardiac muscle tissue." Proc Natl Acad Sci U S A 106(39): 16568-16573.

Sugiura, S., S. Yasuda, H. Yamashita, K. Kato, Y. Saeki, H. Kaneko, Y. Suda, R. Nagai and H. Sugi (2003). "Measurement of force developed by a single cardiac myocyte using novel carbon fibers." Adv Exp Med Biol 538: 381-386; discussion 386-387.

Szentivanyi, A., T. Chakradeo, H. Zernetsch and B. Glasmacher (2011). "Electrospun cellular microenvironments: Understanding controlled release and scaffold structure." Adv Drug Deliv Rev 63(4-5): 209-220.

Tandon, N., A. Marsano, R. Maidhof, K. Numata, C. Montouri-Sorrentino, C. Cannizzaro, J. Voldman and G. Vunjak-Novakovic (2010). "Surface-patterned electrode bioreactor for electrical stimulation." Lab Chip 10(6): 692-700.

Taylor, R. E., K. Kim, N. Sun, S. J. Park, J. Y. Sim, G. Fajardo, D. Bernstein, J. C. Wu and B. L. Pruitt (2012). "Sacrificial layer technique for axial force post assay of immature cardiomyocytes." Biomed Microdevices.

Terrovitis, J., R. Lautamäki, M. Bonios, J. Fox, J. M. Engles, J. Yu, M. K. Leppo, M. G. Pomper, R. L. Wahl, J. Seidel, B. M. Tsui, F. M. Bengel, M. R. Abraham and E. Marbán (2009). "Noninvasive quantification and optimization of acute cell retention by in vivo positron emission tomography after intramyocardial cardiac-derived stem cell delivery." J Am Coll Cardiol 54(17): 1619-1626.

Tulis, D. A., K. S. Bohl Masters, E. A. Lipke, R. L. Schiesser, A. J. Evans, K. J. Peyton, W. Durante, J. L. West and A. I. Schafer (2002). "YC-1-mediated vascular protection through inhibition of smooth muscle cell proliferation and platelet function." Biochem Biophys Res Commun 291(4): 1014-1021.

van der Velden, J., L. J. Klein, M. van der Bijl, M. A. Huybregts, W. Stooker, J. Witkop, L. Eijsman, C. A. Visser, F. C. Visser and G. J. Stienen (1998). "Force production in mechanically isolated cardiac myocytes from human ventricular muscle tissue." Cardiovasc Res 38(2): 414-423.

Vergara, J., M. DiFranco, D. Compagnon and B. A. Suarez-Isla (1991). "Imaging of calcium transients in skeletal muscle fibers." Biophys J 59(1): 12-24.

Villa-Diaz, L. G., H. Nandivada, J. Ding, N. C. Nogueira-de-Souza, P. H. Krebsbach, K. S. O'Shea, J. Lahann and G. D. Smith (2010). "Synthetic polymer coatings for long-term growth of human embryonic stem cells." Nat Biotech 28(6): 581-583.

Wang, F. and J. Guan (2010). "Cellular cardiomyoplasty and cardiac tissue engineering for myocardial therapy." Adv Drug Deliv Rev 62(7-8): 784-797.

Webber, M. J., J. Tongers, C. J. Newcomb, K. T. Marquardt, J. Bauersachs, D. W. Losordo and S. I. Stupp (2011). "Supramolecular nanostructures that mimic VEGF as a strategy for ischemic tissue repair." Proc Natl Acad Sci U S A 108(33): 13438-13443.

Webber, M. J., J. Tongers, M. A. Renault, J. G. Roncalli, D. W. Losordo and S. I. Stupp (2010). "Development of bioactive peptide amphiphiles for therapeutic cell delivery." Acta Biomater 6(1): 3-11.

Yoshida, Y. and S. Yamanaka (2011). "iPS cells: a source of cardiac regeneration." J Mol Cell Cardiol 50(2): 327-332.

You, J. O., M. Rafat, G. J. Ye and D. T. Auguste (2011). "Nanoengineering the heart: conductive scaffolds enhance connexin 43 expression." Nano Lett 11(9): 3643-3648.

Young, J. L. and A. J. Engler (2011). "Hydrogels with time-dependent material properties enhance cardiomyocyte differentiation in vitro." Biomaterials 32(4): 1002-1009.

Yu, J., K. T. Du, Q. Fang, Y. Gu, S. S. Mihardja, R. E. Sievers, J. C. Wu and R. J. Lee (2010). "The use of human mesenchymal stem cells encapsulated in RGD modified alginate microspheres in the repair of myocardial infarction in the rat." Biomaterials 31(27): 7012-7020.

Yuan Ye, K., K. E. Sullivan and L. D. Black (2011). "Encapsulation of cardiomyocytes in a fibrin hydrogel for cardiac tissue engineering." J Vis Exp(55).

Zhang, B., Y. Xiao, A. Hsieh, N. Thavandiran and M. Radisic (2011). "Micro- and nanotechnology in cardiovascular tissue engineering." Nanotechnology 22(49): 494003.

Zhang, G., X. Wang, Z. Wang, J. Zhang and L. Suggs (2006). "A PEGylated fibrin patch for mesenchymal stem cell delivery." Tissue Eng 12(1): 9-19.

Zhang, S., M. A. Greenfield, A. Mata, L. C. Palmer, R. Bitton, J. R. Mantei, C. Aparicio, M. O. de la Cruz and S. I. Stupp (2010). "A self-assembly pathway to aligned monodomain gels." Nat Mater 9(7): 594-601.

Zimmermann, W. H., K. Schneiderbanger, P. Schubert, M. Didié, F. Münzel, J. F. Heubach, S. Kostin, W. L. Neuhuber and T. Eschenhagen (2002). "Tissue engineering of a differentiated cardiac muscle construct." Circ Res 90(2): 223-230.

3. DEVELOPMENT OF AN OPTICAL MAPPING PLATFORM FOR ELECTROPHYSIOLOGICAL ANALYSIS OF CULTURED CARDIOMYOCYTES

3.1. Introduction

The creation of functioning engineered cardiac tissue remains an ongoing challenge as demand for clinical solutions for heart disease and diagnostic research applications continues to increase. Pluripotent stem cells, either embryonic or induced pluripotent in origin, have been routinely differentiated into robust, contracting cardiomyocytes using a combination of different strategies (Takahashi, Lord et al. 2003, Zwi, Caspi et al. 2009, Lian, Zhang et al. 2013). While these approaches provide methods for the generation of cardiomyocytes for different applications, the cells produced using these techniques are often lacking the functional properties that are observed among cells in mature adult myocardium (Harding, Ali et al. 2007, Yang, Pabon et al. 2014, Bedada, Wheelwright et al. 2015). The inability to generate functionally-mature cardiomyocytes, including cells which have adult-like electrophysiology or calcium handling properties, can lead to the formation of arrhythmias when implanted in vivo, disqualifying their use in clinical applications.

To address this need for functional quantification, a range of methods and platforms have been established over several decades for the assessment of cardiomyocyte and cardiac tissue properties and function. These systems include electrophysiological (Herron, Lee et al. 2012, Becker, Stoelzle et al. 2013), mechanical (Malkin, Kramer et al. 2005), and metabolic assays (Malkin, Kramer et al. 2005, Dedkova and Blatter 2012, Robertson, Tran et al. 2013). Initially, these systems were utilized and optimized for the evaluation of whole heart tissue or adult cardiomyocytes

(Wang, Lee et al. 2015); however, these systems have been further refined for characterization of cell-derived cardiomyocytes. Among these, characterization of cardiomyocyte electrophysiological properties remains a critical step for assessing cell-cell connectivity and for predicting the formation of arrhythmias.

In general, the electrophysiological properties of cardiomyocytes can be evaluated using several different techniques, including microelectrode arrays (MEAs), whole cell patch clamp, and optical mapping. Patch clamp and MEA systems have been effective means for evaluating individual ion channel currents and cell membrane potential; however, electrical artifacts, invasive equipment, and cellular inaccessibility in situ are potential drawbacks when implementing microelectrode-based techniques. Patch clamping, which provides detailed information about individual cellular electrical activity, is not suitable for assessment of multicellular systems. While MEAs are suitable for evaluating electrophysiological properties of cellular monolayers or cardiac tissues, cardiomyocytes must be cultured directly on specialized glass substrates with embedded electrodes; this severely limits the overall feasibility (and potentially total spatial resolution) of this technique when evaluating signal propagation between adjacent cardiomyocytes cultured on biomimetic materials or within engineered tissues. To address these shortcomings, optical mapping has emerged as a valuable technique for characterizing electrophysiological properties of cardiomyocyte monolayers and cardiac tissue. In contrast to techniques which rely on electrodes to directly record current or voltage, optical mapping utilizes calcium or voltage-sensitive fluorescent dyes which bind to intracellular calcium or membrane-bound proteins or genetically-induced reporter proteins to obtain recordings. Voltage-sensitive dyes enable visualization of changes

intransmembrane potential; this data can be used to evaluate cellular depolarization, spatial distribution of action potential duration, or repolarization events (Malkin, Kramer et al. 2005). Calcium-sensitive dyes, in contrast, bind to intracellular calcium, allowing for determination of calcium transients during excitation-contraction coupling. In addition to identifying and quantifying functionality of cardiomyocytes and cardiac tissue, optical mapping analysis can also be used to identify reentrant waves among cardiomyocytes which could lead to arrhythmias after clinical implantation.

A number of optical mapping platforms have been previously developed and optimized for acquisition of data from specific kinds of samples; these include whole hearts (Laurita, Chuck et al. 2003, Efimov, Nikolski et al. 2004, Nygren, Baczko et al. 2006), cardiac tissue (Radisic, Fast et al. 2009, Blazeski, Kostecki et al. 2015) and cardiomyocyte monolayers (Bursac, Parker et al. 2002). While these systems are highly efficacious for their individualized applications, a growing need persists for mapping systems which can acquire data from a variety of engineered platforms; such samples require mapping systems that are adaptable to different shapes, sizes, and structures. For example, the ability to acquire signals at either the macro- or microscopic size ranges (from 0.5 to 10+ mm) at high spatial and temporal resolution may be valuable when evaluating either a small region or an entire engineered heart construct; however, this setup typically requires specialized, often costly, hardware solutions. Given the extensive differences in optics, illumination, and other acquisition hardware required to attain signal capture at macro- and microscopic ranges, extending a system to accommodate mapping at both size scales is a formidable endeavor. Additionally, engineered cardiac platforms which utilize different materials of varying optical clarity (from transparent to

opaque) and those with varying structures and shapes present their own unique challenges in the context of signal acquisition. Thus, the ability to evaluate electrical or calcium signaling of cardiomyocytes incorporated in engineered biomaterial systems on either the microscopic and macroscopic scales would be advantageous.

Herein, the authors have described a method for creating an adaptable multi-scale, multi-platform optical mapping system leveraging frequently-available research hardware. Development of a flexible, relatively inexpensive optical mapping system to effectively quantify fluorescent signals from cardiomyocyte layers would provide a valuable research apparatus for investigators attempting to characterize complex samples prepared on a wide array of different size scales and platforms; this tool also facilitates for investigation of local and global electrophysiological activity on the same sample. The described platform is capable of capturing and quantifying cardiac electrical and calcium signals at the micro- (approximately 100-200 μm) and macro-scales (>1 cm). This platform provides a method for quantifying a diverse range of cardiac samples cultured on a range of different materials. Furthermore, this system employs hardware which can be leveraged for use in other laboratory applications.

3.2. Materials and methods

Design of optical mapping chamber

In order to support cell viability throughout the mapping experiments, a chamber was designed to support a high rate of perfusion (greater than 5 mL/min) of Tyrode's solution while minimizing imaging artifacts associated with mixing or moving liquid. Furthermore, In designing the internal chamber geometry, it was required that the total volume of the chamber would be sufficient to support optical measurement of whole

cardiac tissue constructs. Additionally, the geometry of the chamberAdditionally, in the designing of the external chamber geometry, it was required to that the shape be compatible with both the macroscopic mapping apparatus stage as well as the fluorescence microscope stage. A design for the mapping chamber was initially prepared using Solidworks software (Fig. 3.1).

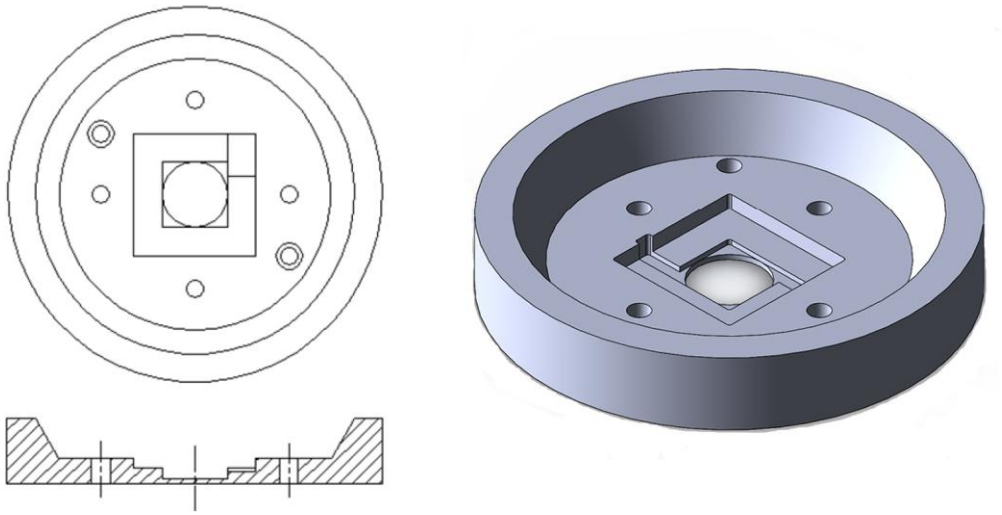

Figure 3.1. Optical mapping chamber design.

Fabrication of the optical mapping chamber was carried out using a CNC milling machine (EZ Trak-SX, Bridgeport); the main structure of the chamber was fabricated from a solid polycarbonate billet in order to form a durable, chemically-resistant cellular environment. In order to visualize the sample, a circular area was hollowed out in the center of the chamber; the resulting void space that was sealed using a 35 mm cover glass fixed on top of a rubber gasket. An aluminum base was fabricated and bolted into the polycarbonate chamber to form a leak-free seal around the glass coverslip. A compatible top was fabricated using high quality glass, which was selected to minimize motion

imaging artifacts as well as auto-fluorescence. An array of 1 mm sized holes was drilled evenly over the area of the glass to allow for electrical point stimulation and temperature monitoring at multiple sites within the chamber. An image of the completed chamber design is shown in Figure 3.2.

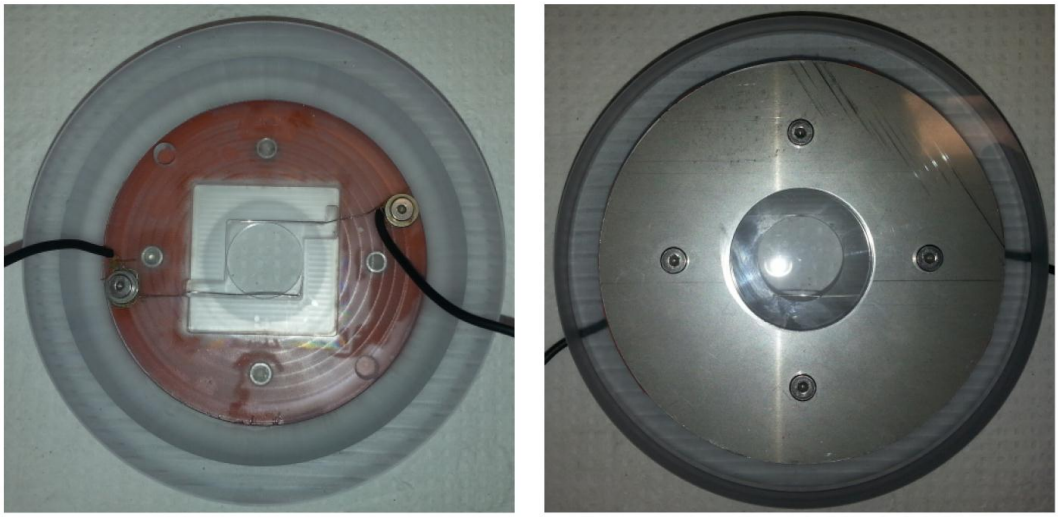

Figure 3.2. Fabricated optical mapping chamber.

Macroscopic imaging apparatus

A macroscopic imaging apparatus was assembled to allow for optical mapping of samples greater than 0.5 cm. The primary structure of the apparatus was fashioned from a vertical rail (X95, Thor Labs), which was attached to a magnetic base (Model 200, Newport Corporation). To minimize vibrational artifacts, a desktop air table (Benchmate 2212, Warner Apparatus) was selected for the bottom of the device. To allow for flexible positioning of the mapping chamber on the apparatus, sliding mechanical rail supports (Thor Labs) were incorporated to facilitate movement of hardware in order to improve spatial resolution of the sample (Fig. 3.3). When mounting the mapping chamber onto the

sliding rail, it was considered how to implement X-Y control of the sample location to ensure that the chamber was always within the camera viewing range. A novel solution to this problem was to retrofit a microadjuster-containing microscope stage (Nikon) with a custom-made bracket for holding the chamber. An aluminum bracket was fabricated and fixed to the mechanical features of the microscope stage. A second aluminum block was designed an attached to the stage to allow the mechanism to be mounted to the sliding rail mount.

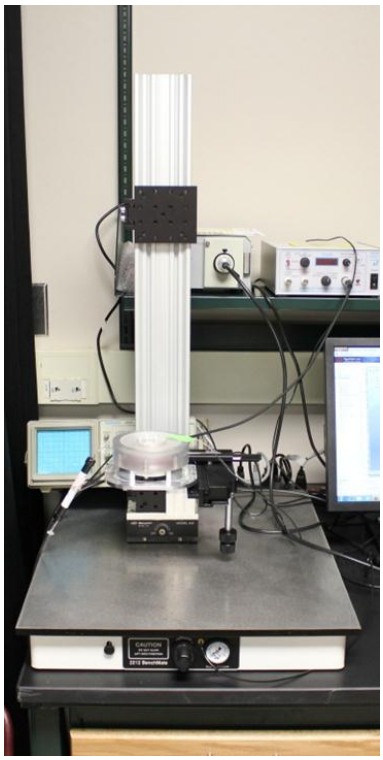

Figure 3.3. Optical mapping setup containing bench-top air table, magnetic base, and sliding rail.

In order to illuminate the cardiac sample and capture the fluorescence signal, a light source, filter, and camera set were selected to coincide with the parameters of the

apparatus. A Prior Lumen 200 metal halide fiber optic illuminator was selected as the light source for the setup due to its broad spectrum of emitted wavelengths and strong light intensity, allowing for illumination of multiple types of fluorescent dyes. A liquid light guide (Edmund Optics) was purchased and mounted onto the rail to position the illuminating light directly at the sample. An attachable C-mount lens was purchased for the light guide with the capacity of incorporating interchangeable filters, allowing for illumination of the sample at specific wavelengths to coincide with excitation band of the fluorescent dye.

An Andor iXon Ultra DU897 CCD camera (Andor) was selected for signal capture due to the high frame rate of the device and sensitivity to low light. To further increase the frame rate of the camera, an Optomask system was equipped to the device which allows for adjustable shortening of the CCD sensor. Focal adjustment was addressed by attaching a Xenon .95/17 mm lens (Schneider Optics) containing an emission filter mount to the Optomask system. Video recordings were acquired using the Elements (Nikon) software package.

In order to maintain temperature and constant perfusion within the mapping chamber, a pump and heating system were selected to fit the geometry of the system. A peristaltic pump (MS Regalo, Ismatic) was fitted with Easy Load 2 pump heads with size 14 Tygon tubing (Cole-Parmer); this tubing has an inside diameter of 1.6 mm and provides a volumetric flow rate of 1.3 to 130 ml/min, providing a wide range of flow rates compatible with the optical mapping system. In order to maintain a constant temperature of 37°C within the chamber, a TC-324B temperature controller and an SH-27B inline heater (Warner Apparatus) was incorporated into the tubing inlet. Removal of

liquid was carried out using a glass pipet attached to a vacuum line. Generation of exogenous pacing was controlled using a Grass stimulator (SD9) via platinum electrodes that were fixed within the chamber to allow for field pacing across the entire area of the sample. Additional platinum electrodes were fabricated to allow for placement through the top of the chamber to supply point stimulation at multiple locations throughout the sample. An image of the full macroscopic mapping system is shown in Figure 3.4.

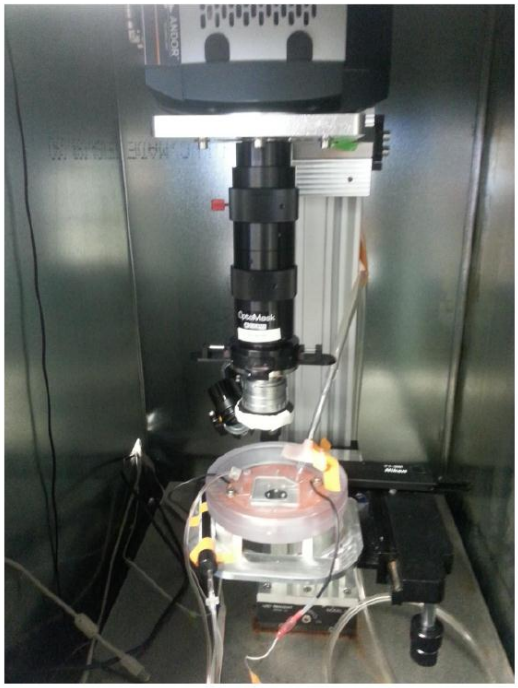

Figure 3.4. Macroscopic imaging apparatus containing the optical mapping chamber.

Microscopic imaging apparatus

A micro-scale mapping system was developed to allow for optical mapping of samples less than 0.5 cm. A Nikon Ti inverted microscope was converted to allow for positioning of the optical mapping chamber within the microscope stage (Fig. 3.5). Visualization of the sample was carried out using a Plan Apo 2x objective (NA 0.10).

The iXon Ultra CCD camera containing the Optomask was fitted onto the microscope using a 0.5x relay lens. The light source, computer, and perfusion setup was consistent between the microscopic and macroscopic systems.

Figure 3.5. Micromapping imaging apparatus containing the mapping chamber.

Optimization of acquisition parameters

In order to maximize the spatiotemporal resolution acquired from the CCD camera, a series of recordings were used to benchmark the camera performance using a number of hardware and software settings. Videos were recorded on both the microscopic and macroscopic imaging systems with and without the Optomask system; microscopic recordings were taken using a 2x, 4x, and 10x objective. The field of view was adjusted to incorporate recordings using: the full CCD chip resolution (for the microscopic setup),

the full mapping area (for the macroscopic setup), or horizontally- or vertically-masked regions of the sample. Vertical shift speed of the CCD was adjusted between 0.5 μs and 0.3 μs; a +1 overclock setting was used in combination with 0.3 μs vertical shift speed in order to stabilize the acquired signal. The CCD sensor was maintained at -70°C during all recordings to minimize temperature-dependent effects associated which could negatively impact acquisition speed. All camera settings were controlled using the Nikon Elements software package.

Cell culture

HL-1 atrial myocytes, a cell line derived from adult mouse atria, were obtained from Dr. William Claycomb (Louisiana State University Health Sciences Center, New Orleans, LA) for use in evaluating the performance of the optical mapping system. HL-1 cells were cultured in vitro using Claycomb media (Sigma-Aldrich) supplemented with 10% fetal bovine serum (Sigma-Aldrich), 0.1 mM norepinephrine (Sigma-Aldrich), 2 mM L-glutamine (Lonza), and 100 μg mL-1 penicillin-streptomycin (Lonza). HL-1 cells were expanded and passaged onto 22 mm PDMS-coated glass cover slips and allowed to expand for 72 hours prior to mapping analysis.

Optical mapping of cells

Optical mapping was performed on confluent HL-1 cell monolayers 72 hours post-seeding on PDMS-coated cover slips. A working concentration of Rhod-2 AM (Invitrogen) intracellular calcium staining dye was prepared by combining 5 μl of 1 mM Rhod-2 AM stock solution, 5 μl of 1% Pluronic F-127 into 1 ml of Tyrode's solution.

Samples were incubated in calcium indicator solution at room temperature for 20 min and subsequently rinsed with Tyrode's solution prior to imaging.

Recordings of calcium wave propagation across the HL-1 cell sheets were acquired using the microscopic and macroscopic imaging systems. Propagating calcium waves were recorded in Tyrode's solution at room temperature (22 °C) in the presence and absence of exogenous stimulation (i.e., spontaneous wave propagation). For each film, a minimum of three recordings were taken with an average length of 10 sec at a rate of approximately 500 frames per second. Data was analyzed using a modified version of a previously established MATLAB (MathWorks, Natick, MA) script. Using this script, calcium transient velocity, calcium transient duration (time to 50% recovery), and calcium wave frequency were quantified for each condition.

3.3. Results

Evaluation of system efficacy

As an initial determination of equipment performance, samples of HL-1 cardiomyocytes were evaluated using the microscopic and macroscopic imaging systems. Recordings of HL-1 monolayers collected using the microscopic apparatus show capture of 5.8 x 5.8 mm^2 samples at 108 frames per second. Incorporation of the Optomask lens system in conjunction with the CCD camera allowed for capture of calcium waves within smaller sample areas using greater acquisition speeds. The acquisition hardware also demonstrated efficacy within the macroscopic system, which supported capture of calcium signaling for samples of 3.8 x 1.2 mm^2 at 503 frames per second.

Optimization of system parameters

In order to maximize the spatiotemporal resolution of the mapping system, a series of video recordings were collected for different conditions using the macroscopic and microscopic imaging systems. In the evaluation of the macroscopic apparatus, videos were captured using the full field of view of the sample area (2.75 x 2.75 cm) and using a representative area (2 x 1 cm) which was masked either horizontally or vertically (Fig 3.6). Full field of view recordings demonstrated a non-multiplicative increase in FPS when the binning was increased from 0x to 2x to 4x (109.2, 207.9, and 377.0 FPS, respectively).

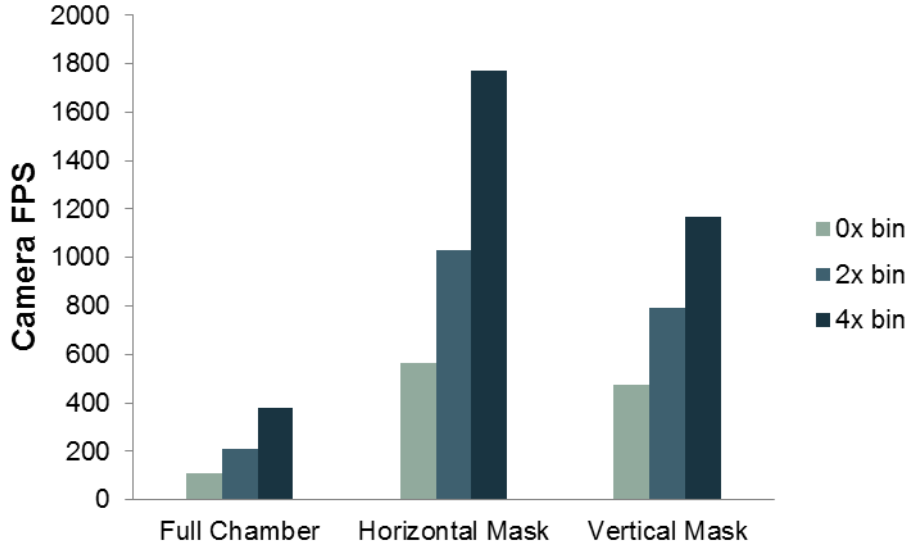

Figure 3.6. Macroscopic imaging apparatus acquision rate at varying masking orientations and binning sizes.

The masking orientation demonstrated a pronounced effect on total FPS captured with each recording; videos captured using a horizontally-positioned mask contained frame rates that were over 19% greater than equivalent videos captured with a vertically-positioned mask (567.0 vs. 475.5 FPS). This disparity in frame rate between horizontally-

and vertically-oriented acquisitions was further exacerbated when increasing the binning to 4x (a 51.8% difference was observed between conditions). Increasing the vertical shift speed (from 0.5 to 0.3 µs) was able to partially ameliorate the disparity between masking conditions (Fig. 3.7).

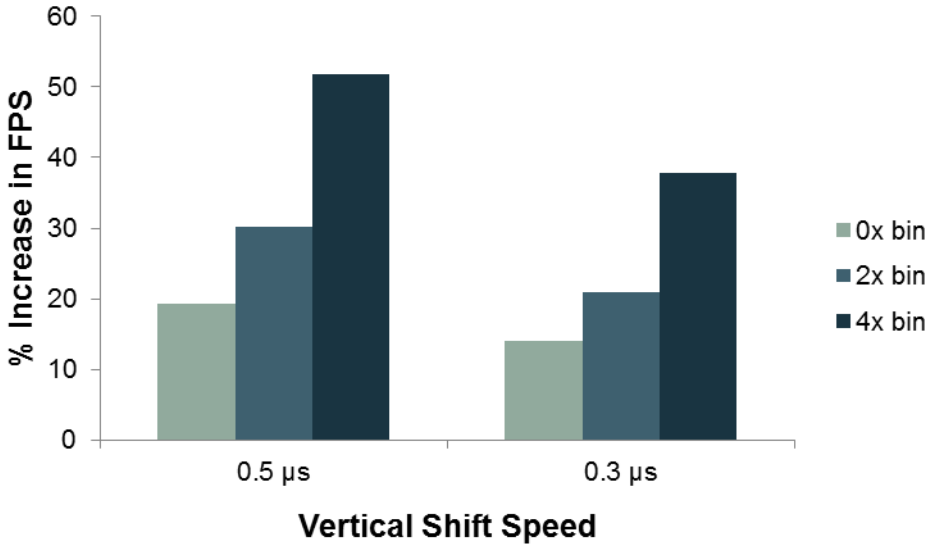

Figure 3.7. Percentage increase in FPS when using horizontal over vertical masking.

While the horizontally-masked videos demonstrated a 2.5-8.5% (0x to 4x bin) increase in FPS, the vertically-masked videos showed a 7.3-19.6% increase in FPS by increasing the vertical shift speed (Fig. 3.8).

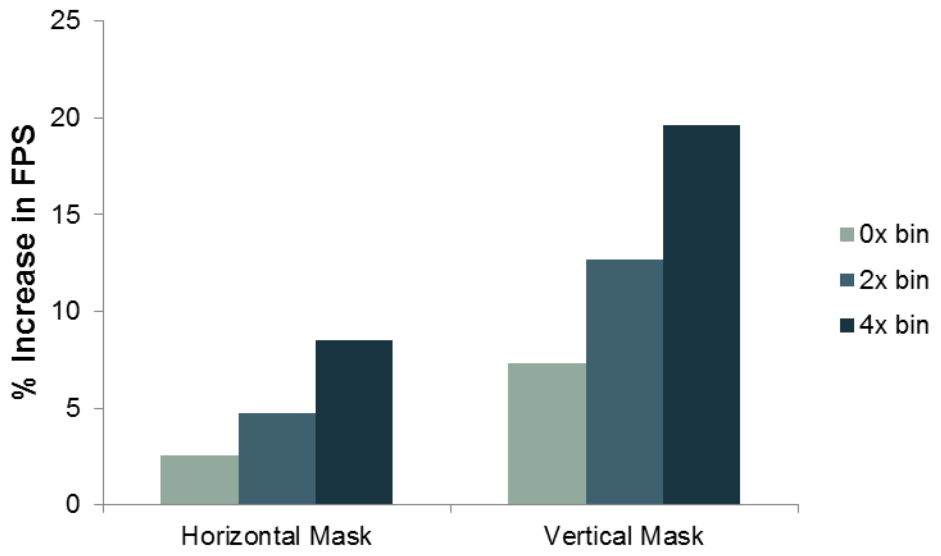

Figure 3.8. Percentage increase in FPS when using 0.3 over 0.5 µs shift speed.

Because an equivalent acquisition system was utilized for both imaging platforms, it was anticipated that similar trends involving masking orientation and shift speed would be observed for videos captured using the microscopic apparatus. To better identify additional trends in capture rate, a series of recordings were taken at different size intervals, at different masking orientations, and utilizing different objectives. Capturing the full field of view yielded frame rates of 55.5 to 201.7 FPS as the binning was increased from 0x to 4x (Fig. 3.9); little change in frame rate was observed through adjustment of the vertical shift speed (55.9 to 210.8 FPS for 0x to 4x bin). However, on a per pixel basis, videos acquired at the full field of view using the 4x bin provided only 22% as much data as videos captured using 0x bin setting (Fig. 3.10).

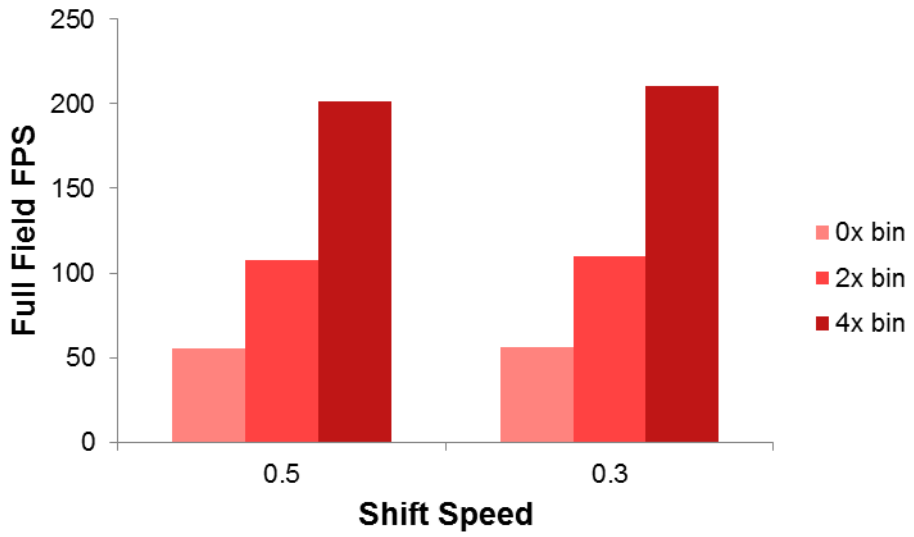

Figure 3.9. Full field FPS captured using the microscopic imaging apparatus at different shift speeds and bin settings.

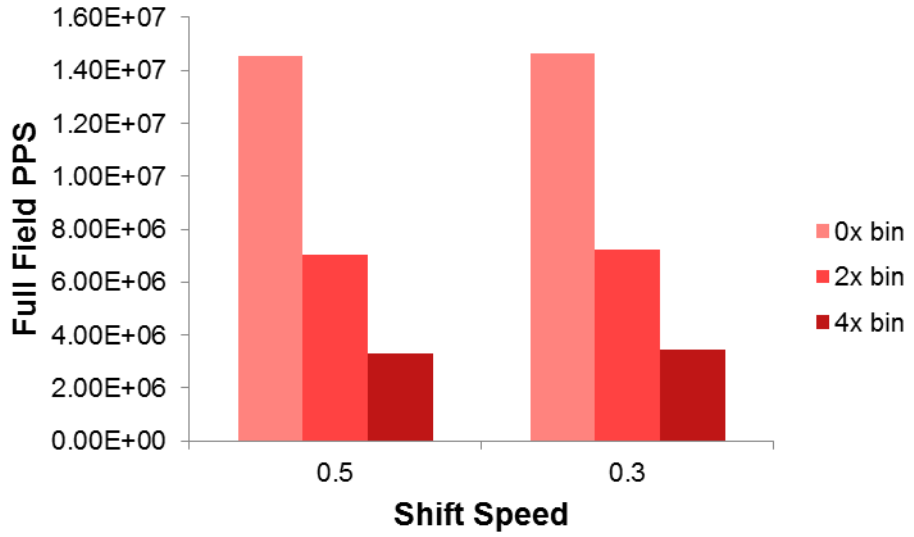

Figure 3.10. Full field pixels per second captured using the microscopic apparatus at varying shift speeds and bin settings.

Videos captured using a 2x objective at different size scales demonstrated the effects of masking and vertical video height on the total speed of acquisition. As

expected, videos captured using horizontal masking contained consistently higher FPS than vertically-masked videos of equivalent measureable area (with the exception of 3x1 mm) (Fig. 3.11).

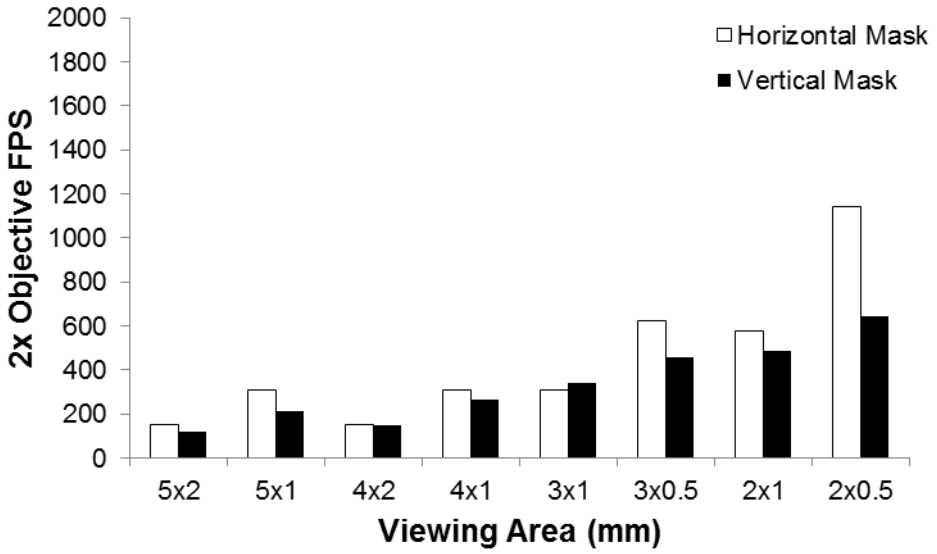

Figure 3.11. Effect of masking orientation on frame rate at different viewing areas.

However, it was observed that the frame rates of horizontally-masked recordings were dependent almost entirely on the number of vertical pixels; these videos produced the same frame rates independently of the number of horizontal pixels (for horizontal sizes 5x1, 4x1, and 3x1 mm, and for 5x2 and 4x2 mm) (Fig. 3.12).

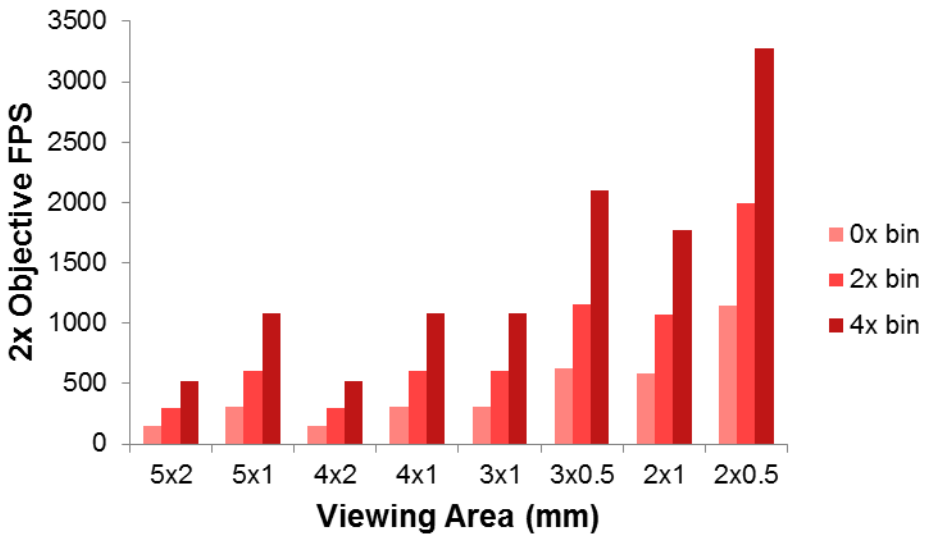

Figure 3.12. Effect of viewing area and bin setting on horizontally-masked frame rate.

Adjusting the objective size to accommodate the same visualized area (0.5x1 mm) produced the expected pixel number-dependent reduction in FPS as the objective was changed between 2x to 4x to 10x (Fig. 3.13).

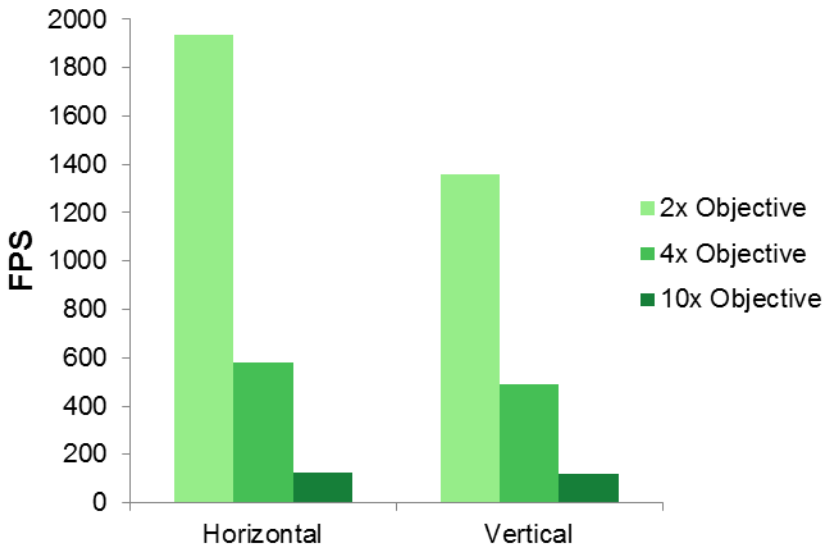

Figure 3.13. Effect of masking orientation and objective size on frame rate. Videos were acquired from a 1 x 0.5 mm region.

Optical mapping of cardiomyocytes

In order to evaluate the efficacy of the optical mapping platform, calcium wave propagations were captured from HL-1 cardiomyocyte monolayers using the microscopic and macroscopic imaging systems. Spontaneously propagating calcium waves captured using the microscopic system demonstrated similar transient velocities in comparison to those captured using the macroscopic system (0.26 ± 0.03 vs. 0.62 ± 0.67 cm/s). Furthermore, the calcium transient duration at 50% (604.8 ± 102.5 ms) and 80% (767.2 ± 117.6 ms) acquired using the microscopic system was also consistent with values obtained using the macroscopic system (50%: 418.7 ± 242.3 ms, 80%: 480.0 ± 288.8 ms). HL-1 cardiomyocytes were able to be successfully paced up to 1 Hz using exogenous stimulation in both systems.

3.4. Discussion

The purpose of this work was to create an adaptable multi-scale, multi-platform optical mapping system using frequently-available research hardware. This equipment represents a viable alternative to other custom or commercially available platforms, capable of quantifying mapping data from a range of different cardiac samples at macro- or micro-scale size ranges. Furthermore, fabrication of this system was carried out using laboratory equipment that is frequently available, with the addition of a relatively small number of easily-attainable components. Together, the ability to fabricate an optical mapping platform with these parameters provides not only a tool to acquire data from a wide gamut of different samples, but also offers an affordable means for researchers who want to enter into the field of optical mapping.

Existing optical imaging platforms, while effective at obtaining mapping data, are often limited to specific applications, such as acquisition of a single data type from a particular kind of sample. To address this limitation, additional work by others has led to the creation of more complex mapping systems capable of acquiring multiple data types, including capture of dual calcium-voltage data (Lee, Klos et al. 2012, Scull, McSpadden et al. 2012) and simultaneous voltage-mechanical movement data (Bourgeois, Bachtel et al. 2011). However, the creation of an existing optical mapping system into a flexible platform capable of acquiring data from a diverse range of sample types is a relatively novel concept in practice. In contrast, the described mapping system provides a means for quantifying electrophysiology for samples that were not previously compatible with a number of existing systems. The Andor iXon Ultra 897 CCD camera was selected specifically for this setup because it maintains high sensitivity to emitted light and

supports adjustable resolution at high frame rates via Optomask-assisted sensor cropping. Furthermore, the ability to mount the camera in a large-scale platform (in addition to a microscope port) allows for sampling from a wide range of different scales.

Benchmarking of the acquisition equipment validates the flexibility of the mapping system for obtaining data from a range of sample sizes. The engineered macroscopic mapping apparatus is capable of obtaining frame rates of the entire internal chamber (2.75x2.75 cm) in excess of 400 FPS (using 4x binning at 0.3 μs vertical shift speed). Furthermore, horizontally- and vertically- masked sections (2 x 1 cm) were capable of acquiring videos in excess of 500 FPS without the loss of resolution through binning. The authors established this size scale (184 x 92 pixels) as the minimum working resolution for the macromapping system due to challenges associated with analysis of smaller resolutions at this physical size scale. Because some samples could require sampling using a specific orientation, it was important to establish the relationship between masking direction and frame rate. Since CCD cameras are designed to scan horizontally, it was expected that horizontal masking would allow for faster data acquisition in comparison to vertically-masked videos. This increase in speed was between 19 and 52% depending on the binning conditions. This disparity in frame rate can be reduced by increasing the vertical shift speed; adjusting the vertical shift speed was able to increase the total frame rate by 7.3 to 19.6% for vertically-masked videos. In order to stabilize the signal at a higher vertical shift speed, the camera voltage was overclocked using the smallest setting available (+1); higher overclock settings are not recommended, as this will cause signal distortion between adjacent pixels, reducing the accuracy of the data analysis.

Evaluation of the acquisition system using the micro-scale apparatus revealed similar trends in FPS and masking orientation. In general, horizontally-masked videos contained higher frame rates than vertically-masked videos of the same size. Adjusting the vertical shift speed increased the FPS, with a greater improvement observed among vertically-masked videos.

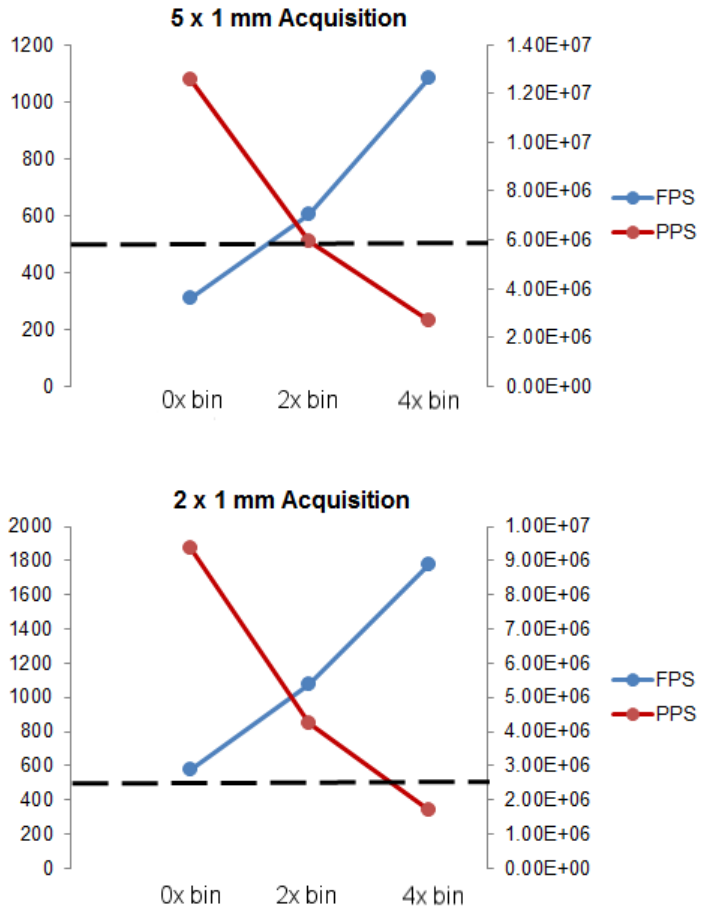

Figure 3.14. Frame rates (left, FPS) and total pixel acquisiton rates (right, PPS) from videos collected with a 2x objective. Dashed line represents a 500 FPS cut-off speed.

While adjusting the physical acquisition area, it was observed that video FPS was almost entirely dependent on the number of vertical pixels; this allows for the acquisition of

videos of large, narrow regions without significant loss in frame rate. For this reason, a 5 x 1 mm (448 x 90 pixels) and a 2 x 1 mm (180 x 90 pixels) region of interest (using a 2x objective) are recommended as the optimal size ranges depending on the sample and required rate of acquisition (Fig. 3.14).

A series of recordings taken of a specific physical range (1 x 0.5 mm) highlights the relationship between lost frame rate and increased resolution when progressing from a 2x to a 10x objective (Fig. 3.15). More importantly, this ability to acquire data with multiple objectives allows for fine-tuning of system parameters depending on the required resolution and inherent conditions of each sample (Fig. 3.16).

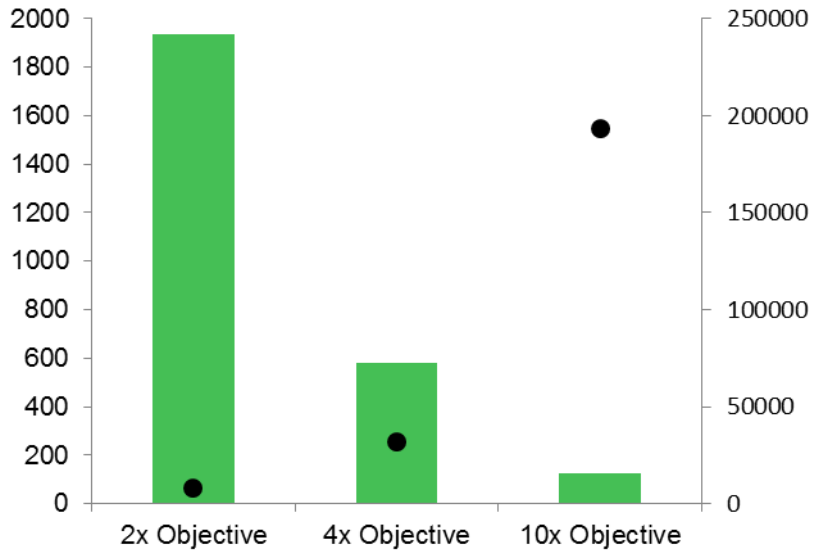

Figure 3.15. Relationship between FPS (left, bars) and resolution (total pixels, dots) when acquiring the same sized samples using different objectives.

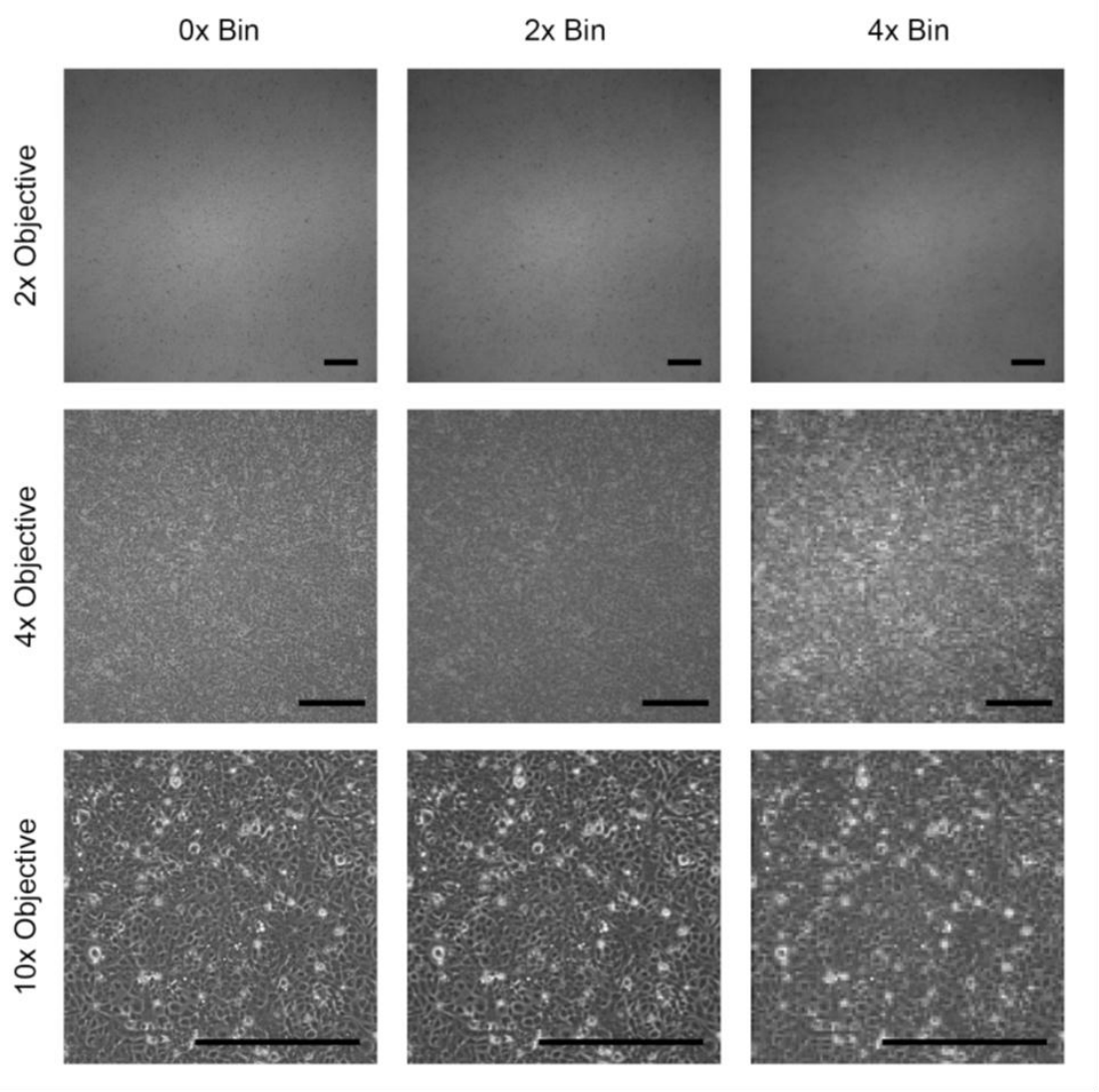

Figure 3.16. Images of HL-1 cardiomyocytes taken at different objective and bin settings. Scale bar represents 0.1 mm.

Analysis of calcium transients captured using the macroscopic and microscopic imaging systems demonstrates the range of sample sizes that can be processed using the novel mapping apparatus. A comparison of calcium transients recorded using each system reveals consistency among calcium transient velocities and calcium transient durations of HL-1 cardiomyocyte monolayers; analysis shows values of calcium transient velocities and durations to be on the same order of magnitude when data is collected from

either system. A small increase in calcium transient velocity was observed among recordings collected using the macroscopic system in comparison to those collected using the microscopic apparatus. While this change may be attributed to inherent variability among samples, the ability to evaluate larger areas of the HL-1 cardiomyocyte monolayer may have also contributed to this measured difference in calcium transient velocity. This ability to acquire and quantify data among larger sample areas underlines the value of the macroscopic apparatus and may be necessary for accurate evaluation of certain sample types.

3.5. Conclusions

The goal of this work was to develop a flexible optical mapping platform capable of acquiring data from samples of different size scales. Furthermore, it was of interest to construct this apparatus using commonly utilized laboratory equipment, making the construction of the system feasible for a wide range of research groups. A CNC-fabricated mapping chamber was fabricated to operate between a microscopic and macroscopic imaging apparatus. A CCD camera used in conjunction with an Optomask relay lens provided a method for acquiring video recordings at varying size scales and frame rates. Together, this device provides a novel system for capturing optical mapping data.

References

Becker, N., S. Stoelzle, S. Gopel, D. Guinot, P. Mumm, C. Haarmann, D. Malan, H. Bohlen, E. Kossolov, R. Kettenhofen, M. George, N. Fertig and A. Bruggemann (2013). "Minimized cell usage for stem cell-derived and primary cells on an automated patch clamp system." J Pharmacol Toxicol Methods 68(1): 82-87.

Bedada, F. B., M. Wheelwright and J. M. Metzger (2015). "Maturation status of sarcomere structure and function in human iPSC-derived cardiac myocytes." Biochim Biophys Acta.

Blazeski, A., G. M. Kostecki and L. Tung (2015). "Engineered heart slices for electrophysiological and contractile studies." Biomaterials 55: 119-128.

Bourgeois, E. B., A. D. Bachtel, J. Huang, G. P. Walcott and J. M. Rogers (2011). "Simultaneous optical mapping of transmembrane potential and wall motion in isolated, perfused whole hearts." J Biomed Opt 16(9): 096020.

Bursac, N., K. K. Parker, S. Iravanian and L. Tung (2002). "Cardiomyocyte cultures with controlled macroscopic anisotropy: a model for functional electrophysiological studies of cardiac muscle." Circ Res 91(12): e45-54.

Dedkova, E. N. and L. A. Blatter (2012). "Measuring mitochondrial function in intact cardiac myocytes." J Mol Cell Cardiol 52(1): 48-61.

Efimov, I. R., V. P. Nikolski and G. Salama (2004). "Optical imaging of the heart." Circ Res 95(1): 21-33.

Harding, S. E., N. N. Ali, M. Brito-Martins and J. Gorelik (2007). "The human embryonic stem cell-derived cardiomyocyte as a pharmacological model." Pharmacol Ther 113(2): 341-353.

Herron, T. J., P. Lee and J. Jalife (2012). "Optical imaging of voltage and calcium in cardiac cells & tissues." Circ Res 110(4): 609-623.

Kim, D. H., E. A. Lipke, P. Kim, R. Cheong, S. Thompson, M. Delannoy, K. Y. Suh, L. Tung and A. Levchenko (2010). "Nanoscale cues regulate the structure and function of macroscopic cardiac tissue constructs." Proc Natl Acad Sci U S A 107(2): 565-570.

Laurita, K. R., E. T. Chuck, T. Yang, W. Q. Dong, Y. A. Kuryshev, G. M. Brittenham, D. S. Rosenbaum and A. M. Brown (2003). "Optical mapping reveals conduction slowing and impulse block in iron-overload cardiomyopathy." J Lab Clin Med 142(2): 83-89.

Lee, P., M. Klos, C. Bollensdorff, L. Hou, P. Ewart, T. J. Kamp, J. Zhang, A. Bizy, G. Guerrero-Serna, P. Kohl, J. Jalife and T. J. Herron (2012). "Simultaneous voltage and

calcium mapping of genetically purified human induced pluripotent stem cell-derived cardiac myocyte monolayers." Circ Res 110(12): 1556-1563.

Lian, X., J. Zhang, S. M. Azarin, K. Zhu, L. B. Hazeltine, X. Bao, C. Hsiao, T. J. Kamp and S. P. Palecek (2013). "Directed cardiomyocyte differentiation from human pluripotent stem cells by modulating Wnt/beta-catenin signaling under fully defined conditions." Nat Protoc 8(1): 162-175.

Malkin, R. A., N. Kramer, B. Schnitz, M. Gopalakrishnan and A. L. Curry (2005). "Advances in electrical and mechanical cardiac mapping." Physiol Meas 26(1): R1-14.

Nygren, A., I. Baczko and W. R. Giles (2006). "Measurements of electrophysiological effects of components of acute ischemia in Langendorff-perfused rat hearts using voltage-sensitive dye mapping." J Cardiovasc Electrophysiol 17 Suppl 1: S113-S123.

Radisic, M., V. G. Fast, O. F. Sharifov, R. K. Iyer, H. Park and G. Vunjak-Novakovic (2009). "Optical mapping of impulse propagation in engineered cardiac tissue." Tissue Eng Part A 15(4): 851-860.

Robertson, C., D. D. Tran and S. C. George (2013). "Concise review: maturation phases of human pluripotent stem cell-derived cardiomyocytes." Stem Cells 31(5): 829-837.

Scull, J. A., L. C. McSpadden, H. D. t. Himel, N. Badie and N. Bursac (2012). "Single-detector simultaneous optical mapping of V(m) and [Ca(2+)](i) in cardiac monolayers." Ann Biomed Eng 40(5): 1006-1017.

Takahashi, T., B. Lord, P. C. Schulze, R. M. Fryer, S. S. Sarang, S. R. Gullans and R. T. Lee (2003). "Ascorbic acid enhances differentiation of embryonic stem cells into cardiac myocytes." Circulation 107(14): 1912-1916.

Yang, X., L. Pabon and C. E. Murry (2014). "Engineering adolescence: maturation of human pluripotent stem cell-derived cardiomyocytes." Circ Res 114(3): 511-523.

Zwi, L., O. Caspi, G. Arbel, I. Huber, A. Gepstein, I. H. Park and L. Gepstein (2009). "Cardiomyocyte differentiation of human induced pluripotent stem cells." Circulation 120(15): 1513-1523.

4. ENHANCED STEM CELL-DERIVED CARDIOMYOCYTE DIFFERENTIATION IN SUSPENSION CULTURE BY DELIVERY OF NITRIC OXIDE USING *S*-NITROSOCYSTEINE

4.1. Introduction

Heart disease has emerged as the leading cause of mortality among people living in developed nations, with coronary heart disease being responsible for approximately one in six deaths in the United States alone (Go, Mozaffarian et al. 2013). Chronic shortages of donor organs, coupled with the questionable long-term reliability of artificial hearts and ventricular assist devices have prompted the development of alternative treatments, such as novel cell therapies, to augment current methods for treating patients with heart disease. Interest in creating functional engineered heart tissue has led to further advancements in the design of cardiac constructs capable of integrating or repairing damaged myocardium in vivo, or emulating specific diseased phenotypes for in vitro diagnostic testing of pharmaceutical drug efficacy and toxicity (Wang and Guan 2010, Itzhaki, Maizels et al. 2011, Park, Larson et al. , Pok and Jacot 2011, Nunes, Miklas et al. 2013). Despite these developments, the ability to generate the quantities of functional cardiomyocytes necessary for clinical and diagnostic research applications remains an elusive goal. Pluripotent stem cells, with their ability to replicate indefinitely while maintaining the potential to differentiate into cell types from all three germ layers, hold promise in a multitude of tissue engineering applications, including myocardial repair (Zimmermann, Schneiderbanger et al. 2002, Serena, Figallo et al. 2009, W. Limpitikul 2011, Christoforou, Liau et al. 2013). While pluripotent stem cells have been heralded as a promising solution for treatment of heart disease, cardiomyocytes created from these cells often exhibit electromechanical properties which are markedly different from those

in native tissue; such differences would effectively disqualify the use of these cell types for regenerative cardiac clinical therapies and limit their usefulness as a diagnostic platform (Liau, Zhang et al. 2012). However, the ability to manipulate the behavior of these cell types during differentiation, such as through the induction of cardiogenic signaling pathways, may provide a platform for influencing the maturation of stem cell-derived cardiomyocytes (SC-CMs), yielding populations of cells which exhibit physiologically-relevant electromechanical properties. Enhanced electrical conduction, preferably anisotropic in nature, resilient mechanical structure and elongated shape of in vitro-derived cardiomyocytes would ultimately reduce the risk of arrhythmia formation and increase cardiac output post-implantation.

Although a number of methods have been utilized to differentiate pluripotent cells down the cardiomyocyte lineage (Burridge, Keller et al. 2012, Zwi-Dantsis and Gepstein 2012, Kadari, Mekala et al. 2014), many of these approaches are not readily scalable and the resulting cells are generally electrophysiologically immature. Immature cardiomyocytes may be characterized by a rounded and undersized morphology, incomplete calcium handling, and circumferential gap junction expression or organization resulting in reduced cell-cell coupling and slower calcium transient and electrical propagation (Robertson, Tran et al. 2013, Yang, Pabon et al. 2014). The use of electrical pacing or mechanical stretching of cells (W. Limpitikul 2011, Wang, Wang et al. 2013) and the use of chemical stimulation (Mummery, Zhang et al. 2012, Lian, Zhang et al. 2013, Lieu, Fu et al. 2013) to activate signaling pathways through supplementation of soluble growth factors, have shown beneficial effects for directing non-fated cells toward specific cardiac cell types, and, more importantly, for enhancing cardiomyocyte maturity

(Nunes, Miklas et al. 2013). Methods used by others to guide cardiac differentiation include: exposure to hypoxia (Millman, Tan et al. 2009, Niebruegge, Bauwens et al. 2009), mechanical stimulation (Schmelter, Ateghang et al. 2006), electrical pacing (W. Limpitikul 2011, Wang, Wang et al. 2013), or the introduction of signaling factors such as BMP-4 and ascorbic acid (Lieu, Fu et al. 2013). While these previous studies have demonstrated the efficacy of directed electromechanical and chemical stimulation, these approaches face significant challenges in scale-up due to implementation and cost constraints. Therefore, creation of an inexpensive, suspension-based cardiogenesis platform is crucial for advancing the capabilities of large-scale cell culture vessels for cardiac tissue engineering (Niebruegge, Bauwens et al. 2009, Sargent, Berguig et al. 2009, Jing, Parikh et al. 2010).

Whereas many of the described techniques are effective at cardiac differentiation in static culture environments, cell signaling via electrical and mechanical pacing or growth factor delivery is often limited by lack of homogeneity in cell stimulation, poor diffusivity of soluble factors, and high implementation cost in larger suspension culture systems. One potential option for inducing cardiac differentiation of stem cells, by overcoming these drawbacks, is through the delivery of nitric oxide (NO)-donating compounds. NO, a free radical gas with a relatively short half-life, is a potent signaling molecule responsible for a multitude of physiological operations including: vasodilation, neurotransmission, inflammation, inhibition of platelet activation, and direction of developmental and stem cell differentiation processes (Pelster, Grillitsch et al. 2005, Conti, Russomanno et al. 2013). Additionally, NO is known to play important roles in the pathology of certain diseases, while also simultaneously controlling several aspects of

healthy cardiovascular physiology. NO is synthesized naturally by the catalytic oxidation of L-arginine via upregulation of nitric oxide synthase (NOS) in response to changes in physical stress, intracellular ion concentrations, and extracellular matrix signaling. Binding of NO to the heme complex within the enzyme soluble guanylyl cyclase (sGC) leads to the conversion of guanosine triphosphate (GTP) into cyclic guanosine monophosphate (cGMP). In turn, cGMP further regulates gene expression, ion channel activity, and other signaling pathways (i.e. phosphate kinase G (PKG)) within the developing cardiomyocyte. Evidence has shown that inhibition of the NO-sGC signaling pathway leads to a marked decrease in the number of cardiomyocytes generated through differentiation (Kanno, Kim et al. 2004), further demonstrating the importance of the pathway in proper cardiomyocyte development. Previous studies have correlated the increase in spontaneous contraction of SC-CMs or embryoid bodies (EBs) with treatment from NO-donating compounds or sGC activators (Kanno, Kim et al. 2004, Mujoo, Sharin et al. 2008); however, these experiments did not examine the effects of NO on cardiac function and maturation. Further investigation is required to determine whether NO-donating compounds can be used to direct stem cells into electrophysiologically-consistent cardiac phenotypes, particularly in suspension culture systems.

The overall goal of this study was to establish the effects of NO donor addition on the yield and function of SC-CMs. We hypothesized that the addition of an NO donor during the course of differentiation would lead to higher yields of cardiomyocytes with well-developed structural and electrical properties. The concentration dependent effect of NO donor addition was quantified through changes in spontaneous contractile activity. Immunostaining, quantitative PCR, and calcium transient analysis were performed to

characterize the effects of the NO donor supplementation on the structural and functional phenotypes of these differentiated cell types.

4.2. Materials and Methods

All materials were obtained from Sigma-Aldrich (St. Louis, MO) unless labeled otherwise.

Expansion and differentiation of embryonic stem cells

A D3 mouse embryonic stem cell (mESC) line (kind gift of Drs. L. Tung and J. Gearhart), genetically modified for neomycin resistance on an α-MHC promoter, was used in all experiments (Klug, Soonpaa et al. 1996, W. Limpitikul 2011). Cultures of undifferentiated mESCs were expanded and maintained on mouse embryonic fibroblast (mEF) feeder layers (mitotically inactivated using gamma irradiation) in mESC culture medium containing: DMEM (Lonza, Walkersville, MD) with 10% (v/v) ESC-defined fetal bovine serum (FBS, Atlanta Biologicals, Norcross GA), 2 mM Glutamax (Gibco, Life Technologies, Grand Island, NY), 100 μM non-essential amino acids (Gibco), 1 mM sodium pyruvate (Gibco), 50 μg/mL gentamicin sulfate (Lonza), 55 μM β-mercaptoethanol (Gibco), and 103 U/mL leukemia inhibitory factor (LIF, Millipore, Billerica, MA). Prior to initiating differentiation, feeder layers were removed and mESCs were further expanded on gelatin-coated plates. Embryoid bodies (EBs) were formed via hanging drop method (at ~1000 cells per EB); after 48 hours EBs were collected and transferred into poly(hydroxyl)ethyl-methacrylate (poly(HEMA))-coated dishes. Ascorbic acid (at a working concentration of 570 μM) was added to culture media to facilitate cardiac differentiation. Media without ascorbic acid (non-treated control) was

used for all flow cytometry experiments so as to not bias results. Media was replaced in each dish after 96 hours of culture time.

Preparation and treatment of NO donor

A soluble NO donor was created and administered as the source of NO for use in cell signaling during differentiation. *S*-nitrosocysteine (CysNO) was prepared by adjusting a solution of L-cysteine and sodium nitrite in HEPES buffered saline (HBS) to pH 2 at 37°C for 30 min. A sterile-filtered, working stock of CysNO was adjusted to a pH 7.4 and administered at two different concentrations (50 µM and 100 µM) to separate populations of EBs in cell culture media; the volume of HBS added to each cell group was kept equal.

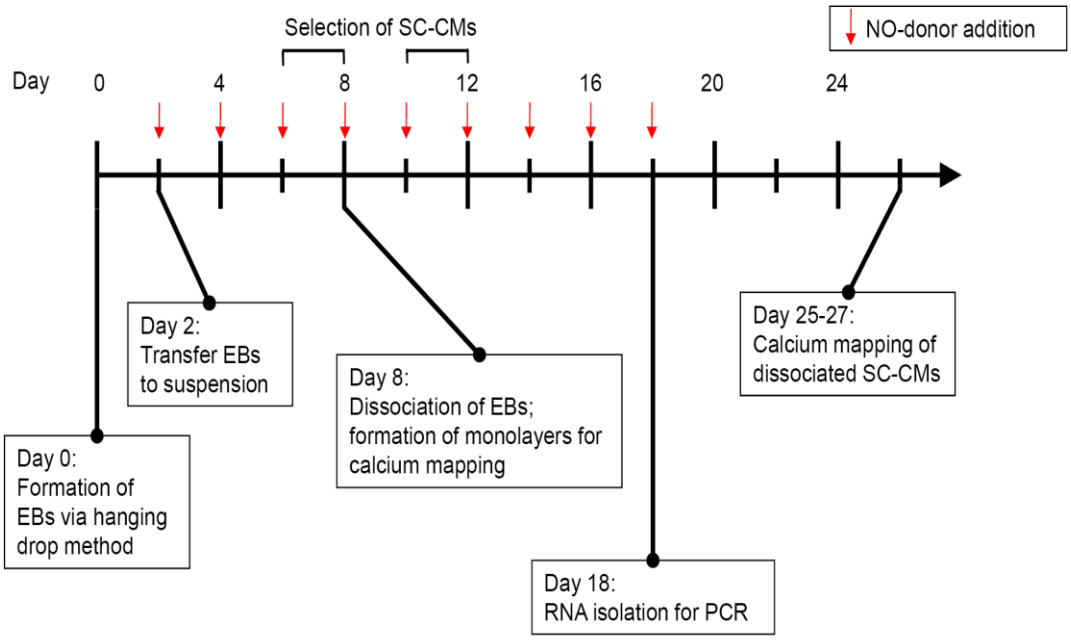

Figure 4.1. Timeline of CysNO delivery and experiments.

To assess release of NO, CysNO was also added to HBS and incubated at 37ºC; release of NO was characterized via Griess assay (Kushwaha, Anderson et al. 2010), a colorimetric assay which detects the presence of organic nitrites; results were quantified using a plate reader at an absorbance of 540 nm. EBs were treated with CysNO every 48 hours through day 18 in culture (Fig. 4.1). To block endogenous NO production by cGMP, a solution containing NOS inhibitor L-NAME (1 mM) was prepared in HBS and used in the treatment of one group of EBs. Treatment with HBS alone was also included as a control group.

Assessment of cell viability in response to CysNO treatment

Following CysNO treatment, the viability of differentiated cells was assessed; this is relevant due to the fact that, NO acts as a cell signaling molecule at low concentrations and is cytotoxic at high concentrations. On day 21, EBs from each treatment condition were incubated in Live/Dead® reagent (Invitrogen, Carlsbad, CA), containing calcein-AM and ethidium homodimer-1, for 30 minutes. Live cells are characterized by intracellular esterase activity which cleaves the calcein-AM to form fluorescent green calcein. Dead cells are identified by presence of red fluorescent ethidium homodimer-1, which enters the cytosol through the ruptured cell membrane and binds to nucleic acids. EBs were imaged using an inverted fluorescence microscope (Nikon Eclipse Ti-U) and an Andor Luca S camera. Viability of EBs was quantified using the 3D Object Counter plugin in ImageJ software (NIH). For each condition, a minimum of 5 EBs were assessed to determine viability.

Characterization of spontaneous contractile activity, size, and morphology of EBs

Spontaneous contractile activity assessment provides the ability to track cardiac differentiation (Niebruegge, Bauwens et al. 2009). EBs in suspension culture were observed for spontaneous contractile activity using visual microscopy. At each time point, data was collected prior to media change and the addition of fresh CysNO, thereby eliminating the effects of any actively released NO during observations. Measurements were carried out over days 8 through 14 and percentage of spontaneously contracting EBs, as well as the frequency of contractions, were recorded for each condition. For each condition, a minimum of 3 differentiation batches, each containing at least 30 EBs, were assessed at each time point to determine percentage of contracting EBs. Frequency of contraction was assessed by examining video recordings of contracting EBs and averaging the number of contractions over a 30 s period; a minimum of 8 EBs per day per condition were quantified from at least 4 differentiation batches. To determine the effect of CysNO treatment on EB morphology, phase contrast images were taken of EBs on days 5, 10 and 14. EB size and sphericity was quantified using ImageJ; a minimum of 30 EBs per condition were quantified from at least 3 differentiation batches.

Analysis of cardiomyocyte population with flow cytometry

On day 8, EBs were dissociated into single cells for use in flow cytometry analysis. Samples of EBs underwent a 90 min incubation in a defined dissociation solution containing: potassium chloride (5.4 mM), magnesium sulfate (5 mM), sodium pyruvate (5 mM), glucose (20 mM), taurine (20 mM), HEPES (10 mM), type 2 collagenase (Worthington, 1 mg/mL), and calcium chloride (30 µM) (pH 6.9), followed by 5 minute incubation in 0.25% trypsin; all cells were singularized by pipetting.

Approximately $5x10^5$ cells were incubated in 1 µL Zombie-NIR viability dye (BioLegend) for 15 min prior to neutralization using a 10% FBS solution. Dissociated cells were then incubated in 4% (vol/vol) paraformaldehyde (Electron Microscopy Sciences) for 20 minutes at room temperature. Cells were subsequently incubated in 90% (vol/vol) cold methanol (Fisher Scientific) at 4 ºC for 15 minutes. Cells were washed with 10% (vol/vol) FBS in PBS, followed by incubation in primary antibody (cardiac troponin T (cTnT), Thermo Fisher Scientific) diluted in 1% (vol/vol) FBS and 0.1% (vol/vol) Triton X-100 in PBS at 4 ºC overnight. Cells were then washed with 1% (vol/vol) FBS and 0.1% (vol/vol) Triton X-100 in PBS and incubated in 100 µL secondary antibody (Alexa Fluor 488 goat anti-mouse, Invitrogen) diluted in 1% (vol/vol) FBS and 0.1% (vol/vol) Triton X-100 in PBS for 30 minutes at room temperature. Labeled cells were washed with 1% (vol/vol) FBS and 0.1% (vol/vol) Triton X-100 in PBS and resuspended in 10% (vol/vol) FBS in PBS. Analysis was carried out using BD Accuri and FlowJo software.

Dissociation of stem cell-derived cardiomyocytes

Dissociation of EBs was performed to create monolayers of SC-CMs for immunocytochemistry and calcium transient analysis (Kehat, Kenyagin-Karsenti et al. 2001). Briefly, PDMS-coated glass coverslips were prepared using a spin coater and sterilized overnight in ethanol. After drying the coverslips with a nitrogen gun, a solution of PBS containing fibronectin (25 µL/mL) was added on the coverslips and incubated at room temperature for 1 hour. EBs from control and CysNO-treated populations were rinsed with PBS; EBs were then agitated in dissociation solution in a 37°C water bath for 45 min. In order to maximize recovery of SC-CMs, the digested material was further

agitated in a resuspension solution containing: potassium chloride (85 mM), potassium phosphate dibasic (30 mM), magnesium sulfate (5 mM), EGTA (1 mM), magnesium-ATP (2 mM), sodium pyruvate (5 mM), creatine (5 mM), taurine (20 mM), and glucose (20 mM) for an additional 15 min. After centrifugation and resuspension in media, the cell suspension was dispensed at approximately $1x10^5$ SC-CMs per cm^2 onto the sterile, PDMS-coated glass cover slips in well plates. To ensure cellular confluency on the material surface, SC-CMs in concentrated suspension were allowed to adhere for four hours prior to filling wells with additional media.

Analysis of protein expression with immunocytochemistry

Monolayers of SC-CMs were subjected to immunocytochemistry to identify expression patterns of cardiac-specific proteins. Monolayers of SC-CMs were selected for cardiomyocytes by addition of 16 μL/mL of G418 neomycin in culture media starting at 48 hours and continued through 96 hours post-dissociation. Selected SC-CMs were fixed using a 50:50 mixture of ethanol and acetone, permeabilized using a 0.1% Triton X-100 solution in PBS, and blocked using a 10% solution of FBS in PBS. SC-CMs were subsequently incubated with rabbit-anti-connexin-43 antibody (1:200, Sigma) and either mouse-anti-α-sarcomeric-actinin (1:400, Sigma) or mouse-anti-cardiac troponin I (1:200, Millipore) for 3 hours at room temperature. After washing, SC-CMs were incubated in secondary antibodies, Alexa Fluor 488 goat-anti-rabbit (1:200, Invitrogen) and Alexa Fluor 568 goat-anti-mouse (1:200, Invitrogen), for 2 hours at room temperature. SC-CMs were counterstained with DAPI (1:36000 from stock, Invitrogen), dehydrated and mounted in Prolong Gold (Life Technologies). Images were captured using confocal microscopy (Nikon AI Confocal Scanning Laser Microscope).

Quantification of gene expression with qPCR

To identify the effect of NO on the genetic phenotype of cell types resulting from differentiation, populations of EBs were treated with CysNO as described previously. RNA was isolated from 5 separate differentiation batches from day 18 EBs using MicroElute Total RNA Kit (Omega Biosciences, Norcross, GA). Briefly, EBs were physically disrupted in lysis buffer prior to homogenization (homogenization columns, Omega Biosciences); RNA was isolated and purified according to the manufacturer's instructions. The concentration of diluted RNA was determined via spectroscopy (NanoDrop, Thermofisher) prior to synthesis of cDNA (qScript cDNA SuperMix, Quanta Biosciences, Gaithersburg, MD). Quantification of genes was carried out via qPCR using a SYBR green amplification kit (PerfeCTa SYBR Green SuperMix, Quanta Biosciences). Thermocycler settings for PCR were 95°C for 5 minutes, followed by 40 cycles of amplification at 95°C for 10 seconds, and 53°C for 30 seconds. GAPDH was used as a housekeeping gene for all trials. Analysis of gene expression was carried out using the ΔΔCt method. A list of all primers used for quantification is available in Table 4-1.

Table 4-1. Primers for qPCR

Gene	**Forward**	**Reverse**
Cx43	GGTGGACTGCTTCCTCTCAC	ATCGCTTCTTCCCTTCACG
αMHC	CTTCAACCACCACATGTTCG	TGTCATACAGCTTGGCCTTG
βMHC	GCCAAAACACCAACCTGTCCAAGTTC	CTGCTGGAGAGGTTATTCCTCG
Cav1.2	ATGATTCGGGCCTTTGTTCAG	TGGAGTAGGGATGTGCTCG
Serca2a	AAGCTATGGGAGTGGTGGTG	GCAATGCAAATGAGGGAGAT
GAPDH	GAAGGGCATCTTGGGCTAC	GCCTCTCTTGCTCAGTGTCC
RyR2	TGAGTTCCTGCTGTCCTGTG	CTCTGCCAACTCCAAGAAGG

Assessment of calcium handling

To assess changes in the electrophysiological function of SC-CMs differentiated in the presence of NO, calcium transients of SC-CMs were characterized (Ding, Zou et al. 2006). Monolayers of SC-CMs were selected for cardiomyocytes by addition of 16 µL/mL of G418 neomycin in culture media starting at 48 hours and continued through 96 hours post-dissociation. Selected SC-CM monolayers were stained using 1 mM Fura-2AM dye in DMSO (5 µL/mL media) for 30 minutes. Slides were immediately washed with Tyrode's Solution and transferred to an IonOptix Myocyte Calcium and Contractility Recording System (IonOptix, Milton, MA). Cells were initially paced at the minimum threshold voltage at 0.5 Hz; pacing frequency was increased until reaching the maximum capture rate, the highest frequency at which a 1:1 correspondence between pacing and cell response was observed. Recordings of contracting cells were taken over a period of at least 60 seconds. A total of 12 calcium transients per condition were assessed using samples from at least 3 separate differentiations.

Recordings of spontaneously propagating calcium waves of SC-CM monolayers were acquired using optical mapping. The calcium dye was prepared by adding 5 µl of 100 µM Rhod-2 (Invitrogen) and 5 µl of Pluronic/ml to Tyrode's solution. 1 ml of this solution was added to each well and allowed to incubate at room temperature for 20 minutes before rinsing with Tyrode's solution. Videos of propagating calcium waves were recorded at room temperature (22°C) without exogenous stimulation (i.e., spontaneous contraction). After recording, the samples were analyzed using a modified version of a previously described MATLAB (Mathworks, Natick, MA) script (Lim, Maskara et al. 2006, Weinberg, Lipke et al. 2010). Using this script, samples were

analyzed for calcium transient velocity, calcium transient duration (at 50% and 80% repolarization), and calcium transient frequency.

Statistical analysis

All data is presented as means ± standard deviations. Statistical analysis was carried out using Minitab software (State College, PA). Multivariate differences between groups were identified using 2-way ANOVA followed by Tukey's test for multiple comparisons. Univariate differences between groups were determined using a two-tailed, unpaired Student's t-test. The normality of each condition was determined using the Anderson-Darling Normality Test; the assumption of normality was confirmed for individual treatments at each time point for use in ANOVA. Significance was determined in cases where $p < 0.05$. Unless otherwise noted, a minimum of 3 samples per condition from at least 3 differentiation batches were evaluated. All figure error bars represent standard deviations.

4.3. Results

Analysis of NO delivery from CysNO

Because NO has a half-life of only a few seconds when administered in a gaseous form, a NO-donating compound was generated to extend the release time of the molecule (Liu, Miller et al. 1998). CysNO, an *S*-nitrosothiol NO donor, was selected for this study, to mimic the release characteristics of NO in native physiology; in vivo systems rely on *S*-nitrosothiols for NO storage, transport, and metabolism, as well as mediation in NO-signaling pathways (Seneviratne, Godoy et al. 2013). In order to evaluate duration, release profile and total concentration of NO released, delivery of NO from CysNO was

quantified by measuring changes in nitrite concentration using the Griess assay. NO release curves for solutions of HBS containing 50 µM or 100 µM CysNO at 37ºC are shown in Figure 4.2.

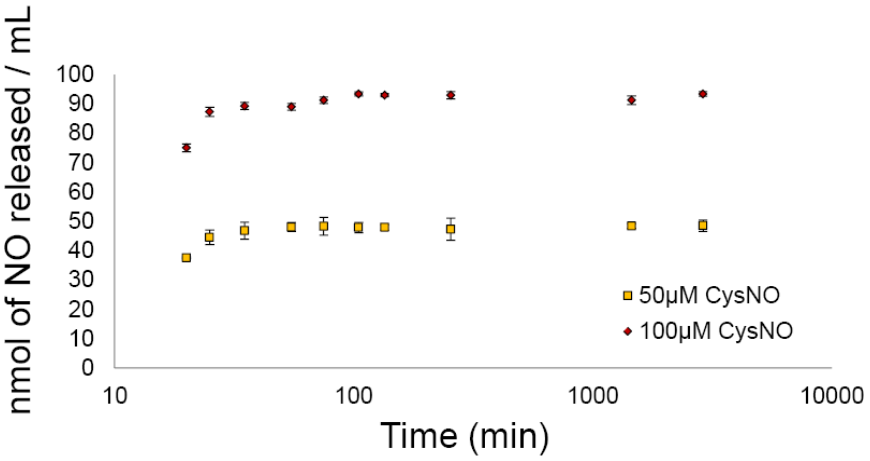

Figure 4.2. Profile and extent of nitric oxide release was characterized for 50 and 100 µM CysNO solutions in HBS using the Griess assay.

Analysis of nitrite concentrations in solution via Griess assay indicated 90% to 95% release of NO occurred within 90 minutes with the remaining NO released over the course of 48 hours. Although this release profile is highly rapid, the effects of NO released from similar soluble NO-donating compounds have shown lasting effects for 1-2 weeks in culture (Kanno, Kim et al. 2004).

Morphology and viability retained in CysNO-treated EBs

Smooth, dense, highly round EB morphologies have been associated with high yields of contracting cells. Therefore, as a first assessment of EB response to CysNO treatment, the size and morphology of EBs was observed over the course of differentiation. EBs were formed using the hanging droplet method to ensure initial

uniformity. To confirm consistency of EB morphology and size between treatment conditions over time, EBs were visualized using phase contrast microscopy. Representative images taken on day 7 are shown in Figure 4.3. EB size on days 5, 10, and 14 was quantified for the control and 100 µM CysNO-treated samples (Fig. 4.3).

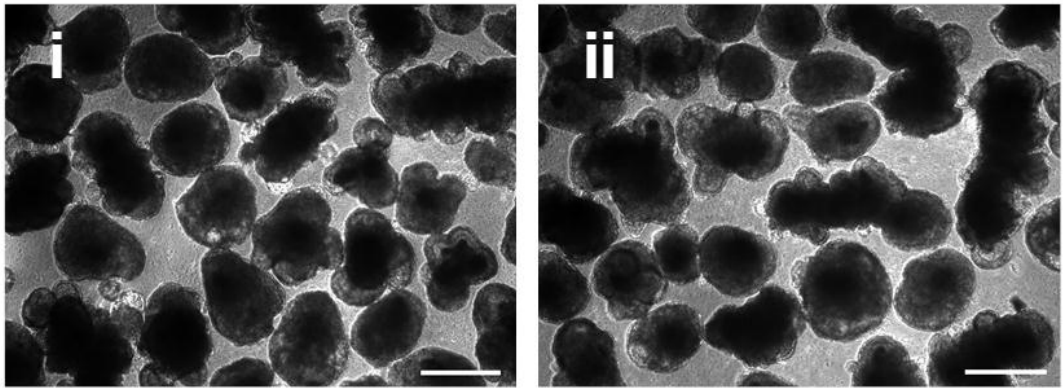

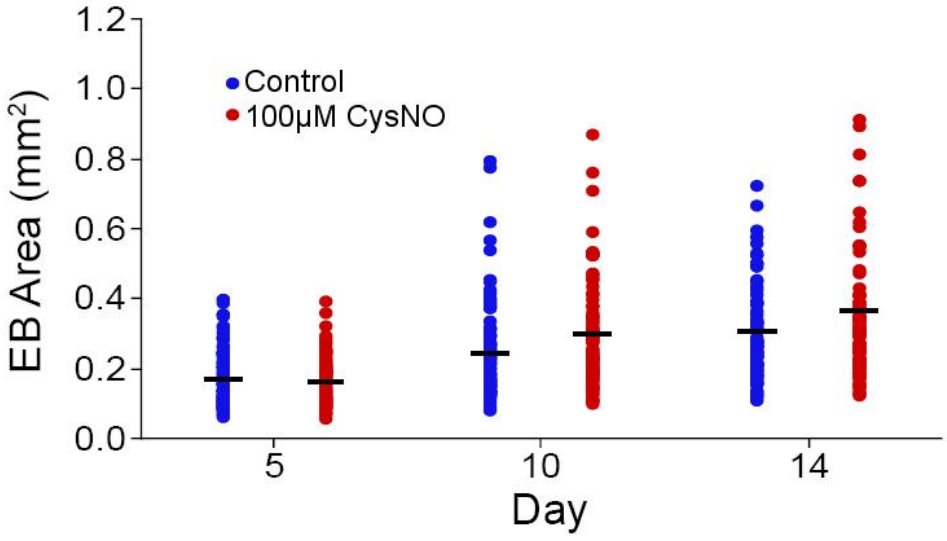

Figure 4.3. (i) CysNO treated EBs were morphologically-consistent with (ii) control EBs. Scale bars represent 500 µm.

Average EB size was consistent between control (D5: 0.180±0.090 mm^2, D10: 0.245±0.140 mm^2, D14: 0.300±0.155 mm^2) and CysNO-treated EBs (D5: 0.170±0.070 mm^2, D10: 0.290±0.150 mm^2, D14: 0.350±0.220 mm^2) on each day. Additionally, no significant difference was observed for the sphericity of control EBs (D5: 0.940±0.030, D10: 0.920±0.050, D14: 0.900±0.070) or CysNO-treated EBs (D5: 0.940±0.020, D10: 0.930±0.035, D14: 0.930±0.045) on each day (data not shown).

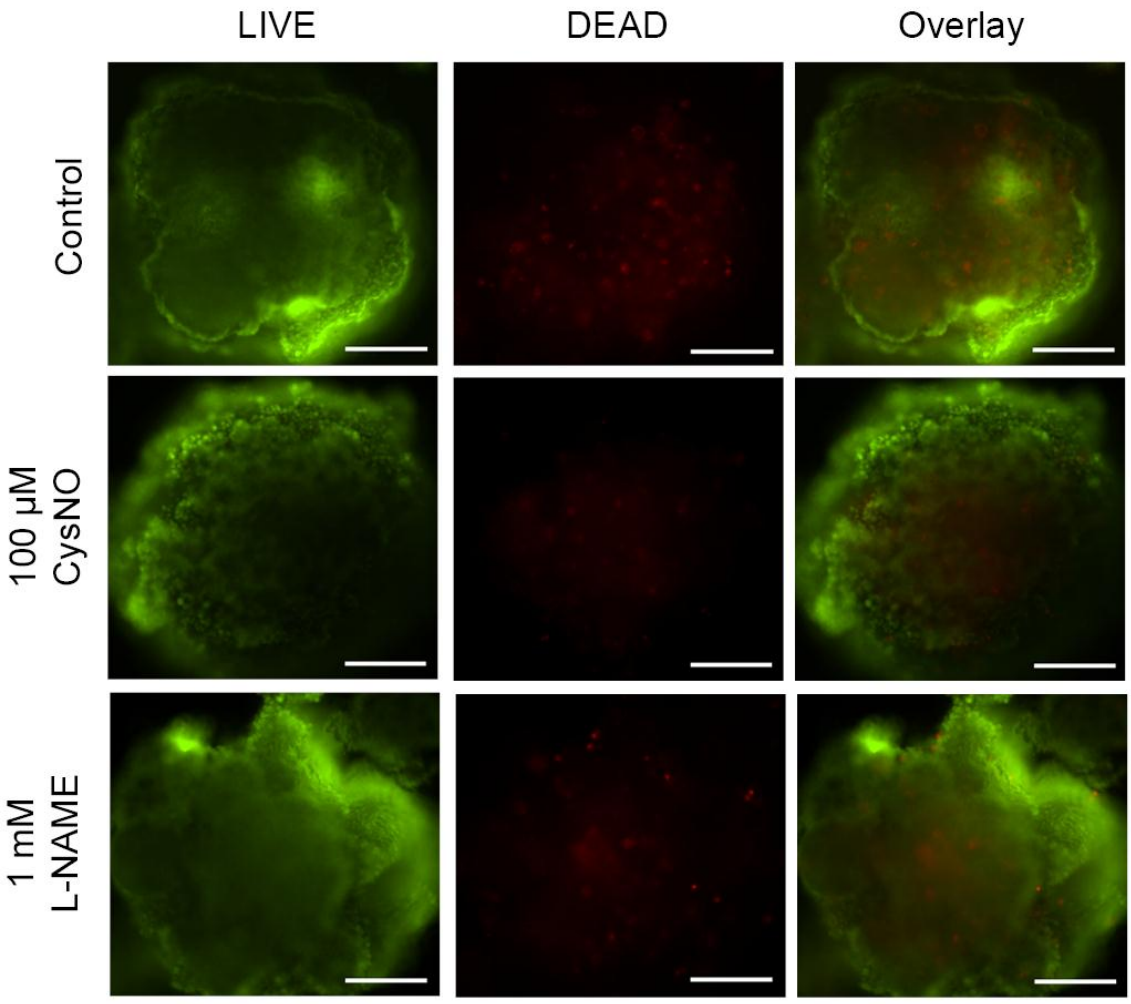

Figure 4.4. CysNO and L-NAME EBs stained with LIVE/DEAD reagent. Scale bars represent 200 µm.

The effect of NO on cellular function is concentration and cell type dependent; NO acts as an important cell signaling molecule at lower concentrations and as a cytotoxin at higher concentrations. It was therefore important to determine whether treatment with CysNO or the NOS inhibitor L-NAME resulted in differing numbers of viable cells within EBs. After analysis of Live/Dead stained images, high cell viability was observed for all treatment groups (Fig. 4.4) with no quantitative difference in viability observed between CysNO- (94.4±4.6%) or L-NAME-treated EBs (94.1±2.4%) and the control EBs (92.2±4.8%) (Fig. 4.5).

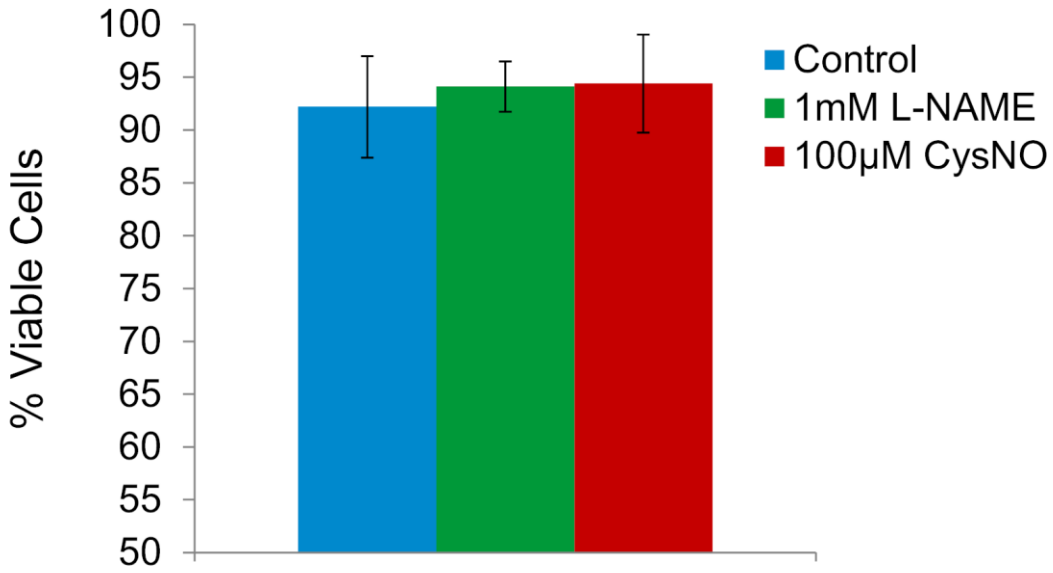

Figure 4.5. CysNO and L-NAME treatment had no effect on cellular viability.

Spontaneous contractile activity increased in NO-treated EBs

The percentages of spontaneously contracting EBs and the frequencies of contraction were evaluated for populations of suspension-cultured EBs treated with either CysNO or L-NAME. The percentage of spontaneously contracting EBs was dependent both on treatment condition and the time elapsed since initiation of differentiation. Some

populations of EBs elicited spontaneous contraction as early as 6 days after the onset of differentiation and every group demonstrated pronounced contraction by day 8. By day 14, many of the EBs within each treatment group demonstrated a reduction in spontaneous contractile activity (or complete absence of contraction), as is typical in static suspension culture (Shafa, Krawetz et al. 2011). NO treatment was able to partially ameliorate this reduction in contractile activity of suspension-cultured EBs as detailed below.

The percentage of EBs exhibiting spontaneous contraction on day 8, ranged from 70% to 85% depending on the treatment and the batch; a slightly higher percentage of CysNO treated EBs contracted spontaneously (81.0±13.5% and 85.3±11.1% for 50 μM and 100 μM, respectively) than for control (70.7±15.1%) or L-NAME (71.4±20.3%) treated EBs (Fig. 4.6). On day 10, the percentage of EBs exhibiting spontaneous contraction remained similar to day 8 for all conditions. By day 12, however, the percentage of EBs exhibiting spontaneous contraction was lower, particularly for control and L-NAME treated EBs where only approximately 45% and 42%, respectively, still exhibited spontaneous contraction. As alluded to above, the percentage of spontaneously contracting EBs in CysNO treated groups did not decrease as rapidly with time. In comparison to the control EBs, the percentage of spontaneously contracting EBs receiving 50 μM or 100 μM CysNO treatment remained higher after 14 days in culture (control: 42.2±10.7%; 50 μM: 53.5±10.0%; 100 μM: 64.7±17.0%, $p^{*}<0.05$ compared to control). The percentage of spontaneously contracting L NAME treated EBs was similar to control at all time points, with an even slightly lower percentage of spontaneously contracting EBs by day 14 (35.1±3.3%). On days 10, 12 and 14, the percentage of

spontaneously contracting EBs in the 100μM CysNO-treated group was statistically greater than the percentage in the L-NAME treated group and significantly greater than the percentage of contracting EBs in the control group on day 12 (Fig. 4.6).

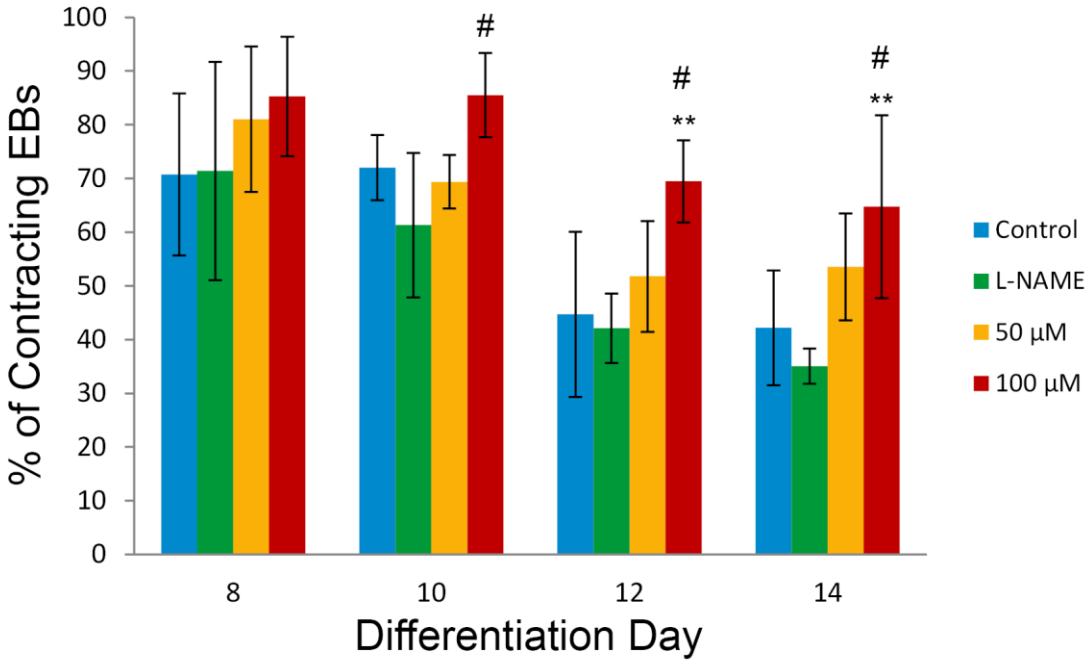

Figure 4.6. Percentage of contracting EBs in culture by day.

Analysis of total cardiomyocyte number via flow cytometry revealed that CysNO-treated EBs were composed of a significantly greater number of cardiac troponin T positive cells (100 μM CysNO, 21.5±9.7%) as compared to non-treated control EBs (14.1±7.5%, $p^{*}<0.05$) on day 8 (Fig. 4.7). High standard deviations are the result of batch-to-batch variability, which is typical for this type of static suspension differentiation technique; however, when compared on a batch-wise basis, CysNO-treated EBs demonstrate a 70% increase in total cardiomyocyte number over the non-treated control EBs (Fig. 4.8).

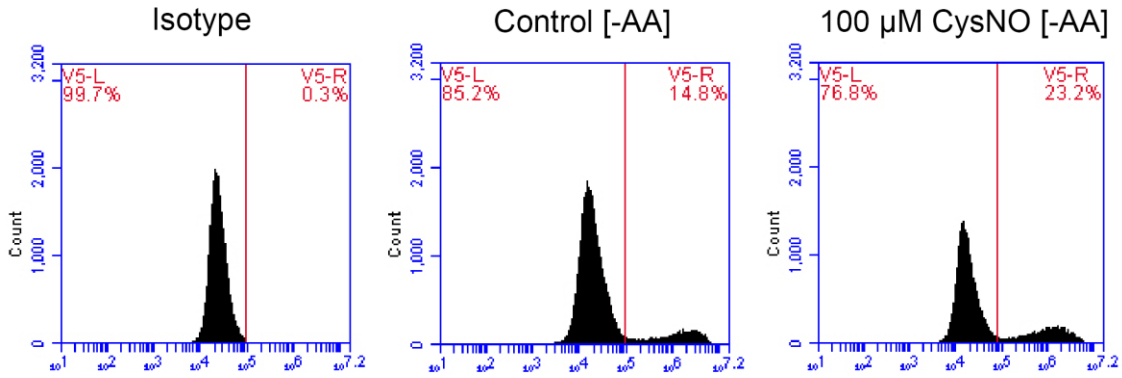

Figure 4.7. Day 8 EBs contain a higher percentage of cardiac troponin T positive cells after CysNO treatment.

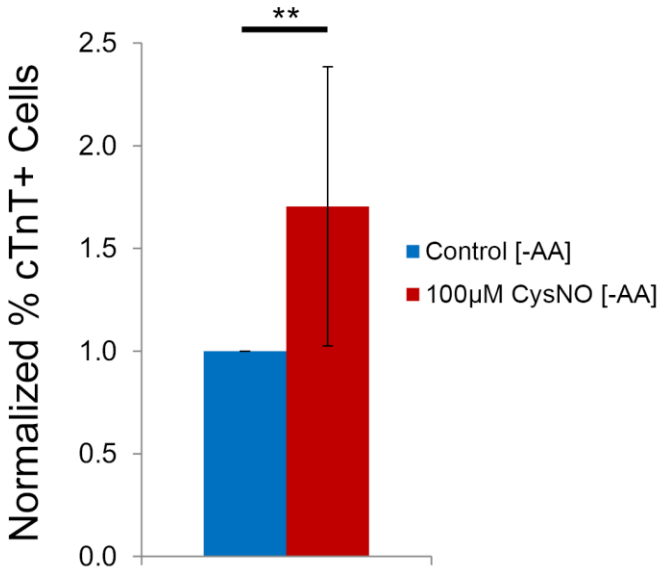

Figure 4.8. Normalized flow cytometry values show a 70% increase in cardiac troponin T positive cells from EBs with CysNO treatment.

To better visualize time point specific differences in spontaneous contraction between treatment groups, data from each time point was normalized batch-wise with respect to control EBs. As shown in Figure 4.9, CysNO treatment during differentiation resulted in a higher percentage of EBs exhibiting spontaneous contraction at each time

point. The greatest differences were observed at late differentiation time points. At the highest concentration CysNO treatment tested (100 µM), the normalized percentage of spontaneously contracting EBs was significantly higher than that of control group on day 14 and that of L-NAME group on day 10 (1.19±0.14) and day 14 (1.53±0.08, $p < 0.05$). Additionally, the 50 µM CysNO treated EBs also experienced a significantly larger contraction percentage than control or L-NAME EBs on day 14 (1.42±0.03, $p < 0.05$). Overall, CysNO treatment resulted in EBs maintaining spontaneous contraction at higher percentages than controls throughout the course of this study; this increase in percentage of contracting EBs with CysNO treatment was dose-dependent.

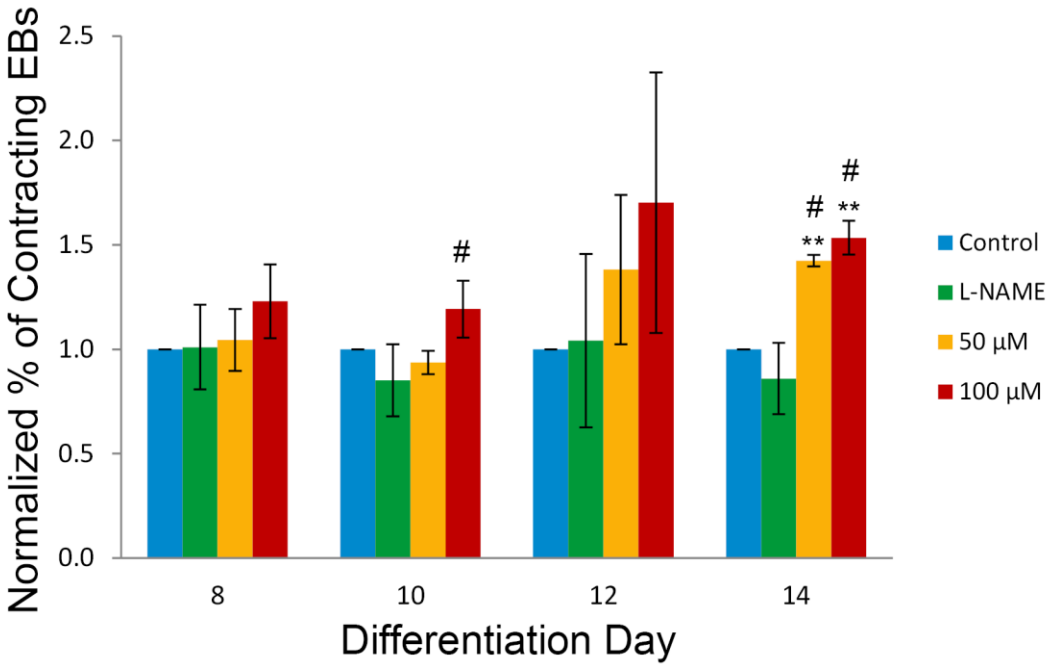

Figure 4.9. Normalized percentages of contracting EBs by day.

In addition to CysNO treatment enhancing the percentage of spontaneously contracting EBs, the average frequency of contraction for CysNO-treated EBs was higher

than that for control or L-NAME treated EBs. As differentiation progressed, trends in the frequency of contraction differed between treatment groups (Fig. 4.10). All groups exhibited a similar frequency of contraction on day 8. From day 8 to day 14, the frequency of contraction of control EBs decreased slightly from approximately 1.3 to 1.1 Hz. In contrast, the frequency of contraction for CysNO-treated EBs trended upward with time. To make comparisons between conditions on a particular day of differentiation, frequency of contraction data from each time point was again normalized by batch against control values (Fig. 4.11).

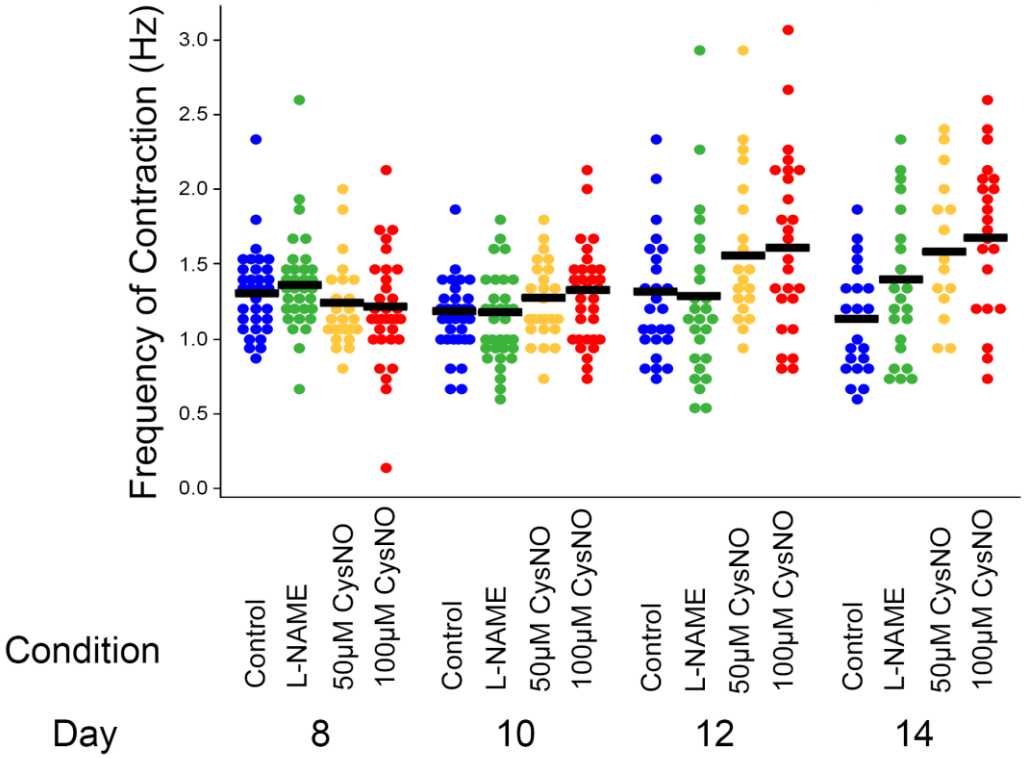

Figure 4.10. Frequency of EB contraction by day.

EBs treated with 50 µM and 100 µM CysNO exhibited significant higher spontaneous contractile frequency on day 14 as compared to control (50µm: 1.36±0.39; 100µm:

1.52±0.41). No significant difference was observed in normalized spontaneous contractile frequency of EBs receiving L-NAME compared to control EBs (1.19±0.41). Additionally, similar ranges of frequency of contraction were observed among each day across all groups. In summary, CysNO treatment resulted in EBs exhibiting increased spontaneous contraction frequencies as compared to control EBs after a period of approximately two weeks.

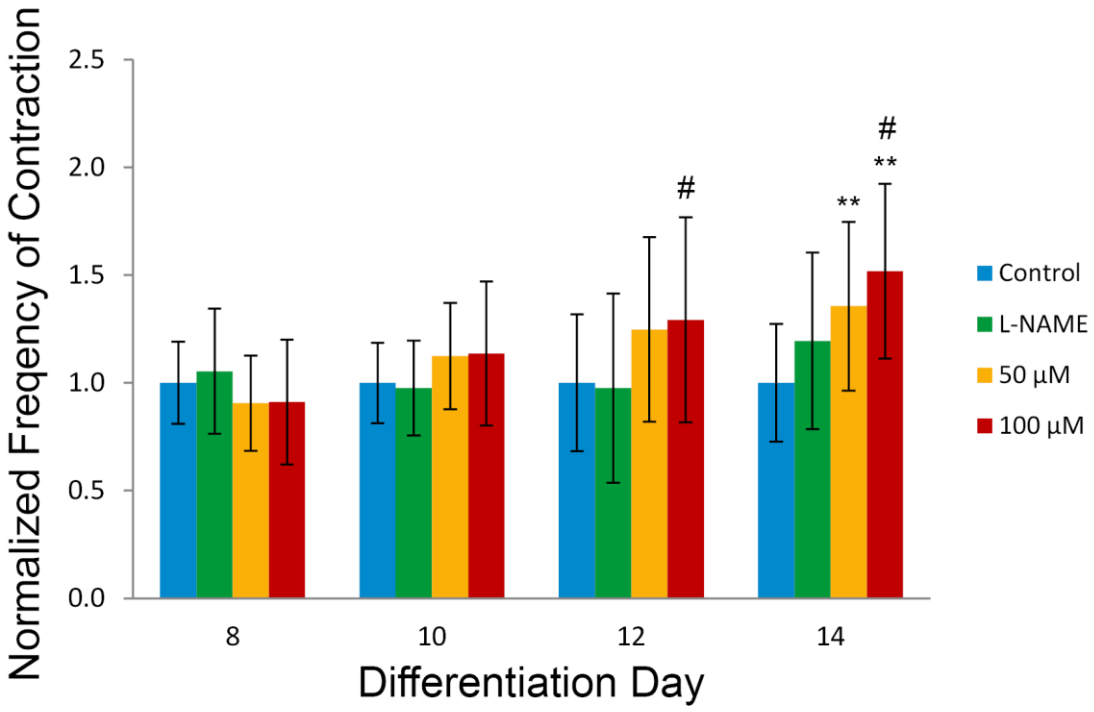

Figure 4.11. Normalized frequency of contracting EBs by day.

Expression of βMHC enhanced via treatment with CysNO

Monolayers of both 100µM CysNO-treated and control SC-CMs (day 18) showed positive expression of cardiomyocyte proteins α-sarcomeric actinin, cardiac troponin I, and connexin-43 (Cx43) (Fig. 4.12).

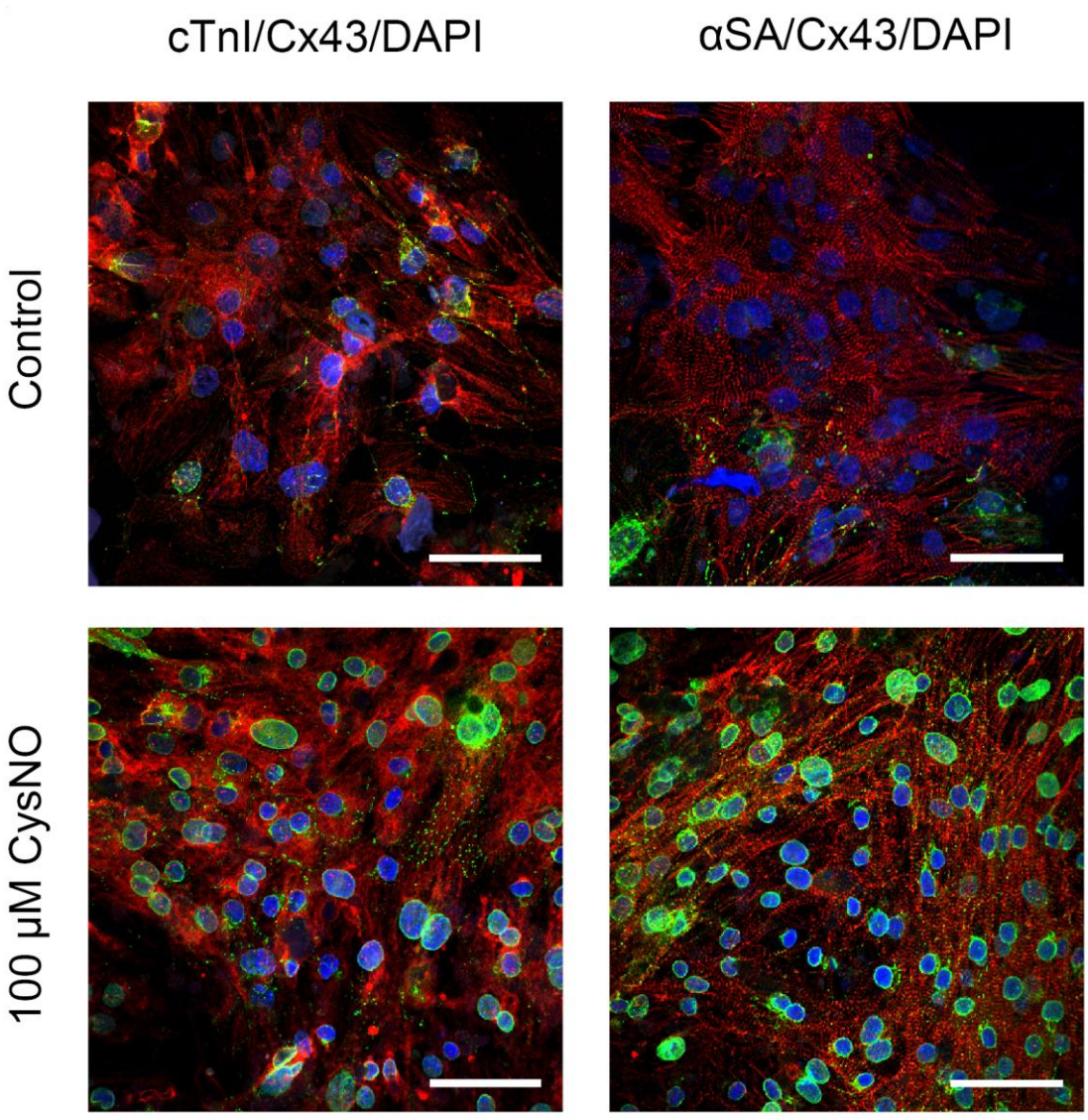

Figure 4.12. Immunocytochemistry images of day 18 SC-CMs. Scale bars represent 100μm.

In order to quantify changes in cardiac gene expression in response to CysNO treatment, day 18 EBs were harvested and characterized via qPCR (Fig. 4.13). Expression of the gap junction protein Cx43 as well as the myofibrillar protein αMHC did not change in response to CysNO treatment. However, βMHC was significantly up-regulated among CysNO-treated EBs in comparison to control EBs. Consequently, the ratio of βMHC to

αMHC was significantly increased for the CysNO-treated EBs. None of the cardiac genes which regulate formation of calcium transporter proteins (RyR2, Serca2a, and CaV1.2) demonstrated changes in expression level in response to CysNO treatment (Fig. 4.14).

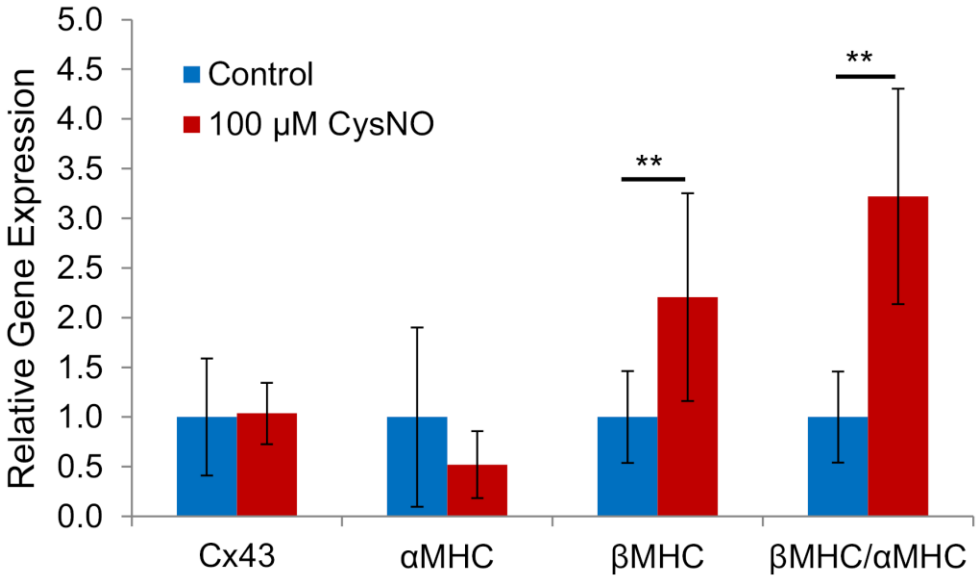

Figure 4.13. CysNO-treated EBs demonstrate significant increase in myosin heavy chain (MHC) ratio.

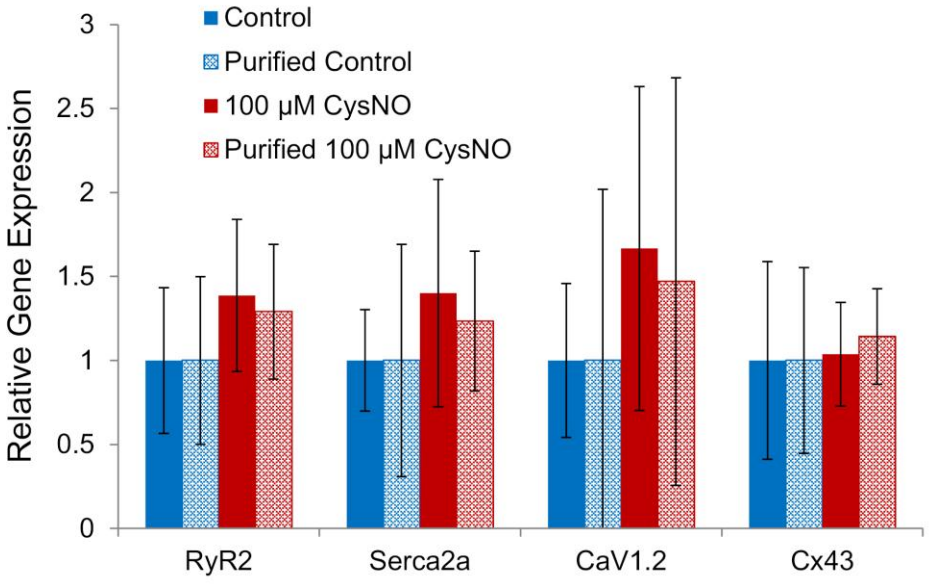

Figure 4.14. Functional gene expression remained unchanged after CysNO addition.

NO-treated cardiomyocytes demonstrate reduced calcium transient duration

Calcium transients analyzed from day 25 SC-CMs revealed differences in calcium handling properties in response to NO treatment during differentiation. Calcium traces collected from SC-CMs (Fig. 4.15) were processed using IonWizard (IonOptix); calcium transient durations were assessed by measuring the time to reach 50% (T50) and 80% (T80) calcium transient ratio decline (Fig. 4.16). SC CMs from both control and treatment populations demonstrated the expected reduction in calcium transient duration in response to increasing pacing frequency. SC-CMs differentiated in the presence of 100 μM CysNO demonstrated a significant reduction in T80 (0.21±0.08 s) compared to control SC-CMs (0.32±0.13 s) when paced at 0.5 Hz (Fig. 4.16); no difference in T80 was observed at higher pacing frequencies. NO-treated SC-CMs had an average maximum capture rate of 1.83 ± 0.86 Hz, which was not statistically different than the maximum capture rate of control SC-CMs (1.32 ±0.46 Hz, Fig. 4.17).

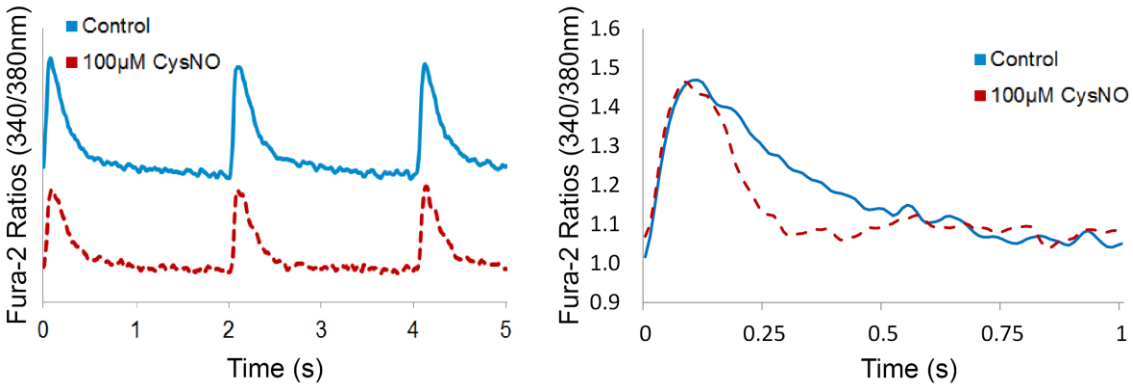

Figure 4.15. Representative calcium transient traces of control and CysNO-treated SC-CMs.

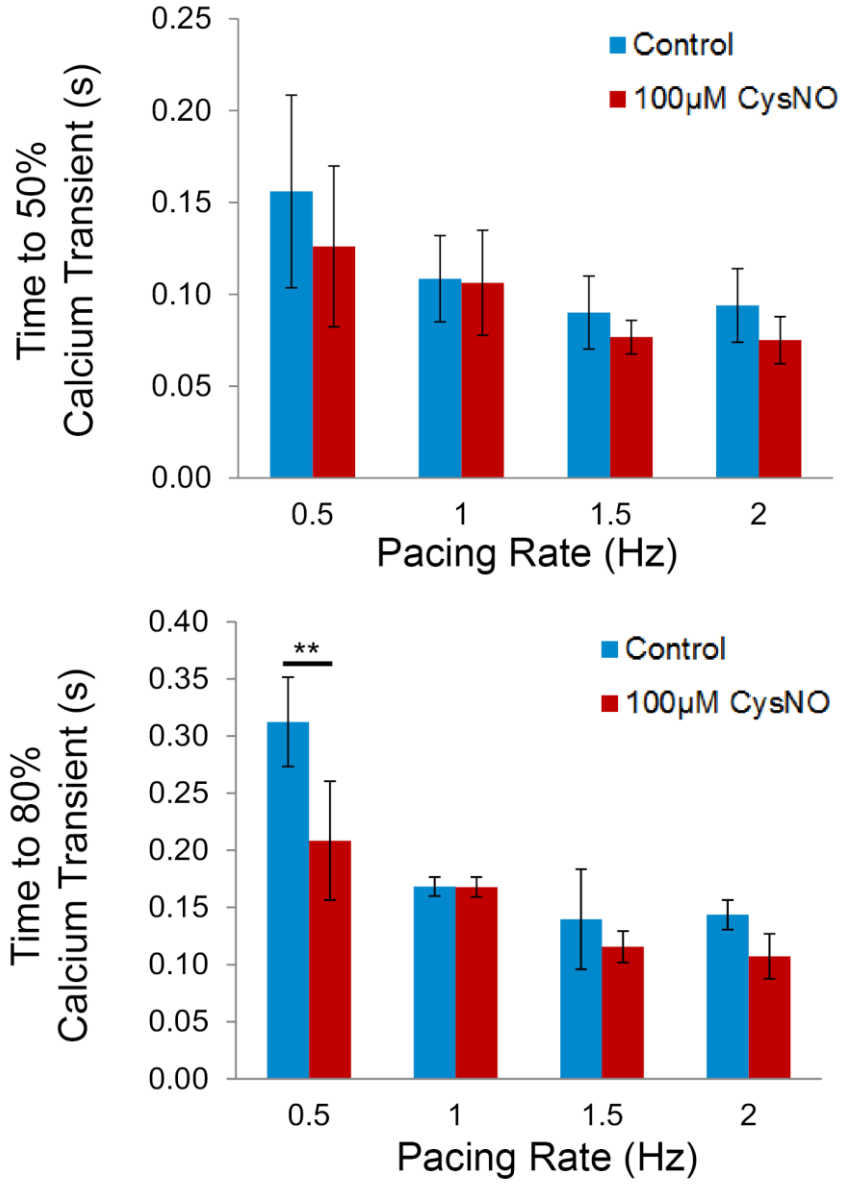

Figure 4.16. Times to 50% and 80% calcium transient ratios.

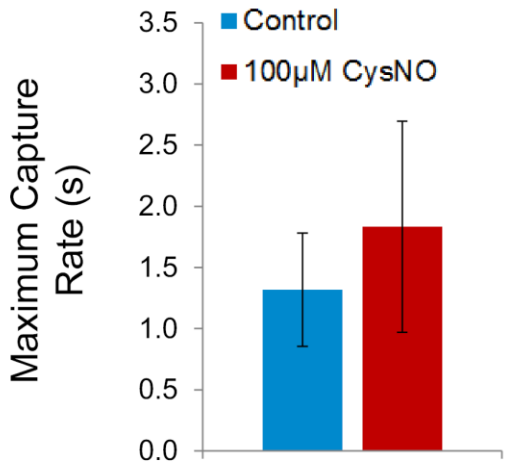

Figure 4.17. Maximum capture rates for control and CysNO-treated SC-CMs.

Comparisons of spontaneous calcium wave propagation across confluent sheets of CysNO treated and control SC-CMs by optical mapping (Fig. 4.18) supported the data found using the IonWizard system. Calcium transient durations were significantly shorter among NO-treated monolayers (50%: 0.24±0.08 s; 80%: 0.25±0.09 s) in comparison to control monolayers (50%: 0.40±0.11 s; 80%: 0.47±0.15 s, n=8 independent samples, Fig. 4.19). Calcium transient wave velocity was significantly higher across NO-treated monolayers than control (Control: 2.43±1.56 cm/s; Treatment: 4.35±1.73 cm/s; n=8 independent samples, Fig. 4.20). Additionally, the frequency of the spontaneous wave propagation was significantly greater among NO-treated monolayers relative to the control (Control: 0.87±0.53 Hz; Treatment: 1.99±0.79 Hz; n=8 independent samples, Fig. 4.21).

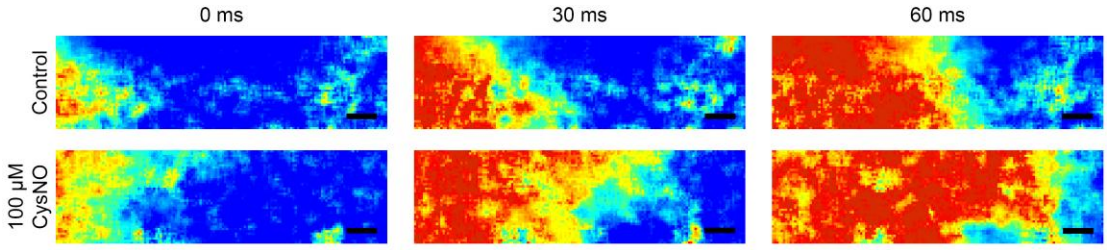

Figure 4.18. Calcium wave propagations from SC-CM monolayers. Scale bars represent 200 µm.

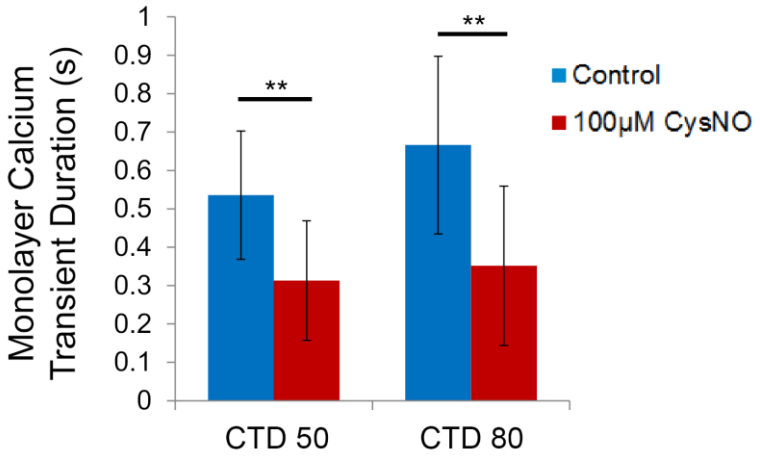

Figure 4.19. Calcium transient durations (at 50% and 80%) of SC-CM monolayers.

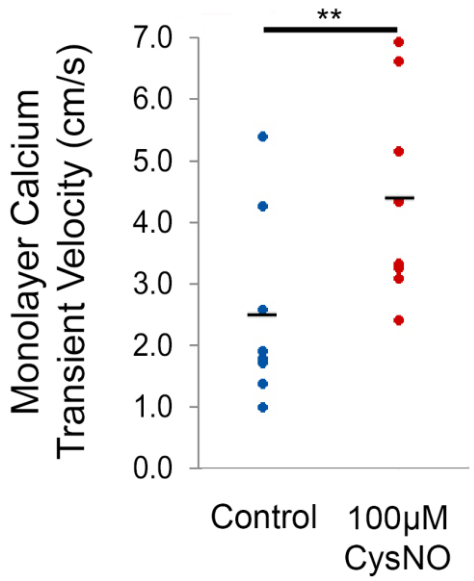

Figure 4.20. Calcium transient wave velocities of SC-CM monolayers.

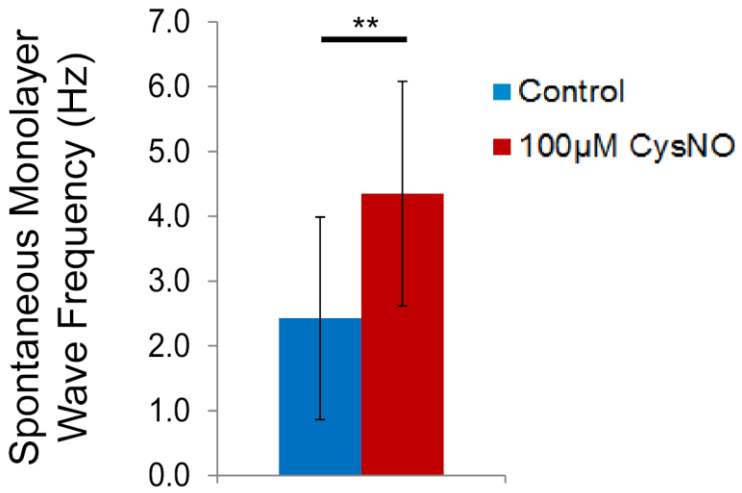

Figure 4.21. Frequency of spontaneous calcium wave propagations (from SC-CM monolayers).

4.4. Discussion

The purpose of this study was to establish the effects of NO donor addition on the yield and maturation of pluripotent stem cell-derived cardiomyocytes. Incorporation of CysNO into culture media had a pronounced effect on the spontaneous contractile activity of EBs in suspension culture, resulting in significant increases in both the percentage of spontaneously contracting EBs and the frequency of contraction. EBs receiving CysNO treatment demonstrated significant up-regulation of βMHC with a greater ratio of βMHC to αMHC. Superior calcium handling capabilities were observed in CysNO-treated SC-CMs in comparison to control SC-CMs, as exhibited through increased calcium transient velocities and reduced calcium transient durations. Furthermore, these changes occurred without differences in EB size and cellular viability. Taken together, these results indicate that CysNO, represents a potential component for use in the creation of structurally- and electrically-mature SC-CMs.

The results of this study provide new information on the effects of NO treatment on the maturation of SC-CMs. Previous studies examining the effect of NO on the differentiation of SC-CMs have not characterized calcium handling of resulting cells, which is an important consideration for application of SC-CMs in cardiac regeneration strategies. Additionally, the use of soluble NO donors for directing cardiac maturation has distinct advantages over other mechanical, electrical, or biochemical factors in terms of cost and ease of delivery, particularly for cells in scalable suspension culture systems. While the experiments performed in this study provide a method for evaluating the properties of maturing SC-CMs, certain necessary discrepancies in the handling of cells between testing protocols may produce questions regarding the consistency of results. In particular, differences in cell handling were necessary to carry out the calcium handling analysis, in which some of the EBs were reconfigured into monolayers with high cell-cell coupling and minimal viability loss. When analyzing the spontaneous contractile activity of SC-CMs, whole EBs were treated with CysNO and characterized over a period of 18 days; however, SC-CMs that were used in calcium transient acquisition were dissociated and purified using antibiotic selection starting on day 8 of differentiation. While consistency was maintained when handling mESCs before and during differentiation, large variances in spontaneous contractile activity were observed between differentiation batches, as is typical for this type of differentiation protocol. Although these batch-to-batch differences were present, they affected each treatment condition similarly and do not change the overall conclusions in this study. Addition of control mechanisms to tightly regulate EB formation and culture conditions throughout differentiation, such as

EB formation through forced plate centrifugation, would significantly reduce the level of batch-to-batch variation observed.

Previous investigation has identified important roles for NO signaling and NOS activation in cardiac differentiation and development (Krumenacker, Katsuki et al. 2006). NO has been identified as an important molecule in the upregulation of certain genes as well as alteration of specific protein functions. The effects of NO on differentiation of stem cells and development of cardiac systems in whole organisms has also been investigated. NOS, the enzyme responsible for endogenous synthesis of NO, has three identified isoforms: endothelial (eNOS), neuronal (nNOS), and inducible (iNOS) NOS. The expression level of each isoform of NOS is dependent on timing during differentiation or development, culture environment of cells (embryonic or in vitro culture), and species. In mice and rats, iNOS and eNOS have been detected in both atrial and ventricular cardiomyocytes starting at E8.5 (Bloch, Fleischmann et al. 1999); however, the concentrations of these two enzymes decline in ventricular tissue at E14.5 until birth (Sachinidis, Fleischmann et al. 2003). When mESCs are cultured in vitro, these cell types also experience a unique, defined change in NOS expression during the course of differentiation. Isolated mRNA for eNOS and nNOS have been identified in undifferentiated mESCs, with scarce amounts of iNOS detected in these cells (Krumenacker, Katsuki et al. 2006). Upon differentiation, expression levels of nNOS are reduced substantially while eNOS and iNOS levels rise significantly (Krumenacker, Katsuki et al. 2006), which is consistent with the observed levels of the respective NOS isoforms in the developing mouse embryo. Bartsch, et al. observed an increase in expression level of eNOS after the onset of differentiation with a decline in protein

expression after 8 days (Bartsch, Bekhite et al. 2011). Similarly, NO produced via iNOS has also been shown as a pertinent component of the signaling cascade involved in cardiomyocyte differentiation (Bloch, Fleischmann et al. 1999). These previous findings indicate that NO signaling, resulting from endogenous NO production, operates in a controlled mechanism to direct cardiomyocyte formation. This data may also suggest that exogenous supplementation of NO may facilitate the same signaling cascade to initiate and direct cardiogenesis.

I have demonstrated the ability of NO delivery by donor compounds to drive differentiation in vitro, similar to the developmental effects of NO, supplied by endogenous production via NOS complexes, during in vivo development. Because endogenous NO production in in vitro culture systems is inherently limited without shear-induced production from endothelial cells (a major source of NO in the developing heart), exogenous NO supplementation may be critical in NO-driven maturation of suspension-cultured SC CMs. Another approach may include the overexpression of NOS isoforms to increase endogenous NO production; incorporation of the iNOS gene into EB outgrowths has been shown to induce cardiomyocyte formation (Kanno, Kim et al. 2004). Taken together, the complex series of NOS activation and deactivation and subsequent NO signaling is important in the process of cardiac development. By delivering an exogenous NO donor to the differentiating stem cells over an extended time course, the results reported here are initial steps in mimicking in vivo NO signaling during in vitro SC-CM differentiation.

In the present study, mESCs differentiated as EBs were characterized for changes in spontaneous contractile activity, cardiomyocyte-specific protein and gene expression,

and calcium handing in response to CysNO treatment. Starting on day 8, the percentage of spontaneously contracting EBs was higher when EBs were differentiated in the presence of 100 μM CysNO; this trend continued through 14 days in culture. Previous work illustrates a similar trend when EBs treated with NO donor *S*-nitroso-N-acetylpenicillamine (SNAP), experienced a significantly greater incidence of contraction than non-treated controls after a period of 14 days in culture (Kanno, Kim et al. 2004). However, the EBs treated with SNAP experienced a doubling in spontaneously contracting outgrowths from days 7 to 14, whereas the percentage of spontaneously contracting EBs treated with CysNO in the present study decreased by 20% over the same period. This difference may be a result of ascorbic acid supplementation to EBs in all treatment groups, which produced a marked increase in the overall number of contracting EBs in comparison to the study by Kanno et al. (25% total incidence of contraction at day 8 among NO-treated EBs in the previous study, as compared to approximately 80% in the current study). In many conventional differentiation protocols, EBs are removed from suspension culture after approximately 5 days and plated onto gelatin, resulting in a general increase in spontaneous contraction over time (Mummery, Ward et al. 2002, Taha and Valojerdi 2008). The addition of growth factors has been used in other studies to enhance the duration of spontaneous contraction among adherent EBs; for instance, a defined media containing FGF-2 and BMP-2 was shown to maintain large populations of adherent contracting EBs over a 30-40 day period (Yamasaki, Nabeshima et al. 2013). In contrast, this experiment maintained EBs for up to 18 days in suspension culture with individual EBs showing a decrease in contraction after 8 to 10 days. This result is similar to other studies operating solely in suspension culture; a reduction in the

percentage of contracting EBs has been observed by others after 10 to 14 days in suspension (Sargent, Berguig et al. 2009, Shafa, Krawetz et al. 2011). Furthermore, while L-NAME did not significantly reduce the percentage of spontaneously contracting EBs in the present study, Kanno et al. observed a reduction in the incidence of contracting outgrowths with L-NAME treatment. This discrepancy may also have been as a result of the ascorbic acid treatment.

In our study, SC-CMs expressed the cardiomyocyte-specific proteins, sarcomeric α-actinin and cardiac troponin-I, and the gap junction protein Cx43. SC-CMs examined using immunocytochemistry had undergone αMHC-dependent selection after being dissociated into monolayers; therefore, the similarity in protein expression between NO-treated and control SC-CMs is justified. In EBs that had not undergone selection, Cx43 gene expression was similar for control and NO-treated SC-CMs (Fig. 4.13). However, differences were observed in βMHC expression, as well as for the ratio of βMHC to αMHC expression. Because expression of αMHC and βMHC changes over the course of differentiation, the relative expression levels of each myofibrillar protein type may be a useful parameter for evaluating changes in maturation (Yang, Pabon et al. 2014). In the context of mouse development, it is understood that expression of βMHC decreases after birth while αMHC levels are increased, correlating with increased postnatal heart rate (Yang, Pabon et al. 2014); however, expression of αMHC is expressed at high levels among atrial cardiomyocytes while ventricular cardiomyocytes express higher levels of βMHC beginning around E8 (Morkin 1993). In this study, CysNO treatment was found to increase levels of βMHC, as well as the ratio of βMHC to αMHC (Fig. 4.13). Changes in differentiating mESC cardiac gene expression in response to NO donor treatment has

been reported in previous studies as well, including increases in Nkx2.5 (Mujoo, Sharin et al. 2008) and myosin light chain and cardiac troponin-I (Kanno, Kim et al. 2004).

SC-CMs often have immature calcium handling, leading to spontaneous depolarization and slow calcium re-uptake, which could contribute to the formation of arrhythmias in vivo. Whereas the effect of NO on SC-CM calcium handling has not been previously reported, the effects of NO on calcium handling by mature cardiomyocytes are better understood. Previous work has demonstrated that influential effects of NO on mature cardiomyocytes are widespread in terms of cell signaling and protein modification (Hammond and Balligand 2012). Critical ion channel proteins, such as those regulating the function of mechanical gated potassium channels (Kazanski, Kamkin et al. 2010) and ryanodine receptor (Wang, Viatchenko-Karpinski et al. 2010), have demonstrated improved function from short-term NO exposure. The use of exogenous NO and nitrate compounds has also been shown to improve calcium current and calcium cycling in mature cardiomyocytes (Vandecasteele, Eschenhagen et al. 1998, Dulce, Yiginer et al. 2013). Extensive evidence has shown that NO acts in a cardio-protective manner after ischemia-reperfusion injury, reducing oxidative damage on ion channel proteins. In turn, the biochemical modifications made by NO have been suggested to both reduce the incidence of calcium overload after injury as well as reduce calcium diffusion into mitochondria (Hotta, Otsuka-Murakami et al. 1999, Stromer, de Groot et al. 2000, Suessenbacher, Lass et al. 2002, West, Rokosh et al. 2008), thereby improving the viability of cells within the injured tissue.

Despite the volume of evidence linking NO to improvement in calcium handling in mature cardiomyocytes, the effects of NO on differentiating cardiomyocytes, both

acute and chronic, have not yet been elucidated. The SC-CMs used in this study demonstrate long-term improvement in maturity through treatment with CysNO during differentiation. For instance, the CysNO-treated SC-CMs exhibited a significant decrease in calcium transient duration (T80 at 0.5 Hz = 0.21±0.08 s) in comparison to controls (T80 at 0.5 Hz = 0.32±0.13 s); this analysis was performed a week after the final CysNO treatment. Calcium transient durations for spontaneously-depolarizing confluent SC-CM monolayers were also reduced among CysNO-treated samples. Furthermore, CysNO-treated SC-CM monolayers exhibited faster calcium wave propagation and increased spontaneous wave frequency than the control monolayers (Fig. 4.20). This improvement in calcium handling was observed one week following the final CysNO treatment. Thus, these results suggest that the differences observed in calcium activity in CysNO-treated SC-CMs may constitute changes in calcium-transporting proteins which regulate ion presence in the intercellular space, cytosol, and sarcoplasmic reticulum, rather than being a short-term direct effect of CysNO on the SC-CMs.

4.5. Conclusions

Treatment of SC-CMs with the NO-donor CysNO resulted in an increased percentage of spontaneously contracting EBs, increased frequency of contraction of EBs, and increased expression of βMHC. CysNO-treated SC-CMs demonstrated increased calcium transient velocity and spontaneous propagation frequency and reduced calcium transient duration. The changes observed in calcium handling occur long after CysNO treatment is discontinued. This study supports the notion that NO induces development of SC-CMs and may prove valuable as a cardiogenic factor in large-scale suspension cell production.

References

Bartsch, C., M. M. Bekhite, A. Wolheim, M. Richter, C. Ruhe, B. Wissuwa, A. Marciniak, J. Muller, R. Heller, H. R. Figulla, H. Sauer and M. Wartenberg (2011). "NADPH oxidase and eNOS control cardiomyogenesis in mouse embryonic stem cells on ascorbic acid treatment." Free Radic Biol Med 51(2): 432-443.

Bloch, W., B. K. Fleischmann, D. E. Lorke, C. Andressen, B. Hops, J. Hescheler and K. Addicks (1999). "Nitric oxide synthase expression and role during cardiomyogenesis." Cardiovasc Res 43(3): 675-684.

Burridge, P. W., G. Keller, J. D. Gold and J. C. Wu (2012). "Production of de novo cardiomyocytes: human pluripotent stem cell differentiation and direct reprogramming." Cell Stem Cell 10(1): 16-28.

Christoforou, N., B. Liau, S. Chakraborty, M. Chellapan, N. Bursac and K. W. Leong (2013). "Induced pluripotent stem cell-derived cardiac progenitors differentiate to cardiomyocytes and form biosynthetic tissues." PLoS One 8(6): e65963.

Conti, V., G. Russomanno, G. Corbi, V. Izzo, C. Vecchione and A. Filippelli (2013). "Adrenoreceptors and nitric oxide in the cardiovascular system." Front Physiol 4: 321.

Ding, Y., R. Zou, R. L. Judd and J. Zhong (2006). "Effects of gender difference on cardiac myocyte dysfunction in streptozotocin-induced diabetic rats." Endocrine 29(1): 135-141.

Dulce, R. A., O. Yiginer, D. R. Gonzalez, G. Goss, N. Feng, M. Zheng and J. M. Hare (2013). "Hydralazine and organic nitrates restore impaired excitation-contraction coupling by reducing calcium leak associated with nitroso-redox imbalance." J Biol Chem 288(9): 6522-6533.

Go, A. S., D. Mozaffarian, V. L. Roger, E. J. Benjamin, J. D. Berry, W. B. Borden, D. M. Bravata, S. Dai, E. S. Ford, C. S. Fox, S. Franco, H. J. Fullerton, C. Gillespie, S. M. Hailpern, J. A. Heit, V. J. Howard, M. D. Huffman, B. M. Kissela, S. J. Kittner, D. T. Lackland, J. H. Lichtman, L. D. Lisabeth, D. Magid, G. M. Marcus, A. Marelli, D. B. Matchar, D. K. McGuire, E. R. Mohler, C. S. Moy, M. E. Mussolino, G. Nichol, N. P. Paynter, P. J. Schreiner, P. D. Sorlie, J. Stein, T. N. Turan, S. S. Virani, N. D. Wong, D. Woo, M. B. Turner, C. American Heart Association Statistics and S. Stroke Statistics (2013). "Heart disease and stroke statistics--2013 update: a report from the American Heart Association." Circulation 127(1): e6-e245.

Hammond, J. and J. L. Balligand (2012). "Nitric oxide synthase and cyclic GMP signaling in cardiac myocytes: from contractility to remodeling." J Mol Cell Cardiol 52(2): 330-340.

Hotta, Y., H. Otsuka-Murakami, M. Fujita, J. Nakagawa, M. Yajima, W. Liu, N. Ishikawa, N. Kawai, T. Masumizu and M. Kohno (1999). "Protective role of nitric oxide synthase against ischemia-reperfusion injury in guinea pig myocardial mitochondria." Eur J Pharmacol 380(1): 37-48.

Itzhaki, I., L. Maizels, I. Huber, L. Zwi-Dantsis, O. Caspi, A. Winterstern, O. Feldman, A. Gepstein, G. Arbel, H. Hammerman, M. Boulos and L. Gepstein (2011). "Modelling the long QT syndrome with induced pluripotent stem cells." Nature 471(7337): 225-229.

Jing, D., A. Parikh and E. S. Tzanakakis (2010). "Cardiac cell generation from encapsulated embryonic stem cells in static and scalable culture systems." Cell Transplant 19(11): 1397-1412.

Kadari, A., S. Mekala, N. Wagner, D. Malan, J. Koth, K. Doll, L. Stappert, D. Eckert, M. Peitz, J. Matthes, P. Sasse, S. Herzig, O. Brustle, S. Ergun and F. Edenhofer (2014). "Robust Generation of Cardiomyocytes from Human iPS Cells Requires Precise Modulation of BMP and WNT Signaling." Stem Cell Rev.

Kanno, S., P. K. Kim, K. Sallam, J. Lei, T. R. Billiar and L. L. Shears, 2nd (2004). "Nitric oxide facilitates cardiomyogenesis in mouse embryonic stem cells." Proc Natl Acad Sci U S A 101(33): 12277-12281.

Kazanski, V. E., A. G. Kamkin, E. Y. Makarenko, N. N. Lysenko, P. V. Sutiagin, T. Bo and I. S. Kiseleva (2010). "Role of nitric oxide in activity control of mechanically gated ionic channels in cardiomyocytes: NO-donor study." Bull Exp Biol Med 150(1): 1-5.

Kehat, I., D. Kenyagin-Karsenti, M. Snir, H. Segev, M. Amit, A. Gepstein, E. Livne, O. Binah, J. Itskovitz-Eldor and L. Gepstein (2001). "Human embryonic stem cells can differentiate into myocytes with structural and functional properties of cardiomyocytes." J Clin Invest 108(3): 407-414.

Klug, M. G., M. H. Soonpaa, G. Y. Koh and L. J. Field (1996). "Genetically selected cardiomyocytes from differentiating embronic stem cells form stable intracardiac grafts." J Clin Invest 98(1): 216-224.

Krumenacker, J. S., S. Katsuki, A. Kots and F. Murad (2006). "Differential expression of genes involved in cGMP-dependent nitric oxide signaling in murine embryonic stem (ES) cells and ES cell-derived cardiomyocytes." Nitric Oxide 14(1): 1-11.

Kushwaha, M., J. M. Anderson, C. A. Bosworth, A. Andukuri, W. P. Minor, J. R. Lancaster, Jr., P. G. Anderson, B. C. Brott and H. W. Jun (2010). "A nitric oxide releasing, self assembled peptide amphiphile matrix that mimics native endothelium for coating implantable cardiovascular devices." Biomaterials 31(7): 1502-1508.

Lian, X., J. Zhang, S. M. Azarin, K. Zhu, L. B. Hazeltine, X. Bao, C. Hsiao, T. J. Kamp and S. P. Palecek (2013). "Directed cardiomyocyte differentiation from human

pluripotent stem cells by modulating Wnt/beta-catenin signaling under fully defined conditions." Nat Protoc 8(1): 162-175.

Liau, B., D. Zhang and N. Bursac (2012). "Functional cardiac tissue engineering." Regen Med 7(2): 187-206.

Lieu, D. K., J. D. Fu, N. Chiamvimonvat, K. C. Tung, G. P. McNerney, T. Huser, G. Keller, C. W. Kong and R. A. Li (2013). "Mechanism-based facilitated maturation of human pluripotent stem cell-derived cardiomyocytes." Circ Arrhythm Electrophysiol 6(1): 191-201.

Lim, Z. Y., B. Maskara, F. Aguel, R. Emokpae, Jr. and L. Tung (2006). "Spiral wave attachment to millimeter-sized obstacles." Circulation 114(20): 2113-2121.

Liu, X., M. J. Miller, M. S. Joshi, H. Sadowska-Krowicka, D. A. Clark and J. R. Lancaster, Jr. (1998). "Diffusion-limited reaction of free nitric oxide with erythrocytes." J Biol Chem 273(30): 18709-18713.

Millman, J. R., J. H. Tan and C. K. Colton (2009). "The effects of low oxygen on self-renewal and differentiation of embryonic stem cells." Curr Opin Organ Transplant 14(6): 694-700.

Morkin, E. (1993). "Regulation of myosin heavy chain genes in the heart." Circulation 87(5): 1451-1460.

Mujoo, K., V. G. Sharin, N. S. Bryan, J. S. Krumenacker, C. Sloan, S. Parveen, L. E. Nikonoff, A. Y. Kots and F. Murad (2008). "Role of nitric oxide signaling components in differentiation of embryonic stem cells into myocardial cells." Proc Natl Acad Sci U S A 105(48): 18924-18929.

Mummery, C., D. Ward, C. E. van den Brink, S. D. Bird, P. A. Doevendans, T. Opthof, A. Brutel de la Riviere, L. Tertoolen, M. van der Heyden and M. Pera (2002). "Cardiomyocyte differentiation of mouse and human embryonic stem cells." J Anat 200(Pt 3): 233-242.

Mummery, C. L., J. Zhang, E. S. Ng, D. A. Elliott, A. G. Elefanty and T. J. Kamp (2012). "Differentiation of human embryonic stem cells and induced pluripotent stem cells to cardiomyocytes: a methods overview." Circ Res 111(3): 344-358.

Niebruegge, S., C. L. Bauwens, R. Peerani, N. Thavandiran, S. Masse, E. Sevaptisidis, K. Nanthakumar, K. Woodhouse, M. Husain, E. Kumacheva and P. W. Zandstra (2009). "Generation of human embryonic stem cell-derived mesoderm and cardiac cells using size-specified aggregates in an oxygen-controlled bioreactor." Biotechnol Bioeng 102(2): 493-507.

Nunes, S. S., J. W. Miklas, J. Liu, R. Aschar-Sobbi, Y. Xiao, B. Zhang, J. Jiang, S. Masse, M. Gagliardi, A. Hsieh, N. Thavandiran, M. A. Laflamme, K. Nanthakumar, G. J. Gross, P. H. Backx, G. Keller and M. Radisic (2013). "Biowire: a platform for maturation of human pluripotent stem cell-derived cardiomyocytes." Nat Methods 10(8): 781-787.

Park, H., B. L. Larson, M. D. Guillemette, S. R. Jain, C. Hua, G. C. Engelmayr, Jr. and L. E. Freed (2011). "The significance of pore microarchitecture in a multi-layered elastomeric scaffold for contractile cardiac muscle constructs." Biomaterials 32(7): 1856-1864.

Pelster, B., S. Grillitsch and T. Schwerte (2005). "NO as a mediator during the early development of the cardiovascular system in the zebrafish." Comp Biochem Physiol A Mol Integr Physiol 142(2): 215-220.

Pok, S. and J. G. Jacot (2011). "Biomaterials advances in patches for congenital heart defect repair." J Cardiovasc Transl Res 4(5): 646-654.

Robertson, C., D. D. Tran and S. C. George (2013). "Concise review: maturation phases of human pluripotent stem cell-derived cardiomyocytes." Stem Cells 31(5): 829-837.

Sachinidis, A., B. K. Fleischmann, E. Kolossov, M. Wartenberg, H. Sauer and J. Hescheler (2003). "Cardiac specific differentiation of mouse embryonic stem cells." Cardiovasc Res 58(2): 278-291.

Sargent, C. Y., G. Y. Berguig and T. C. McDevitt (2009). "Cardiomyogenic differentiation of embryoid bodies is promoted by rotary orbital suspension culture." Tissue Eng Part A 15(2): 331-342.

Schmelter, M., B. Ateghang, S. Helmig, M. Wartenberg and H. Sauer (2006). "Embryonic stem cells utilize reactive oxygen species as transducers of mechanical strain-induced cardiovascular differentiation." FASEB J 20(8): 1182-1184.

Seneviratne, U., L. C. Godoy, J. S. Wishnok, G. N. Wogan and S. R. Tannenbaum (2013). "Mechanism-based triarylphosphine-ester probes for capture of endogenous RSNOs." J Am Chem Soc 135(20): 7693-7704.

Serena, E., E. Figallo, N. Tandon, C. Cannizzaro, S. Gerecht, N. Elvassore and G. Vunjak-Novakovic (2009). "Electrical stimulation of human embryonic stem cells: cardiac differentiation and the generation of reactive oxygen species." Exp Cell Res 315(20): 3611-3619.

Shafa, M., R. Krawetz, Y. Zhang, J. B. Rattner, A. Godollei, H. J. Duff and D. E. Rancourt (2011). "Impact of stirred suspension bioreactor culture on the differentiation of murine embryonic stem cells into cardiomyocytes." BMC Cell Biol 12: 53.

Stromer, H., M. C. de Groot, M. Horn, C. Faul, A. Leupold, J. P. Morgan, W. Scholz and S. Neubauer (2000). "Na(+)/H(+) exchange inhibition with HOE642 improves postischemic recovery due to attenuation of Ca(2+) overload and prolonged acidosis on reperfusion." Circulation 101(23): 2749-2755.

Suessenbacher, A., A. Lass, B. Mayer and F. Brunner (2002). "Antioxidative and myocardial protective effects of L-arginine in oxygen radical-induced injury of isolated perfused rat hearts." Naunyn Schmiedebergs Arch Pharmacol 365(4): 269-276.

Taha, M. F. and M. R. Valojerdi (2008). "Effect of bone morphogenetic protein-4 on cardiac differentiation from mouse embryonic stem cells in serum-free and low-serum media." Int J Cardiol 127(1): 78-87.

Vandecasteele, G., T. Eschenhagen and R. Fischmeister (1998). "Role of the NO-cGMP pathway in the muscarinic regulation of the L-type Ca2+ current in human atrial myocytes." J Physiol 506 (Pt 3): 653-663.

W. Limpitikul, N. C., S. Edmonds, J. Gearhart, L. Tung, E.A. Lipke (2011). "Influence of Electromechanical Activity on Cardiac Differentiation of Mouse Embryonic Stem Cells." Cardiovascular Engineering and Technology 1(3): 179–193.

Wang, B., G. Wang, F. To, J. R. Butler, A. Claude, R. M. McLaughlin, L. N. Williams, A. L. de Jongh Curry and J. Liao (2013). "Myocardial scaffold-based cardiac tissue engineering: application of coordinated mechanical and electrical stimulations." Langmuir 29(35): 11109-11117.

Wang, F. and J. Guan (2010). "Cellular cardiomyoplasty and cardiac tissue engineering for myocardial therapy." Adv Drug Deliv Rev 62(7-8): 784-797.

Wang, H., S. Viatchenko-Karpinski, J. Sun, I. Gyorke, N. A. Benkusky, M. J. Kohr, H. H. Valdivia, E. Murphy, S. Gyorke and M. T. Ziolo (2010). "Regulation of myocyte contraction via neuronal nitric oxide synthase: role of ryanodine receptor S-nitrosylation." J Physiol 588(Pt 15): 2905-2917.

Weinberg, S., E. A. Lipke and L. Tung (2010). "In vitro electrophysiological mapping of stem cells." Methods Mol Biol 660: 215-237.

West, M. B., G. Rokosh, D. Obal, M. Velayutham, Y. T. Xuan, B. G. Hill, R. J. Keith, J. Schrader, Y. Guo, D. J. Conklin, S. D. Prabhu, J. L. Zweier, R. Bolli and A. Bhatnagar (2008). "Cardiac myocyte-specific expression of inducible nitric oxide synthase protects against ischemia/reperfusion injury by preventing mitochondrial permeability transition." Circulation 118(19): 1970-1978.

Yamasaki, S., K. Nabeshima, Y. Sotomaru, Y. Taguchi, H. Mukasa, M. K. Furue, J. D. Sato and T. Okamoto (2013). "Long-term serial cultivation of mouse induced pluripotent

stem cells in serum-free and feeder-free defined medium." Int J Dev Biol 57(9-10): 715-724.

Yang, X., L. Pabon and C. E. Murry (2014). "Engineering adolescence: maturation of human pluripotent stem cell-derived cardiomyocytes." Circ Res 114(3): 511-523.

Zimmermann, W. H., K. Schneiderbanger, P. Schubert, M. Didie, F. Munzel, J. F. Heubach, S. Kostin, W. L. Neuhuber and T. Eschenhagen (2002). "Tissue engineering of a differentiated cardiac muscle construct." Circ Res 90(2): 223-230.

Zwi-Dantsis, L. and L. Gepstein (2012). "Induced pluripotent stem cells for cardiac repair." Cell Mol Life Sci 69(19): 3285-3299.

5. NOVEL ELECTROACTIVE SUBSTRATE SUPPORTS GROWTH AND PROLIFERATION OF HL-1 CARDIOMYOCYTES

5.1. Introduction

Heart disease is the leading cause of mortality in the United States, accounting for about 25% of all deaths in 2009 (Heron 2012). Better treatment options to enable true cardiac regeneration are needed to augment total heart transplant, for which donor organs are in chronic short supply. Engineered cardiac tissues having properties similar to native myocardium have the potential to contribute to reaching this goal, both through their use in drug-testing platforms for the identification of more effective pharmaceutical therapies and directly in future clinical treatments. However, creating tissues in vitro that have the electromechanical properties of adult native cardiac tissue remains an elusive goal. By replicating microenvironmental cues present in native myocardium, biomimetic materials may facilitate formation and maturation of functional engineered cardiac tissues (Dunn, Hodge et al. 2014, Hodge 2014).

Electrical signaling and conductivity are important considerations in designing a substrate that mimics the properties of native cardiac tissue. The propagation of electrical signals through native myocardium trigger the organized contraction of the heart, resulting in blood being pumped throughout the body. Improper conduction of electrical signals can result in deadly arrhythmias. Electrical stimulation has been previously shown to be important in directing the structure and electrophysiological properties of cardiomyocytes and engineered cardiac tissue during in vitro culture. Electrical stimulation of cardiac cell monolayers has been shown to increase alignment of neonatal rat ventricular myocytes (Radisic, Park et al. 2004, Dvir, Timko et al. 2011), increase cell coupling (Radisic, Park et al. 2004, Dvir, Timko et al. 2011), decrease the heterogeneity

of conduction velocity (Limpitikul 2010), and increase the amplitude of cardiac construct synchronous contractions (Radisic, Park et al. 2004). Shortened action potential durations and decreased spontaneous contractile activity have also been reported in neonatal rat ventricular myocytes undergoing electrical stimulation (Sathaye, Bursac et al. 2006). In aligned cardiac tissues created using human pluripotent stem cell-derived cardiomyocytes, electrical stimulation resulted in higher conduction velocities and improved electrophysiological properties (Nunes, Miklas et al. 2013). Use of conductive substrates, including the electrically conductive polymer scaffold polyaniline-poly(glycerol-sebacate) (Qazi, Rai et al. 2014), has also resulted in enhanced engineered cardiac tissue function.

Multiple avenues for creating conductive substrates for cell growth have been explored, including the use of carbon nanotubes (Hu, Ni et al. 2004, McKenzie, Waid et al. 2004, Webster 2004), use of homogenously dispersed gold particles (You, Rafat et al. 2011), and entirely polymer-based scaffolds incorporating electrically-conductive polymers such as polypyrrole (PPy) (Bechara, Wadman et al. 2011, Hardy, Lee et al. 2013). The cost of gold nanoparticles may prohibit their large-scale application as electroactive biomaterials, whereas the potential cytotoxicity of carbon nanotubes may limit their use within biodegradable implantable scaffolds (Shvedova, Castranova et al. 2003). PPy has been used widely as an electrically conductive polymer for neural tissue engineering applications (Lee, Bashur et al. 2009, Bechara, Wadman et al. 2011). The selection of the dopant counterions during the synthesis of electroactive polymers has an effect on the biocompatibility of the electroactive polymer (PPy) in vitro, with high molecular weight dopants (typically polyanions such as polystyrene sulfonate) being

attractive because they will not readily leach from the polyelectrolyte complex formed with the (typically) polycationic PPy (Fonner, Forciniti et al. 2008, Guimard, Sessler et al. 2009, Higgins 2012, Moulton 2012). Interestingly, in vivo studies of electroactive scaffolds have been carried out and histological analyses of tissue surrounding polypyrrole-based tissue scaffolds implanted subcutaneously or intramuscularly in rats reveal immune cell infiltration comparable to FDA-approved poly(lactic acid-co-glycolic acid) (Schmidt, Shastri et al. 1997) or FDA-approved poly(D,L-lactide-co-glycolide) (Wang, Roberge et al. 2004). Likewise, no significant inflammatory response was observed with polypyrrole-based sciatic nerve guidance channels implanted in rats after 8 weeks (Durgam, Sapp et al. 2010), polypyrrole-coated electrodes in rat brains after 3 or 6 weeks (George, Lyckman et al. 2005), or most pertinently, polypyrrole-based tissue scaffolds implanted in the coronary artery of rats after 5 weeks (Mihardja, Sievers et al. 2008). Although differences in the individual studies (i.e. the chemical/mechanical/topological properties of the scaffolds, the site of implantation, and the methodology used to evaluate the immune response) make it challenging to compare the results of each study, PPy-based biomaterials exhibit levels of immunogenicity that are comparable with other FDA-approved biomaterials and have potential for clinical translation, in addition to use for cell growth in vitro.

Polycaprolactone (PCL) has previously demonstrated strong compatibility as an underlying base material in the formation of conductive polymer substrates. Electroactive composites of PCL and polyaniline have been previously shown to support the adhesion and proliferation of H9c2 cells (derived from rat heart tissue) (Li, Guo et al. 2006) and the differentiation of human mesenchymal stem cells towards cardiogenic outcomes

(Borriello, Guarino et al. 2011), whereas electroactive composites of PCL and PPy were demonstrated to support the adhesion and proliferation of primary rabbit cardiomyocytes and the expression of cardiac-specific proteins (α-actinin, troponin-T, and connexin 43 (Cx43)) (Kai, Prabhakaran et al. 2011). Consequently, interpenetrating networks of PPy and PCL (PPy-PCL) may offer a commercially viable, electrically conductive alternative to existing materials used for culturing cardiac tissue monolayers and for cardiac differentiation of pluripotent stem cells. PCL is a biodegradable polyester that has been FDA-approved for use clinically in drug delivery devices and as a component of biomaterials used for bone regeneration (Woodruff 2010). Interpenetrating networks of PPy and PCL have demonstrated physiological levels of conductivity (Bechara, Wadman et al. 2011), and copolymers of PPy and PCL have been shown to enhance neurite outgrowth from rat PC12 cells (Durgam, Sapp et al. 2010), which, like cardiomyocytes, respond to electrical stimuli. The conductivity of the PPy-PCL creates an environment conducive to electrical stimulation, thereby mimicking conditions found in the heart. Measurements of cardiac tissue resistivity vary, but are typically around 0.5 kΩ cm (Rush, Abildskov et al. 1963). Based on these properties, PPy-PCL-based materials are interesting substrates for in vitro studies of cardiomyocytes and are of potential clinical relevance for cardiac tissue engineering.

Conductive materials that provide an electrical environment which effectively mimics the physiological conditions in the heart may enhance electrical signaling in engineered cardiac tissues, similar to changes observed in response to exogenous electrical pacing. Cx43 is a vital gap junction protein found within the myocardium responsible for establishing electrical and chemical coupling between cardiomyocytes,

and is therefore a critical feature in the formation of mature engineered heart tissue. For instance, engineered heart tissue composed of anisotropically aligned cells and well-organized Cx43 demonstrated improved twitch force relative to isotropic scaffolds (Black, Meyers et al. 2009). Application of exogenous electrical pacing to condition engineered heart tissue has been shown to improve Cx43 density and organization (Hirt, Boeddinghaus et al. 2014). Exogenous electrical pacing has also been demonstrated to influence electrical and calcium wave propagation and may also be implicated in reduced heterogeneity of engineered heart tissue. Providing a more physiological electrical environment for formation of engineered cardiac tissues may contribute to enhanced Cx43 organization, improving electrical signal propagation in the engineered myocardium.

The overall objective of this study was to determine the efficacy of the conductive PPy-PCL interpenetrating networks for use as electroactive substrates for cardiomyocyte culture. We first assessed the ability of PPy-PCL to support the adhesion and growth of cardiomyocytes and thereafter the differences between cardiomyocyte monolayers cultured on either PCL or PPy-PCL. A simple three step fabrication method was established and the surface resistivity and hydrophobicity of the materials were characterized. Cardiomyocyte cell sheets were formed on the PPy-PCL and PCL substrates and cell adhesion, cell viability, cell size, cell morphology, and Cx43 expression and organization were quantified. Propagation of calcium transients across the cardiomyocyte cell sheets was visualized through optical mapping; calcium transient velocity, duration and frequency of spontaneous propagation were quantified. Comparing cardiomyocyte phenotype and the resulting cardiac monolayer tissue properties on the

non-conductive and conductive substrates allows us to assess the usefulness of mimicking the inherent conductivity of native myocardium in an in vitro setting.

5.2. Materials and methods

All materials were purchased from Sigma-Aldrich (St. Louis, MO) unless noted otherwise.

Fabrication of PCL-Based Films

The fabrication process for NaOH-treated PCL, as well as for PPy-PCL, is represented in Figure 5.1 and detailed below.

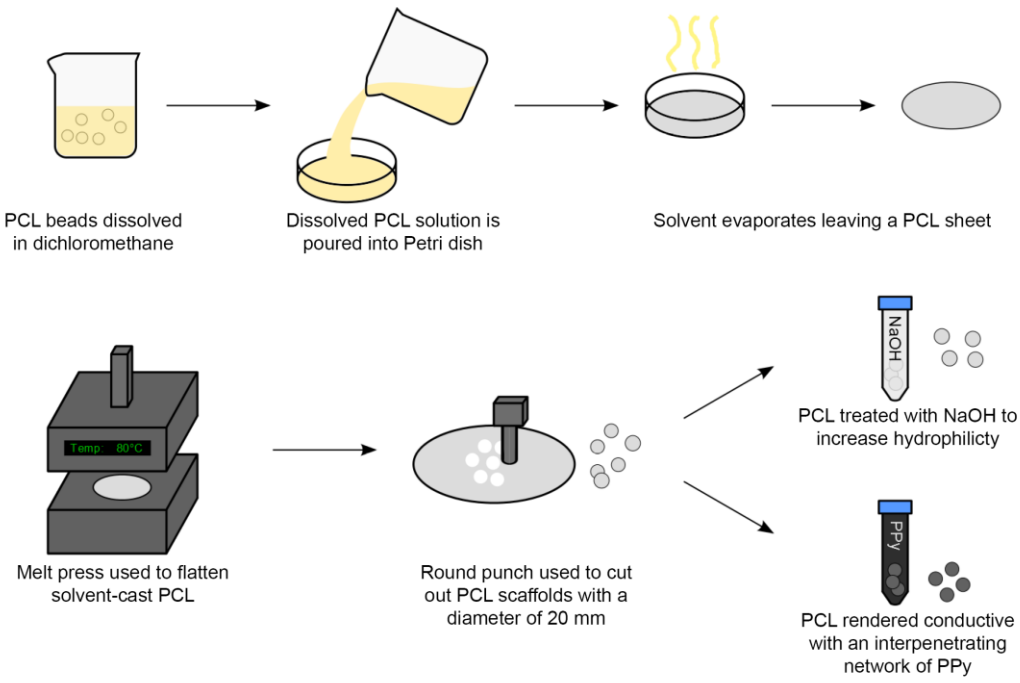

Figure 5.1. Process for generating films of PCL and PPy-PCL.

PCL Film Preparation

Heat-pressed PCL films were prepared by dissolving PCL beads (20 w/v%) in dichloromethane (Acros Organics, Thermo Fisher Scientific, Waltham, MA), casting on a flat surface and allowing the solvent to evaporate overnight. The solvent-cast PCL films were flattened between 1/8" mirror finished 316 stainless steel sheets (McMaster-Carr, Atlanta, GA) on a Wabash G30H hydraulic press (Wabash MPI, Wabash, IN) at 80˚C with 1 ton of force for five min. After cooling, films were cut out of the resulting PCL sheet using a 20 mm diameter punch.

NaOH Treatment of PCL

To optimize PCL surfaces for cell adhesion, PCL films were subjected to NaOH treatment (Serrano, Portoles et al. 2005, Wang, Teo et al. 2013). PCL films were treated with 3 N NaOH for periods of 0, 1.5, 3, 24, or 48 h, rinsed in PBS (Lonza, Walkersville, MD) and incubated in deionized water such that all samples were subjected to aqueous conditions for a duration of 48 h. Samples were then dried using a nitrogen gun and characterized or sterilized for cellular experiments. Hereafter these films are referred to as PCL-0 (for PCL that was not exposed to NaOH), or PCL-1.5, PCL-3, PCL-24 or PCL-48 respectively, depending on the duration of exposure to NaOH.

Preparation of conductive PPy-PCL

To generate conductive PCL-based materials, an interpenetrating network of PPy was grown within PCL films by adaptation of a previously described polymerization technique (Lee, Bashur et al. 2009, Bechara, Wadman et al. 2011). Briefly, a solution of polystyrene sulfonic acid (70,000 MW, 15.98 g L-1) and pyrrole (5.99 g L-1, 0.084 M)

was prepared in deionized (DI) water and mixed well. PCL films were added and the solution was incubated at room temperature for 1 h. Subsequently, ferric chloride (37.0 g L-1, 0.228 M) was added to the mixture. This final mixture was incubated at 4º C for 24 h, at which point the PPy-PCL samples were removed, rinsed with DI water, and air-dried prior to testing.

Material Characterization

PCL and PPy-PCL material characterization included assessment of: water contact angle (WCA), electrical resistivity, material hardness and elasticity, surface chemistry, and imaging using scanning electron microscopy (SEM) as described below.

Water Contact Angle (WCA)

To assess the hydrophobicity of the treated films, the WCA of the PCL was measured. The WCA of the NaOH-treated PCL and the PPy-PCL was quantified using a ramé-hart contact angle goniometer and DROPimage software (ramé-hart, Succasunna, NJ). Three separately prepared samples were tested for each treatment condition.

Nanoindentation

To determine the elastic modulus and stiffness for PCL and PPy-PCL films, material mechanical analysis was carried out using nanoindentation. Samples were loaded into an MTS Nanoindenter XP with a Berkovich diamond tip under continuous stiffness operation. Parameters were set to include a harmonic displacement target of 2 nm and a minimum thermal drift rate of 0.05 nm/s. The samples were indented to a depth of at least 2 μm and the values of elastic modulus and hardness were continually recorded

throughout displacement. Arrays of at least five indents were performed for each experimental condition to obtain a statistical response.

Quantification of Surface Chemistry

To confirm surface modification of PCL films via NaOH treatment or PPy synthesis, samples were evaluated using X-ray photoelectric spectroscopy (XPS). XPS analyses were performed using AXIS Ultra DLD with monochromatic Al Kα radiation as the X-ray source. Survey and high resolution spectra were recorded with a pass energy of 160 eV and 20 eV, respectively, at constant analyzer transmission energy mode. The binding energy of the system was referenced to Ag 3d5/2 at 368.3 eV.

Scanning Electron Microscopy (SEM)

PCL and PPy-PCL samples, both with and without cells, were imaged using SEM to observe the surface properties of the material. Briefly, samples with cells were fixed in a solution of 3% paraformaldehyde for 2 h at room temperature, followed by incubation in 2% osmium tetroxide for 2 h. Material samples were dried using serial dilutions of ethanol followed by a chemical drying step in hexamethyldisilazane for 30 min. All samples were allowed to dry completely in air prior to mounting on aluminum stubs and sputter-coating using gold (EMS 550X Auto Sputter Coating Device, Electron Microscope Services, Hatfield, PA). Gold-coated samples imaged using SEM (Zeiss EVO 50 SEM, Carl Zeiss Microscopy, Jena, Germany).

Surface resistivity

The surface resistivity of PCL and PPy-PCL films was determined with a Keithley 4200-SCS Parameter Analyzer (Keithley, Cleveland, OH) and the four-point probe method; this approach is optimal for flat materials such as those described herein and helps to eliminate the influence of instrumentation internal resistance on the recorded resistance. Four probes, spaced equidistantly from one another, were applied to the surface of a sample. A known current was applied to the outer two probes while the inner two probes were used to measure the voltage on the sample surface. Ohm's Law was then used to solve for the surface resistivity of each sample. The resistivity of each sample was confirmed prior to sterilization and culture of cardiomyocytes.

Cell Culture

HL-1 Maintenance

HL-1 atrial myocytes, a cell line derived from adult mouse atria (Claycomb, Lanson et al. 1998) were obtained from Dr. William Claycomb (Louisiana State University Health Sciences Center, New Orleans, LA) and cultured in vitro using Claycomb media supplemented with 10% fetal bovine serum (FBS), 0.1 mM norepinephrine, 2 mM L-glutamine (Lonza), and 100 μg mL-1 penicillin-streptomycin (Lonza). HL-1 cells were expanded and passed according to standard protocols (Claycomb, Lanson et al. 1998) prior to use in all experiments.

HL-1 Cell Response to PCL-Based Films

PCL-based films were placed in a 12-well plate and sterilized by incubation in 70% ethanol (Pharmco-AAPER, Brookfield, CT) solution and exposure to UV light for 1

h. The ethanol solution was aspirated and the films were washed with PBS and dried. Films were incubated in a solution of (0.02 w/v%) gelatin-(5 x 10-6 g/mL) fibronectin for at least 1 hr at 37°C to better promote cellular attachment to each surface. HL-1 cells were then seeded on the film surface at a density of 1,300 cells mm 2. Cell culture medium was exchanged every 24 h.

LIVE/DEAD Assay

A LIVE/DEAD assay (Invitrogen, Life Technologies, Grand Island, NY) was used to quantify the viability of the cells on each surface 6 days post-seeding. Briefly, cells were incubated at room temperature for 20 min in a solution of calcein-AM (2 mM) and ethidium homodimer-1 (4 mM) in PBS. The solution was aspirated, cells were rinsed with PBS and PBS was added prior to imaging using fluorescence microscopy. Live cells were characterized by intracellular esterase activity which cleaves the calcein-AM to form fluorescent green calcein. Dead cells were reported by the presence of red fluorescent ethidium homodimer-1, which enters through the ruptured cell membrane and binds to nucleic acids in the nucleus. HL-1 cells were imaged using a Nikon Eclipse-Ti inverted fluorescence microscope (Nikon Instruments Inc., Melville, NY) and an Andor Luca S camera (Andor, Belfast, UK). Viability of cells on three separate films per condition was quantified using the cell counter plugin for ImageJ (NIH).

Analysis of Adherent Cell Density and Cellular Size

HL-1 cells were fluorescently labeled to quantify the density of adherent cells and the average surface area of individual cells on the films 10 days post-seeding; PPy-PCL is opaque, meaning cells are unable to be visualized under bright field microscopy. After

fixation with a 50:50 acetone (Macron Chemicals, Center Valley, PA)/ethanol solution, HL-1 cells were permeabilized using a 0.1% Triton X-100 solution in PBS, washed with PBS and incubated in a 2.5 (v/v)% solution of Alexa Fluor® 488 Phalloidin (Invitrogen) in PBS for 20 min at room temperature. HL-1 cells were then counterstained with DAPI (Invitrogen, 1:36000 from stock) and samples were dehydrated and mounted in Prolong Gold (Life Technologies). Images of HL-1 cells on the film surfaces were acquired using a Nikon confocal microscope (Nikon Instruments Inc).

Morphological analysis was performed using ImageJ by outlining five to ten individual cells in each of 3-4 images per film. The average cell size was determined for each film and used for statistical analysis (n = 3 to 4). Analysis of adherent cell density was carried out using ImageJ. All nuclei within each image were counted and then divided by the unit area of each image to find the cell density (n = 3 films per condition).

Immunocytochemistry

Qualitative assessment of the expression and localization of the gap junction protein Cx43 in HL-1 cells adhered on PCL-based films was achieved with immunocytochemistry at 10 days post-seeding. HL-1 cells were fixed using a 50:50 acetone/ethanol solution for 10 min at -20°C. The HL-1 cells were then permeabilized using a 0.1% Triton X-100 solution in PBS and blocked using a 3% solution of FBS in PBS. Following blocking, samples were incubated in rabbit-anti-Cx43 antibody (diluted 1:200 in blocking buffer) for 2 h at room temperature. After rinsing, the secondary antibody Alexa Fluor 488 goat-anti-rabbit (Invitrogen, diluted 1:200 in blocking buffer) was added and incubated for 2 h at room temperature. To quantify the number of cells per area, HL-1 cells were counterstained with DAPI (Invitrogen, 1:36000 from stock) and

samples were dehydrated and mounted in Prolong Gold (Life Technologies). Images of HL-1 cells on the film surfaces were acquired using a Nikon confocal microscope.

To eliminate the potential for bias, this analysis was carried out by a blinded observer and automated image re-naming and order randomization was employed. Image analysis was performed using the cell counter plugin for ImageJ. For each image, the number of cells with positive peripheral staining for Cx43 was counted. Then the number of remaining cells, i.e. those without peripheral Cx43 expression, was counted. For each individual film, three images were quantified; the percentage of cells with peripheral Cx43 expression was then calculated and the average value used for statistical analysis (n = 4 films per condition).

Analysis of Connexin-43 expression by qPCR

To quantify the effect of film type on gap junction gene expression, HL-1 cells were evaluated using qPCR. Cells were seeded on PCL and PPy-PCL films. After 7 days of culture, RNA was isolated using a MicroElute Total RNA Kit (Omega Bio Tek, Norcross, GA). Cells were physically disrupted in lysis buffer prior to homogenization (Homogenizer Spin Columns, Omega Bio Tek). The solution containing nucleic acid was transferred to collection columns and treated according to the manufacturer's instructions; the concentration of diluted RNA was determined via spectroscopy (NanoDrop, Thermo Fisher) prior to generation of a cDNA library (qScript cDNA SuperMix, Quanta Biosciences, Gaithersburg, MD). Quantification of Cx43 (Forward: GGTGGACTGCTTCCTCTCAC, Reverse: ATCGCTTCTTCCCTTCACG) was carried out via qPCR using a SYBR green amplification kit (PerfeCTa SYBR Green SuperMix, Quanta Biosciences) in an iCycler iQ5 (Bio-Rad, Hercules, CA). PCR conditions were

95°C for 5 min, followed by 40 cycles of amplification at 95℃ for 10s, and 55℃ for 30s. GAPDH (Forward: GAAGGGCATCTTGGGCTAC, Reverse: GCCTCTCTTGCTCAGTGTCC) was used as a housekeeping gene for all trials. Relative quantification of Cx43 was determined using the ΔΔCt method; a total of n = 5 samples were analyzed from each treatment group.

Optical Mapping

Optical mapping was performed on confluent HL-1 cell monolayers 10 to 12 days post-seeding on PCL-based films. Tyrode's solution was prepared as previously described (Weinberg, Lipke et al. 2010). Rhod 2 (Invitrogen) calcium indicator was prepared by first creating a 1 mM stock solution through addition of anhydrous dimethylsulfoxide followed by sonication at 50º C for 30 min. To prepare the working calcium indicator solution, 5 µl of 1 mM Rhod-2 stock solution and 5 µl of Pluronic F-127 were added per 1 ml of Tyrode's solution. Following removal of cell culture media, 1 ml of calcium indicator solution was added to each well and allowed to incubate at room temperature for 20 min. After the incubation period, the wells were rinsed three times with Tyrode's solution prior to imaging.

Recordings of calcium wave propagation across the HL-1 cell sheets were acquired using an iXon Ultra DU897 EMCCD camera (Andor) coupled to an Optomask Adjustable Field Mask (Andor), which was utilized to enhance frame rate in cropped sensor mode, and Nikon Elements software. Propagating calcium waves were recorded in Tyrode's solution at room temperature (22 °C) in the absence of exogenous stimulation (i.e., spontaneous wave propagation). For each film, a minimum of three recordings were taken with an average length of 10 sec at a rate of approximately 500 frames per second.

Data was analyzed using a modified version of a previously established MATLAB (MathWorks, Natick, MA) script (Weinberg, Lipke et al. 2010, Blazeski, Zhu et al. 2012, Blazeski, Zhu et al. 2012). Using this script, calcium transient velocity, calcium transient duration (time to 50% recovery), and calcium wave frequency were quantified for each condition (n = 3 to 4).

Image and Statistical Analysis

As detailed above, quantification of cell viability, cell density, cell size, and Cx43 location was performed using ImageJ. Non-treated PCL was used as an initial control for viability and cell density experiments comparing the effect of PCL NaOH pre-treatment duration; NaOH-treated PCL films shown to support comparable cellular viability and density to PPy-PCL were used as a control for gap junction and calcium handling experiments. After quantification, the data was imported into MATLAB (MathWorks) where statistical analysis was performed and plots were generated. Images from three to four films were quantified for each treatment condition and averaged (n = 3 to 4). For statistical analysis involving two treatment conditions, a two tailed, two sample t-test was performed assuming equal variances. For statistical analysis involving more than two conditions, one way ANOVA was performed and significant differences between groups were identified using the Tukey-Kramer method. A p-value of less than 0.05 was considered statistically significant. All error bars represent standard deviations.

5.3. Results

NaOH Treatment of PCL Decreases WCA of Films

Based on previous studies, treatment with NaOH was anticipated to affect the surface chemistry of PCL by hydrolysis of the ester group, yielding materials displaying carboxylic acid and hydroxyl groups on their surfaces (Woodruff 2010, Oh and Lee 2013). NaOH treatment of PCL resulted in an exposure time-dependent decrease in hydrophobicity, as demonstrated by the change in WCA measurements (Fig. 5.2).

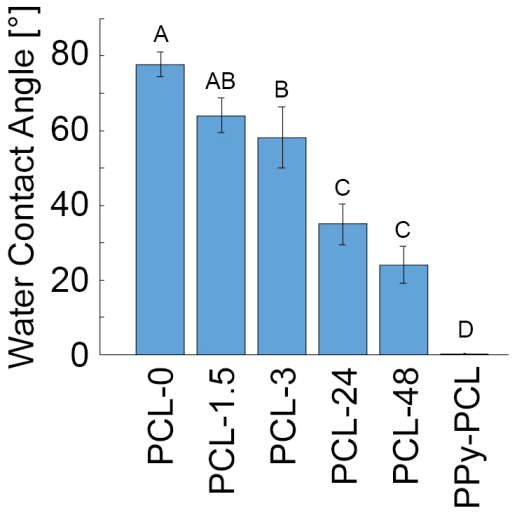

Figure 5.2. Water contact angle measurements taken from NaOH-treated PCL, PPy-PCL samples.

PCL films that were treated with water alone (PCL-0) had an average contact angle of 78 ± 3°; values for WCA decreased incrementally as the time of NaOH treatment was increased (denoted by PCL-hours of NaOH treatment: PCL-1.5: 64 ± 5°, PCL-3: 58 ± 8°, PCL-24: 35 ± 5°, PCL-48: 24 ± 5°). PPy-PCL showed super-hydrophilic characteristics, consistent with previous studies (Zhong 2006); the water droplet spread across the surface of the material upon contact giving an effective WCA of 0°.

PCL and PPy-PCL Material Properties

XPS analysis confirmed the surface modification of NaOH-treated PCL and polymerization of PPy-PCL (Fig. 5.3, Table 5-1). Treatment of the PCL with NaOH over 24 h period resulted in a shift of the carbon 1s peak, which is indicative of formation of carbonyl and alcohol groups (via hydrolysis of the ester bond). Successful polymerization of PPy within the PCL backbone was confirmed through identification of a nitrogen 1s peak (at ~400 eV) which was not present in the PCL films.

Table 5-1. Analysis of XPS peaks

XPS Analysis of Carbon 1s Peak

Sample	Peak (eV)		
	1	2	3
PCL-0	285.1	286.6	289.2
PCL-24	293.7	297.1	301.6
PPy-PCL	284.8	286.3	289.1

XPS Analysis of Nitrogen 1s Peak

Sample	Peak (eV)	
	1	2
PPy-PCL	401.9	400.0

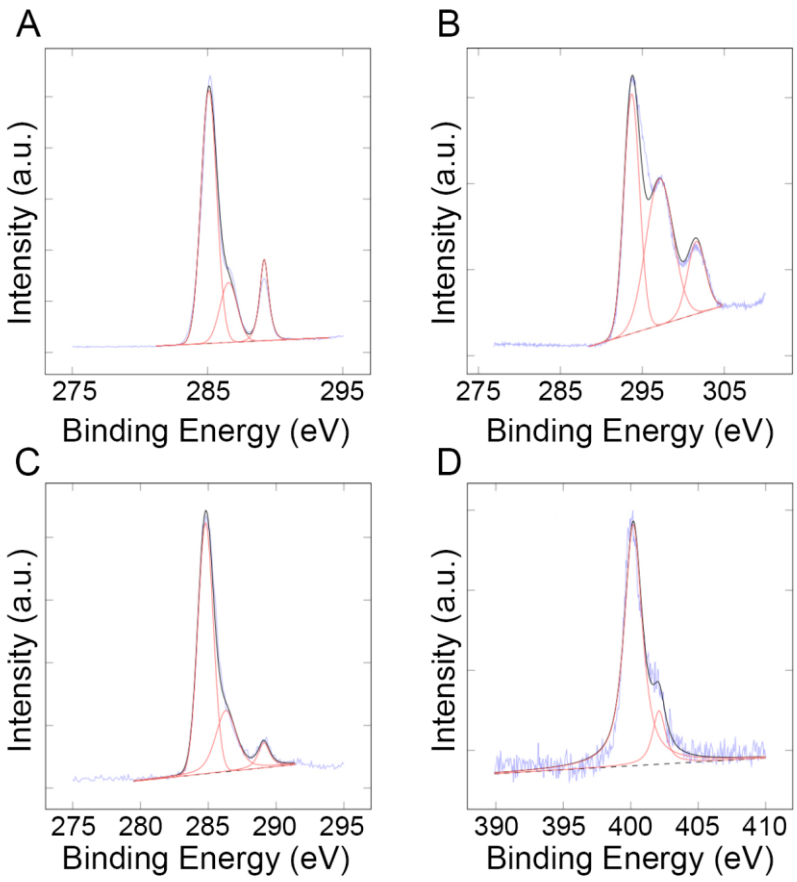

Figure 5.3. XPS peaks for (A) PCL-0, (B) PCL-24, (C) PPy-PCL, (D) PPy-PCL high energy.

Because material stiffness is known to affect phenotype of developing cardiomyocytes, nanoindentation was used to evaluate the mechanical properties of PCL after NaOH treatment and PPy polymerization. Both the PCL-24 and the PPy-PCL films exhibited similar elastic modulus (1.07 ± 0.05 GPa, 0.93 ± 0.19 GPa) and hardness (0.073 ± 0.008 GPa, 0.071 ± 0.02 GPa)(Fig. 5.4).

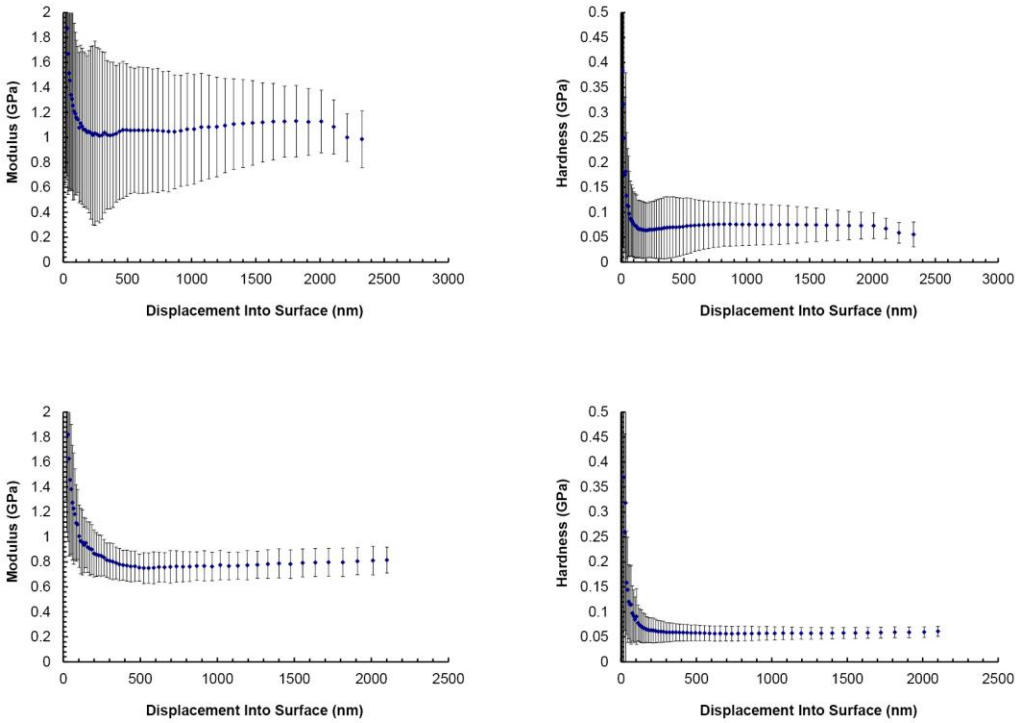

Figure 5.4. Modulus and hardness of (Top) PCL-24 and (Bottom) PPy-PCL films.

Conductive PPy-PCL Films Have Biomimetic Resistivity

Generation of an interpenetrating network of PPy within the non-conductive PCL films produced materials with electrical resistivities that closely mimicked the resistivity of native cardiac muscle. PCL and NaOH-treated films had infinite resistivity indicating that they did not conduct electricity, while the interpenetrating networks of PPy-PCL had an average resistivity of 1.0 ± 0.4 kΩ cm (Table 5-2). In comparison, native cardiac muscle has approximate resistivity of 0.5 kΩ cm (Rush, Abildskov et al. 1963), which is a factor of two lower than the PPy-PCL, and adipose tissue has approximate resistivity of 2.6 kΩ cm (Rush, Abildskov et al. 1963), which is a factor of two higher than the PPy-PCL films (Table 5-2). We therefore conclude that generation of an interpenetrating

network of PPy within PCL generates films with resistivities that closely mimic that of native cardiac muscle.

Table 5-2. Comparison of PPy-PCL, PCL resistivities to other materials

Material	Composition	Resistivity (kΩ cm)	Source
PCL-24		∞	This study
PPy-PCL		1.00±0.40	This study
Body Tissue			
Cardiac muscle		0.50	Rush et al, 1963
Skeletal muscle		0.70	Rush et al, 1963
Adipose tissue		2.60	Rush et al, 1963
Conductive Polymer Systems			
PCL/PANi	80:20	12.50	Borriello et al, 2011
aniline-dimer end-functionalized PU		100.00	Baheiraei et al, 2014
PANi/gelatin fibers	60:40	0.05	Li et al, 2005
PPy-PCL/gelatin	30:70	2.70	Kai et al, 2011
PLCL/PANi	70:30	> 0.01	Jun et al, 2009
PANi/PLGA fiber matrix	0.5%/8%	0.32	Hsiao et al, 2013
PANi/PGS	30:70	0.06	Qazi et al, 2014

High Cell Viability Observed on all Films

HL-1 cells adhered and remained viable when seeded on the surface of PCL-based films. PPy-PCL and PCL-24 surfaces were visualized both with and without cells using SEM imaging (Fig. 5.5). PCL-based films were mostly smooth with the presence of nano-scale cracks with respective thickness of 100-200 nm. The presence of an interpenetrating network of PPy increased the surface roughness somewhat (Fig. 5.5) with the thickness of the films increasing by less than 500 nm after generation of the PPy network. PCL-24 supported the attachment of HL-1 cells with a combination of

elongated and rounded morphologies; in contrast, HL-1 cells on PPy-PCL films appeared more elongated with fewer rounded cells adherent to the underlying HL-1 cell monolayer.

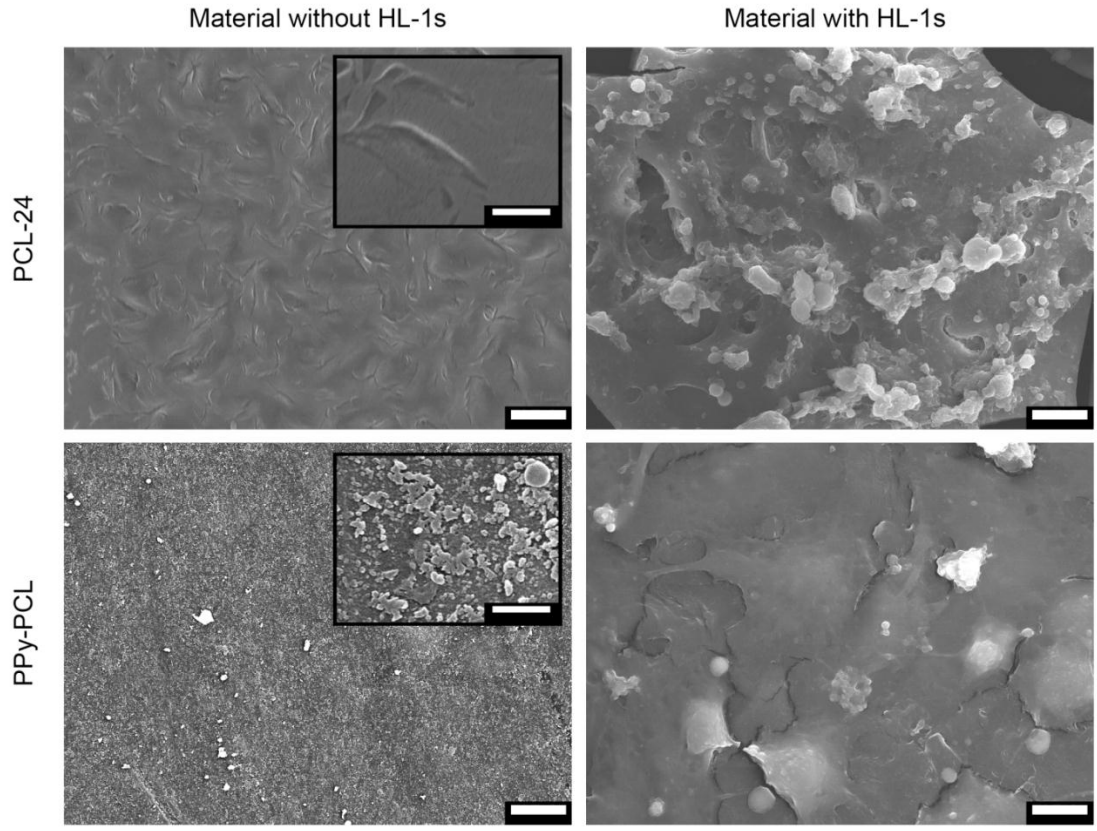

Figure 5.5. SEM images of PCL-24, PPy-PCL with and without HL-1 cells. Scale bars represent 10 µm (windowed scale bars represent 1 µm).

The surface chemistry of the films was found to have no effect on the viability of the cells (Fig. 5.6). Based on quantification following LIVE/DEAD staining, cell viability was found to be approximately 90% on all films (Fig. 5.7).

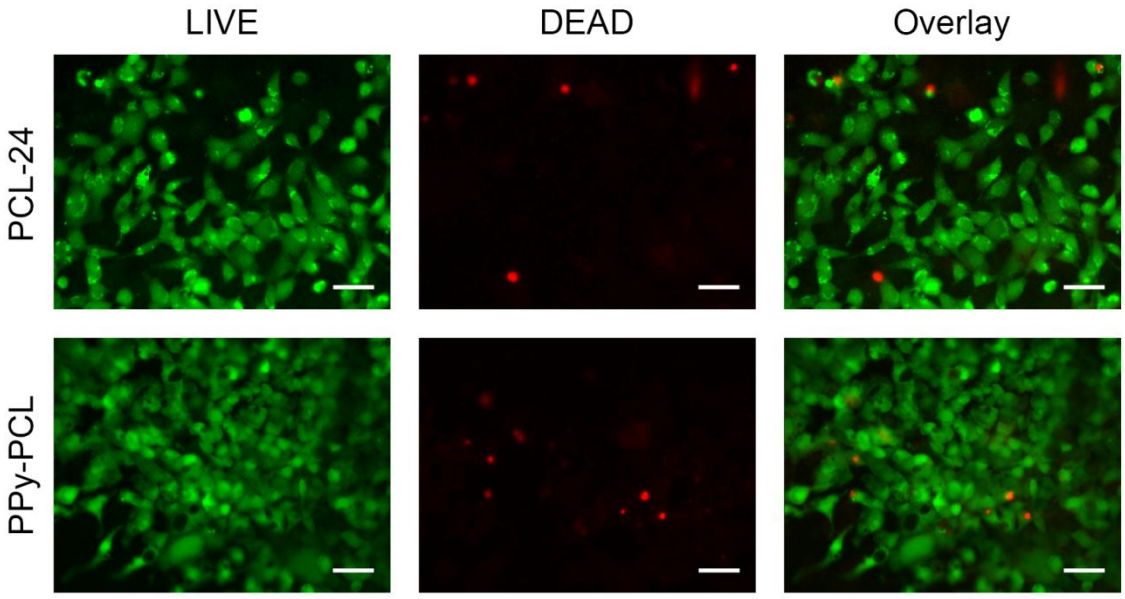

Figure 5.6. LIVE/DEAD images of HL-1 cells on PCL-24, PPy-PCL. Scale bars represent 40 µm.

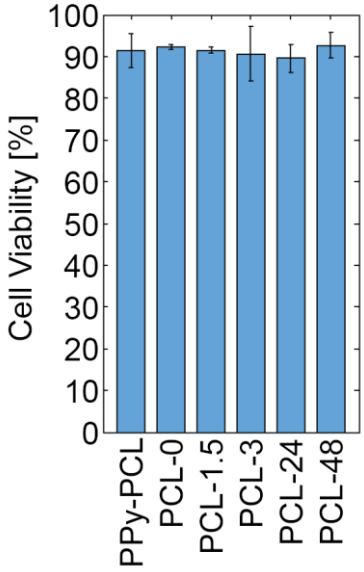

Figure 5.7. HL-1 viability is independent of film material type.

NaOH Treatment of PCL Increases Cell Adhesion

Achieving high densities of adherent cardiomyocytes on film materials is necessary in creating engineered cardiac tissues and can be challenging depending on the

material. As NaOH treatment time of the PCL films was increased and hydrophobicity decreased, there was a significant increase in the number of cells on the film surface per unit area (PCL-0: 1,568 ± 126 cells mm^{-2}, PCL-24: 2,880 ± 439 cells mm^{-2}, PCL-48: 3,623 ± 456 cells mm^{-2}, Fig. 5.8). Furthermore, increasing the NaOH treatment times led to an overall decrease in the area of individual adhered HL-1 cells (PCL-0: 419 ± 120 μm^2, PCL-24: 270 ± 48 μm^2, PCL-48: 270 ± 60 μm^2, Fig. 5.8).

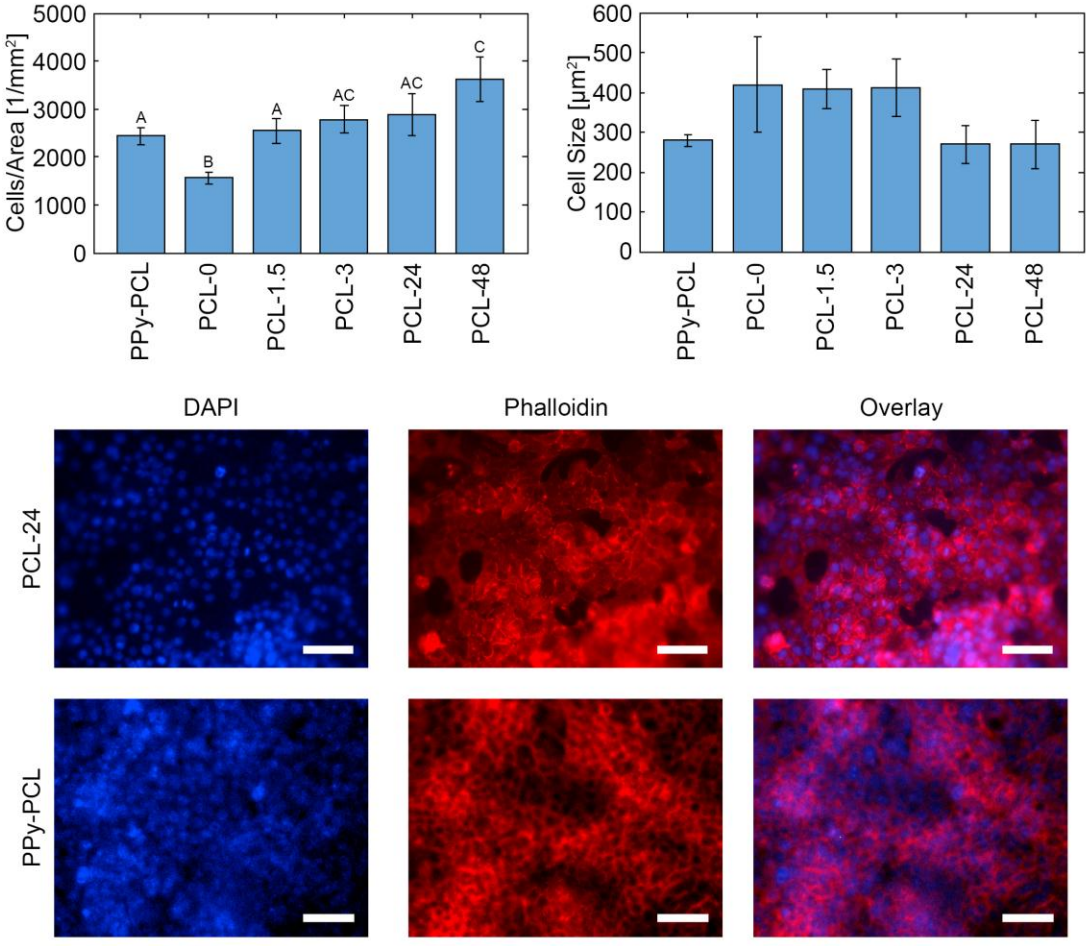

Figure 5.8. (Top) HL-1 cell size and cells per area on different films. (Bottom) Actin/nuclear stains of HL-1 cells on PCL-24 and PPy-PCL. Scale bars represent 40 µm.

HL-1 adhesion and cell size on PPy-PCL was most similar to PCL-24, with PPy-PCL films having 2,434 ± 166 cells mm^{-2} and the average area of HL-1 cells on PPy-PCL being 279 ± 15 μm^2; PCL-24 was selected, therefore, for comparison with PPy-PCL in functional and gene expression experiments.

Conductive PPy-PCL Films Encourage Peripheral Localization of Cx43

Cardiomyocyte growth on conductive PPy-PCL films resulted in a change in intracellular location of the gap junction Cx43, but did not significantly alter Cx43 gene expression.

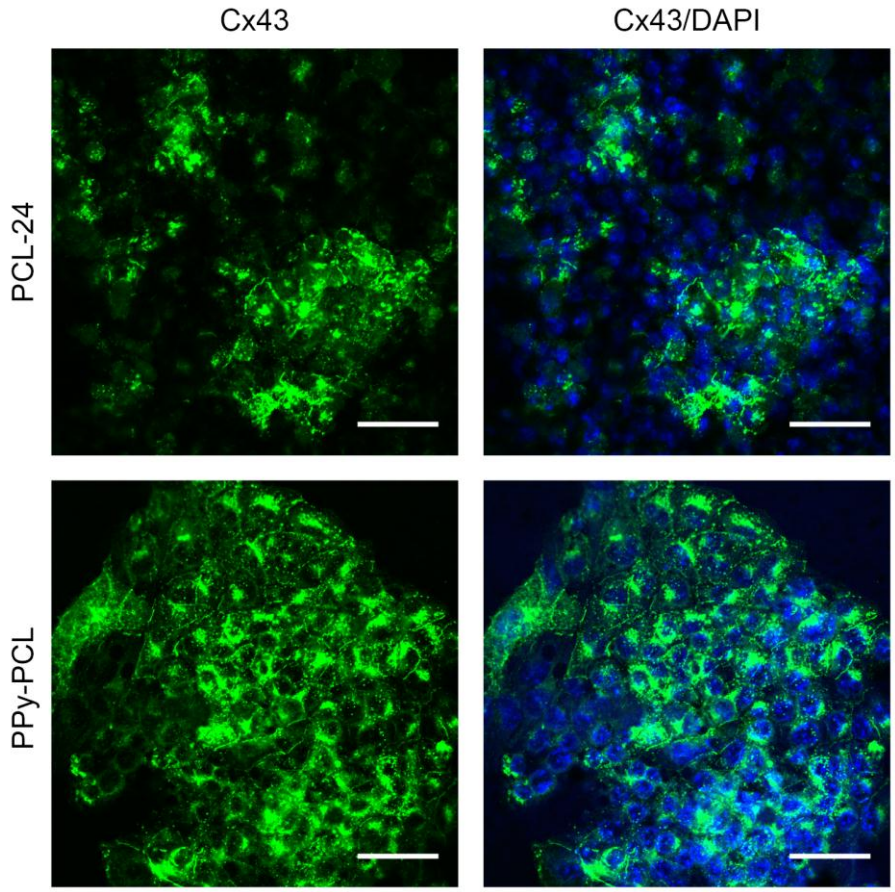

Figure 5.9. Immunocytochemistry images showing connexin-43/nuclei of HL-1 cells on PCL-24, PPy-PCL. Scale bars represent 40 µm.

In HL-1 cells grown on the electrically-conductive PPy-PCL, the gap junction protein Cx43 was frequently observed to be located around the cell periphery, whereas in HL-1 cells grown on PCL this was less frequently the case (Fig. 5.9). Based on analysis of immunofluorescence imaging, when cultured on PPy-PCL films, 60 ± 4% of HL-1 cells expressed peripheral Cx43, whereas 47 ± 6% of HL-1 cells expressed peripheral Cx43 when cultures on PCL-24 films ($p<0.05$, Fig. 5.10). No significant difference in Cx43 gene expression was observed between HL-1 cells cultured on PPy-PCL versus PCL-24 films based on qPCR analysis (Fig. 5.10).

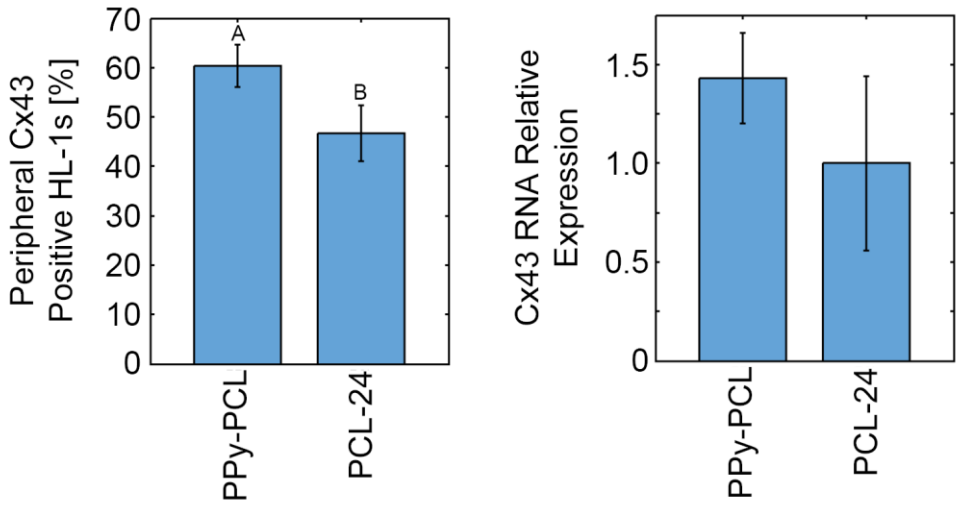

Figure 5.10. (Left) Percentage of HL-1 cells with peripheral Cx43 expression. (Right) Cx43 relative gene expression of HL-1 cells on PCL-24, PPy-PCL.

Calcium Transient Wave Propagation Improves on Conductive PPy-PCL Films

Growth of cardiac cell monolayers on conductive PPy-PCL films positively influenced functional properties. HL-1 cell monolayers grown on PPy-PCL demonstrated

an overall increase in the average velocity of calcium transient wave propagation in comparison to cells grown on PCL-24 (Fig. 5.11).

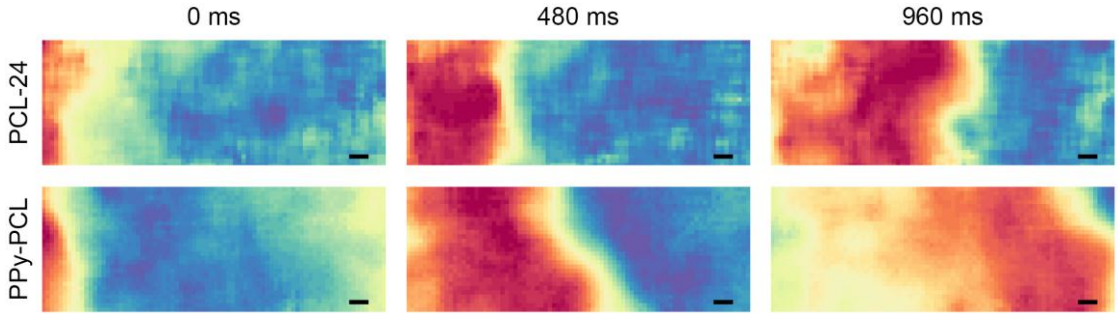

Figure 5.11. Representative calcium transient propagations for HL-1 cells on PCL-24, PPy-PCL films. Scale bars represent 100 μm.

Following 10-12 days of culture on the films, the average calcium transient wave velocity across HL-1 cell monolayers on PPy-PCL (1612 ± 143 μm/s) was significantly higher than that across HL-1 cell monolayers on PCL-24 (1,129 ± 247 μm/s, $p<0.05$, Fig. 5.12). Moreover, HL-1 cells cultured on PPy PCL also demonstrated improved calcium transient recovery relative to cells cultured on PCL 24; calcium transient durations, specifically the time to reach 50% recovery, were significantly shorter for HL 1 cells on PPy PCL (910 ± 60 ms) relative to HL-1 cells on PCL-24 (1,130 ± 20 ms, $p<0.01$, Fig. 5.12). Additionally, the frequency of spontaneous calcium transient propagation was higher for HL-1 cell monolayers on PPy-PCL as compared to on PCL-24 (0.48 ± 0.03 Hz and 0.31 ± 0.02 Hz, respectively, $p<0.01$ Fig. 5.13).

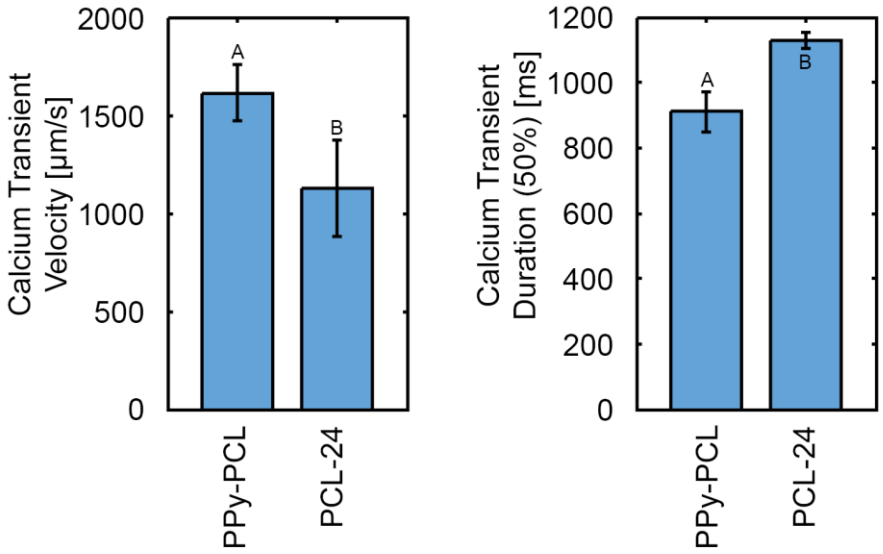

Figure 5.12. Calcium transient wave velocity and duration of HL-1 cells on PCL-24, PPy-PCL.

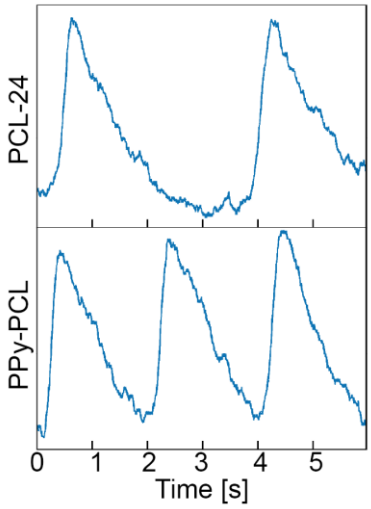

Figure 5.13. Representative calcium transient traces for HL-1 cells on PCL-24, PPy-PCL materials.

5.4. Discussion

The overall goal of this study was to determine the efficacy of conductive PPy-PCL interpenetrating networks for use as electroactive substrates for cardiomyocyte culture. To accomplish this goal, HL-1, a murine cardiomyocyte cell line, was employed in this first study examining the potential of PPy-PCL films for use in cardiac tissue engineering applications. Unlike primary cardiomyocytes, such as neonatal rat cardiomyocytes, HL-1 cells are capable of being expanded in vitro. HL-1 cells have previously been used in studies aiming to increase homogeneity of cardiomyocyte contraction (White, Constantin et al. 2004, Smith, Segar et al. 2012). Additionally, HL-1 cells, in contrast to other contractile cell types, are often limited to spontaneous contraction among isolated, independent clusters of cells. This provided a greater opportunity to evaluate changes in response to culture on the electrically-conductive PPy-PCL films, including changes in gene expression and functional properties, i.e. calcium transient propagation and duration, related to calcium and electrical signal handling. Future examination of other types of cardiomyocytes cultured on PPy-PCL will provide additional insights into the usefulness of this material as a conductive cardiac tissue engineering platform.

The resistivity of PPy-PCL films used in this study was 1.0 ± 0.4 kΩ cm, which is similar to the reported resistivity of cardiac tissue (approximately 0.5 kΩ cm) (Rush, Abildskov et al. 1963). A variety of methods for preparing PPy-PCL films were tested including employing only solvent casting or heat pressing to prepare the PCL; however, the most consistent method was found to be the one utilizing both solvent casting and a heat press as described above. This method resulted in the creation of films with

consistent topography and shape, as well as conductive substrates with reproducible resistivities. Furthermore, the PPy-PCL films exhibit elastic moduli and hardness similar to NaOH-treated PCL films (Fig. 5.4), as well as resistivities which are comparable to those of other conductive polymer systems that have been synthesized for use in other tissue engineering platforms (Table 5-2).

Changes in PCL surface chemistry as a result of NaOH treatment and PPy polymerization may be important factors contributing to the significant increase in numbers of cells (and concomitant decrease in the average size of cells) on each material relative to the PCL-0. NaOH treatment of PCL was found to result in increased cell adhesion to the PCL films, consistent with studies using a multitude of different cell sources (Thapa, Webster et al. 2003, Serrano, Portoles et al. 2005, Yeo, Wong et al. 2010, Wang, Teo et al. 2013). NaOH treatment causes hydrolysis of the ester bonds within the PCL films, thereby exposing carboxylic acid and hydroxyl groups on the surface which renders the surfaces more hydrophilic (Vance, Miller et al. 2004). Under physiologically-mimetic conditions (i.e. PBS, pH 7.4), the carboxyl groups exposed after hydrolysis of the PCL will be deprotonated and therefore negatively charged, as indeed would the sulfonate groups displayed on the polystyrene sulfonate dopant for PPy. Although all films were coated with a gelatin-fibronectin solution prior to HL-1 seeding, differing electrostatic interactions could result in differences in the relative amount and distribution of proteins adsorbed, particularly following one week in culture. Cell adhesion, which is typically mediated by the cell-matrix interactions, is heavily dependent on the distribution of different proteins that adsorb on the surface of a biomaterial (Higgins 2012). While surface chemistry strongly influences cellular attachment, modifications to surface

structure or topography via chemical polymerization or hydrolization may also contribute to greater adherent cell numbers observed on PCL-24 and PPy-PCL films.

Inability to form a syncytium through poor re-formation of gap junctions is a serious impediment to creation of engineered cardiac tissue from dissociated cardiomyocytes. One potential reason for this lack of cellular interconnectivity is the inability of the cells to sense each other electrically on the substrate. For instance, junctional conductance is lower in developing neonatal rat cardiomyocytes compared to adult rat cardiomyocytes, which may result from decreased expression or poor organization of Cx43 (Fishman, Moreno et al. 1991). Cell adhesion to conductive polymers is typically mediated via both integrin and non-integrin interactions with surface-adsorbed proteins (Higgins 2012). Although the underlying material is likely separated from the adherent cells by a layer of adsorbed and secreted proteins, conductive polymers influence the electrical charge within a local cellular environment, which in turn can result in changes in cell phenotype. Another issue that hinders the creation of engineered cardiac tissue is the inability to induce synchronous contraction of cardiac cells during in vitro culture. Induction of synchronous contraction of cardiac cells used to create engineered cardiac tissue, either through electrical pacing or by mechanical stimulation, has led to reduced heterogeneity (Limpitikul 2010) and improved maturation (Radisic, Park et al. 2004), including maintenance of differentiated cell phenotypes (Radisic, Park et al. 2004), elongation and alignment of cells (Radisic, Park et al. 2004), and increased gap junction formation among cells (Radisic, Park et al. 2004, Sathaye, Bursac et al. 2006).

Some studies employing conductive substrates for cardiomyocyte culture have demonstrated increased Cx43 gene expression, including neonatal rat cardiomyocytes cultured in hydrogels containing gold nanoparticles (You, Rafat et al. 2011) or gold nanowires (Dvir, Timko et al. 2011), whereas others have seen functional improvements in engineered cardiac tissues without changes in Cx43 expression (Shin, Jung et al. 2013). In this study, analysis of Cx43 gene expression via qPCR did not reveal significant differences between HL-1 cells cultured on PPy PCL versus on PCL. This finding suggests that the functional differences observed between cells cultured on each film may be due to improved organization and formation of gap junctions in HL-1 cells on the PPy-PCL, which has been demonstrated through fluorescence image analysis of HL-1 cells stained for Cx43 (Fig. 5.9). Other studies support this observed correlation between changes in cellular function and altered localization of Cx43. For instance, exogenous electrical pacing, which has shown improvement in functional maturation of cardiomyocytes, has resulted in increased presence of Cx43 structures within engineered rat myocardium (Hirt, Hansen et al. 2014) as well as increased Cx43 along the membranes of individual neonatal rat cardiomyocytes relative to non stimulated myocardium (Lasher, Pahnke et al. 2012). Similarly, cyclical mechanical stretching of cardiomyocytes has been shown to enhance overall Cx43 presence (Zhang, Wan et al. 2012), which can include increased gap junction expression at the poles of each cell (Salameh, Wustmann et al. 2010). While the exact mechanism for cellular communication on conductive surfaces hasn't been elucidated, it has been postulated by others that enhanced localization of connexins and formation of gap junctions is a consequence of increased spontaneous depolarization which may be a result of cells

detecting electrical signals from the local environment (You, Rafat et al. 2011). Enhancing Cx43 expression and organization is also of particular importance for differentiation of stem cell-derived cardiomyocytes from pluripotent stem cells and results suggest employing a conductive polymer film may be an effective tool to aid in this process.

Electrophysiological maturation, as evidenced through changes in ion channel currents, electrical propagation, and calcium handling, is a fundamental characteristic for assessing the efficacy of cardiac tissue models. In this study, optical mapping of calcium waves demonstrated increased calcium transient velocities and decreased calcium transient durations among HL-1 cells cultured on PPy-PCL in comparison to cells on PCL alone (Fig. 5.12). These results are consistent with observations of maturation in neonatal cardiomyocytes cultured in vitro for extended periods, resulting in reduction in action potential duration (Guo, Kamiya et al. 1996). While fundamental knowledge elucidating the mechanism by which conductive materials improve electrophysiology is incomplete, parallels may be drawn between systems which subject in vitro cardiomyocytes to exogenous electrical stimulation or mechanical stretch. In such cases, improvements in conduction velocity and action potential duration are associated with transient activity of specific ion channel currents, including I_{t0}, I_{NaCa}, and $I_{Ca,L}$ (Alseikhan, DeMaria et al. 2002, Sathaye, Bursac et al. 2006). However, improvement in conduction velocity, or calcium transient wave propagation, is also mediated by changes in cell cell coupling which may be influenced by exogenous electrical or mechanical pacing. This idea is consistent with the increased peripheral Cx43 presence observed among HL-1 cells cultured on PPy-PCL films (Fig. 5.10). Together, these data demonstrate the

efficacy of conductive substrates to aid electrophysiological maturation of cells cultured on their surfaces, which may be of clinical relevance for the future design and manufacture of engineered heart tissues.

5.5. Conclusions

This study demonstrated that conductive PPy-PCL films effectively support cardiomyocyte culture and could be useful in enhancing the functional properties and maturation of cardiomyocyte cell sheets. Treatment of PCL films with NaOH resulted in decreased surface hydrophobicity, increased cardiomyocyte attachment and decreased cell size. PPy-PCL substrates promoted cellular attachment at comparable densities and cell areas relative to NaOH-treated PCL films and without a change in cellular viability. Cx43 gene expression was similar for HL-1 cardiomyocytes grown on PPy-PCL and PCL films. However, localization of Cx43 protein differed; when HL-1 cells were cultured on PPy-PCL, Cx43 was more frequently observed to be along the cell periphery. Additionally, HL-1 cells grown on conductive PPy-PCL films supported significantly faster calcium transient velocities and significantly lower calcium transient durations relative to HL-1 cells grown on control PCL films. These data encourage the use of conductive materials as substrates for cardiac tissue engineering; providing enhanced substrate conductivity, similar to that of native cardiac tissue, may constitute an important component in achieving proper electrophysiological development of cardiac cell types, and may have clinical relevance for cardiac tissue engineering applications.

References

Alseikhan, B. A., C. D. DeMaria, H. M. Colecraft and D. T. Yue (2002). "Engineered calmodulins reveal the unexpected eminence of Ca2+ channel inactivation in controlling heart excitation." Proc Natl Acad Sci U S A 99(26): 17185-17190.

Bechara, S., L. Wadman and K. C. Popat (2011). "Electroconductive polymeric nanowire templates facilitates in vitro C17.2 neural stem cell line adhesion, proliferation and differentiation." Acta Biomater 7(7): 2892-2901.

Black, L. D., 3rd, J. D. Meyers, J. S. Weinbaum, Y. A. Shvelidze and R. T. Tranquillo (2009). "Cell-induced alignment augments twitch force in fibrin gel-based engineered myocardium via gap junction modification." Tissue Eng Part A 15(10): 3099-3108.

Blazeski, A., R. Zhu, D. W. Hunter, S. H. Weinberg, K. R. Boheler, E. T. Zambidis and L. Tung (2012). "Electrophysiological and contractile function of cardiomyocytes derived from human embryonic stem cells." Prog Biophys Mol Biol 110(2-3): 178-195.

Blazeski, A., R. Zhu, D. W. Hunter, S. H. Weinberg, E. T. Zambidis and L. Tung (2012). "Cardiomyocytes derived from human induced pluripotent stem cells as models for normal and diseased cardiac electrophysiology and contractility." Prog Biophys Mol Biol 110(2-3): 166-177.

Borriello, A., V. Guarino, L. Schiavo, M. A. Alvarez-Perez and L. Ambrosio (2011). "Optimizing PANi doped electroactive substrates as patches for the regeneration of cardiac muscle." J Mater Sci Mater Med 22(4): 1053-1062.

Claycomb, W. C., N. A. Lanson, Jr., B. S. Stallworth, D. B. Egeland, J. B. Delcarpio, A. Bahinski and N. J. Izzo, Jr. (1998). "HL-1 cells: a cardiac muscle cell line that contracts and retains phenotypic characteristics of the adult cardiomyocyte." Proc Natl Acad Sci U S A 95(6): 2979-2984.

Dunn, D. A., A. J. Hodge and E. A. Lipke (2014). "Biomimetic materials design for cardiac tissue regeneration." Wiley Interdiscip Rev Nanomed Nanobiotechnol 6(1): 15-39.

Durgam, H., S. Sapp, C. Deister, Z. Khaing, E. Chang, S. Luebben and C. E. Schmidt (2010). "Novel degradable co-polymers of polypyrrole support cell proliferation and enhance neurite out-growth with electrical stimulation." J Biomater Sci Polym Ed 21(10): 1265-1282.

Dvir, T., B. P. Timko, M. D. Brigham, S. R. Naik, S. S. Karajanagi, O. Levy, H. Jin, K. K. Parker, R. Langer and D. S. Kohane (2011). "Nanowired three-dimensional cardiac patches." Nat Nanotechnol 6(11): 720-725.

Fishman, G. I., A. P. Moreno, D. C. Spray and L. A. Leinwand (1991). "Functional analysis of human cardiac gap junction channel mutants." Proc Natl Acad Sci U S A 88(9): 3525-3529.

Fonner, J. M., L. Forciniti, H. Nguyen, J. D. Byrne, Y. F. Kou, J. Syeda-Nawaz and C. E. Schmidt (2008). "Biocompatibility implications of polypyrrole synthesis techniques." Biomed Mater 3(3): 034124.

George, P. M., A. W. Lyckman, D. A. LaVan, A. Hegde, Y. Leung, R. Avasare, C. Testa, P. M. Alexander, R. Langer and M. Sur (2005). "Fabrication and biocompatibility of polypyrrole implants suitable for neural prosthetics." Biomaterials 26(17): 3511-3519.

Guimard, N. K., J. L. Sessler and C. E. Schmidt (2009). "Towards a Biocompatible, Biodegradable Copolymer Incorporating Electroactive Oligothiophene Units." Macromolecules 42(2): 502-511.

Guo, W., K. Kamiya and J. Toyama (1996). "Modulated expression of transient outward current in cultured neonatal rat ventricular myocytes: comparison with development in situ." Cardiovasc Res 32(3): 524-533.

Hardy, J. G., J. Y. Lee and C. E. Schmidt (2013). "Biomimetic conducting polymer-based tissue scaffolds." Curr Opin Biotechnol 24(5): 847-854.

Heron, M. (2012). "Deaths: leading causes for 2009." Natl Vital Stat Rep 61(7): 1-94.

Higgins, M. J. M., P. J.; Yue, Z.; Wallace, G. G. (2012). "Organic Conducting Polymer-Protein Interactions." Chemistry of Materials 24(5): 828-839.

Hirt, M. N., J. Boeddinghaus, A. Mitchell, S. Schaaf, C. Bornchen, C. Muller, H. Schulz, N. Hubner, J. Stenzig, A. Stoehr, C. Neuber, A. Eder, P. K. Luther, A. Hansen and T. Eschenhagen (2014). "Functional improvement and maturation of rat and human engineered heart tissue by chronic electrical stimulation." J Mol Cell Cardiol 74: 151-161.

Hirt, M. N., A. Hansen and T. Eschenhagen (2014). "Cardiac tissue engineering: state of the art." Circ Res 114(2): 354-367.

Hodge, A. J. K., P.; Dunn, D. A.; Lipke, E. A. (2014). Biomimetic Materials for Cardiac Regeneration, World Scientific Publishing Co.

Hu, H., Y. Ni, V. Montana, R. C. Haddon and V. Parpura (2004). "Chemically Functionalized Carbon Nanotubes as Substrates for Neuronal Growth." Nano Lett 4(3): 507-511.

Kai, D., M. P. Prabhakaran, G. Jin and S. Ramakrishna (2011). "Polypyrrole-contained electrospun conductive nanofibrous membranes for cardiac tissue engineering." J Biomed Mater Res A 99(3): 376-385.

Lasher, R. A., A. Q. Pahnke, J. M. Johnson, F. B. Sachse and R. W. Hitchcock (2012). "Electrical stimulation directs engineered cardiac tissue to an age-matched native phenotype." J Tissue Eng 3(1): 2041731412455354.

Lee, J. Y., C. A. Bashur, A. S. Goldstein and C. E. Schmidt (2009). "Polypyrrole-coated electrospun PLGA nanofibers for neural tissue applications." Biomaterials 30(26): 4325-4335.

Li, M., Y. Guo, Y. Wei, A. G. MacDiarmid and P. I. Lelkes (2006). "Electrospinning polyaniline-contained gelatin nanofibers for tissue engineering applications." Biomaterials 27(13): 2705-2715.

Limpitikul, W. C., N.; Thompson, S. A.; Gearhart, J. D.; Tung, L.; Lipke, E. A. (2010). "Influence of Electromechanical Activity on Cardiac Differentiation of Mouse Embryonic Stem Cells." Cardiovascular Engineering Technology 1: 179-193.

McKenzie, J. L., M. C. Waid, R. Shi and T. J. Webster (2004). "Decreased functions of astrocytes on carbon nanofiber materials." Biomaterials 25(7-8): 1309-1317.

Mihardja, S. S., R. E. Sievers and R. J. Lee (2008). "The effect of polypyrrole on arteriogenesis in an acute rat infarct model." Biomaterials 29(31): 4205-4210.

Moulton, M. J. H., M. J.; Kapsa, R. M. I.; Wallace, G. G. (2012). "Organic Bionics: A New Dimension in Neural Communications." Advanced Functional Materials 22: 2003-2014.

Nunes, S. S., J. W. Miklas, J. Liu, R. Aschar-Sobbi, Y. Xiao, B. Zhang, J. Jiang, S. Masse, M. Gagliardi, A. Hsieh, N. Thavandiran, M. A. Laflamme, K. Nanthakumar, G. J. Gross, P. H. Backx, G. Keller and M. Radisic (2013). "Biowire: a platform for maturation of human pluripotent stem cell-derived cardiomyocytes." Nat Methods 10(8): 781-787.

Oh, S. H. and J. H. Lee (2013). "Hydrophilization of synthetic biodegradable polymer scaffolds for improved cell/tissue compatibility." Biomed Mater 8(1): 014101.

Qazi, T. H., R. Rai, D. Dippold, J. E. Roether, D. W. Schubert, E. Rosellini, N. Barbani and A. R. Boccaccini (2014). "Development and characterization of novel electrically conductive PANI-PGS composites for cardiac tissue engineering applications." Acta Biomater 10(6): 2434-2445.

Radisic, M., H. Park, H. Shing, T. Consi, F. J. Schoen, R. Langer, L. E. Freed and G. Vunjak-Novakovic (2004). "Functional assembly of engineered myocardium by electrical

stimulation of cardiac myocytes cultured on scaffolds." Proc Natl Acad Sci U S A 101(52): 18129-18134.

Rush, S., J. A. Abildskov and McFeer (1963). "Resistivity of body tissues at low frequencies." Circ Res 12: 40-50.

Salameh, A., A. Wustmann, S. Karl, K. Blanke, D. Apel, D. Rojas-Gomez, H. Franke, F. W. Mohr, J. Janousek and S. Dhein (2010). "Cyclic mechanical stretch induces cardiomyocyte orientation and polarization of the gap junction protein connexin43." Circ Res 106(10): 1592-1602.

Sathaye, A., N. Bursac, S. Sheehy and L. Tung (2006). "Electrical pacing counteracts intrinsic shortening of action potential duration of neonatal rat ventricular cells in culture." J Mol Cell Cardiol 41(4): 633-641.

Schmidt, C. E., V. R. Shastri, J. P. Vacanti and R. Langer (1997). "Stimulation of neurite outgrowth using an electrically conducting polymer." Proc Natl Acad Sci U S A 94(17): 8948-8953.

Serrano, M. C., M. T. Portoles, M. Vallet-Regi, I. Izquierdo, L. Galletti, J. V. Comas and R. Pagani (2005). "Vascular endothelial and smooth muscle cell culture on NaOH-treated poly(epsilon-caprolactone) films: a preliminary study for vascular graft development." Macromol Biosci 5(5): 415-423.

Shin, S. R., S. M. Jung, M. Zalabany, K. Kim, P. Zorlutuna, S. B. Kim, M. Nikkhah, M. Khabiry, M. Azize, J. Kong, K. T. Wan, T. Palacios, M. R. Dokmeci, H. Bae, X. S. Tang and A. Khademhosseini (2013). "Carbon-nanotube-embedded hydrogel sheets for engineering cardiac constructs and bioactuators." ACS Nano 7(3): 2369-2380.

Shvedova, A. A., V. Castranova, E. R. Kisin, D. Schwegler-Berry, A. R. Murray, V. Z. Gandelsman, A. Maynard and P. Baron (2003). "Exposure to carbon nanotube material: assessment of nanotube cytotoxicity using human keratinocyte cells." J Toxicol Environ Health A 66(20): 1909-1926.

Smith, A. W., C. E. Segar, P. K. Nguyen, M. R. MacEwan, I. R. Efimov and D. L. Elbert (2012). "Long-term culture of HL-1 cardiomyocytes in modular poly(ethylene glycol) microsphere-based scaffolds crosslinked in the phase-separated state." Acta Biomater 8(1): 31-40.

Thapa, A., T. J. Webster and K. M. Haberstroh (2003). "Polymers with nano-dimensional surface features enhance bladder smooth muscle cell adhesion." J Biomed Mater Res A 67(4): 1374-1383.

Vance, R. J., D. C. Miller, A. Thapa, K. M. Haberstroh and T. J. Webster (2004). "Decreased fibroblast cell density on chemically degraded poly-lactic-co-glycolic acid, polyurethane, and polycaprolactone." Biomaterials 25(11): 2095-2103.

Wang, Z., C. Roberge, L. H. Dao, Y. Wan, G. Shi, M. Rouabhia, R. Guidoin and Z. Zhang (2004). "In vivo evaluation of a novel electrically conductive polypyrrole/poly(D,L-lactide) composite and polypyrrole-coated poly(D,L-lactide-co-glycolide) membranes." J Biomed Mater Res A 70(1): 28-38.

Wang, Z. Y., E. Y. Teo, M. S. Chong, Q. Y. Zhang, J. Lim, Z. Y. Zhang, M. H. Hong, E. S. Thian, J. K. Chan and S. H. Teoh (2013). "Biomimetic three-dimensional anisotropic geometries by uniaxial stretch of poly(epsilon-caprolactone) films for mesenchymal stem cell proliferation, alignment, and myogenic differentiation." Tissue Eng Part C Methods 19(7): 538-549.

Webster, T. J. W., M. C.; McKenzie, J. L.; Price, R. L.; Ejiofor, J. U. (2004). "Nano-biotechnology: carbon nanofibres as improved neural and orthopaedic implants." Nanotechnology 15(1): 48-54.

Weinberg, S., E. A. Lipke and L. Tung (2010). "In vitro electrophysiological mapping of stem cells." Methods Mol Biol 660: 215-237.

White, S. M., P. E. Constantin and W. C. Claycomb (2004). "Cardiac physiology at the cellular level: use of cultured HL-1 cardiomyocytes for studies of cardiac muscle cell structure and function." Am J Physiol Heart Circ Physiol 286(3): H823-829.

Woodruff, M. A. H., D. W. (2010). "The return of a forgotten polymer—Polycaprolactone in the 21st century." Progress in Polymer Science 35(10): 1217–1256.

Yeo, A., W. J. Wong, H. H. Khoo and S. H. Teoh (2010). "Surface modification of PCL-TCP scaffolds improve interfacial mechanical interlock and enhance early bone formation: an in vitro and in vivo characterization." J Biomed Mater Res A 92(1): 311-321.

You, J. O., M. Rafat, G. J. Ye and D. T. Auguste (2011). "Nanoengineering the heart: conductive scaffolds enhance connexin 43 expression." Nano Lett 11(9): 3643-3648.

Zhang, T., L. Q. Wan, Z. Xiong, A. Marsano, R. Maidhof, M. Park, Y. Yan and G. Vunjak-Novakovic (2012). "Channelled scaffolds for engineering myocardium with mechanical stimulation." J Tissue Eng Regen Med 6(9): 748-756.

Zhong, W. L., S.; Chen, X.; Wang, Y.; Yang, W. (2006). "High-Yield Synthesis of Superhydrophilic Polypyrrole Nanowire Networks." Macromolecules 39(9): 3224–3230.

6. DIFFERENTIATION ON CONDUCTIVE POLYMERS FACILITATES MATURATION OF STEM CELL-DERIVED CARDIOMYOCYTES

6.1. Introduction

Creation of mature cardiomyocytes is a critical step towards the implementation of cells in clinical or diagnostic research applications. In recent years, the field of cardiac tissue engineering has focused on methods for directing functional maturation of stem cell-derived cardiomyocytes (SC-CMs), which are typically similar to fetal or neonatal cardiomyocytes (van den Berg, Okawa et al. 2015). The development of engineered biomaterial platforms has led to the formation of SC-CMs in vitro with gene expression, protein phenotypes, and functional properties that are more physiologically accurate than cells created using standard differentiation protocols (Chun, Balikov et al. 2015). Additionally, novel engineered substrates have been developed which generate cardiac monolayers and tissue with well-defined structure, facilitating anisotropic electrical propagation and mechanical stretch (Feinberg, Alford et al. 2012, Khan, Xu et al. 2015, Pilarczyk, Raulf et al. 2016). Despite the advancements made in this area, the production of physiologically-viable cardiomyocytes in vitro for cardiac regenerative therapies remains a challenging endeavor. For instance, many novel materials are limited in their capacity to actively facilitate cell-cell signaling, impeding the progression of electrical signaling and increasing the likelihood of arrhythmias after engraftment into the diseased myocardium.

Incorporation of mechanisms within the local cellular environment which promote the formation of cell-cell coupling may comprise a necessary step for improving electrical signaling within engineered cardiac tissue. Electrical propagation through the myocardium is regulated strongly through the formation of gap junctions which localize

along the intercalated discs of the cardiomyocytes; these low resistance pathways act to regulate the synchronicity of action potentials (Ye and Black 2011). On average, cardiomyocytes couple adjacently to 11 other cells, accomplished by the formation of tight junctions, gap junctions, and integrin binding (Saffitz 1994, Stoppel, Hu et al. 2015). Together, these features not only ensure electrical signaling between cardiomyocytes, but also help define anisotropic propagation through the myocardium (Rohr, Fluckiger-Labrada et al. 2003). Connexins, the proteins which comprise the structure of gap junctions, play complex roles in cardiomyocyte development, including the development of conduction system of the heart (Salameh, Wustmann et al. 2010). Differentiation strategies which actively promote the development of gap junctions (and enhance expression of connexins) will be critical for the creation of functional myocardium.

Implementation of exogenous electrical signaling has been utilized as a method for improving cell-cell signaling among SC-CMs in vitro. Exogenous electrical pacing, while demonstrating improvement in alignment and contraction strength of engineered cardiac tissue by influencing the expression of gap junction proteins, is difficult to transition into large scale culture of SC-CMs. The incorporation of conductive materials into scaffolds may offer one alternative solution for increasing cell-cell signaling and improved electrical conductivity through engineered tissues. A number of materials have been employed previously in the creation of biomimetic conductive scaffolds, including gold nanoparticles, carbon nanotubes, and semi-conductive polymers. Incorporation of these conductive materials has led to increases in expression of Nkx2.5 (Mooney, Mackle et al. 2012), connexin-43 (You, Rafat et al. 2011), and sarcomeric actinin (Dvir, Timko et

al. 2011) utilizing different stem and cardiac cell types. However, employment of these materials for large-scale cell culture or clinical applications may be hindered by high costs and toxicity concerns. Polypyrrole (PPy), a semi-conductive polymer used in neural tissue engineering applications, is known for having strong biocompatibility and physiologically-relative conductive properties (Durgam, Sapp et al. 2010). Additionally, PPy can be synthesized readily and constructed into different structures and geometries to form scaffolds for tissue engineering (Hardy, Lee et al. 2013). The brittle mechanical properties of PPy, in addition to being markedly different from native myocardium, make the material difficult to work with outright; however, PPy can be doped or combined with a more workable material, such as polycaprolactone (PCL), in order to create a material suitable for tissue engineering applications. PPy-PCL scaffolds have demonstrated effectiveness in neural and cardiac tissue applications, supporting the culture of primary cardiomyocytes in a three-dimensional environment (Kai, Prabhakaran et al. 2011).

The use of PPy-PCL scaffolds in the differentiation of stem cells offers a novel approach to directing the fate and maturation of SC-CMs. In this study, pluripotent stem cells were differentiated and subsequently cultured on PCL or PPy PCL scaffolds using previously investigated techniques. Viability, as well as protein expression of SC-CMs, was assessed over the course of differentiation. Electrophysiological maturation of SC-CMs was also assessed by quantifying calcium transients via optical mapping. This study offers new insight into how developing cardiomyocytes behave on conductive polymer systems.

6.2. Materials and Methods

Fabrication of PPy-PCL

Production of PPy-PCL constructs was performed using established protocols. Briefly, solid PCL beads were dissolved in 3 wt% dichloromethane and poured into glass petri dishes. After solvent evaporation, cast PCL disks were flattened using a melt press and individual constructs were cut using a stainless steel punch. PCL scaffolds were treated with 3M NaOH for 24 hours to adjust surface chemistry to allow for improved cell attachment. PCL was doped with PPy using established protocols. All materials were dried and sterilized prior to use. A solution of fibronectin (25 ng/μL) was used to coat PCL and PPy-PCL constructs for 1 hour prior to experiments to promote cell attachment.

Culture and Differentiation of SC-CMs

A D3 mouse embryonic stem cell (mESC) line (kind gift of Drs. L. Tung and J. Gearhart), genetically modified for neomycin resistance on an α-MHC promoter, was used in all experiments (Klug et al. 1996; W. Limpitikul 2011). Cultures of undifferentiated mESCs were expanded and maintained on mitotically inactivated mouse embryonic fibroblast (mEF) feeder layers in mESC culture medium containing: DMEM (Lonza, Walkersville, MD) with 10% (v/v) ESC-defined fetal bovine serum (FBS, Atlanta Biologicals, Norcross GA), 2 mM Glutamax (Gibco, Life Technologies, Grand Island, NY), 100 μM non-essential amino acids (Gibco), 1 mM sodium pyruvate (Gibco), 50 μg/mL gentamicin sulfate (Lonza), 55 μM β-mercaptoethanol (Gibco), and 103 U/mL leukemia inhibitory factor (LIF, Millipore, Billerica, MA). Prior to initiating differentiation, feeder layers were removed and mESCs were further expanded on gelatin-coated plates. Embryoid bodies (EBs) were formed via hanging drop method (at

~1000 cells per EB); after 48 hours EBs were collected and transferred into poly(hydroxyl)ethyl-methacrylate (poly(HEMA))-coated dishes. Ascorbic acid (at a working concentration of 570 μM) was added to culture media to facilitate cardiac differentiation. On day 5 of differentiation, EBs were transferred into gelatin coated-dishes to promote attachment. Media was replaced in each dish after 96 hours of culture time.

Dissociation of stem cell-derived cardiomyocytes

Dissociation of EBs was performed to create uniform monolayers of SC-CMs on the PCL and PPy-PCL films (Kehat et al. 2001). Briefly, PDMS-coated glass coverslips were prepared using a spin coater and sterilized overnight in ethanol. After drying the coverslips with a nitrogen gun, a solution of PBS containing fibronectin (25 μL/mL) was added on the coverslips and incubated at room temperature for 1 hour. EBs from control and CysNO-treated populations were rinsed with PBS; EBs were then agitated in dissociation solution (potassium chloride (5.4 mM), magnesium sulfate (5 mM), sodium pyruvate (5 mM), glucose (20 mM), taurine (20 mM), HEPES (10 mM), type 2 collagenase (Worthington, 1 mg/mL), and calcium chloride (30 μM) (pH 6.9)) in a 37°C water bath for 45 min. In order to maximize recovery of SC-CMs, the digested material was further agitated in a resuspension solution containing: potassium chloride (85 mM), potassium phosphate dibasic (30 mM), magnesium sulfate (5 mM), EGTA (1 mM), magnesium-ATP (2 mM), sodium pyruvate (5 mM), creatine (5 mM), taurine (20 mM), and glucose (20 mM) for an additional 15 min. After centrifugation and resuspension in media, the cell suspension was dispensed at approximately 1x105 SC-CMs per cm2 onto the sterile, PDMS-coated glass cover slips in well plates. To ensure cellular confluency

on the material surface, SC CMs in concentrated suspension were allowed to adhere for four hours prior to filling wells with additional media.

Assessment of Viability

The viability of SC-CMs was monitored throughout differentiation to ensure successful attachment and development of cardiac cells. At Day 10 and Day 14 of differentiation, SC-CMs were stained using LIVE/DEAD kit to determine viability. Live cells are characterized by intracellular esterase activity which cleaves the calcein-AM to form fluorescent green calcein. Dead cells are identified by presence of red fluorescent ethidium homodimer-1, which enters the cytosol through the ruptured cell membrane and binds to nucleic acids. SC-CMs stained with LIVE/DEAD were imaged using fluorescence microscopy and viability was quantified using ImageJ.

A LIVE/DEAD assay (Invitrogen, Life Technologies, Grand Island, NY) was used to quantify the viability of the cells on each surface 6 days post-seeding. Briefly, cells were incubated at room temperature for 20 min in a solution of calcein-AM (2 mM) and ethidium homodimer-1 (4 mM) in PBS. The solution was aspirated, cells were rinsed with PBS and PBS was added prior to imaging using fluorescence microscopy. Live cells were characterized by intracellular esterase activity which cleaves the calcein-AM to form fluorescent green calcein. Dead cells were reported by the presence of red fluorescent ethidium homodimer-1, which enters through the ruptured cell membrane and binds to nucleic acids in the nucleus. HL-1 cells were imaged using a Nikon Eclipse-Ti inverted fluorescence microscope (Nikon Instruments Inc., Melville, NY) and an Andor Luca S camera (Andor, Belfast, UK). Viability of cells on three separate films per condition was quantified using the cell counter plugin for ImageJ (NIH).

Characterization of cardiac protein expression

In order to evaluate expression of cardiac-specific proteins, Day 15 SC-CMs were subjected to immunocytochemistry. Cardiomyocytes were fixed using a 50:50 acetone/ethanol solution for 10 min at -20°C. The SC-CMs were then permeabilized using a 0.1% Triton X-100 solution in PBS and blocked using a 3% solution of FBS in PBS. Following blocking, samples were incubated in either mouse-anti-sarcomeric actinin or mouse-anti-cardiac troponin I and rabbit-anti-Cx43 antibody (diluted 1:200 in blocking buffer) for 2 h at room temperature. After rinsing, the secondary antibodies Alexa Fluor 488 goat-anti-rabbit and Alexa Fluor 568 goat-anti-mouse (Invitrogen, diluted 1:200 in blocking buffer) were added and incubated for 2 h at room temperature. To quantify the number of cells per area, SC-CMs cells were counterstained with DAPI (Invitrogen, 1:36000 from stock) and samples were dehydrated and mounted in Prolong Gold (Life Technologies). Images of SC-CMs on the film surfaces were acquired using a Nikon confocal microscope.

Electrophysiological analysis using optical mapping

Optical mapping was performed on confluent day 15 SC-CM monolayers on PCL-based films. Rhod 2 (Invitrogen) calcium indicator was prepared by first creating a 1 mM stock solution through addition of anhydrous dimethylsulfoxide followed by sonication at 50^{o} C for 30 min. To prepare the working calcium indicator solution, 5 µl of 1 mM Rhod-2 stock solution and 5 µl of Pluronic F-127 were added per 1 ml of Tyrode's solution. Following removal of cell culture media, 1 ml of calcium indicator solution was added to each well and allowed to incubate at room temperature for 20 min. After the

incubation period, the wells were rinsed three times with Tyrode's solution prior to imaging.

Recordings of calcium wave propagation across the SC-CM were acquired using an iXon Ultra DU897 EMCCD camera (Andor) coupled to an Optomask Adjustable Field Mask (Andor), which was utilized to enhance frame rate in cropped sensor mode, and Nikon Elements software. Propagating calcium waves were recorded in Tyrode's solution at room temperature (22 °C) in the absence of exogenous stimulation (i.e., spontaneous wave propagation). For each film, a minimum of three recordings were taken with an average length of 10 sec at a rate of approximately 500 frames per second. Data was analyzed using a modified version of a previously established MATLAB (MathWorks, Natick, MA) script (Weinberg, Lipke et al. 2010). Using this script, calcium transient velocity, calcium transient duration (time to 50% and 80% recovery), and calcium wave frequency were quantified for each condition.

6.3. Results

Attachment of SC-CMs to PCL, PPy-PCL films

It was expected that incorporation of PPy networks in to the PCL polymer would affect the attachment of SC-CMs to the material surface. To assess whether or not viable cardiomyocytes would readily adhere to the PCL and PPy-PCL films, fluorescence images were captured of day 12 SC-CMs labeled using a LIVE/DEAD stain (Fig. 6.1). The resulting images confirm that large numbers of viable SC-CMs were attached to each material 72 hours post-dissociation. A negligible percentage of dead cells were observed for each condition.

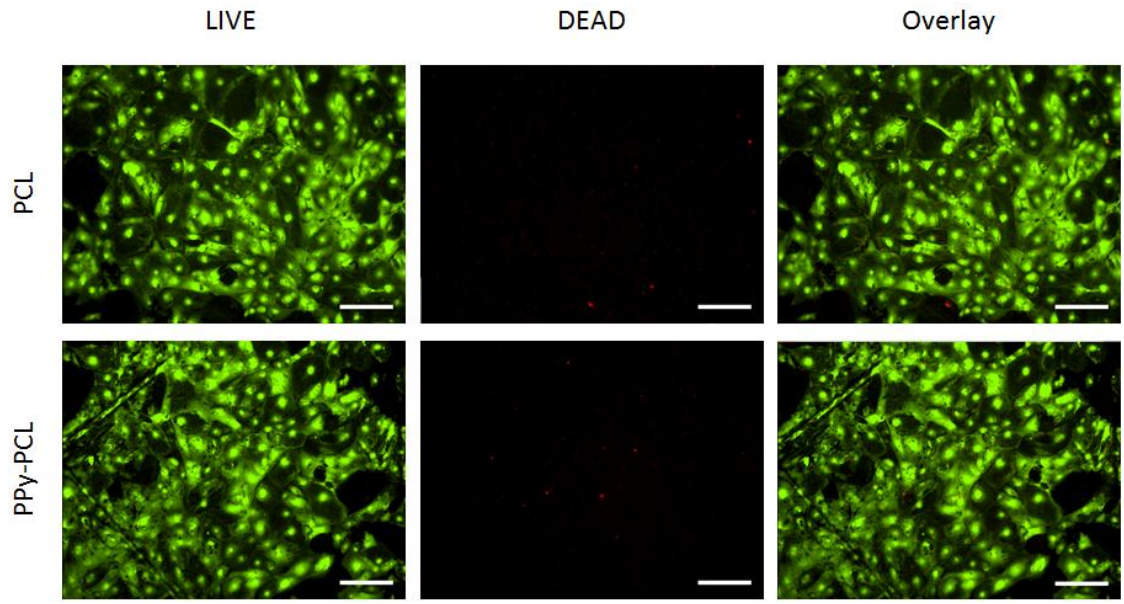

Figure 6.1. LIVE/DEAD images taken of day 12 SC-CMs on PCL, PPy-PCL. Scale represents 100 μm.

PPy-PCL, PCL facilitate formation of gap junctions

Monolayers of SC-CMs cultured on PCL and PPy-PCL films (day 15) showed positive expression of cardiomyocyte proteins α-sarcomeric actinin, cardiac troponin I, and connexin-43 (Cx43) (Fig. 6.2). While images of SC-CMs on each substrate demonstrate positive expression of Cx43 along the membranes of adjacent cells, no observable difference in total Cx43 organization was seen on either PCL or PPy-PCL films (Fig. 6.3).

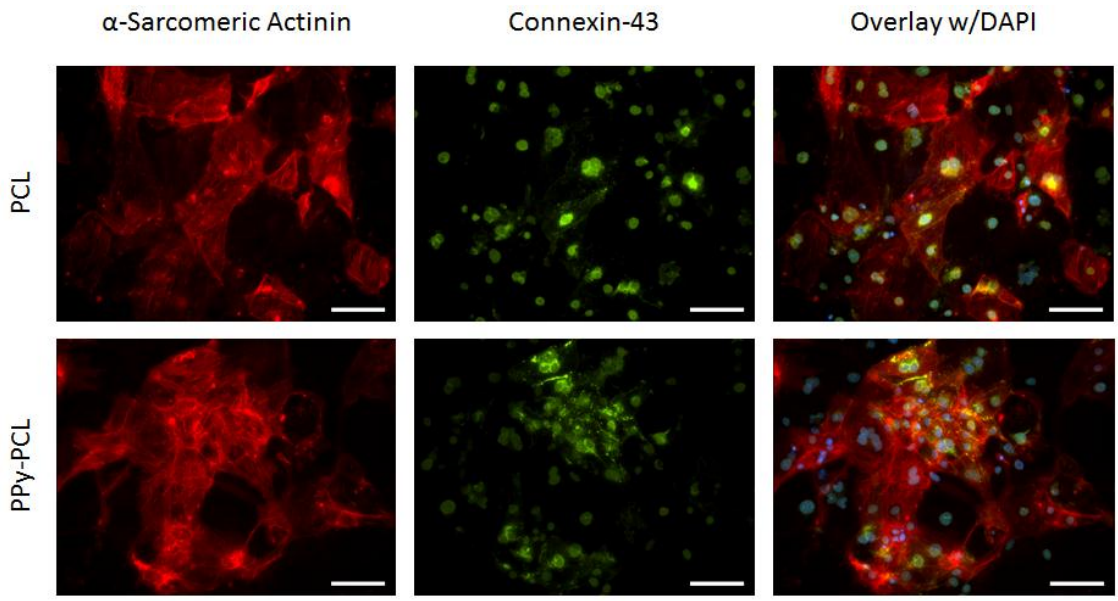

Figure 6.2. Immunocytochemistry images taken of day 15 SC-CMs. Scale represents 100 μm.

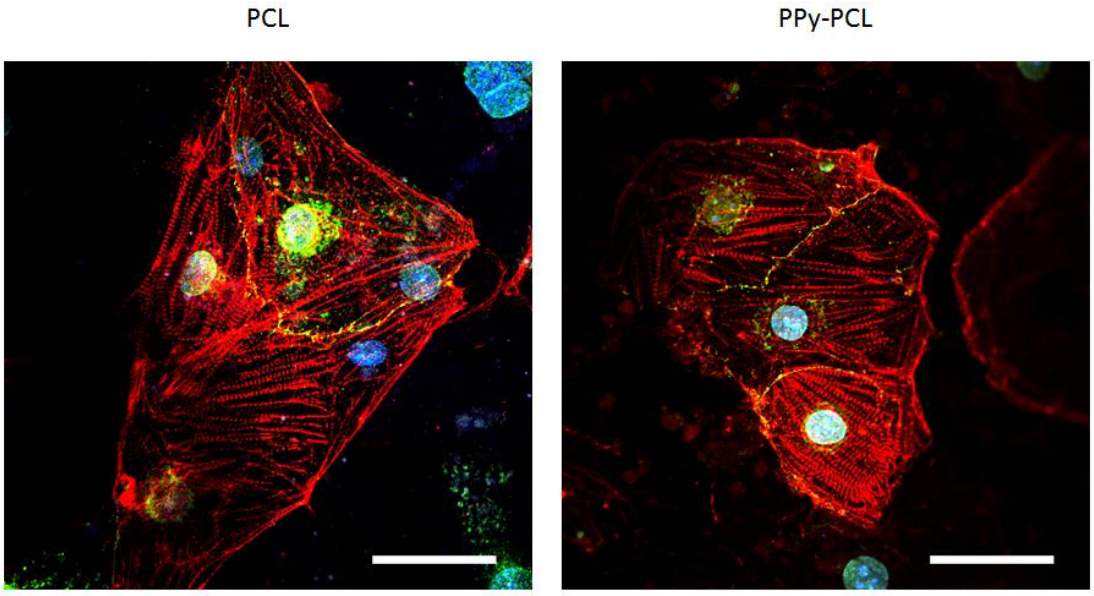

Figure 6.3. Confocal images of SC-CMs on each material. Scale represents 100 μm.

Preliminary calcium transient data

In order to evaluate the effect of film type on SC-CM calcium handling, day 15 films were evaluated using optical mapping analysis. Spontaneous calcium transient propagation was sparse and non-uniform throughout SC-CM monolayers on both film types. Exogenous electrical stimulation resulted in signal capture among a limited number of SC-CM monolayers.

In an effort to increase the Rhod-2 signal output on PCL and PPy-PCL films, monolayers were augmented by seeding HL-1 cardiomyocytes (at 50,000 cells per film) 72 hours prior to optical mapping analysis. Although this adjustment resulted in calcium transient data acquisition from additional samples, only a limited number of recordings were collected from each condition. This preliminary data was insufficient to allow for comparison of: calcium transient velocities (PCL: 4.00 ± 1.76 cm/s; PPy-PCL: 2.99 ± 0.82 cm/s; n=2 independent cover slips, Fig. 6.4), calcium transient durations at 50% (PCL: 649.8 ± 511.5 ms; PPy-PCL: 687.8 ± 18.9 ms) and 80% (PCL: 787.6 ± 679.6 ms; PPy-PCL: 900.2 ± 4.5 ms) recovery (Fig. 6.5), or spontaneous propagation frequency (PCL: 1.05 ± 0.98 Hz; PPy-PCL: 0.49 ± 0.04 Hz) (Fig. 6.6) for SC-CM/HL-1 monolayers cultured on the PCL and PPy-PCL films.

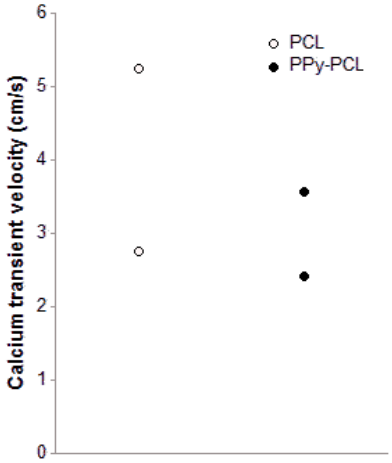

Figure 6.4. Calcium transient velocities of SC-CM/HL-1 monolayers on each material evaluated via optical mapping.

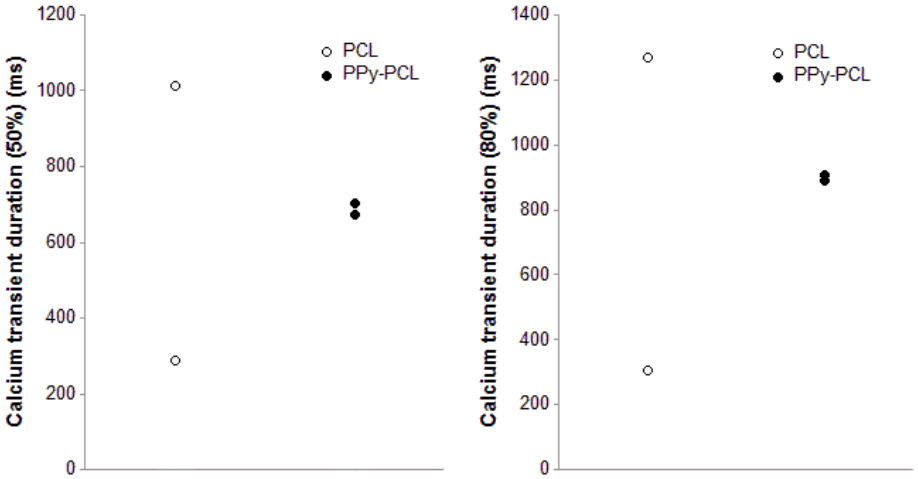

Figure 6.5. Calcium transient durations of SC-CM/HL-1 monolayers on each material evaluated via optical mapping.

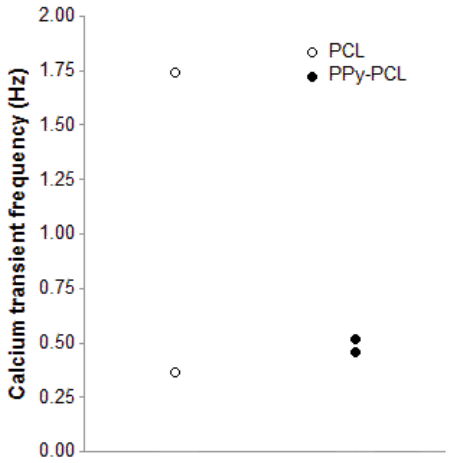

Figure 6.6. Calcium transient frequencies of SC-CM/HL-1 monolayers on each material evaluated via optical mapping.

6.4. Discussion

The purpose of this experiment was to determine the outcome of mSC-CMs undergoing cardiac differentiation on a conductive PPy-PCL substrate. Based on previous work observing HL-1 cardiomyocytes on PPy-PCL, it has been determined that the conductive PPy-PCL substrates are compatible with contractile cell types, supporting cell densities and cellular viabilities comparable to NaOH-treated PCL substrates alone. Furthermore, HL-1 cells grown on PPy-PCL scaffolds exhibited much higher Cx43 expression than HL-1 cells grown on PCL with high gap junction protein expression in proximity to the cell membrane. Taken together, these findings suggest that cardiomyocytes derived from stem cells grown on PPy-PCL could exhibit a significant increase in gap junction protein expression, translating into significantly higher conduction velocities than cardiomyocytes differentiated on PCL alone. The results of this study provide novel insight into the development of stem cell-derived cardiomyocytes on conductive materials and offer a new platform for creation of electrophysiologically-mature cardiomyocytes for clinical and diagnostic applications.

Significant evidence suggests that differentiating SC-CMs in materials containing conductive elements improves the maturation state of cardiomyocytes. For instance, culturing neonatal rat cardiomyocytes in a hydrogel containing gold nanoparticles increased the expression of Cx43 by 1 to 4 orders of magnitude in comparison to cardiomyocytes grown in hydrogels alone (You, Rafat et al. 2011). Similar results have been observed in cell scaffolds prepared with carbon nanotubes (Meng, Stout et al. 2013, Shin, Jung et al. 2013) and polypyrrole (Kai, Prabhakaran et al. 2011). Taken together, these findings indicate that conductive materials can improve expression and performance of maturing cardiomyocytes. In contrast, the effects of incorporating undifferentiated or immature cell types into conductive materials are not well understood.

In this experiment, pre-differentiated SC-CMs were dissociated and cultured on PCL and PPy-PCL films for a period of 7 days. LIVE/DEAD staining revealed that SC-CMs on both materials demonstrate robust viability and qualitatively-similar cellular adhesion. This result is consistent with a previous study utilizing HL-1 cardiomyocytes on PPy-PCL and PCL films; HL-1 cardiomyocytes were shown to adhere at a similar cellular density while maintaining over 90% viability in each case (Chapter 5). Additionally, SC-CMs on both films developed cardiomyocyte structural protein (α-sarcomeric actinin) and established circumferential gap junction proteins (Cx43), as evidenced through immunocytochemistry. These findings provide evidence that differentiating SC-CMs may be cultured and allowed to develop (and potentially mature) on the novel film material.

It was expected that changes in calcium handling would be observed via culture on conductive PPy-PCL films. In a previous study, HL-1 cardiomyocytes demonstrated

an increase in calcium transient velocity and decrease in calcium transient duration when cultured on PPy-PCL relative to a PCL control (Chapter 5). Initially, it was found that day 15 SC-CMs cultured on PPy-PCL and PCL films generated limited observable calcium transient activity. While the cause of this limited calcium transient activity is not understood, the addition of HL-1 cardiomyocytes to each film was utilized to increase the latent calcium transient activity on each sample. Preliminary calcium transient data collected via optical mapping revealed no significant difference in transient velocities, durations, or frequencies among SC-CM/HL-1 monolayers on PCL and PPy-PCL. Because SC-CMs exhibit batch-to-batch variability in addition inherent differences in individual sample preparation, evaluation of additional samples will be necessary to elucidate any changes in calcium transient activity that results from maturation on PPy-PCL films.

6.5. Conclusions

The purpose of this study was to determine changes in maturation of differentiating SC-CMs cultured on PPy-PCL films. This study demonstrates that SC-CMs maintain high viability and attach to conductive PPy-PCL and PCL films. SC-CMs grown on this material also develop cardiomyocyte structural proteins as well as gap junctions as evidenced through the formation of Cx43. Preliminary data recorded using optical mapping analysis revealed calcium transient activity present among cardiomyocytes cultured on PPy-PCL and PCL; however, quantification of additional samples is necessary to evaluate possible changes in calcium handling among cardiomyocytes on the novel material. Future work in this area could help to elucidate the

changes in maturation of SC-CMs which result from culture on conductive polymer substrates.

References

Bechara, S., L. Wadman and K. C. Popat (2011). "Electroconductive polymeric nanowire templates facilitates in vitro C17.2 neural stem cell line adhesion, proliferation and differentiation." Acta Biomater 7(7): 2892-2901.

Chun, Y. W., D. A. Balikov, T. K. Feaster, C. H. Williams, C. C. Sheng, J. B. Lee, T. C. Boire, M. D. Neely, L. M. Bellan, K. C. Ess, A. B. Bowman, H. J. Sung and C. C. Hong (2015). "Combinatorial polymer matrices enhance in vitro maturation of human induced pluripotent stem cell-derived cardiomyocytes." Biomaterials 67: 52-64.

Durgam, H., S. Sapp, C. Deister, Z. Khaing, E. Chang, S. Luebben and C. E. Schmidt (2010). "Novel degradable co-polymers of polypyrrole support cell proliferation and enhance neurite out-growth with electrical stimulation." J Biomater Sci Polym Ed 21(10): 1265-1282.

Dvir, T., B. P. Timko, M. D. Brigham, S. R. Naik, S. S. Karajanagi, O. Levy, H. Jin, K. K. Parker, R. Langer and D. S. Kohane (2011). "Nanowired three-dimensional cardiac patches." Nat Nanotechnol 6(11): 720-725.

Feinberg, A. W., P. W. Alford, H. Jin, C. M. Ripplinger, A. A. Werdich, S. P. Sheehy, A. Grosberg and K. K. Parker (2012). "Controlling the contractile strength of engineered cardiac muscle by hierarchal tissue architecture." Biomaterials 33(23): 5732-5741.

Hardy, J. G., J. Y. Lee and C. E. Schmidt (2013). "Biomimetic conducting polymer-based tissue scaffolds." Curr Opin Biotechnol 24(5): 847-854.

Kai, D., M. P. Prabhakaran, G. Jin and S. Ramakrishna (2011). "Polypyrrole-contained electrospun conductive nanofibrous membranes for cardiac tissue engineering." J Biomed Mater Res A 99(3): 376-385.

Kehat, I., D. Kenyagin-Karsenti, M. Snir, H. Segev, M. Amit, A. Gepstein, E. Livne, O. Binah, J. Itskovitz-Eldor and L. Gepstein (2001). "Human embryonic stem cells can differentiate into myocytes with structural and functional properties of cardiomyocytes." J Clin Invest 108(3): 407-414.

Khan, M., Y. Xu, S. Hua, J. Johnson, A. Belevych, P. M. Janssen, S. Gyorke, J. Guan and M. G. Angelos (2015). "Evaluation of Changes in Morphology and Function of Human Induced Pluripotent Stem Cell Derived Cardiomyocytes (HiPSC-CMs) Cultured on an Aligned-Nanofiber Cardiac Patch." PLoS One 10(5): e0126338.

Klug, M. G., M. H. Soonpaa, G. Y. Koh and L. J. Field (1996). "Genetically selected cardiomyocytes from differentiating embronic stem cells form stable intracardiac grafts." J Clin Invest 98(1): 216-224.

Lee, J. Y., C. A. Bashur, A. S. Goldstein and C. E. Schmidt (2009). "Polypyrrole-coated electrospun PLGA nanofibers for neural tissue applications." Biomaterials 30(26): 4325-4335.

Meng, X., D. A. Stout, L. Sun, R. L. Beingessner, H. Fenniri and T. J. Webster (2013). "Novel injectable biomimetic hydrogels with carbon nanofibers and self assembled rosette nanotubes for myocardial applications." J Biomed Mater Res A 101(4): 1095-1102.

Mooney, E., J. N. Mackle, D. J. Blond, E. O'Cearbhaill, G. Shaw, W. J. Blau, F. P. Barry, V. Barron and J. M. Murphy (2012). "The electrical stimulation of carbon nanotubes to provide a cardiomimetic cue to MSCs." Biomaterials 33(26): 6132-6139.

Pilarczyk, G., A. Raulf, M. Gunkel, B. K. Fleischmann, R. Lemor and M. Hausmann (2016). "Tissue-Mimicking Geometrical Constraints Stimulate Tissue-Like Constitution and Activity of Mouse Neonatal and Human-Induced Pluripotent Stem Cell-Derived Cardiac Myocytes." J Funct Biomater 7(1).

Rohr, S., R. Fluckiger-Labrada and J. P. Kucera (2003). "Photolithographically defined deposition of attachment factors as a versatile method for patterning the growth of different cell types in culture." Pflugers Arch 446(1): 125-132.

Saffitz, J. E. (1994). "Myocyte interconnections at gap junctions and the development of anatomic substrates of ventricular arrhythmia's." Cardiovasc Pathol 3(2): 87-91.

Salameh, A., A. Wustmann, S. Karl, K. Blanke, D. Apel, D. Rojas-Gomez, H. Franke, F. W. Mohr, J. Janousek and S. Dhein (2010). "Cyclic mechanical stretch induces cardiomyocyte orientation and polarization of the gap junction protein connexin43." Circ Res 106(10): 1592-1602.

Shin, S. R., S. M. Jung, M. Zalabany, K. Kim, P. Zorlutuna, S. B. Kim, M. Nikkhah, M. Khabiry, M. Azize, J. Kong, K. T. Wan, T. Palacios, M. R. Dokmeci, H. Bae, X. S. Tang and A. Khademhosseini (2013). "Carbon-nanotube-embedded hydrogel sheets for engineering cardiac constructs and bioactuators." ACS Nano 7(3): 2369-2380.

Stoppel, W. L., D. Hu, I. J. Domian, D. L. Kaplan and L. D. Black, 3rd (2015). "Anisotropic silk biomaterials containing cardiac extracellular matrix for cardiac tissue engineering." Biomed Mater 10(3): 034105.

van den Berg, C. W., S. Okawa, S. M. Chuva de Sousa Lopes, L. van Iperen, R. Passier, S. R. Braam, L. G. Tertoolen, A. del Sol, R. P. Davis and C. L. Mummery (2015). "Transcriptome of human foetal heart compared with cardiomyocytes from pluripotent stem cells." Development 142(18): 3231-3238.

Weinberg, S., E. A. Lipke and L. Tung (2010). "In vitro electrophysiological mapping of stem cells." Methods Mol Biol 660: 215-237.

Ye, K. Y. and L. D. Black, 3rd (2011). "Strategies for tissue engineering cardiac constructs to affect functional repair following myocardial infarction." J Cardiovasc Transl Res 4(5): 575-591.

You, J. O., M. Rafat, G. J. Ye and D. T. Auguste (2011). "Nanoengineering the heart: conductive scaffolds enhance connexin 43 expression." Nano Lett 11(9): 3643-3648.

7. CONCLUSIONS

As the number one source of mortality in the United States, heart disease has far-reaching costs in terms of: medical treatment expenses, reduction in quality of life, lost economic potential, and loss of lives. The lack of current therapies for post-infarcted patients has prompted the investigation into novel treatments for individuals with heart disease; many of these approaches rely on engineered materials that provide biomimetic cues to stem cells or differentiating cardiomyocytes. As such, understanding the role by which specific stimuli contribute to the differentiation and development of cardiomyocytes, in conjunction with the development of new materials which effectively demonstrate these biomimetic qualities, is ultimately important for success in this area. Furthermore, because the implantation of immature cardiomyocytes may lead to the development of arrhythmias, the ability to quantify the functional maturation of these cells and tissues is also a necessary step in the development of engineered myocardium.

In this document, I have described a set of studies which evaluate the effects of different biomaterials on the maturation of cardiomyocytes. In order to quantify the functional maturation of these cell types, I have fabricated an optical mapping platform capable of recording propagating calcium waves through cardiac tissue and cardiomyocyte monolayers. To accomplish this endeavor, I created a dual microscopic and macroscopic imaging system which can acquire recordings from samples ranging in size from 21 mm down to 100 μm. The fabrication of a customized optical mapping chamber allowed for perfusion of Tyrode's solution over the sample at physiological temperature while providing a mechanism for exogenous electrical stimulation of cardiomyocytes. The implementation of specialized optical equipment allowed for acquisition from a range of

different sample types. Together, the flexibility of this optical mapping platform was critical in assessing the impact of my biomaterials on resulting engineered cardiac tissue function.

As a small molecule with high diffusivity properties, nitric oxide (NO) has been evaluated by others as a promoter of cardiac differentiation; however, the effects of nitric oxide on cardiomyocyte maturation were not previously understood. Here I have shown that treatment of developing embryoid bodies (EBs) with the nitric oxide donor S-nitrosocysteine resulted in larger populations of cardiomyocytes with EBs demonstrating greater spontaneous contractile activity. Furthermore, developing cardiomyocytes receiving the NO donor demonstrated a more mature phenotype and improvement in calcium handling relative to control samples, as evidenced by increased calcium transient velocities and decreased calcium transient durations via optical mapping. Taken together, these results indicate that NO may play an important role in the maturation of stem cell-derived cardiomyocytes grown in large scale suspension culture platforms.

Cell-cell connectivity via formation of gap junctions between cardiomyocytes is an important facet of cardiac maturation. Because conductive substrates have been known to assist in the formation of these cellular structures, I selected a biocompatible, semi-conducting polymer (polypyrrole-polycaptrolactone (PPy-PCL)) to study as a platform for cardiac maturation. Cardiomyocytes cultured on the novel material demonstrated viabilities and cell densities that were consistent with cells grown on control materials. Cardiomyocytes cultured on PPy-PCL developed greater numbers of peripherally-located gap junction protein (Cx43). Furthermore, cardiomyocytes cultured on the PPy-PCL films developed increased calcium transient velocities and decreased calcium transient

durations relative to controls. These results show the potential importance of mimicking the conductivity of native myocardium in order to facilitate cardiac maturation.

The results of these studies demonstrate how engineering tools and systems can be applied towards the goal of heart regeneration. Implantation of immature cardiomyocytes can lead to the formation of deadly arrhythmias; the ability to drive maturation of cardiomyocytes in vitro is an important step in the adaptation of these cells into clinical or research applications. Through the use of a custom built mapping platform, I have shown how two novel material systems can be implemented to facilitate cardiomyocyte electrophysiological maturation in vitro. These findings contribute to our overall knowledge of cardiac-promoting biomaterials and may assist in establishing future cardiac regeneration technologies.

APPENDIX A: INCORPORATION OF CARDIOGENIC NITRIC OXIDE-RELEASING COMPOUNDS INTO THE CELLULAR NICHE IMPROVES MATURATION OF ENCAPSULATED STEM CELL-DERIVED CARDIOMYOCYTES

Introduction

Nitric oxide (NO) has been shown to increase the potential for cardiac differentiation as well as cardiac maturation of stem cell-derived cardiomyocytes (SC-CMs), as evidenced by improvements in contraction, protein and gene expression, and calcium handling (Chapter 4). The use of exogenous NO in the form of soluble *S*-nitrosocysteine (CysNO) has demonstrated improvement in spontaneous contraction percentage and frequency of contraction of embryoid bodies (EBs), as well as reduction in times to 50% and 80% calcium transient and increases in maximum capture rate among mESCs differentiated in static suspension culture. These data highlight the importance of NO as a cardiogenic signaling molecule with implications in scaled production of SC-CMs.

One important consideration for the implementation of NO signaling in a cardiogenic platform is the transient nature of NO delivery to the EBs and SC-CMs. Soluble CysNO demonstrates rapid release kinetics, delivering over 90% of its NO payload over the course of one hour. Since the biology of developing myocardium relies on continuous signaling via nitric oxide synthase (multiple isoforms), this method of NO delivery may not be successful in driving cardiac maturation in large scale culture platforms. Furthermore, additional considerations may arise with the incorporation of novel biomaterial-based cell carriers. It is not fully understood how mESCs differentiated in such environments will respond to NO signaling. Therefore, identification of the effects of exogenous NO signaling on pluripotent cells grown encapsulated in a

biomaterial carrier is critical in the development of a platform for large scale production of cardiomyocytes for clinical and diagnostic applications.

Polyethylene glycol- (PEG) based hydrogels have many properties which make them conducive for tissue engineering applications. PEG-based hydrogels have a high water content which is similar to naturally occurring tissue. The materials have easily tunable mechanical properties, have controllable chemical formulation, and can be readily formed into specific structures through rapid photopolymerization. PEG is also easy to customize with bioactive factors, proteins, signaling molecules; this allows for creation of a scaffold which promotes cell adhesion and accommodates growth with the incorporation of enzymatically-degradable structures within the material. PEG-fibrinogen, a natural-synthetic hybrid material, has been shown to support a number of cardiac cell types, including neonatal rat ventricular myocytes and human embryonic stem cell derived-cardiomyocytes (Habib, Shapira-Schweitzer et al. 2011). Additionally, PEG-fibrinogen has the potential to incorporate cell signaling peptides for engineering the microenvironment of synthetic tissues (Rufaihah, Vaibavi et al. 2013).

A hydrogel scaffold containing PEG-fibrinogen supplemented with exogenous NO may provide an environment conducive to cardiac differentiation and maturation of SC-CMs. In this study, mESCs were encapsulated in PEG-fibrinogen hydrogel and allowed to differentiate; differentiation of SC-CMs was assessed in micro-island and static microsphere culture. Viability and morphology of SC-CMs was assessed over the course of differentiation.

Materials and Methods

Culture of mESCs

A mouse D3 embryonic stem cell line was used for all experiments. Undifferentiated mESCs were expanded on mouse embryonic fibroblast layers prior to use. mESCs grown on feeder layers were enzymatically removed using a solution of 0.05% trypsin in EDTA, dispersed and counted using a hemocytometer.

Formation of PEG-fibrinogen (PEG-Fb) precursor

PEG-Fb precursor was prepared using established protocols (Shapira-Schweitzer, Habib et al. 2009). Briefly, PEG-Fb powder dissolved in PBS (10 mg/mL) was combined with N-vinylpyrrolidone, eosin Y (1 mM), and pluronic to form the hydrogel precursor that was used in all following experiments.

Encapsulation of mESCs in PEG-Fb using PDMS Molds

mESCs were transferred into a new vial prior to encapsulation and all media was be removed from the suspension. A volume of PEG-Fb precursor was added to the cells such that a cell density of $90x10^6$ cells/mL was achieved. Precursor was mixed well and dispensed into custom-made PDMS molds on acrylated glass slides. Light was applied for approximately 60 seconds to achieve crosslinking. Hydrogel scaffolds were immediately transferred into culture media.

Encapsulation of mESCs in PEG-FB Microspheres

mESCs were transferred into a new vial prior to encapsulation and all media was removed from the suspension. A volume of PEG-Fb precursor was added to the cells such that a cell density of $90x10^6$ cells/mL was achieved. Precursor was mixed well and

dispensed into a glass tube containing mineral oil with I-651 photoinitiator and NVP. The colloidal suspension was vortexed for 2 seconds and crosslinked using light over a period of 20 seconds. Oil was removed using 3 subsequent washing steps using DMEM before transferring microspheres into culture media.

Analysis of Viability using LIVE/DEAD Assay

Following encapsulation, the viability of differentiated cells was assessed. Encapsulated mESCs from each configuration were incubated in Live/Dead® reagent (Invitrogen, Carlsbad, CA), containing calcein-AM and ethidium homodimer-1, for 30 minutes. Live cells are characterized by intracellular esterase activity which cleaves the calcein-AM to form fluorescent green calcein. Dead cells are identified by presence of red fluorescent ethidium homodimer-1, which enters the cytosol through the ruptured cell membrane and binds to nucleic acids. EBs were imaged using an inverted fluorescence microscope (Nikon Eclipse Ti-U) and an Andor Luca S camera.

Results

In this experiment, I was interested in indentifying the effect of soluble NO treatment on the cardiogenic potential of mESCs encapsulated in PEG-Fb hydrogels. I hypothesized that mESCs encapsulated in PEG-Fb in the presence of exogenous NO would exhibit increased levels of cardiac protein and gene expression after two weeks in culture. Furthermore, dissociated SC-CMs differentiated in the presence of NO were expected to produce faster conduction velocities than SC-CMs not receiving the exogenous signal. Taken together, the results of this experiment would provide insight

into the nature of cardiomyocyte differentiation and maturation, producing a novel biomimetic platform for production of cardiomyocytes in a large scale culture system.

Initial tests were been performed to evaluate mESC performance in PEG-Fb hydrogel micro-islands. To optimize the cell encapsulation density and photoinitiator combination in the micro-islands, PEG-Fb precursor was prepared using eosin-Y and Igacure 2959 photoinitiators. mESCs were encapsulated at either 30 or 60 million cells per mL; mESCs were visualized using LIVE/DEAD stain after 72 hours in culture (Fig. A.1).

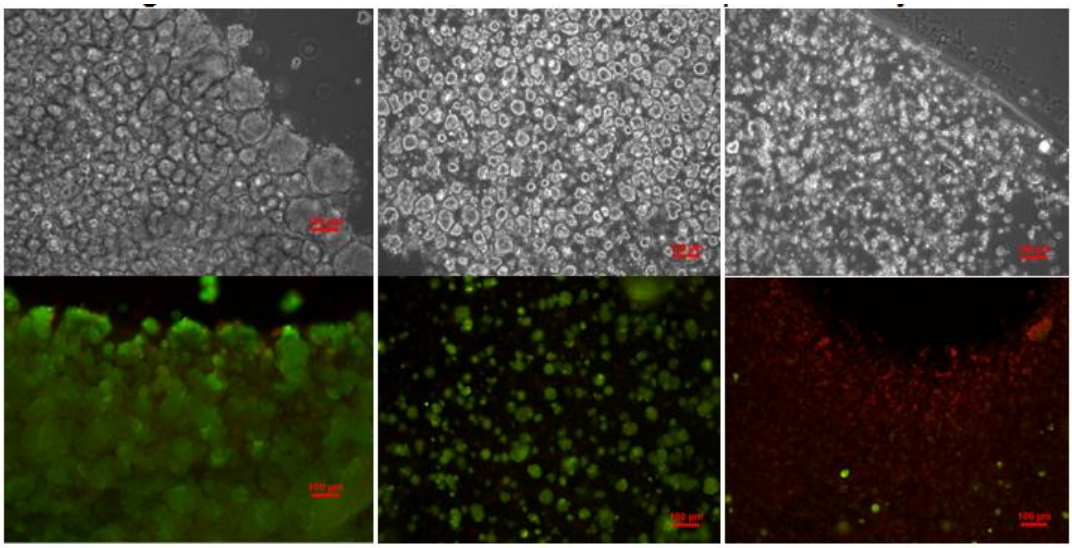

Figure A.1. SC-CMs in PEG-Fb. (Left) 60 million cells/mL, Eosin-Y. (Middle) 30 million cells/mL, Eosin-Y. (Right) 30 million cells/mL, Igacure-2959. (Top) Phase contrast images of SC-CMs in PEG-Fb. (Bottom) LIVE (green)/ DEAD (red) images of SC-CMs. Scale bars represent 100 μm.

Qualitative analysis shows PEG-Fb hydrogels containing 60 million cells per mL cross-linked using eosin-Y as the optimal condition parameters for the formation of micro-islands.

Formation of PEG-Fb microspheres containing mESCs has also been peformed. Microspheres containing mESCs were fabricated according to the previously described protocol (Fig. A.2). LIVE/DEAD analysis has shown that mESCs encapsulated in PEG-Fb microspheres are subject to high cell death (Fig. A.3). Because encapsulation of cells is a manually-intensive activity which requires high operator skill, additional work will be required to improve the viability of encapsulated mESCs.

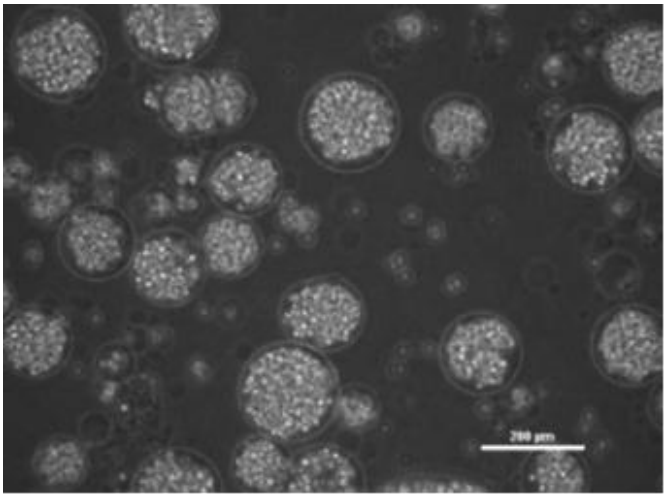

Figure A.2. Microspheres formed from PEG-fibrinogen containing mESCs. Scale bars represent 200μm.

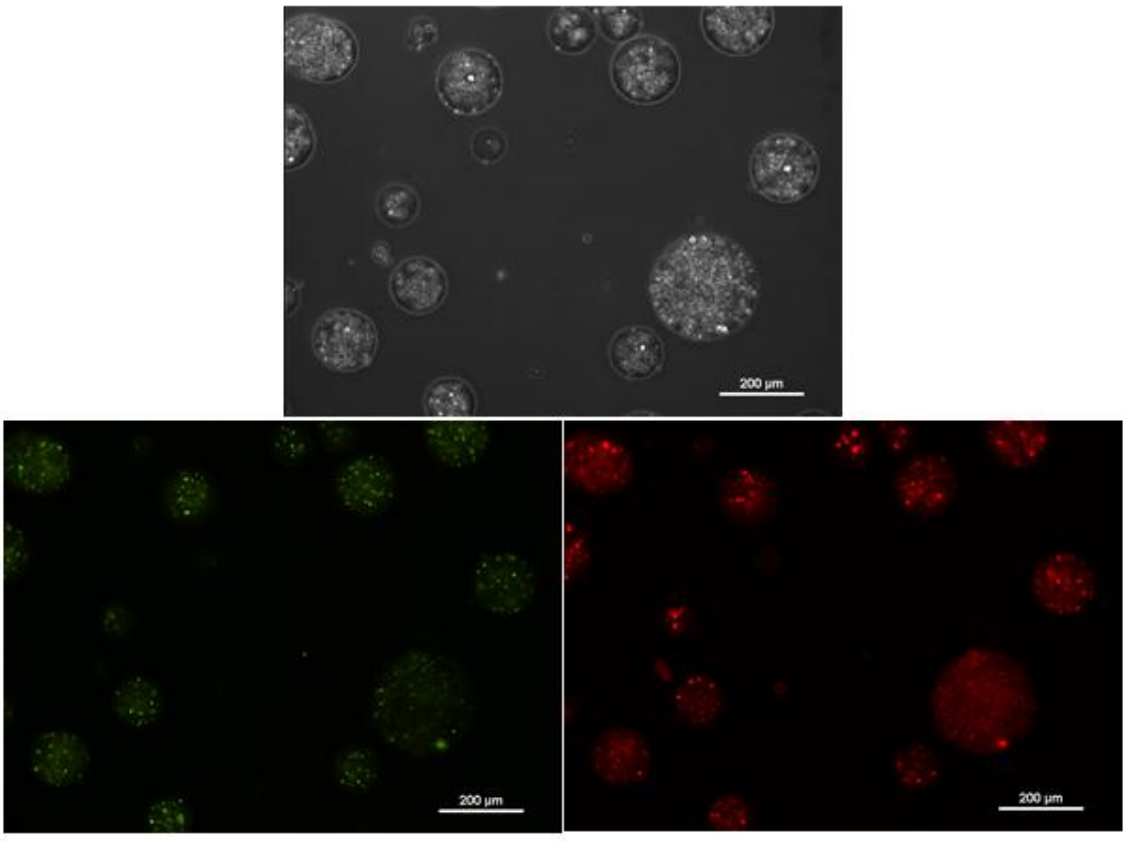

Figure A.3. mESCs in PEG-fibrinogen microspheres were stained using LIVE/DEAD. (Top) Phase contrast; (Bottom-Left) LIVE; (Bottom-Right) DEAD. Scale bars represent 200µm.

Discussion

The use of microcarriers and other biomaterial based cell transport systems is a critical component to large scale cell culture and cell delivery systems. Cell encapsulation for cardiac repair applications has been attempted by others using a variety of materials, including Matrigel (Mayfield, Tilokee et al. 2014) and alginate (Levit, Landazuri et al. 2013). Others have utilized synthetic biomaterials, including PEG-based hydrogels, for large scale cell culture of stem cells (Lei and Schaffer 2013). In the Lipke Lab, Samuel Chang incorporated a technique using PEG based hydrogels to encapsulate mESCs in

microspheres (Olabisi, Lazard et al. 2010). While Sam was successful in encapsulating these cell types, his incorporation of ascorbic acid alone did not produce large numbers of functional SC-CMs. These results indicate that more intricate cell signaling, by virtue of modification of the cellular niche, may be required in order to drive cardiogenesis of pluripotent cell types in this hydrogel environment.

Preliminary data show high cell death of mESCs encapsulated using the microsphere protocol. This result may be a consequence of user variability; however, it has also been postulated that increasing the encapsulation cellular density may be one method for mitigating the damage inflicted onto the mESCs during the procedure. Additionally, it has been suggested that incorporation pre-formed embryoid bodies into the material may also support mESC proliferation and differentiation in the PEG-Fb material (Wilson, Najia et al. 2014).

References

Habib, M., K. Shapira-Schweitzer, O. Caspi, A. Gepstein, G. Arbel, D. Aronson, D. Seliktar and L. Gepstein (2011). "A combined cell therapy and in-situ tissue-engineering approach for myocardial repair." Biomaterials 32(30): 7514-7523.

Kehat, I., D. Kenyagin-Karsenti, M. Snir, H. Segev, M. Amit, A. Gepstein, E. Livne, O. Binah, J. Itskovitz-Eldor and L. Gepstein (2001). "Human embryonic stem cells can differentiate into myocytes with structural and functional properties of cardiomyocytes." J Clin Invest 108(3): 407-414.

Lei, Y. and D. V. Schaffer (2013). "A fully defined and scalable 3D culture system for human pluripotent stem cell expansion and differentiation." Proc Natl Acad Sci U S A 110(52): E5039-5048.

Levit, R. D., N. Landazuri, E. A. Phelps, M. E. Brown, A. J. Garcia, M. E. Davis, G. Joseph, R. Long, S. A. Safley, J. D. Suever, A. N. Lyle, C. J. Weber and W. R. Taylor (2013). "Cellular encapsulation enhances cardiac repair." J Am Heart Assoc 2(5): e000367.

Mayfield, A. E., E. L. Tilokee, N. Latham, B. McNeill, B. K. Lam, M. Ruel, E. J. Suuronen, D. W. Courtman, D. J. Stewart and D. R. Davis (2014). "The effect of encapsulation of cardiac stem cells within matrix-enriched hydrogel capsules on cell survival, post-ischemic cell retention and cardiac function." Biomaterials 35(1): 133-142.

Olabisi, R. M., Z. W. Lazard, C. L. Franco, M. A. Hall, S. K. Kwon, E. M. Sevick-Muraca, J. A. Hipp, A. R. Davis, E. A. Olmsted-Davis and J. L. West (2010). "Hydrogel microsphere encapsulation of a cell-based gene therapy system increases cell survival of injected cells, transgene expression, and bone volume in a model of heterotopic ossification." Tissue Eng Part A 16(12): 3727-3736.

Rufaihah, A. J., S. R. Vaibavi, M. Plotkin, J. Shen, V. Nithya, J. Wang, D. Seliktar and T. Kofidis (2013). "Enhanced infarct stabilization and neovascularization mediated by VEGF-loaded PEGylated fibrinogen hydrogel in a rodent myocardial infarction model." Biomaterials 34(33): 8195-8202.

Shapira-Schweitzer, K., M. Habib, L. Gepstein and D. Seliktar (2009). "A photopolymerizable hydrogel for 3-D culture of human embryonic stem cell-derived cardiomyocytes and rat neonatal cardiac cells." J Mol Cell Cardiol 46(2): 213-224.

Wilson, J. L., M. A. Najia, R. Saeed and T. C. McDevitt (2014). "Alginate encapsulation parameters influence the differentiation of microencapsulated embryonic stem cell aggregates." Biotechnol Bioeng 111(3): 618-631.